The 2003 Chuya sequence (North Altay range): tectonic context and seismological study.

Ulziibat Munkhuu

UNIVERSITE DE NICE-SOPHIA ANTIPOLIS – UFR SCIENCES
Ecole doctorale Sciences Fondamentales et Appliquées

THESE

pour obtenir le titre de

Docteur en Sciences
de l'Université de Nice-Sophia Antipolis

Spécialité : Géophysique

présentée et soutenue par

Ulziibat MUNKHUU

The 2003 Chuya sequence (North Altay range): tectonic context and seismological study

Thèse préparée dans le laboratoire Géosciences Azur (UMR 6526 à Sophia Antipolis) et au Centre de Recherche d'Astronomie et Géophysique (Oulan-Bator, Mongolie) dirigée par Antoine Schlupp et Anne Deschamps

Soutenue le 20 janvier 2006, devant le jury composé de :

Michel Cara	Professeur	Rapporteur
Jacques Déverchère	Professeur	Rapporteur
Jocelyn Guilbert	Chercheur	Examinateur
Jean François Ritz	Directeur de recherche	Examinateur
Jean François Stéphan	Professeur	Examinateur
Anne Deschamps	Directeur de recherche	Co-directrice de thèse
Antoine Schlupp	Physicien Adjoint	Co-directeur de thèse

Acknowledgements

First, I would like to thank my father Munkhuu Daram for giving me the strength, guidance, and determination to complete my thesis.

I would like also to express my heart-felt gratitude and appreciation to my first supervisor Anne Deschamps for her decisive guidance, constructive criticism and constant encouragement whole of my graduate days. My sincere thanks are due to my second supervisor, Antoine Schlupp, for his friendly support and guidance, valuable advice made this dissertation possible. They teach me how to read, to write, to present, to organize thoughts. It has been a wonderful experience and great opportunity to work with them and I can never appreciate Anne and Antoine enough for them understanding of the human problems of them student.

DASE and French Embassy in Mongolia generously provided funding for this research and my dissertation. I am deeply grateful to Mr Jacques Bouchez (Département Analyse Surveillance Environnement /Commissariat à l'Energie Atomique), French Ambassadors and heads of French Cultural Center in Mongolia that gave me a unique opportunity, which made this work possible.

I would like to thank my PhD committee members Michel Cara, Jacques Déverchère, Jean-François Ritz, Jean-François Stéphan for accepting to review my work.

I particularly thank Bertrand Delouis for all the instructive discussions, critical comments and especially for his assistance with the Nabelek inversion code.

I am thankful to Remi Michel and Renaud Binet (DASE/CEA) providing me the results of SPOT image correlation used in my research.

I express my gratitute to Jocelyn Guilbert and for all instructive discussions I had with him. I appreciate the helps I enjoyed at different times given by Bruno Feignier, Thierry Heritier, Cansi Yves, Jean-Paul Santoire, Denis Lubin, Daniel Fouquet from DASE.

I would like to thank Christophe Larroque, Martin Vallée, Marc Régnier, Francoise Courboulex and other colleagues from the "Laboratoire Géosciences Azur" for their support and encouragement in providing me all necessary hardware, software issue and their assistance during my stay in France.

My sincerely gratitude to my colleagues of Research Center of Astronomy and Geophysics of Mongolian Academy of Sciences, who gives me great chance to start my PhD study in France and their supporting during my study time.

Last, but not least, special thanks go to my family. Their love and support made this work possible.

Abstract

The present work is focussed on the seismological study of the September 27th 2003 (M = 7.3) large earthquake in Altay and try to include the results on a tectonical study of the Altay range (Mongolia/Russia).

In the first chapter is presented tectonic and geodynamic aspect of Altay range. A review of existing works on the morphological and geological context is completed by an interpretation of satellite images. We consider four active fault zones from their continuity. On images we interpret several offsets of river streams. The distribution of offsets is similar along the same active zone, but are different from one fault to the other. We propose a partitioning of movements inside the Altay block and discuss the compatibility of the observations with a global rotation of the Altay.

In the second chapter is discussed the seismic catalogue of Mongolia produced by the RCAG and presented different methods to analyse it, in particular the clustering to reduce the impact of the aftershocks. We show distributions of b-values in the different zones and their relation with the abnormal occurrences of large events on the territory of Mongolia. Next, we focus more on Altay region and its observed seismic activity.

The third chapter is focused on the geological context of the Chuya earthquake. We discuss the available field observations and compared the measured displacement values to the results obtained with a SPOT image correlation made on the southern part of the ruptured zone. Surfaces rupture observed on the field and deduced from spot correlation are geometrically very similar, but amplitude of the horizontal displacement are different.

In the fourth chapter we analyze in detail location of the seismic sequence. Relocation of the first period (main shock and stronger aftershocks) is done with regional data. Next, we discuss the location procedure and show the aftershocks distribution obtained for the period covered by a temporary network. Main activity of aftershock occurred on southern margin of Chuya and Kurai depressions. The cluster is 90 km long in a NW-SE direction, superposed to the surface breaks in its central part, and extend to a depth of 20km.

In the fifth chapter is presented a model of the rupture for the mainshock and two large aftershocks obtained using body wave inversion. The 3 analysed events are modeled as complex events with combination of two or more subevents with different focal mechanisms and different rupture velocities. The source duration, and rupture velocities allow to reconstruct from the epicentral locations a rupture which is in agreement with the surface observation but the history of the sequence can be related to the segmentation of the fault and the presence of different tectonic units.

Key words : Mongolia, Altay range, seismicity, large intra-continental earthquake, satellite images analysis, source process, aftershocks, earthquake location.

Résumé

Le travail présenté est consacré à l'étude sismologique du séisme du 27 septembre 2003 qui a eu lieu en Altay (Mongolie, Russie) et à l'interprétation des résultats dans le cadre d'une étude tectonique de la chaîne de l'Altay.

Dans le premier chapitre nous avons collecté les informations morphologiques, géologiques et tectoniques dans la littérature existante. Nous en avons déduit un schéma simple de déformation de la chaîne avec 4 failles NW-SE majeures. Nous avons complété ces informations avec une interprétation d'images satellites sur lesquelles sont mesurés des déplacements horizontaux. Les décalages semblent de même amplitude sur le même faille, mais variables d'une faille à l'autre. Nous proposons un partionnement du mouvement à l'intérieur du bloc Altay et discutons de la compatibilité avec une rotation anti-horaire du bloc.

Dans le second chapitre nous analysons le catalogue de sismicité de Mongolie produit par le RCAG. Nous montrons qu'une grande partie des événements peuvent être considérés comme des répliques des grands séismes qui ont eu lieu au siècle dernier. Nous analysons la distribution de la b-value dans différentes régions en relation avec l'occurrence de grands séismes. L'accent est mis sur la région de l'Altay.

Dans le 3ième chapitre nous introduisons le contexte géologique du séisme de Chuya (Ms = 7.3) et les observations de qui ont pu être faites en surface du déplacement horizontal produit par le séisme. Les mesures sur les traces de surface sont comparées à des mesures plus globales obtenues sur l'auto-corrélation d'image SPOT. La géométrie très semblable contraint très bien la position du séisme.

Dans le 4ième chapitre est analysée la position des séismes majeurs de la séquence sismique à partir de données sismologiques de réseaux permanents. Une meilleure image de la distribution des répliques est produite par l'interprétation des données d'un réseau temporaire déployé sur le zone épicentrale. Cet essaim de séisme montre une activité sur 90 km de long dans la direction NW-SE le long du bord sud des dépressions de Chuya et Kurai et jusqu'à des profondeurs de 20 km.

Dans le 5^{ième} chapitre est présenté un modèle de rupture des 3 événements majeurs de la séquence obtenu par inversion des ondes de volume P et SH. Ces 3 séismes présentent une rupture complexe avec plusieurs sous événements de mécanisme différent et des vitesses de rupture assez variables. Les valeurs de durée de source et de vitesse de rupture sont en bon accord avec les observations de surface.

L'ensemble de ces résultats permet de proposer un schéma global de la séquence cohérent en accord avec la morphologie et la tectonique dans cette partie de la chaîne.

Mots clef : Mongolie, Altay, sismicité, analyse d'image satellite, grands décrochements intra-continentaux, source sismique, répliques, localisation de séismes.

Content

Introduction

Central Asia presents one of unique Earth's laboratories for studying process of intracontinental deformation associated with a major collision. The Indo-Eurasian collision well-known effects on Cenozoic uplift of the Himalayas, Tibet, Pamir and Tien Shan are intensively studied. Longer distance effect including Altay, Gobi-Altay, Sayan, Hangai dome, Khuvsugul and Baikal rift zones are starting to be studied in more details only recently. Active faulting and kinematics of fault were extensively studied in these regions by different international teams (Baljinnyam et al., 1993; Ritz et al., 1995; Schlupp, 1996; Bayasgalan, 1999). Movements in the Altay consists of dextral strike-slip faults oriented NNW and thrust and reverse faults on more E-W trending structures. The Gobi-Altay system is dominated by E-W left lateral strike-slip fault systems also observed in the north of Hangai dome (Bulnay faults). On the east of Hangai occurred right-lateral strike-slip in the Mogod fault system. Although the Khuvsugul graben system appears to be an extension of Baikal, the region shows strike-slip faulting.

The resent GPS studies show northward velocities and N-S shortening in western Mongolia and eastward to southeastward motion and left lateral shear for the central and eastern Mongolia (Calais et al., 2003). However, active deformation and occurrence of large earthquakes over this region are still far to be understood. They still need more detail studies using modern technology and knowledge. Our study is focused more in this region and we hope that our result will help to solve some of the questions related to the active deformation of Central Asia.

The present study focuses on the Altay range which is one of the last great frontier areas for continental tectonics. We are interested in understanding the processes of intracontinental mountain building and in the manner in which continents deformation are internally partitioned. The Altay range is one region of complex active deformation which is difficult to assess by classic geological or geophysical tools. Moreover, it is also one region which is poorly studied.

They are many questions on that area which have been never answered as:

- How a 4000 m high mountain range was formed in the center of Asia;
- The behavior of the tectonic stress field in highly heterogeneous basement terranes and its relation to the tectonic and upper crustal movements;
- The high seismic activity and its relation with active faults;

- How to explain occurrence of several destructive large earthquakes in short time (during last century) under this slow compression and long recurrence time of these large earthquakes;
- What is the relation between dextral major strike-slip faults (southern and internal Altay) oriented NNW, with major reverse and thrust faults (northern Altay)

First, we will focus on the determination of active deformation and Quaternary fault slip, using satellite image interpretation of the Mongolian Altay region. Other information that we will bring to knowledge of Altay region is a complex seismological and image-processing study, using data of Chuya large earthquakes which occurred in Northern Altay (Ms=7.3). The Chuya earthquake is the first large earthquakes recorded in Altay range since the installation of the worldwide digital stations that will give us chance to study in details fault and rupture process of this large event.

The seismological instrumental studies of Mongolia starts relatively recently, just after large Gobi-Altay earthquake of the 04th September, 1957 (M=8.2), with two stations. However more complete observation of seismic activity of the territory started in 1964 after the installation of several other seismic stations. Since that time, our data set starts to be more complete with events of moderate size over the entire region. However, even in this short time period, we have recorded a relatively large number of earthquakes on which can be studied the seismic activity and constrained the tectonic processes of different regions. In the last years, in the framework of CTBTO to monitor potential nuclear test around the world, the distribution of seismic stations increased significantly in the world. As Mongolia is one of the strategic territory for CTBTO (low seismic noise; not far from countries who could make nuclear explosions like Russia, China, Pakistan, India) several stations have been installed through this project. Actually, in Mongolia is working more than 40 seismic stations if we include mini-array group stations and the detection level on the territory increased significantly. Other hand, seismic database of RCAG is also increasing due to these instrumentation developments. The RCAG interest is not only collecting data and maintenance of these stations, but also to work on the data and to developed scientific studies. For this purpose, RCAG try to develop his own scientific studies and collaboration with worldwide institutes. Some international projects already succeed to be supported; one was the MoBal seismological transect project installed in 2003 for the study of deep lithospheric structure from Baikal (Russia) to Gobi-Altay (South Mongolia) in collaboration Geoazur (France) and Earth crust (Russia) institutes.

My work at RCAG starts with the study of tectonics and seismological aspects of Altay range but move soon after to installation and maintenance of seismic stations because of the contracts signed by the RCAG. I was then involved in data managing and localization procedures. During that period I contributed to establish the seismic catalog of Mongolia. Nevertheless, in the last years, when RCAG staff was increasing, I could develop scientific works. I had the chance to participate to the MoBal project and I had the proposition from DASE to support me for a thesis work partly in France. The first proposition was to work on the data of MoBal transect for deep structure determination.

However, at that the time the great Chuya earthquake occurred in Northwestern Altay range and its give interest to continue my work on the Altay region that is one of less studied region of Mongolia.

The first chapter of thesis is focusing on the tectonic and geodynamic aspect of Altay range. For the beginning, we discuss morphological and geological context of the region. Next, we will show our interpretation of satellite images in terms of active faults over the Altay range. To show the activity over these zones, we used the results obtained earlier by several authors who did different field studies on the faults. We have considered four active fault zones from their continuity and observed offsets that are discussing in details. We found in several areas that clear offsets of river streams could be observed. The distribution of offsets is different for each active structure but is constant along the same active fault. These observations lead us to discuss some partitioning of movements inside the Altay block. Based on this study we will propose some model of deformation and will compare our observation with other studies.

In the second chapter, we discuss the seismic network of Mongolia and its recent development. We also describe the seismic data set of RCAG and we present different methods we have used to improve the data base. Next, we show our seismicity analysis of Mongolia and discuss annual radiated energy release over the territory and over some specific zones. We estimated the aftershock clustering to characterize the seismic activity of Mongolia. In addition, we show distributions of ***b***-values in the different zones and their relation with the abnormal occurrences of large events in Mongolia. Next, we will focus more on Altay region and observed seismic active zones.

The third chapter is focused on the geological context of the magnitude Ms=7.3 Chuya earthquake which occurred on 27th September 2003. We discuss the available field observations and the results of a SPOT image correlation.

In the fourth chapter, we analyze in detail aftershock activity recorded after the Chuya earthquake. First, we present the relocation of the main shock of the Chuya earthquake and its two large aftershocks together with the early aftershock sequence. Next, we describe the temporary experiment to record the aftershock sequence. We discuss the location procedure and show the aftershocks distribution obtained for the period covered by the temporary network. Main aftershock activity occurred on the southern margin of the Chuya and Kurai depressions. The cluster is 90 km long in a NW-SE direction. Relocation of main shock and location of aftershocks show that main activity occurred at depth shallower than 20 km.

In chapter V, we introduce our body wave inversion results of main shock and two large aftershocks. The results of inversions show that all earthquakes are modeled as complex events with a combination of two or more subevents with different focal mechanisms and different rupture velocities. Then we will discuss these results and compare them to the information obtained from the previous chapters and to the characteristic of similar large intra-continental events.

Finally, in the "general conclusion and perspectives" we summarize and discuss our results and propose some future possible research that should be done to increase our knowledge of Altay region, but also of global seismic hazard in Mongolia.

Chapter I

Active deformation in Altay range

I.1. Introduction

The India-Eurasia convergence induces the active deformation of Central Asia (Tapponnier and Molnar, 1979) which takes place from the north of Himalayas up to the Baikal rift system. Central Asia has a right-stepping en-echelon mountain range system including Hindu Kush, Pamir, Tien Shan, Altay and Sayan ranges (Fig. I.1). Altay is the youngest system. Its formation has begun at the Cenozoic period (Tapponnier and Molnar, 1979).

The Altay range stretches from southwestern Siberia to the Gobi desert of Mongolia and is located dominantly in Mongolia but also in Russia, China, and Kazakhstan. The Altay range is a tectonically active region and corresponds to an intra-continental uplifted mountain. The system, about 1500 km long, is composed of an alternation of ranges and basins which are mainly oriented in NW-SE direction. The recent deformation observed along the tectonic structures shows mainly compression with right-lateral horizontal movements. The present deformation, deduced from GPS data (Calais et al., 2003), show N-S shortening combined with right-lateral shear in the Altay. The observed velocities, in reference to the Siberian platform, decrease from south to north, from 10 mm/yr at Urumqi, south of the Altay range, down to ~ 4 mm/yr at Altay city, north east of the range. If these values are confirming in the future, they mean that the whole Altay absorb about 10 mm of the convergence between Urumqi and Siberia, thus that individual active faults have a probable rate of horizontal deformation of the order of the millimeter per year.

Compression features can be observed, but also horizontal motion, across alluvial fans. Large north-northwest trending strike-slip faults systems play a key role in the active tectonics of Altay. The major active faults are considered to be at the west and east of the highest relief of the range (Tapponnier and Molnar, 1979). At the SE extremity of Altay takes place dominant thrust faulting with strike-slip component, as at the south west margin of Baatar-Hairhan and Sutai ranges (Fig.I.3 and I.5). In the Sutai and Jargalant range, the deformation is accommodated by right-lateral strike-slip, thrust and oblique-slip displacements (Cunningham *et al.* 1996).

Several major structures have been ruptured by two large destructive earthquakes in the last century; the Fu-Yun (M = 8, 1931) mainly right-lateral strike-slip fault and the Ureg-Nuur (M = 7.0, 1970) which presents mainly compressive motion (Khilko *et al*., 1985) (Fig.I.1). In September 2003 occurred, at the NW edge of the range, the Chuya event (Ms = 7.3) (Fig.I.1), which will be extensively discussed. Besides these large events, the dominant structures of the Altay range are underlined by a background seismic activity which is localized at the RCAG using worldwide and national networks.

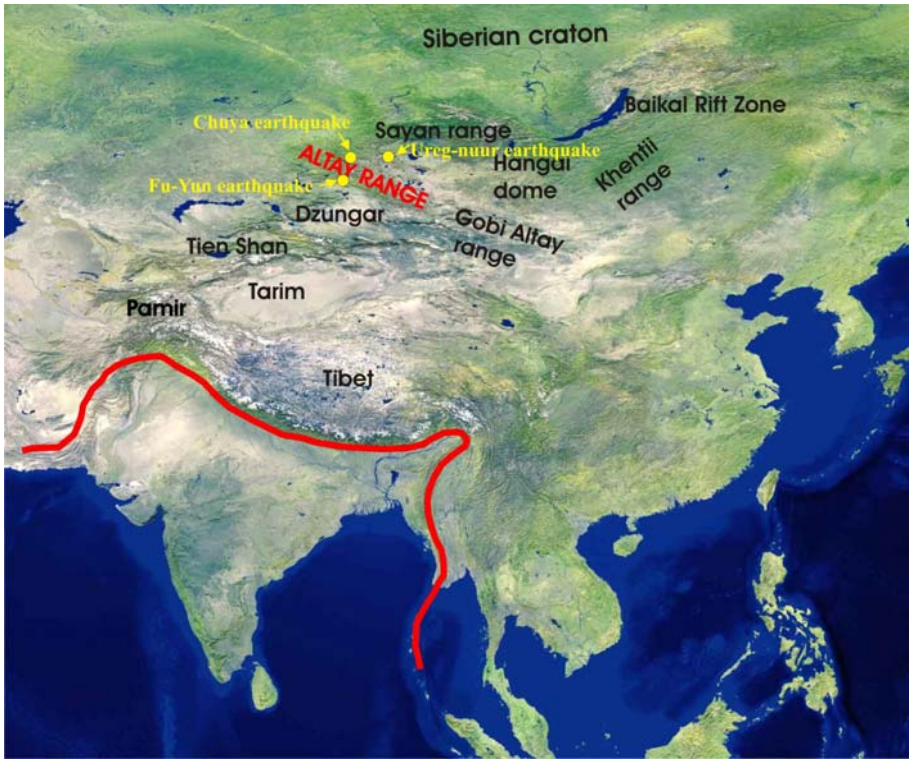

Figure I.1. Location of the Altay Range and the collision front between India and Asia (red line) in a general view of Asia.

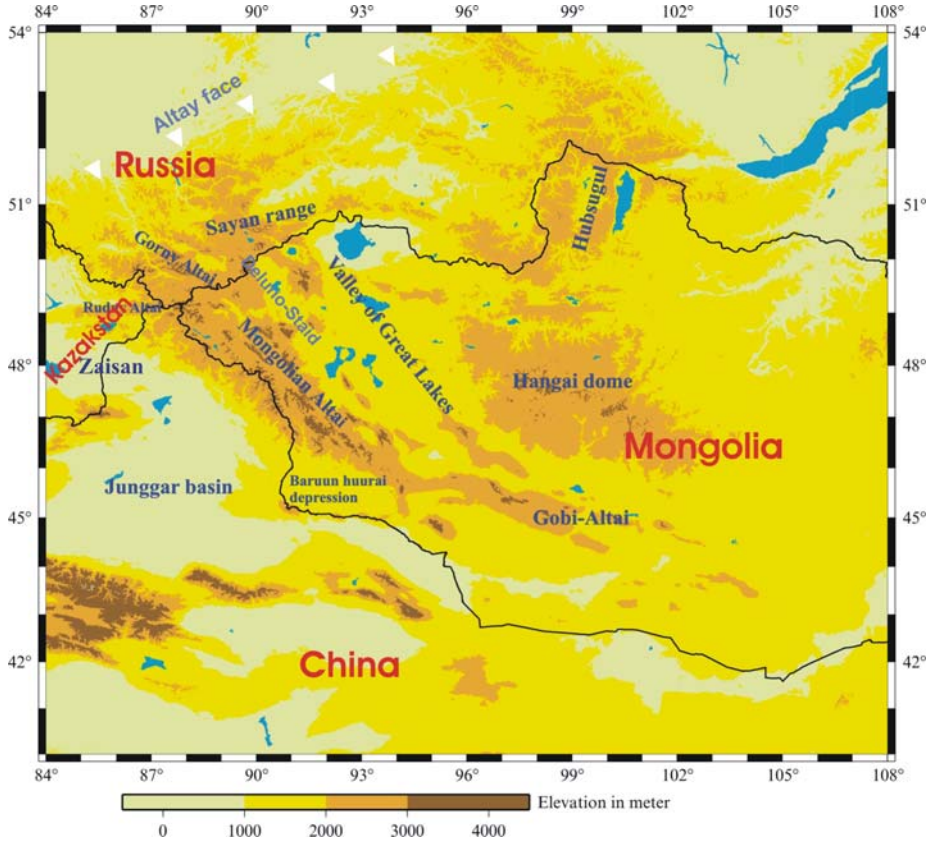

Figure I.2: The various local name of the Altay range related to their hosted country: the Gorny Altay (Russian side) where the Chuya event occurred in September 2003, the Mongolian Altay or Western Altay (Mongolian side), the Rudny Altay (Kazakhstan side) and the Chinese Altay (China part).

Before 1990, most of the information related to the geology and tectonic of Altay range were only in Russian and Mongolian publications (Khilko *et al*., 1977; Khilko *et al*., 1985; Dergunov *et al*., 1972; Devyatkin, 1975; Dobretsov, 1972). Nevertheless, during the last ten years, Altay range and its active deformation were studied by several international teams (Cunningham *et al*., 1996; Cunningham *et al*., 1998; Thomas *et al*., 2002).

As the Altay range intersects four countries (Fig. I.2), most of time studies are covering only parts of the range corresponding to one of these countries and specific terminologies are then used: 1) the Gorny-Altay (Russian side) where the Chuya event occurred in September 2003 is the better described, 2) Mongolian Altay or Western Altay (Mongolian side), 3) the Rudny-Altay (Kazakhstan side) and 4) the Chinese Altay (China part).

I.2. Morphology of the range

The Altay Mountain oriented NW-SE, is a great intercontinental range between the south-western Siberia and to the southern Gobi of Mongolia (Fig. I.2). It is more than 1500 km long if we include the Gobi-Altay range. Its wide is 400 km at the northern part and decrease down to 50 km at the south east termination. The topography (Fig.I.3) consists of a combination of high mountain ranges, up to 4500 m, alternating with inter-mountain compressive basins filled by Mesozoic and Cenozoic detrital sediments.

The range is bounded at the North by the Western Siberian craton (Fig.I.1). The boundary between Altay range and Siberian craton is expressed by reverse faults called “The Altay Face” in most publications (Novikov, 2004) (Fig.I.2). At the northeast, the Altay range is bordered by the Western Sayan range. To the northwest, in Kazakhstan, the Altay range is separated from the Kazakh platform by the Irtysh shear zone (Fig.I.5). Southwest of the Altay range are the Junggar (north western China) and Zaisan (south eastern Kazakhstan) basins (Fig.I.2). The Fu-Yun fault marks a sharp boundary between the Junggar basin and Altay range in China (Tapponnier and Molnar, 1979; Thomas *et al*., 2002). The bottom of the Junggar basin lies at an altitude between 500 and 700 m (Fig.I.4). At the southeast, around 94°E, the NW oriented Altay range is connected to the EW oriented Gobi-Altay range. The two ranges are built along transpressional fault systems with opposite slip directions: right-lateral for the Altay and left lateral for the Gobi-Altay. They present different morphologies: the Altay range is wide and has more continuous mountain topography whereas the Gobi Altay consists of individual narrow linear ranges separated by large intermountain valleys (Cunningham *et al*., 1996).

The Altay range is bounded to the east and northeast sides by the Valley of Great Lakes which separates the Altay range and the Hangai Dome (Fig. I.2). This valley, which follows the eastern Altay front over 600 km, is at an altitude of 740 to 1500 m (from north to south) and is 200 to 250 km wide (Fig.I.2 and I.3). The valley is bounded to the north by Tanun ridge (Fig.I.3) at the foot of which are developed the great lakes Uvs and Hyargas (Fig. I.4). At the SE, the valley turns eastward and follows the north of the Gobi-Altay range until Gobi desert.

The Altay range is characterized by relatively flat-topped summit which corresponds to uplifted erosion surfaces. Maximum elevation reach 4362 m in the Munkh-Hairhan massif at SW, 4355 m in the Taban-Bogd at NW and many other summits are about 3000 to 4000 m high like Harhira (4037 m), Turgen (3965 m), Tsambagarab (4165 m), Sutai (4090 m), Tsast (4193 m), Baatar-Hairhan (3984 m), Jargalant (3797 m) and Munkh-Hairhan (Fig. I.3). Glaciations process has been observed only in the highest part of the mountains, at altitude greater than 3000 m.

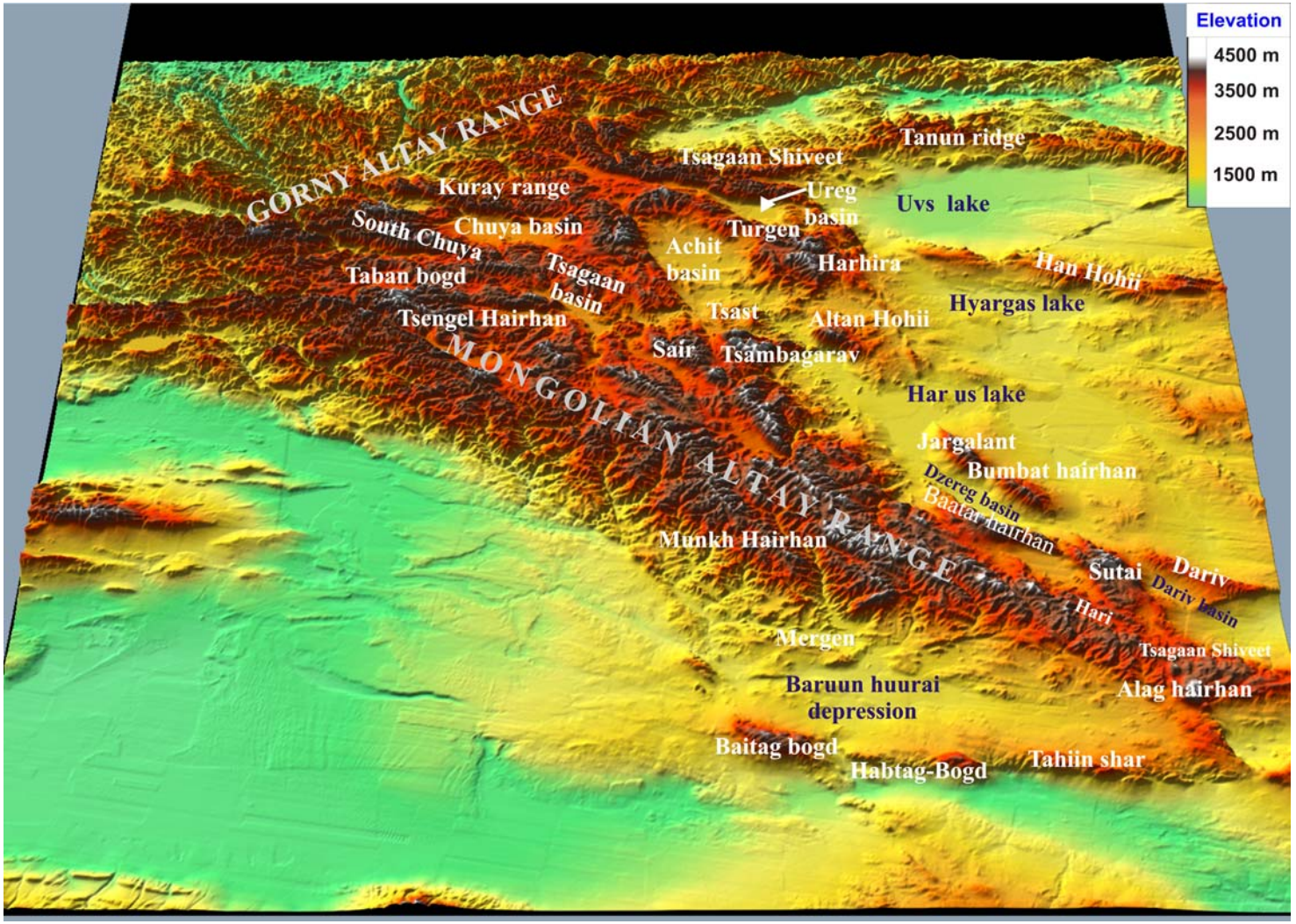

Figure.I.3: Topography and the main geographical names of the relief in the Altay Range.

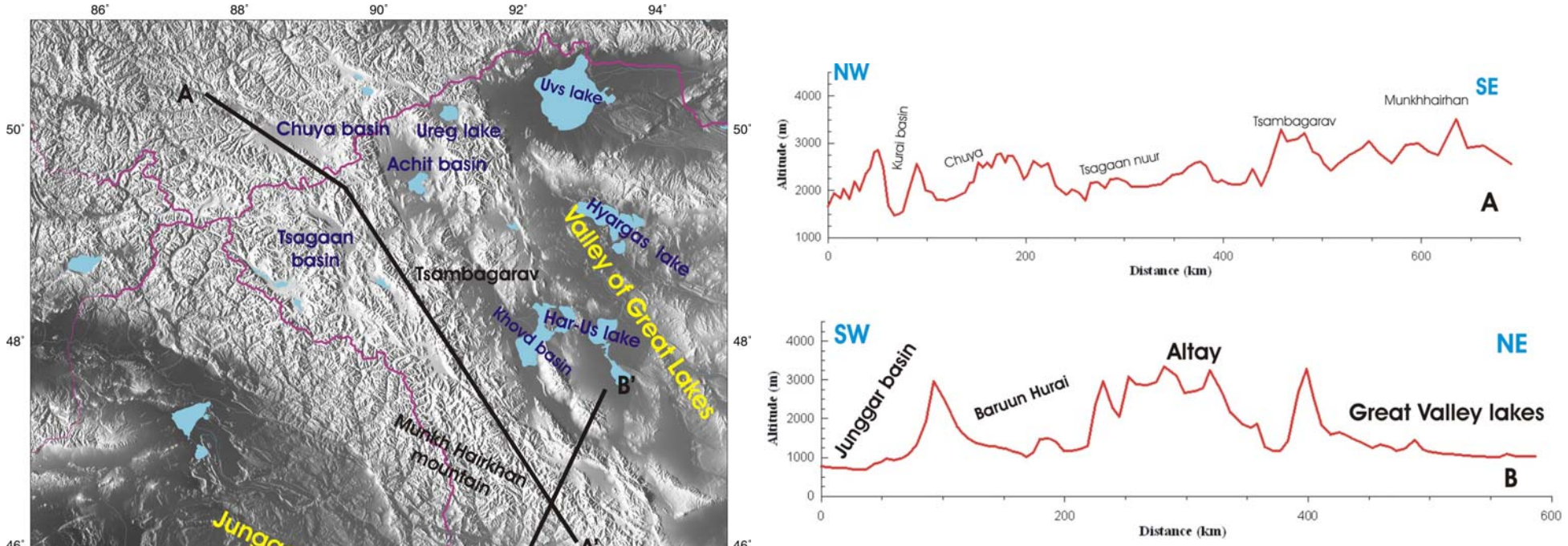

Figure I.4: Topographic cross section of Altay (after SRTM), the map shows the location of A and B cross sections; A: cross section along the axes of the range; B: cross section perpendicular to the range at its southern part.

The largest part of Altay range is situated in Mongolia and called Mongolian Altay, (Fig. I.2). It starts from the highest mountain of the country, Taban-Bogd massif, and extends in southeast direction to the Alag-Hairhan Mountain, over a length of 600 km. Most of the mountain fronts are limited by scarps of active right-lateral strike-slip, thrusts or oblique-slip faults and alluvial fans cut by active structures are widespread (Cunningham *et al.,* 1996). They are clear on satellite images (Fig.I.6).

The Gorny Altay region corresponds to the north western part of Altay range and is situated on the Russian territory. To the north, it is bounded by the Siberian craton and to the east it is topographically connected with the West Sayan Mountain. Gorny Altay is mainly composed by two large ranges striking WNW-ESE: the Kurai range in the north, with a maximum altitude of 3400 and Chuya range in the south with a maximum altitude of 3936 m (Fig. I.3). These ranges are separated by two basins: the Kurai depression, to the NW, at an altitude of 1550 m and the Chuya basin, to the SE, between 1800 - 2100 m. (Delvaux *et al*., 1995) (Fig.I.4)

Important elements of the Mongolian Altay range geomorphology are intermountain valleys which produce complex morphostructures. The largest are Achit and Khovd valleys, several tens of kilometers long and 5 to 20 km wide (Fig. I.4). They are also several smaller valleys as Tsagaangol, Ureg, Tolbo, Uigar and Tsetseg. These valleys are oriented NW along the main direction of the range and their elevations are between 2000 and 2200 m.

At the southern extremity of Mongolian Altay lies the Baruun Huurai basin which is bounded by ridges with elevation between 2300 and 3500 m, as Baitag-Bogd, Habtag-Bogd and Takhiin-Shar (Fig.I.3). The floor of the large Baruun Huurai depression, 300 km long and 100 - 120 km wide, is at 1100 to 1300 m (Fig.I.4).

I.3. Geological and tectonic context of the Altay range

Pre-Cenozoic tectonic structures of Altay range are the result of the Paleozoic accretion-collision of the Paleoasian Ocean (Delvaux *et al*., 1995). The geological history of Altay range can be traced back to the late Precambrian. The main orogenic phases that formed and shaped the geological units of the area are constrained to the Paleozoic and early Mesozoic. During this period, major crustal growth took place in the whole Eurasia. The different phases of crustal accretion and intrusion, separated by primarily strike-slip fault zones, created a complex assemblage of various crustal units (De Grave *et al.*, 2001; Dobretsov *et al.*, 1996).

The **Caledonian** structure of Altay plate is extremely complex, with tectonic slivers of volcano-sedimentary, metamorphic and ophiolitic rocks juxtaposed.

During **Precambrian and early Cambrian,** the region corresponded to an active margin. The oldest rocks in Mongolian Altay consist of Riphean, Vendian-Cambrian volcanic rocks, marine carbonates and clastic sediments. They are generally continental bed reds, volcanic rocks and marine carbonates, tightly folded and metamorphosed sometimes to muscovite schist and augen gneiss grade. They are today mainly in high Altay Mountains, near shear fault zones and on the western or north-western borders of Altay range. For example, these units are along the Bulgan fault zone (South Altay) between Altay from Baruun Huurai depression (Fig.I.5), in Dariv range between Altay range and Valley of Great Lakes (Fig.I.3) and along the west of Tolbo and Khovd faults zone (Fig.1.5). Theses Vendian - Cambrian rocks are not only observable in the Altay but also throughout the Valley of Great Lakes and in the western part of Hangai dome.

During **Ordovician-Silurian**, the Mongolian micro-continent (corresponding at least of today's Altay and Valley of Lake) converged and collided with the Siberian craton, and the

northern part, corresponding approximately to the Gorny Altay and the Cambrian island-arc, were accreted to the West Sayan block (Delvaux *et al.*, 1995). This collision induced the end of island arcs volcanism, the intrusion of collision type granite, the formation of molasses, the accumulation of flays-type sediments in residual troughs and shelf deposits on stable blocks. Ordovician-Silurian greens schist grade meta-sedimentary and meta-volcanic rocks are today at outcrops in the South part of Altay range as west of Sutai, Tsagaan-Shivert and Hari region (Fig.I.3).

The Siberian and "Altay blocks" have been sutured at **Devonian** and a major Caledonian fold belt was developed along the Altay block. The lateral extent of this fold belt shows that it should have been a major sediment source area and continued to rise up during the Devonian, with emplacement of granite plutons (Traynor *et al.*, 1995). A collage of terrain was formed by strike-slip deformation related to collision of the Gondwana during the late Devonian-early Carboniferous.

Devonian-Mid-Permian sequences along the Altay range are interpreted as the record of the continental sedimentation in narrow foreland basins in front of these Caledonian thrust belts, although there is no strong control on it (Traynor *et al.*, 1995). Devonian units are in the Deluno-Staid NS depression (Fig.I.2) which is along the Tolbo and Khovd fault zone and separates Devonian and Cambrian rocks. This depression is filled by Devonian sedimentary-volcanogenic rocks overlapped by sandstones and siltstones. The same feature is also observed locally in Achit basin (fig I.3). The Devonian-Carboniferous sedimentary sandstone, siltstone and locally metamorphosed green siltstone, amphibole-boitite rocks are today widespread throughout the southern slope of Altay range and Baruun Huurai depression. Devonian-Carboniferous rocks, as spilit-diabase, siltstone and andesit, are present in the Baitag, Havtag and Tahiin-Shar mountains (Fig.I.3).

During **Late Carboniferous-Permian**, the collision of the "Kazakhstan plate" and Siberian-Altay continent occurred. The collision episodes and their related strike-slip faults and thrusts broke the accretion-collision margins of both continents into a plethora of tectono-stratigraphic units. Thus, the final stages of the Paleo-Asian Ocean evolution was, during Late Devonian-Early Carboniferous, important left lateral translational between Mongolian Altay terrain and the West Sayan block along the Kurai and Charysh-Terekta fault zones (Delvaux *et al*., 1995) (Fig.I.5).

During the **Mesozoic**, tectonic activity significantly decreased and West-Siberian basin developed at north of Altay range. From **late Triassic-Jurassic**, sedimentary basins started to develop: in early Jurassic developed the West-Siberian basin, north of the Altay region and during middle Jurassic-late Jurassic, several basins in Zaisan zone, Valley of Great Lakes (Fig.I.2). Rare Triassic magmatism, associated with mineralization, is observed in Mongolian Altay range. Around Hangay uplift large fault bounded coal bearing basins of Jurassic-Early Cretaceous time (Delvaux *et al.*, 1995).

Mesozoic clastic sequences are present at the both boundaries of Han-Hohii mountain (Fig.I.3) and continue to WNW, along the seismically active Shapshal fault that undergoes mainly thrust, reverse, dextral oblique slip and underlining the southern bound of Tsagaan-Shiveet mountain (Delvaux *et al.*, 1995) (Fig.I.3). Relatively large Mesozoic structures are in basins between the Valley of Great Lakes and the eastern margin of the Altay such as Dzereg and Dariv basins (Fig.I.3), south east of Har-Us lake. Such structures are also observable in valleys east of Jargalant-Hairhan (Fig. I.3). However, thin sequences of **Jurassic and Cretaceous** clastic sediments occur locally in western Mongolia. They are interpreted to be intra-continental rift deposits related to a regional extension event that had its greatest manifestation in southern and eastern Mongolia but probably affected western Mongolia as well (Cunningham *et al.,* 1996).

The neotectonic structure of Altay range is characterized by a system of NW-SE trending ridges separated by intra-mountain depressions lying at altitudes ranging from 1000 to 2000 meters. This general structure is partly controlled by **Cenozoic** activation or reactivation of major fault zones. Cenozoic uplift has led to the development of thick Neogene and Quaternary alluvial deposits along the outside depressions of Altay range and within some intermountain depressions. These alluvial sediments were deposed in the large depressions of Valley of Great Lake, Junggar and Baruun Huurai. Oldest Miocene sediments are present in the northern part of Uvs and also Hyargas, Har-Us basins. Eocene and Oligocene clays and sandy clays are present locally in the Valley of Great Lakes and South part of Baruun Huurai depressions.

After the initiation of India-Asian collision in the Eocene, large scale mountain building started at the late Oligocene in Tien Shan (Dobretsov *et al*., 1996; Molnar and Tapponnier, 1975; Dehandschutter *et al*., 2002) and more recently, since Pliocene, in Altay range (Dobretsov *et al*., 1996, Dehandschutter *et al.*, 2002). Recent features of the Altay range is dominated by high uplifted region bounded by active right-lateral strike-slip and trust faults that could define asymmetric flower structures (Cunningham *et al.,* 1996).

I.4 Active structures and large earthquakes in Altay

The range is structurally dominated by right-lateral strike-slip faults oriented NW-SE, a transpressive reactivation of Paleozoic shears zones, and by thrust faults oriented EW (Fig. I.5). Inside the range, several intramountain sedimentary depressions are developed mostly along strike-slip or full ramp basins (Delvaux *et al*., 1995; Schlupp, 1996; Dehandschutter *at al*., 2002). The Cenozoic active faults are in good agreement with the main orientation of older basement blocks (Cunningham, 1998).

On the Landsat images of Altay range we can detect many active fault scarps highlighted by triangular facets along scarps and deviations of active alluvial fan deposits or of drainage indicating the recent slip along the faults. All these observations show that Altay range is a tectonically active intra-continental mountain range.

The tectonic activity of the Altay range is illustrated by the high seismic activity with two large earthquakes (Fun-Yun, 1931 $M = 8.1$; Ureg-Nuur 1970, $M = 7.0$) and several moderate earthquakes with magnitude more than $M \geq 5$ during the XX century. These large known events activated only a small part of all the Altay active structures. A challenge is to extend our knowledge to the past to determine historical events. This would bring to us important complementary information to understand the deformation along all these large faults. A detailed study of the seismic activity of Altay will be the topic of chapter II.

Fig.I.5 shows the active faults of Altay obtained from my interpretation of SPOT and Landsat-7 + ETM images (30 meters ground resolution). These data allows us to see in details the main right-lateral strike-slip faults of the range (Khovd, Tolbo, Sagsai) and the left-lateral strike-slip faults associated with reverse slip along structures at the south of the Altay range (Bulgan, Sharga) which are the main features of the active deformation in the Altay. Many late Quaternary surface ruptures, or paleodislocations, are known. They were produced by large earthquakes along Chihtei, Sagsai, Ar-Hotol, Bulgan or Bidj segments. I will discuss in details the available information of these segments and will add new data and interpretation. I have done specific interpretation of satellite images in the way to estimate the main deformation characteristics along these faults as cumulative displacement and average rate of deformation. In the following, the active zones are described from east to west and from north to south. The Fig.I.6 shows locations of these active zones.

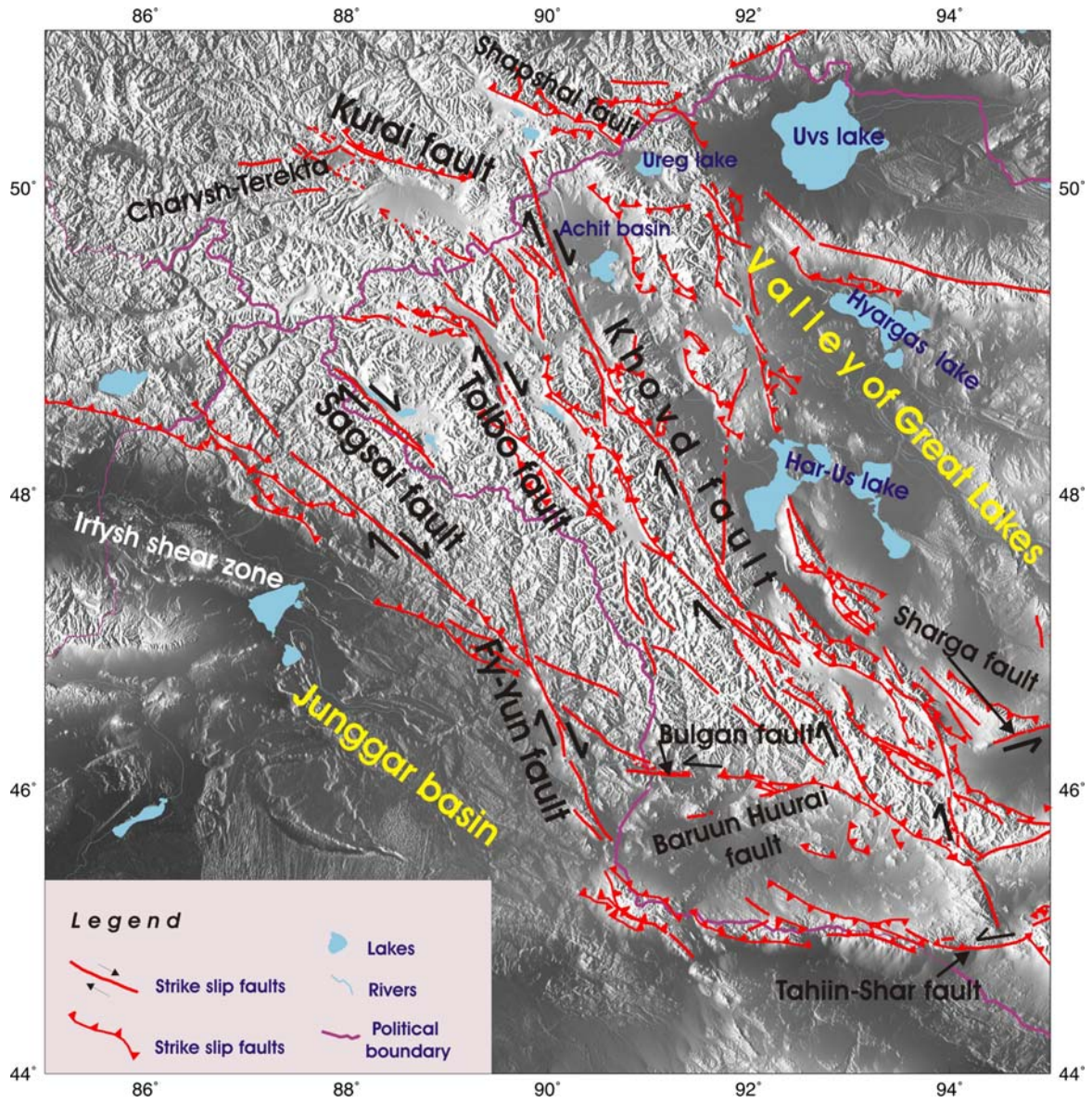

Figure I.5: Main active structures of Altay, interpreted using SPOT and Landsat satellite images, overlapped on GTOPO30 topography.

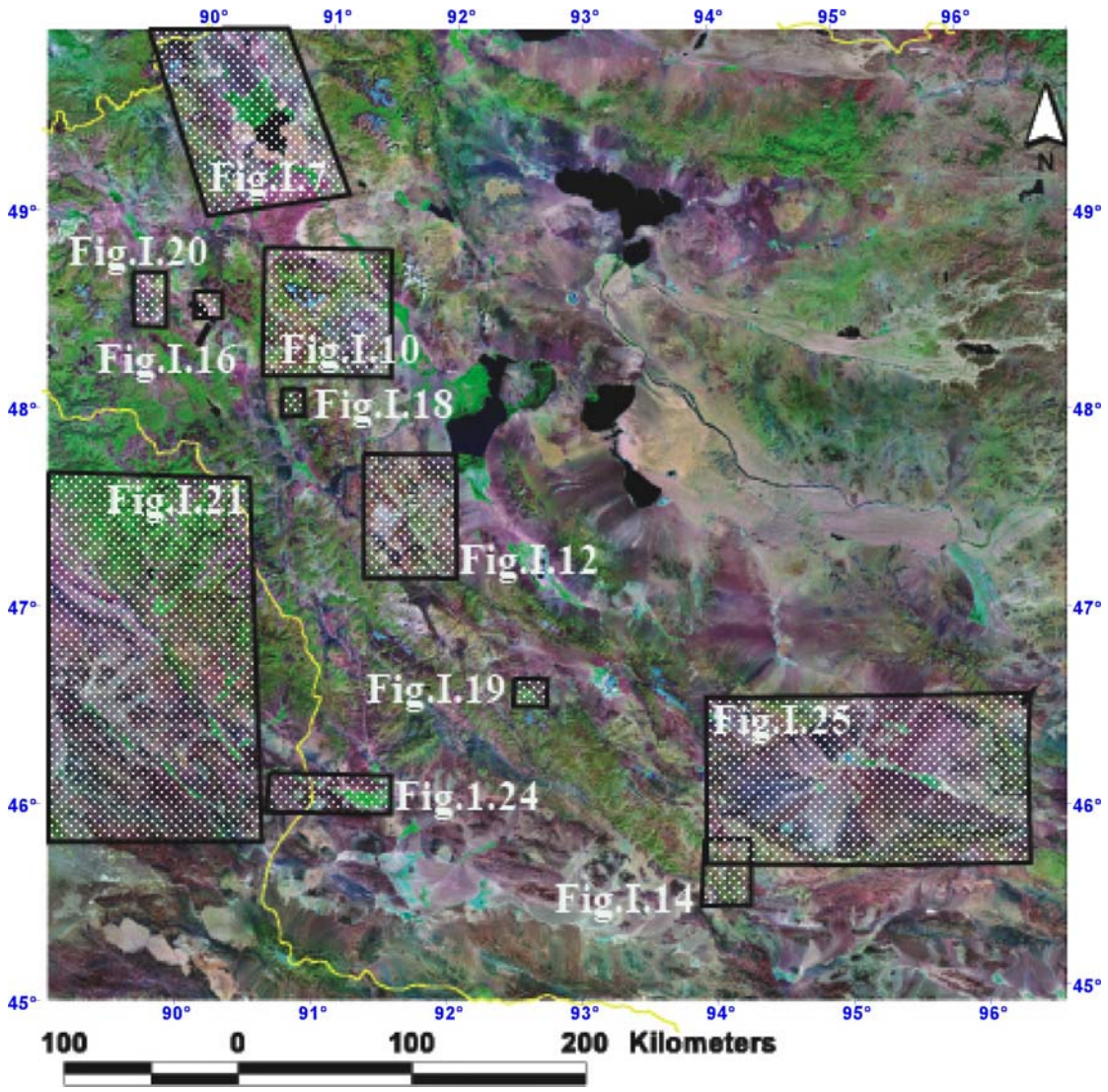

Figure I.6: Landsat-7 + ETM images of the Altay region. The boxes show location of the active zones described in the text. The figure numbers corresponds to each following zoomed maps.

I.4.1 The Khovd fault zone

At the east boundary of the Altay range lays the Khovd fault (Fig.I.5 and I.6). It consists of a right-lateral strike-slip fault with reverse component. The Khovd fault extends several hundred kilometers from about 46°N until the Achit basin, near 50°N. The fault patterns in this zone are complicated by many roughly parallel NNW faults. Khilko *et al.*, (1985) reported two recent surface ruptures along the Khovd fault. The first, at the north near 49.2°N, 90.3°E, is the Chihtei segment (Baljinnyam *et al.*, 1993). The second, at the south, longer and associated with a more recent paleodislocation, is Ar-Hotol. We will describe in detail these structures with the help of Landsat-7 and ETM images (30 meters ground resolution), from North to South.

I.4.1.1 The Chihtei paleodislocation

The Chihtei segment is located at the northern end of Khovd fault and is running along the western margin of Achit basin and at the east border of the Tsahar Mountain (Fig. I.7). To the south, the Chihtei fault scarp ends and disappears, due to the river erosion, when it crosses the Khovd River. It corresponds to a 27 km long rupture. The fault scarp strikes N-S and shows a right-lateral oblique strike-slip with reverse component. The scarp is west-facing and varies in height from 0.5 m to 1.5 or 2.0 m along the central 10 km of the segment (Khilko *et al.*, 1985, Baljinnyam *et al.*, 1993). It decreases further north, where tension crack and mole tracks are the dominant surface manifestations of the rupture. Along much of the rupture, en echelon tension cracks, with azimuth of 10° to 30°, mark the surface trace and attest to a significant component of right-lateral slip (Baljinnyam *et al.* 1993). Near its southern end, along 4-5 km, the fault present also mole tracks of compression and tension zones (Khilko *et al.*, 1977) (Fig.I.7).

On the images, we observe along the Chihtei fault clear straight linear surface ruptures, around 30 km long and oriented NNE (Fig. I.7). They affect Quaternary deposits, when crossing alluvial fans of rivers flowing from Har mountains, at the north of "Chihtei bulag" spring, and the "Helentseg" river alluvial deposits at the south of the spring (Fig. I.8). It demonstrates that the Chihtei surface rupture was activated during the Quaternary. Using the morphology of the features observed along the fault trace, and comparing them with other ruptures in the Mongolian Altay, it has been assigned an age of 1000 to 1500 years for the last Chihtei surface rupture (Khilko *et al.*, 1985).

Along the surface ruptures, no clear offsets have been observed even when the fault crosses alluvial fans or river valleys, except at its northern part. There, the Chihtei surface rupture crosses several old river valleys and we can observe right-lateral displacement but its value is still hard to estimate (Fig.I.9).

The Chihtei fault scarp morphology is smoother than the other segments along the Khovd fault system (Khilko *et al.*, 1985). Either the Chihtei segment is less active than the other segments of Khovd fault systems, but we have no reason to think that because it is a part of a long continuous active structure; or the last break of this segment was older than those on the others segments. Thus, it could be the next segment which will break along the Khovd fault system.

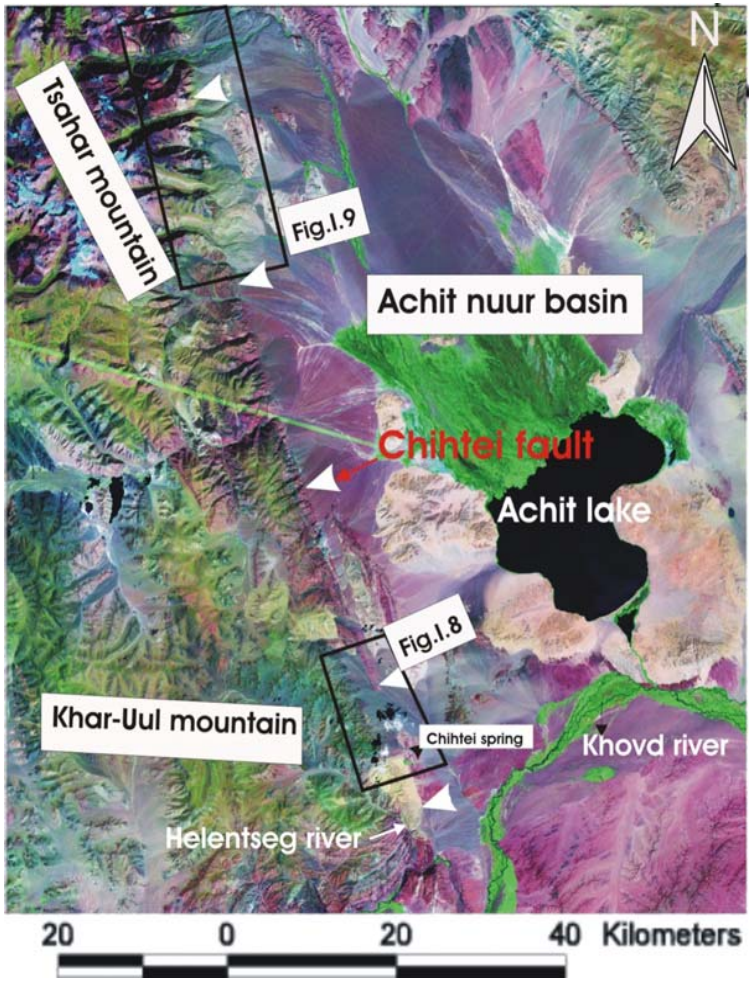

Figure I.7: Landsat ETM+ images of the Chihtei segment (see Fig. I.6 for location) located at the northern end of Khovd fault. White arrows underlined clear traces of the surface rupture on the image; boxes show extends of Fig.I.8 and I.9.

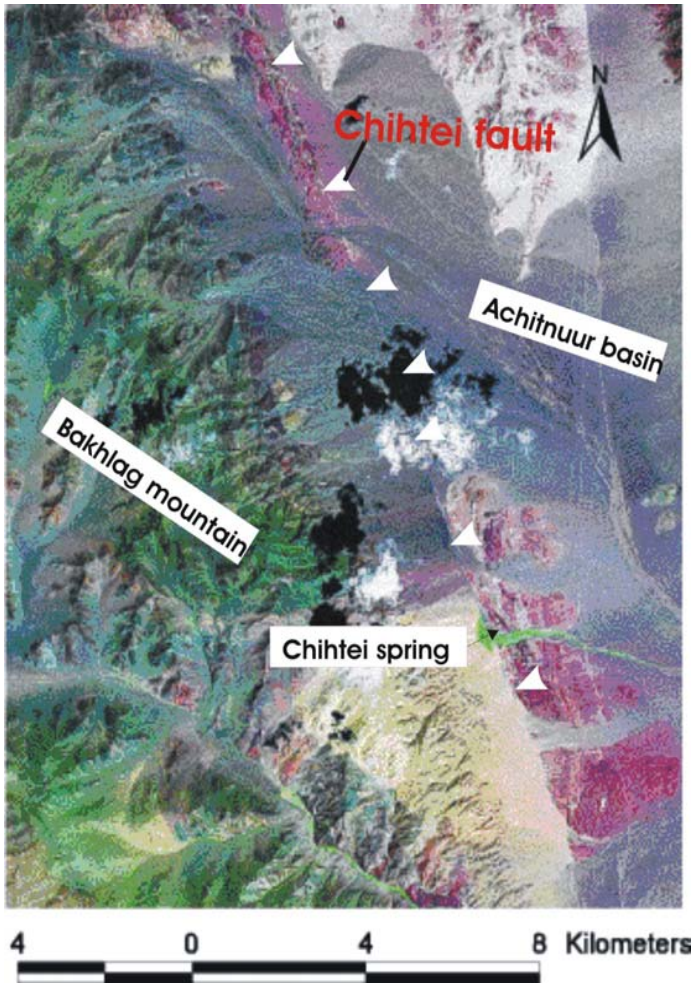

Figure I.8: The Chihtei segment affects quaternary deposits (Landsat images). See Figure I.7 for location.

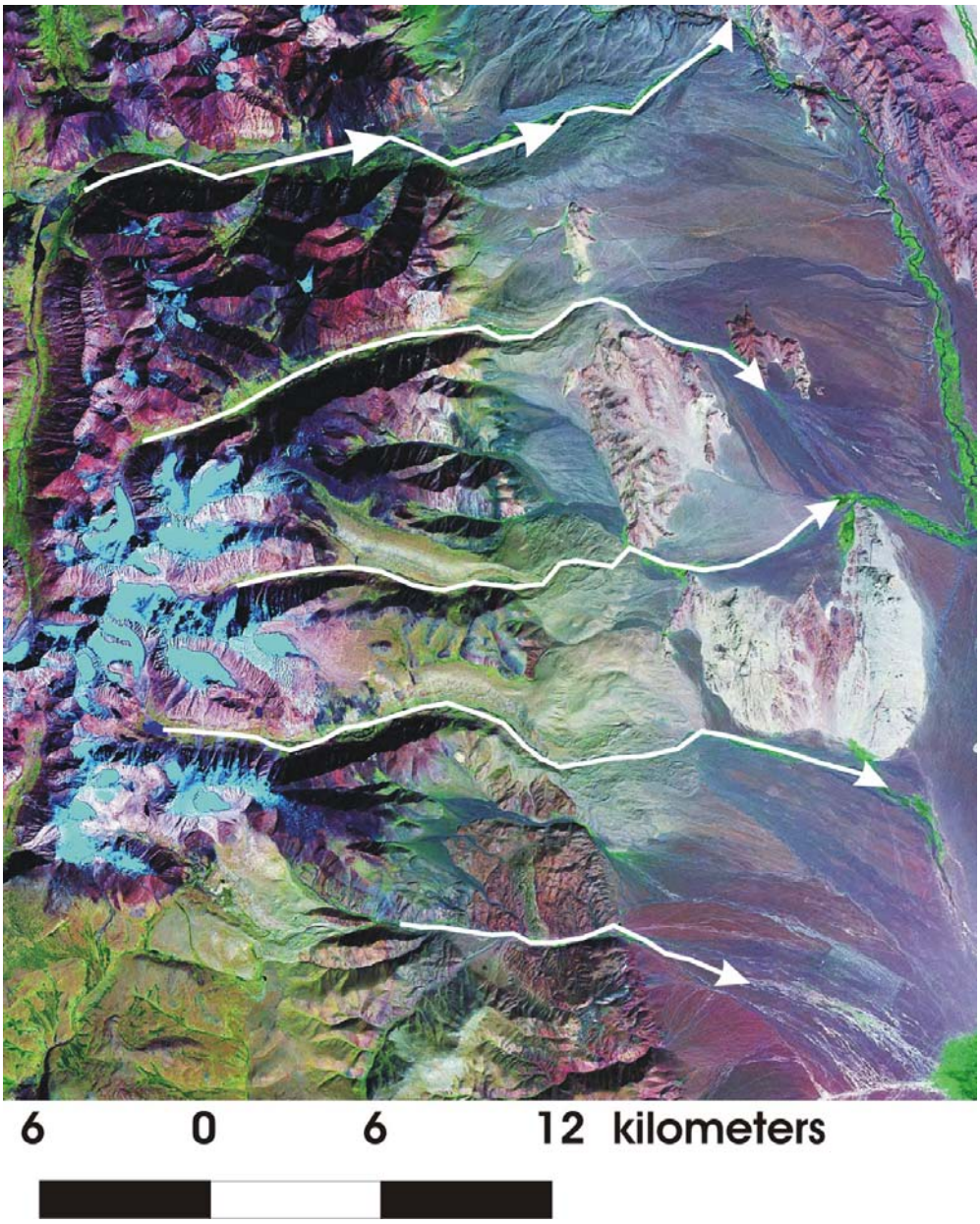

Figure I.9: The right-lateral displacement of rivers due to the Chihtei segment observed on Landsat images. See Figure I.7 for location.

I.4.1.2 The Tsambagarav reverse segment

This fault scarp (Fig. I.10) runs between Tsahar and Yamat Mountains and cuts Neogene's deposits of Khovd River. To the south, the Khovd fault follows the western slope of Tsambagarav massif where the movement becomes reverse. Fault segments with strike-slip faulting are observed on the western side of Tsambagarav reverse fault may be in relation with the Tolbo active fault zone.

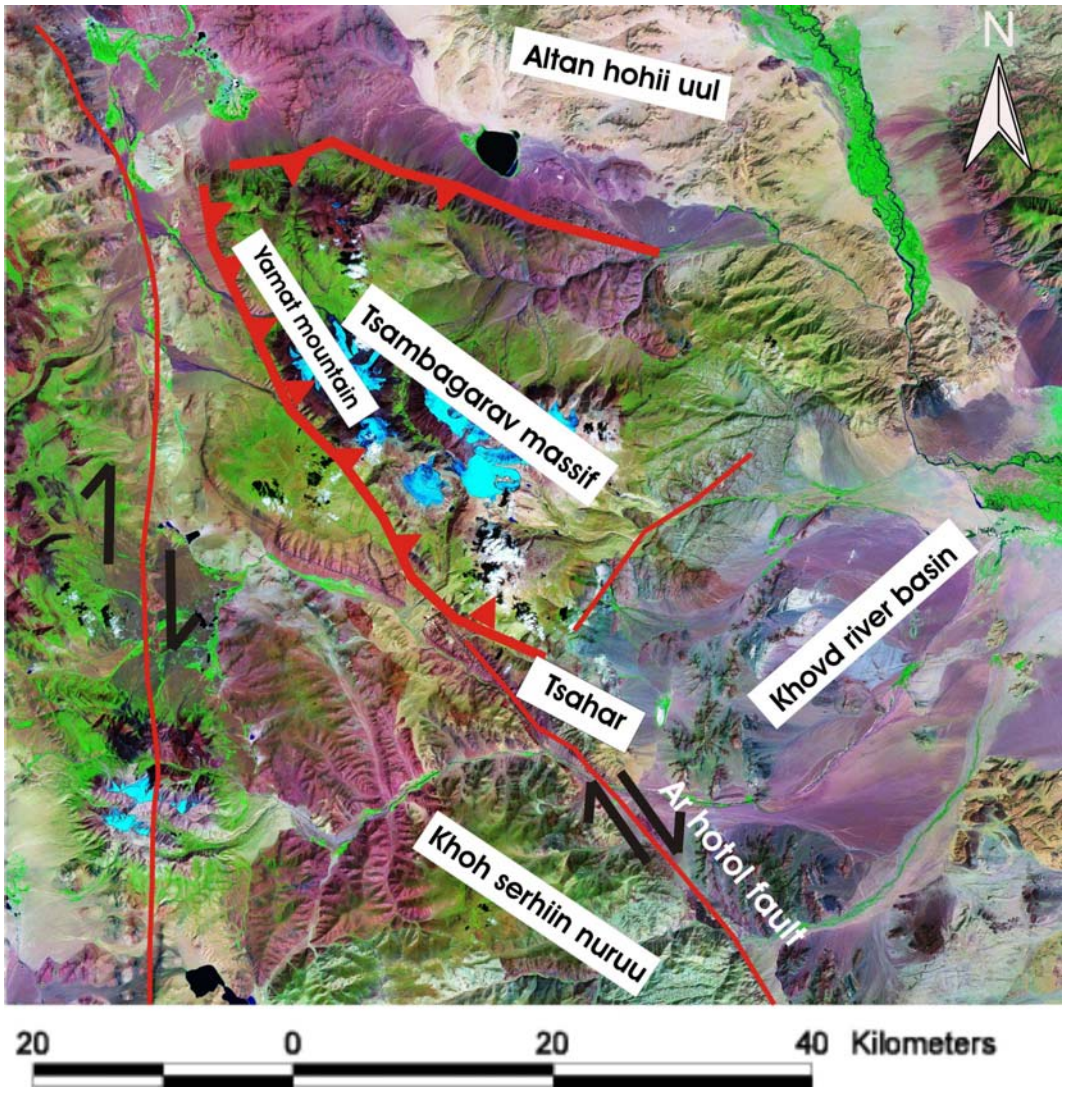

Figure I.10: Ar-Hotol Fault and the Tsambagarav reverse fault observed on Landsat images (see Fig. I.6 for location).

I.4.1.3 The Ar-Hotol paleodislocation

South of Tsambagarav reverse segment starts the Ar-Hotol segment (Fig. I.10). The Ar-Hotol surface rupture is prominent, continuous along more than 215 km (Khilko *et al.*, 1985; Baljinnyam *et al.*, 1993) and can be traced on Landsat images (Fig.I.11). The fault, oriented about N130-150°, starts from river Shurga in the North and continue to the south up to river Bodonch (Khilko *et al.*, 1977) (Fig.I.11). The southern end of the rupture is characterized by several ruptures, roughly 60 km in total.

The northern part of the fault, with an orientation of N130°, extends along the east border of Erdeneburen Mountain and is sharply expressed on the Landsat images. After it crosses the river Dund and continues along the east slope of Tsagduul Mountain.

Most of the clear surface deformations on the field are en echelon extensional open cracks and compressional mole tracks. These features are wider in flat zones with thick sediments as

between Shibert River and Ar-Hotol pass and near Dabst Lake. Numerous left stepping tension cracks, oriented N170° ± 20°, show right-lateral strike-slip on Ar-Hotol structure (oriented N130°). Their sizes are about 40-50 m long, 8-10 m wide and 2.5-3 m deep. Associated to the open cracks, we observe small thrusts or compression ridges with a size of 15-20 m long, 2-3 m high and oriented N100-120°.

Near Dund River, 1 m of vertical offset and 5 m of right-lateral strike-slip has been measured on the field (Khilko *et al*., 1977). The most impressive horizontal displacements are between river Buyant and Dund-Tsenher, where there are several evidences of 4 to 5 m of right-lateral offsets on shallow or dry streambeds. Field observations along river valleys (or along the network of stream channels) show that the last rupture of this structure was associated to 4-5 m right-lateral strike-slip displacements. Even this displacement could reach locally 7 m (Khilko *et al.*, 1977; Khilko *et al.*, 1985) with a maximum of 7.5 m ± 3 m, at roughly 6 km south of Ar-Hotol pass, as reported by Baljinnyam *et al.* (1993). Clear horizontal offsets were observed mostly in the area of Ar-Hotol pass (Ar-Hotol dava), Dabst Lake and Shibert, Tsenher Urt Rivers (Fig.I.11).

One other important information was that the Ar-Hotol surface ruptures cuts two historical graves, called in Mongolia 'heregsuur'. The right-lateral offset measured is 2-2.5 m (Khilko *et al.*, 1985, Baljinnyam *et al.*, 1993). From archeological information, these graves can belong to XIII - XVI centuries (Khilko *et al.*, 1985). So apparently, the corresponding earthquake occurred recently, during the last 400-700 years. Khilko *et al.* (1985) pointed out that a major earthquake was felt over a large part of western Mongolia and southern Siberia on 1761 December 09, with intensities comparable to those associated with the great earthquakes of Bulnay (1905), Fun-Yun (1931) and Gobi-Altay (1957). Consequently, they assigned the Ar-Hotol rupture to that earthquake (Khilko *et al.*, 1985). Baljinnyam (Baljinnyam *et al.*, 1993) also discussed the age of the Ar-Hotol rupture and agreed with Khilko. In the RCAG seismic database, the Ar-Hotol is then assigned to an earthquake in 1761, characterized from macro seismic data. The scale of deformation and the morphology of the surface ruptures are comparable with those associated with the great Bulnay earthquake of 23 July 1905 (Mw = 8.3 to 8.5, Schlupp 1996). Thus, the Ar-Hotol segment broke probably in the past during a single large earthquake. The magnitude has been estimated as about M = 8.0 from the character of the paleodislocation and the measurement of the offsets (Khilko *et al*., 1985).

Relationship between active faulting and the offset of streams is often used to identify active faults (Allen, 1975). As the fault is perpendicular to the general direction of the rivers and as the cumulative offset is similar for each of them, we can consider that they are featuring induced by the movements on the fault. After the reconstruction of these river streams, we can define average displacement along the rupture.

In our case, the local drainage flows, from west to east, from Khoh-Serkh High Mountain to the Har-us Lake Basin, through the Ar-Hotol fault. Along the Ar-Hotol structure, we can clearly see on satellite images large right-lateral offsets, as on the rivers Shibert and Tsagaan-Burgast (Fig. I.12). Using Landsat and ETM images with ground resolution 30 m, we can measure the Ar-Hotol cumulative displacement along at least five sites, i.e. from North to South, on rivers Shibert, Tsagaan-Burgast, Khoit-Tsenkher, Tugreg and Huurai (Fig.I.12).

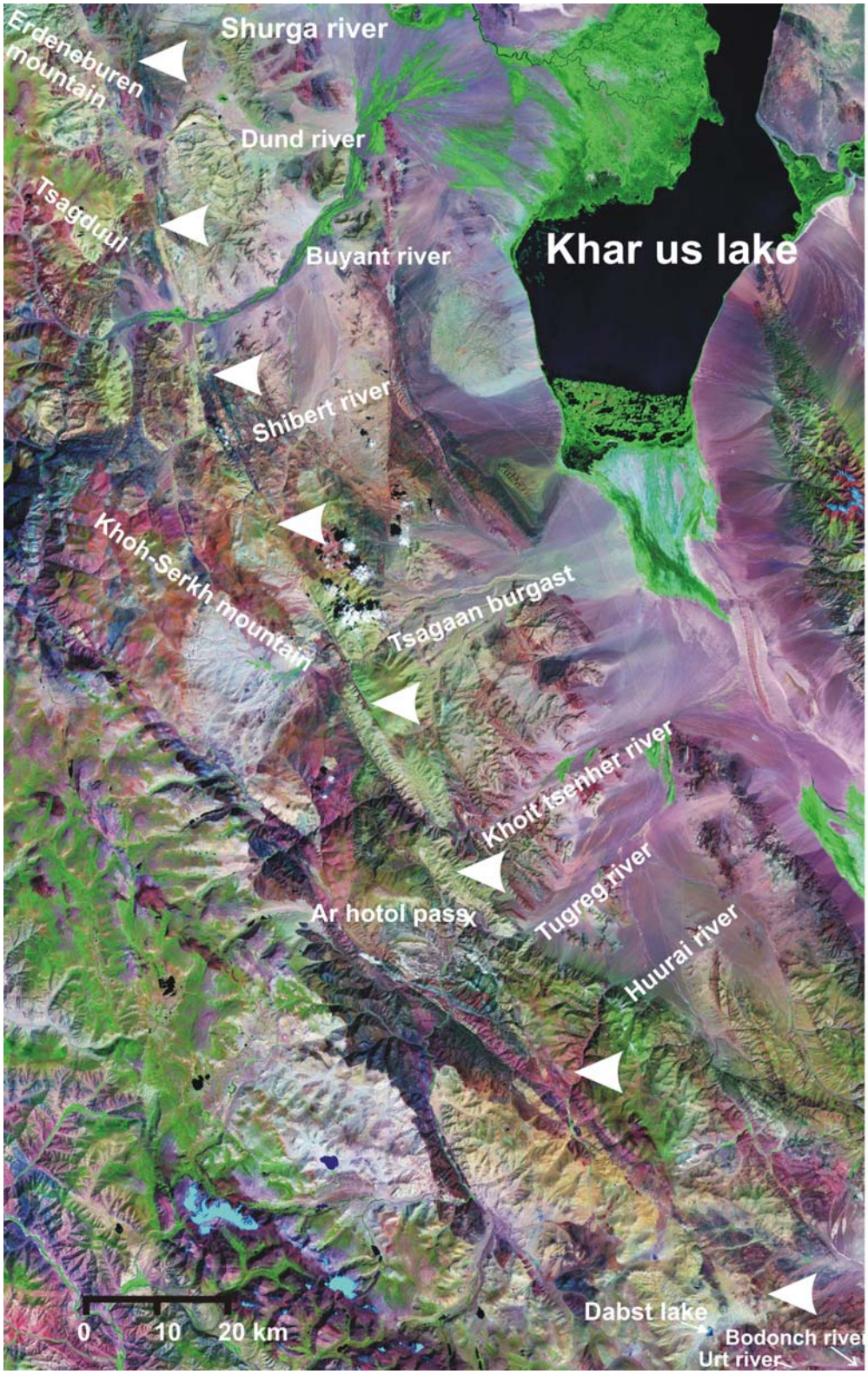

Figure I.11. Landsat + ETM image of the Ar-Hotol fault. The fault scarps are clearly observed along the trace. Several river offsets are also observed along this fault segment.

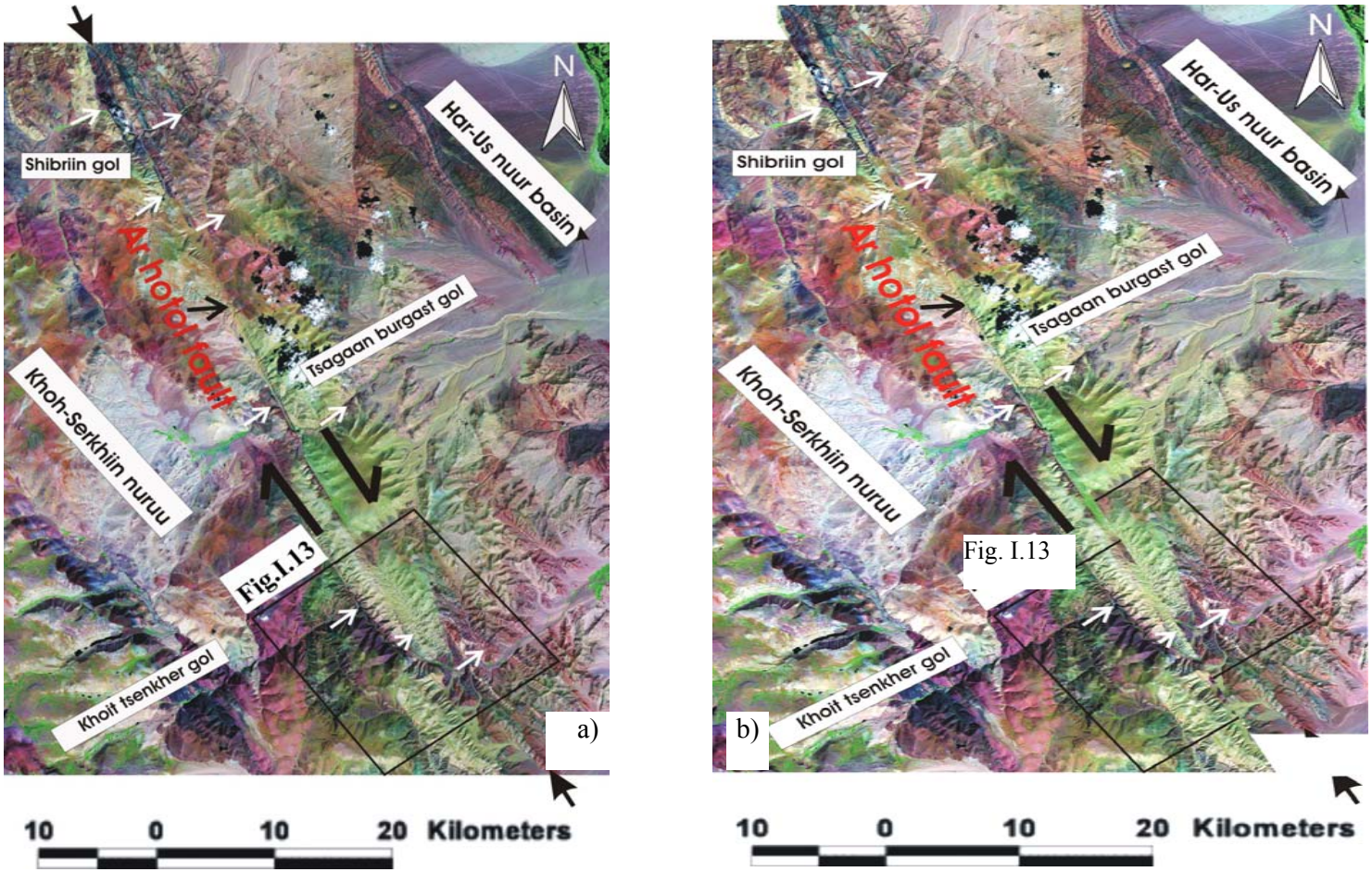

Figure I.12 (a) Large right-lateral river offsets along the Ar-Hotol structure (between white arrows) clearly observable on Landsat satellite images, as on the rivers Shibert and Tsagaan-Burgast. (see Fig.I.6 for location); (b) Reconstruction of linear river streams are giving constant displacements.

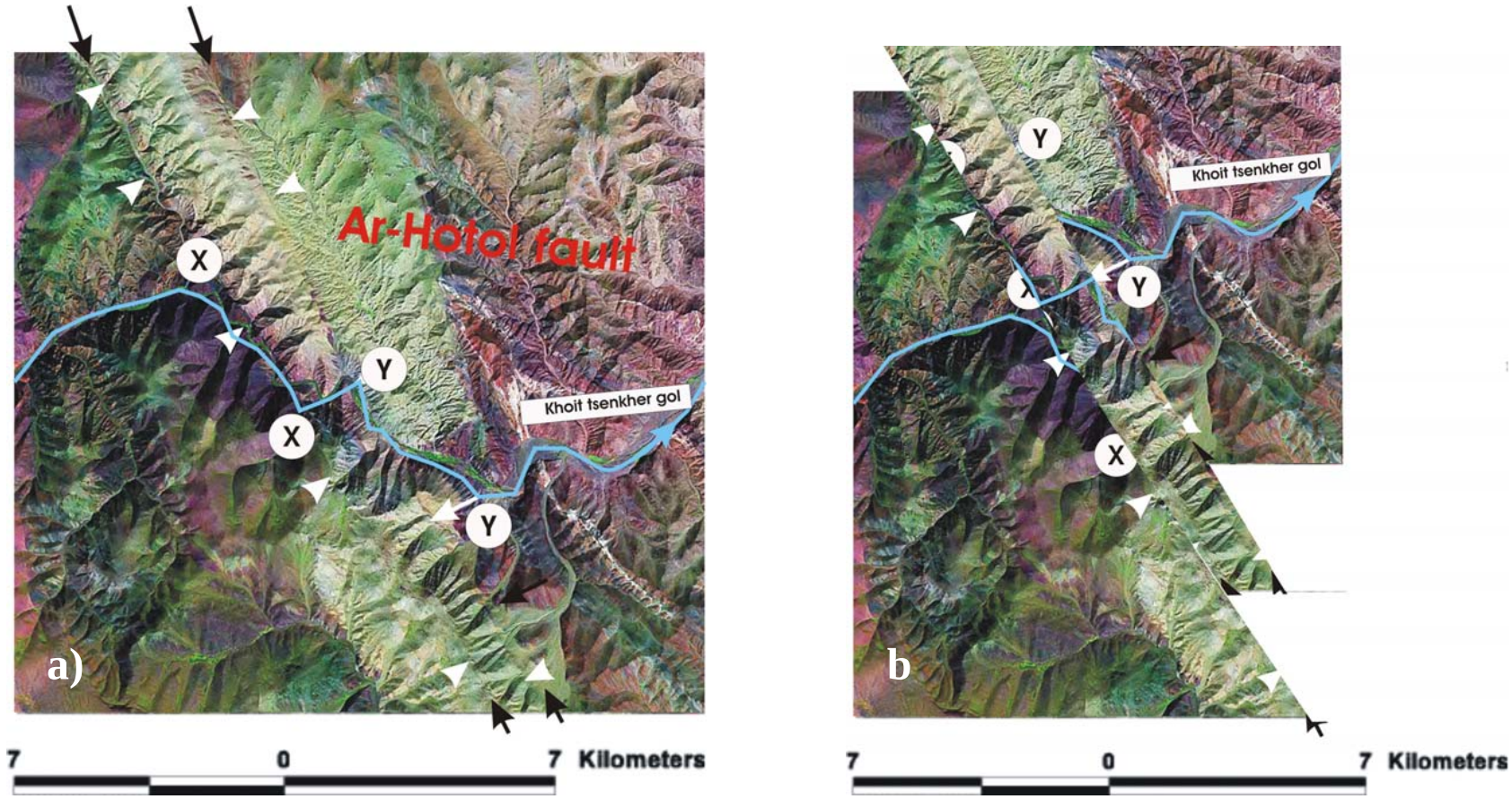

Figure I.13: (a) Ar-Hotol Fault (white arrows) in two segments (black arrows) which displaces the Khoit-Tsenkher River of several kilometers (XX and YY). Background with Landsat images (See Fig.I.12 for location). (b) Reconstruction of river streams are giving the same value along the both faults.

We have measured 3.8 km offset on the Shibert River, 4.0 km on Tsagaan-Burgast River, 4.4 km and 4.8 km for the two ruptures cutting the Khoit-Tsenkher River, 3.6 km on Tugreg River and 4.7 km on Huurai River (Fig.I.12 and I.13). Average offset is about 4 km and the largest offset is observed on Khoit-Tsenkher River, with about 4.6 km offset along each of the two parallel segments (Fig. I.13b).

Several authors (Trifonov, 1983; Khilko *et al*., 1985) noted that the total cumulated stream offsets along the Khovd fault is between 3.5 km to 6 km, but that larger offsets cannot easily be disproved. Their observations are similar to ours except for the 6 km offsets. Our observation shows that the total Khoit-Tsenkher River offset is due to two different segments clearly observed on Landsat + ETM image (Fig.I.13a and I.13b).

Finally, I propose that the total cumulative offset of river streams along the Ar-Hotol fault is between 3.6 km and 4.8 km. We can consider that the rivers were trapping in the mountain since the beginning of the uplift. If the Ar-Hotol fault activity started at the same time and, considering an averaged horizontal displacement of 1 to 5 mm/years, it suggests that the deformation of the Ar-Hotol fault started 1 to 4 My ago. These values are still hypothetical but consistent with the observation along the Gobi-Altay fault (Ritz et al. 1995, and Ritz et al., 2003) and the GPS measurements in Altay (Calais et al., 2003).

I.4.1.4 The Bidj structure

The Bidj paleodislocation is located at the southeastern end of the Altay range, between 45°53' N and 45°35'N, and belongs to the transpressional zone making the junction between the western Altay and the Gobi Altay (Fig.I.14).

The morphology of the region is characterized by series of high mountains: Alag-Hairhan with elevation 3738 m, Bus-Hairhan 3393 m, Nariin-Bus 3042 m. and intramountain basins like Hag and Bidj River (Fig.I.14). The basement of mountains Bus-Hairhan, Nariin-Bus and Alag-Hairhan consist of Paleozoic metamorphic sedimentary rocks, volcanic and late Paleozoic intrusive rocks. The Neogene clastic sedimentary deposits are between these two mountains.

On the Landsat + ETM image, we see clearly the ruptures oriented NS and continuous along most of its 40 km. The paleodislocation follows the west slope of the mountain Nariin-Bus, then the east border of the Bus-Hairhan with a slightly change in orientation where it cuts the alluvial deposits of the Hag basin and finish near the Alag-Hairhan. It is associated to right-lateral strike-slip with reverse component.

I could measure clear horizontal displacements on the river along the slope of Bus-Hairhan Mountain on the field and images but they show apparent left lateral offsets (Fig. I.15). Khilko *et al.* (1977) considered that Bus-Hairhan mountain is moving to the south to explain this apparent left lateral movement. The kinematics associated to such an interpretation is not explained by the authors. Indeed, we observe that the topography of the Hag basin shows lower altitude at the north than at the south, so the rivers are still "attracted" to the north by the slope of the basin despite they are right-laterally displaced. It is a clear example of an apparent offset of rivers opposite to the offset of the fault due to local topography and this show that we have to be very careful when interpreting offsets only using remote data as satellite images.

To the south, the rupture runs through the drainage divide of the Bidj basin, located between Bus-Hairhan and Alag-Hairhan mountains. There, the fault scarps present again clear right-lateral strike-slip with reverse component. From this watershed, footwall of fault changes to the east side. Several tension cracks oriented N40° are observed. They are elongated along the main direction of rupture and show right-lateral strike-slip displacements (Khilko *et al*., 1977). At some place, the measured displacement due to the last event reaches 2 m (Khilko *et al*., 1977 and Baljinnyam *et al.,* 1993, personal measurements).

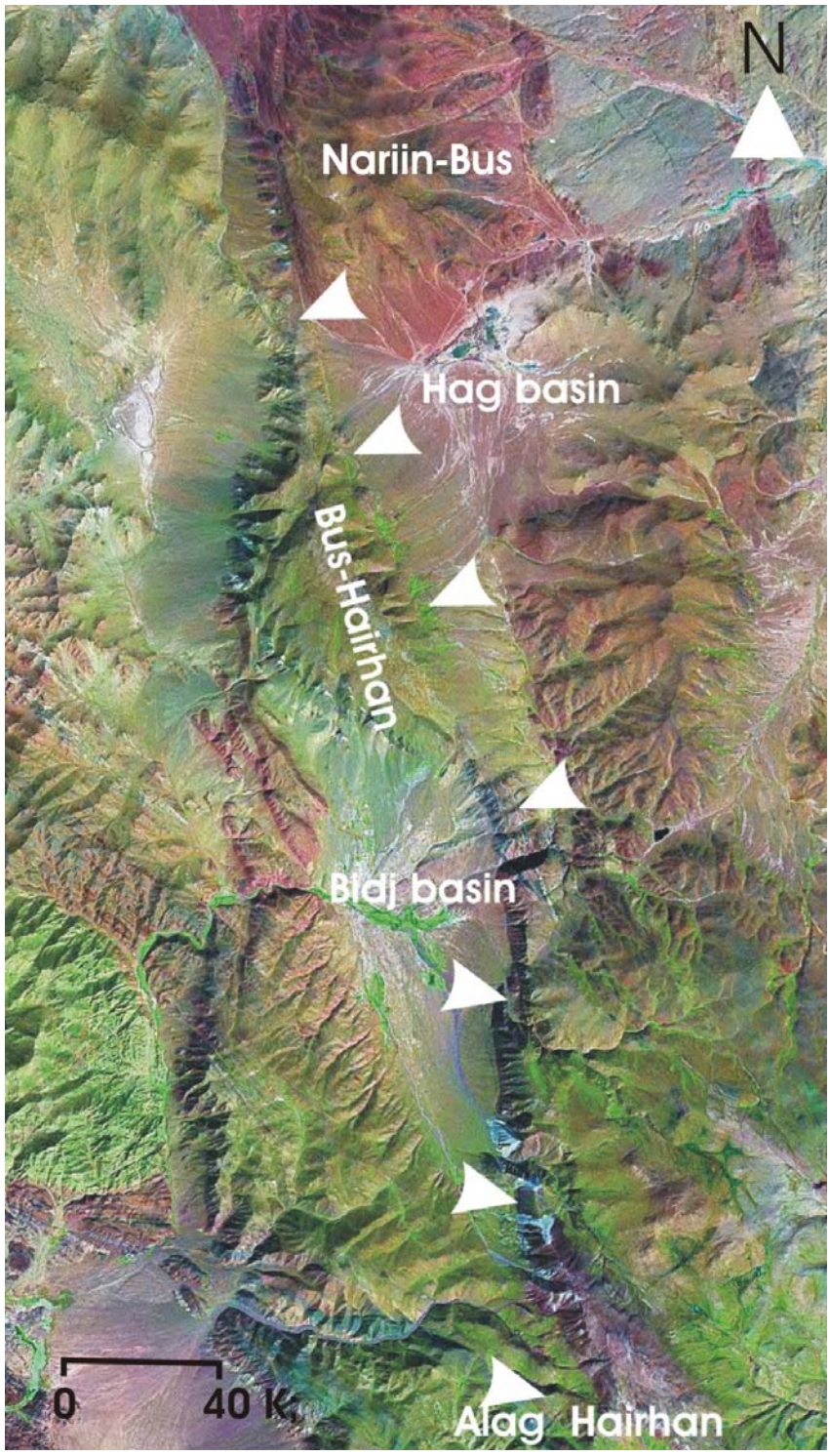

Figure I.14: The Bidj paleodislocation (white arrows), located between 45°53'N and 45°35'N at the southeastern end of the Altay range, observed on Landsat images (see Fig.I.6 for location).

Further to the south, the ruptures appear along the west abrupt slope of Alag-Hairhan Mountain and cut the basement rocks (Fig.I.14). At this place, rupture represents a clear linear scarp 1 m high (Khilko *et al.*, 1977). The deformation of Bidj paleodislocation, right-lateral with

reverse component, is consistent with a general orientation of the main horizontal stress oriented SW-NE.

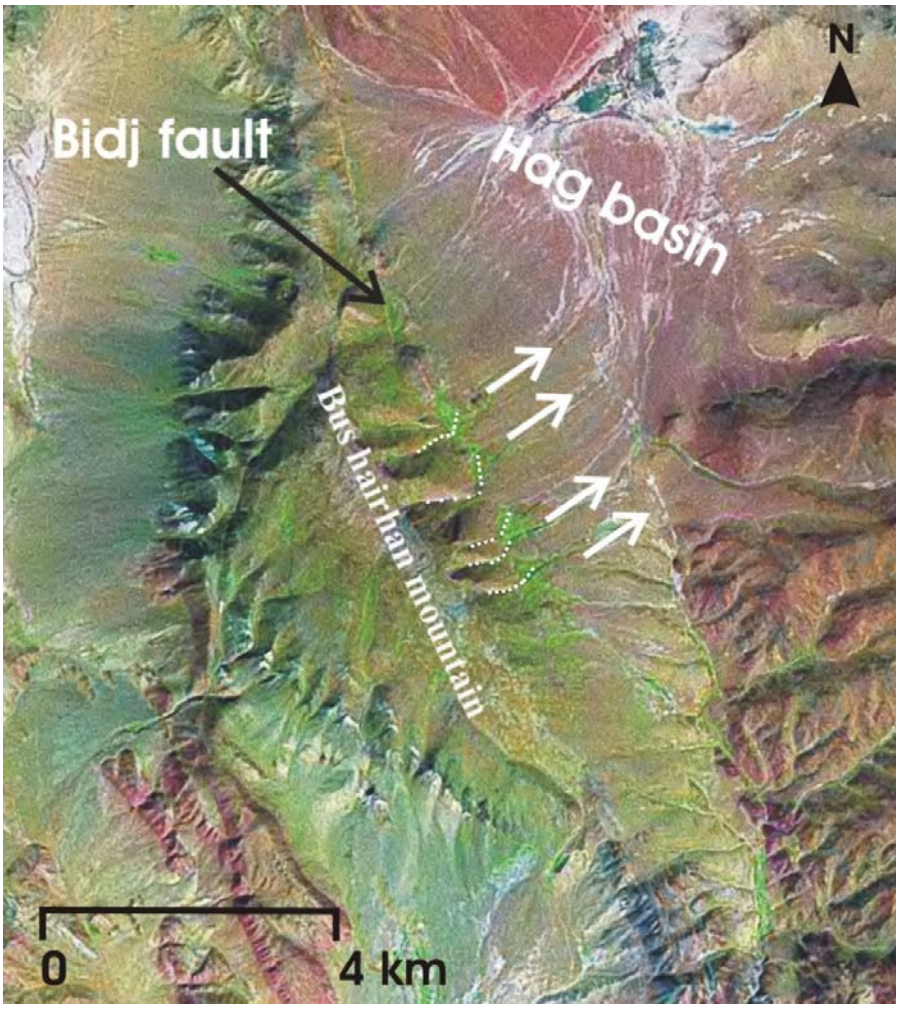

Figure I.15: The Bidj right-lateral paleodislocation (northern part of the Fig. I.14) cut small streams of the Hag Basin underlined by white arrows and with apparent left lateral movement on Landsat images. It is due to the slope of the Hag Basin border that is lower on the north and 'catches' the streams.

I.4.2 The Tolbo fault

The Tolbo fault is a major strike-slip fault between the Sagsai and Khovd faults and also one of less studied zone despite it has been mentioned by many authors (Khilko *et al.*, 1985; Thomas *et al.*, 2002; Novikov, 2002). Tolbo faults trends along the southwestern slope of Khungui range and it separates high summits from long narrow valley of Tolbo (Fig. I.16). Tolbo itself is a long lake oriented NW with flat ridge to its northeast. The Tolbo fault is very clear on the satellite image. Right-lateral slip is revealed by offsets of river valleys and disrupted alluvial fans (Fig. I.16). Three rivers running to the Tolbo Basin recorded clear offset of alluvial fan.

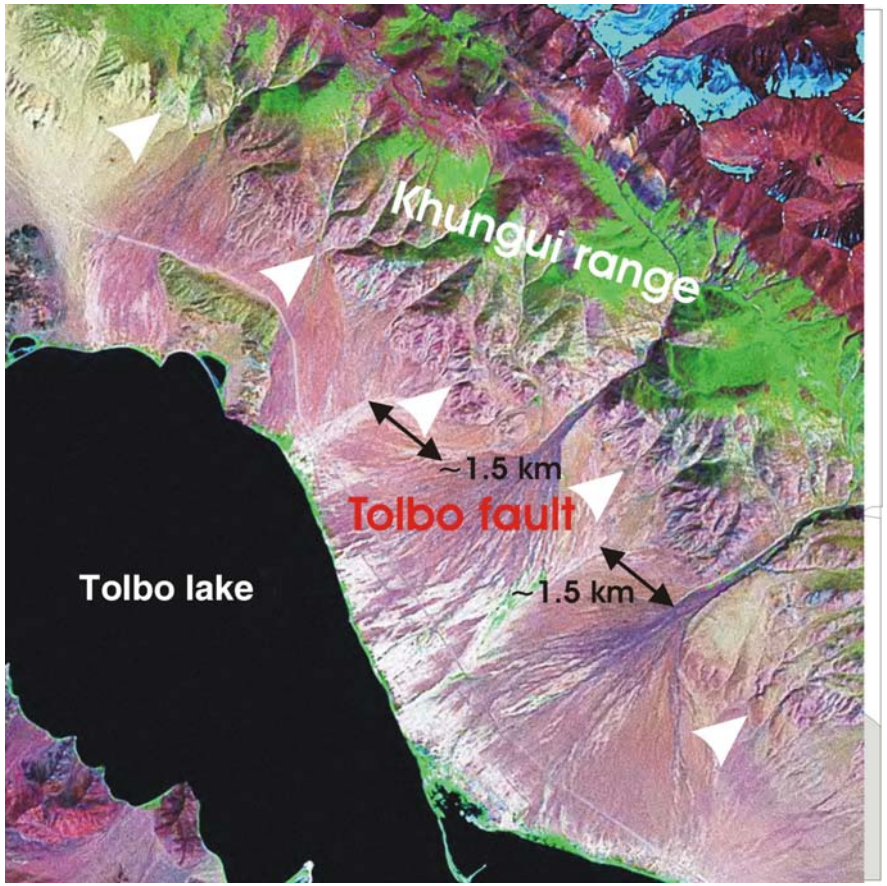

Figure I.16: The Tolbo surface ruptures observed on Landsat images (see Fig.I.6 for location).

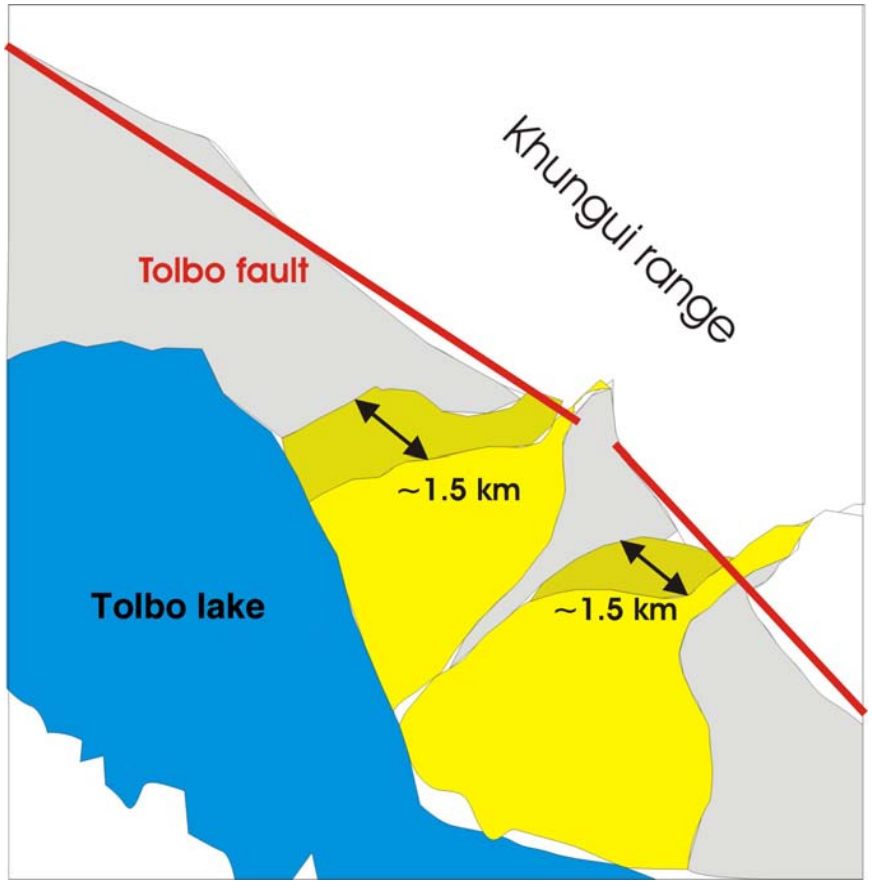

Figure I.17: Interpretation of the Fig.I.16 The actual alluvial fans (yellow) cover the previous alluvial fans (yellow brawn) showing a right-lateral displacement of about 1.5 km.

Along the chosen zone, we tried to measure cumulative displacements from stream offsets. We found several evidences of offsets in three different parts of the fault.

- Near the Tolbo lake area, we can see slip evidence of alluvial fans displaced right-laterally about 1.5 km (Fig.I.17). The observation is based on the offset between two generations of alluvial fans and we found the same amount of offset on both.
- At around 60 km south from Tolbo Lake, we found five clearly expressed offsets of river streams (Fig. I.18). From North to South, we measure offset of 1.4 km; 1.5 km, 1.3 km 1.2 km, 1.3 km So the average total offset of such rivers in that region is about 1.4 km. These observations are well correlated to the previous measurements 60 km to the north.
- At the extreme south of the Tolbo fault, we find on the Landsat images four other evidences of right-lateral strike-slip displacement. Our estimated offsets are from North to South; 1.4 km, 1.3 km, 1.4 km and 1.3 km., respectively (Fig.I.19).

Along the entire Tolbo fault zone we can see and measure many cumulated offsets of streams confirming right-lateral strike-slip displacements of about 1.4 km. As the Tolbo fault follows topography, it should be associated with a vertical component of the displacement. Horizontal offsets are three times less than along the Ar-Hotol fault but the streams could be younger or the fault slower. Dating of displaced alluvial fans could bring very interesting information on the rate of deformation. This could be a focused zone of future work.

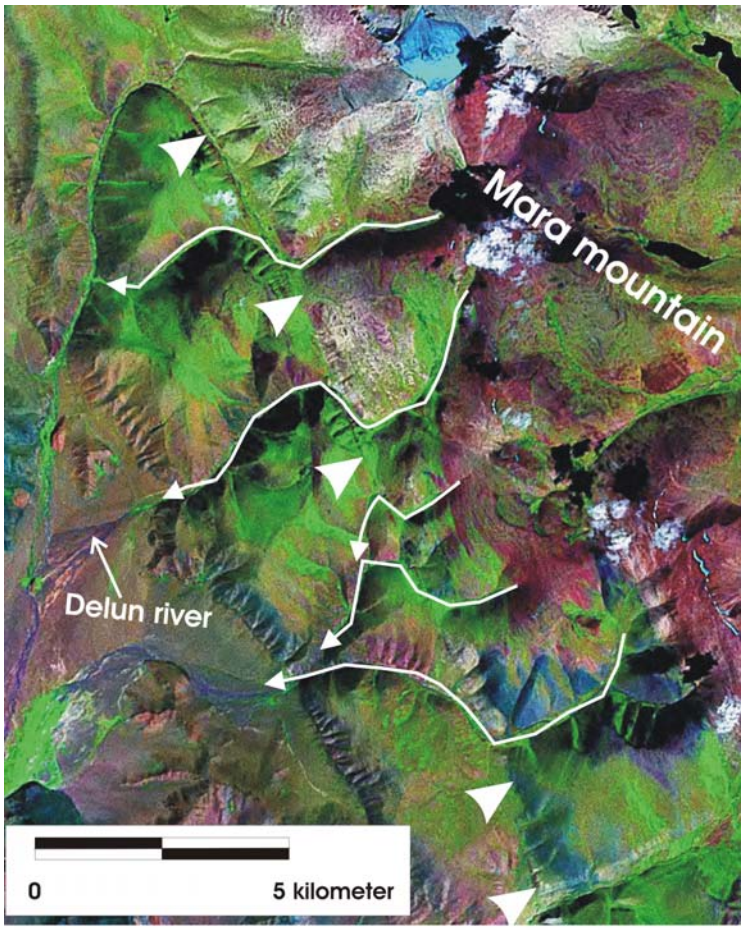

Figure I.18: Tolbo Fault observed on Landsat images at around 60 km south from Tolbo Lake (see Fig.I.6 for location). We can see five right-lateral offset of river streams. From North to South, the displacements are 1.4 km, 1.5 km, 1.3 km, 1.2 km and 1.3 km.

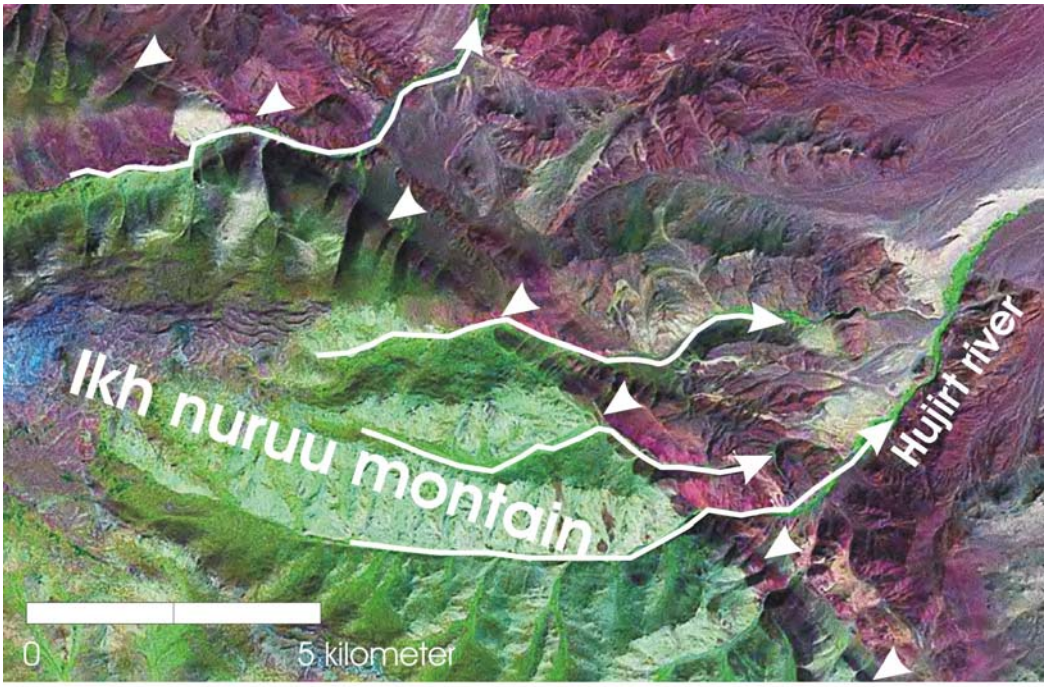

Figure I.19: Tolbo Fault observed on Landsat images: at the extreme south of the Tolbo fault four other evidences of right-lateral strike-slip displacement. From North to South, offsets of 1.4 km, 1.3 km, 1.4 km and 1.3 km are measured.

I.4.3 The Sagsai active structure

The Sagsai paleodislocation, oriented NW-SE as the other main strike-slip faults of Altay, is a Cenozoic fault reactivated in Quaternary. The fault is observed about 40 km SW from Ulgii city, near the Buyant somon, which is located inside high mountain system of the Altay range. The morphology of Sagsai structure consists of intra-mountain basins at the altitude of 2000-2300 m, bounded by high uplifted mountain systems such as Hoh-Sain (3573 m), Chuluut (2742m), Ezerleg (2945 m) (Fig.I.20).

The basement in the region consists of Precambrian-Cambrian metamorphosed volcanoclastic sediments and volcanic rocks cropping out in the Hudsan and Hoh-Sain mountains. Paleozoic metamorphic sedimentary and volcanic rocks bound the Toshint ridge and Hoh-Sain. The Paleozoic granitic intrusive rocks are cropping out in the Chuluut and Buyant mountains. Quaternary alluvial deposits are distributed in the basin of Sagsai River, Zosiin-Hud (Fig.I.20).

The fault starts from drainage divide Bogoch, west side of Toshint Mountain, and next tracing to the SE along the mountains Chuluut, Ezerleg, Hoit-debseg, Hoh-Sain. On the Landsat image, it can be traced following most of time clear surface ruptures but at some places, it is less obvious (Fig.I.20). The clearest and most continuous fault scarp is on the foot of the Hudsan and Hoh-Sain mountains. In theses sites, a vertical offset of 1.8 m has been measured on the field by Khilko *et al.* (1977). A right-lateral strike-slip displacement was also reported at these places with offset of ~ 2 m.

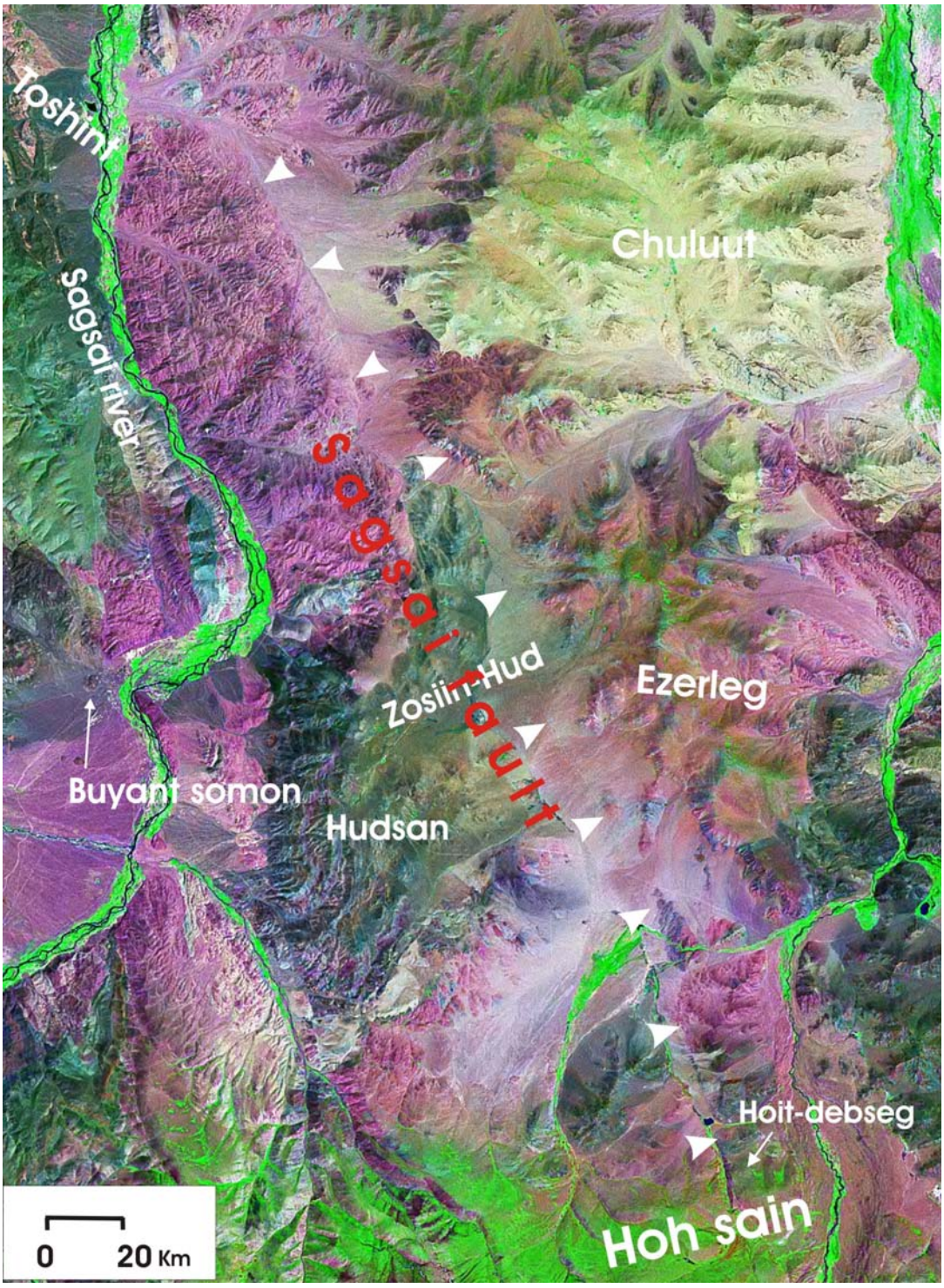

Figure I.20: Landsat ETM+ images of the Sagsai fault (see Fig.I.6 for location). The white arrows show the main trace of the Sagsai fault.

Further south, it runs to the south front of mountain Chuluut and continues to the Zosiin-hud Basin. The most clear linear surface ruptures oriented N150°, are along the flat foot of Ezerleg Mountain (Fig.I.20). Here *en echelon* mole tracks and tension cracks (compression and

extension zones) are respectively oriented about N110 and N180. Compression mole tracks are like small thrusts with height 2-3.5 m and extensional open cracks are 40-50 m long and 2 m deep (Khilko *et al*., 1977). They noted also several horizontal displacements of river channels of less than 3 meters. All these informations show that the fault is associated mainly to right-lateral strike-slip displacement.

The vertical displacement is generally hard to estimate and very variable. The displacements are clearly expressed at the south end of mountain Ezerleg. On southeast termination, especially when crossing river Buyant, character of reverse component of fault is associated to the formation of small lakes and with boggy sites.

In summary, Sagsai paleodislocation is a long right-lateral strike-slip with reverse component, which is consistent with the general deformation characteristics of the region. Unfortunately, we did not reveal evidence of stream or other type of offsets using satellite images.

I.4.4 The Fu Yun active fault

At the southwest of Altay range, the Fu-Yun fault zone, oriented NNW-SSE extends from about 45°N near Barkol-Tagh to the Irtysh River near the 47° N (Fig.I.21). The fault trace appears to be roughly continuous for several hundred kilometers and is characterised by active right-lateral strike slip (Baljinnyam *et al.*, 1993). This fault was associated with the great Fu-Yun earthquake, of 1931 August 10 (46.89°N, 90.06°E, M = 8.0), which produced 180 km of surface ruptures. They trends N-NW (N 160). Right-lateral displacements were observed along most of the faults. Several local measurements of 9 to 11 m were made in the central section, with an isolated maximum measurement of 14.6 m near the centre of the rupture (Baljinnyam *et al.*, 1993; Shi *et al.*, 1984; Zhang Pei-zhen, 1982). Component of normal faulting in the northern part of the rupture and of reverse faulting in the southern part were reported, implying scissors faulting. This suggests that a small component of relative rotation about a vertical axis might have occurred (Baljinnyam *et al*., 1993). Vertical components, between 1 m and 3.6 m, were measured at the south part of the rupture (Molnar, 1984). The southwestern end of the Fun-Yun fault, near 45°N - 91°E, is associated with high-angle thrust faulting (Tapponnier and Molnar, 1979). The right-lateral offsets have been measured by several teams. Shi *et al.* 1984 reported 20 m offsets on some features but consider them as cumulative slips associated with several previous earthquakes. Baljinnyam *et al.* (1993) also reported cumulative right-laterally slip of 100 m to 3 km measured on streams flowing westward from the higher parts of the Altay range, with several clearly offsets of 1.5 to 2 km.

The observations on Landsat -7 + ETM image allow us to measure such large cumulative displacements. I find five places with clear cumulative river streams offsets. Between the Karachora and Chalgir rivers, I estimated four stream offsets; from north to south, with displacements of about 1.6 km; 1.5 km; 1.5 and 1.3 km respectively (Fig.I.22). More to the south, we can observe another evidence of largest stream offsets with 2.4 km (Fig.I.23).

The Fu-Yun active fault is right-lateral strike-slip that produced observable cumulative rivers offsets between 1.3 and 2.4 km.

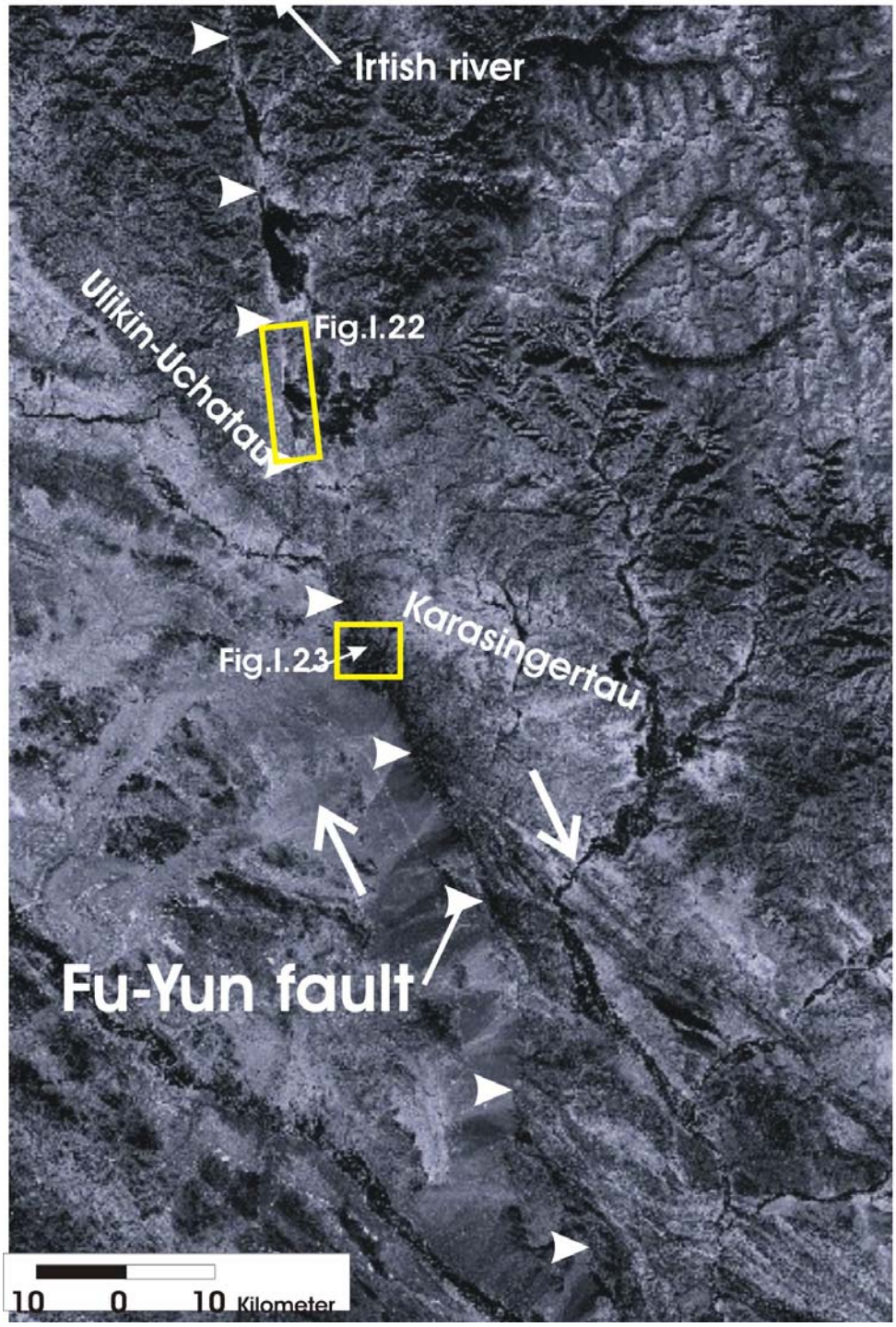

Figure I.21: Extracted of Landsat image which shows the central part of the Fu Yun Fault, which was activated during the magnitude 8.0 August 1931 earthquake (see Fig.I.6 for location). The boxes show the location of next zoomed maps.

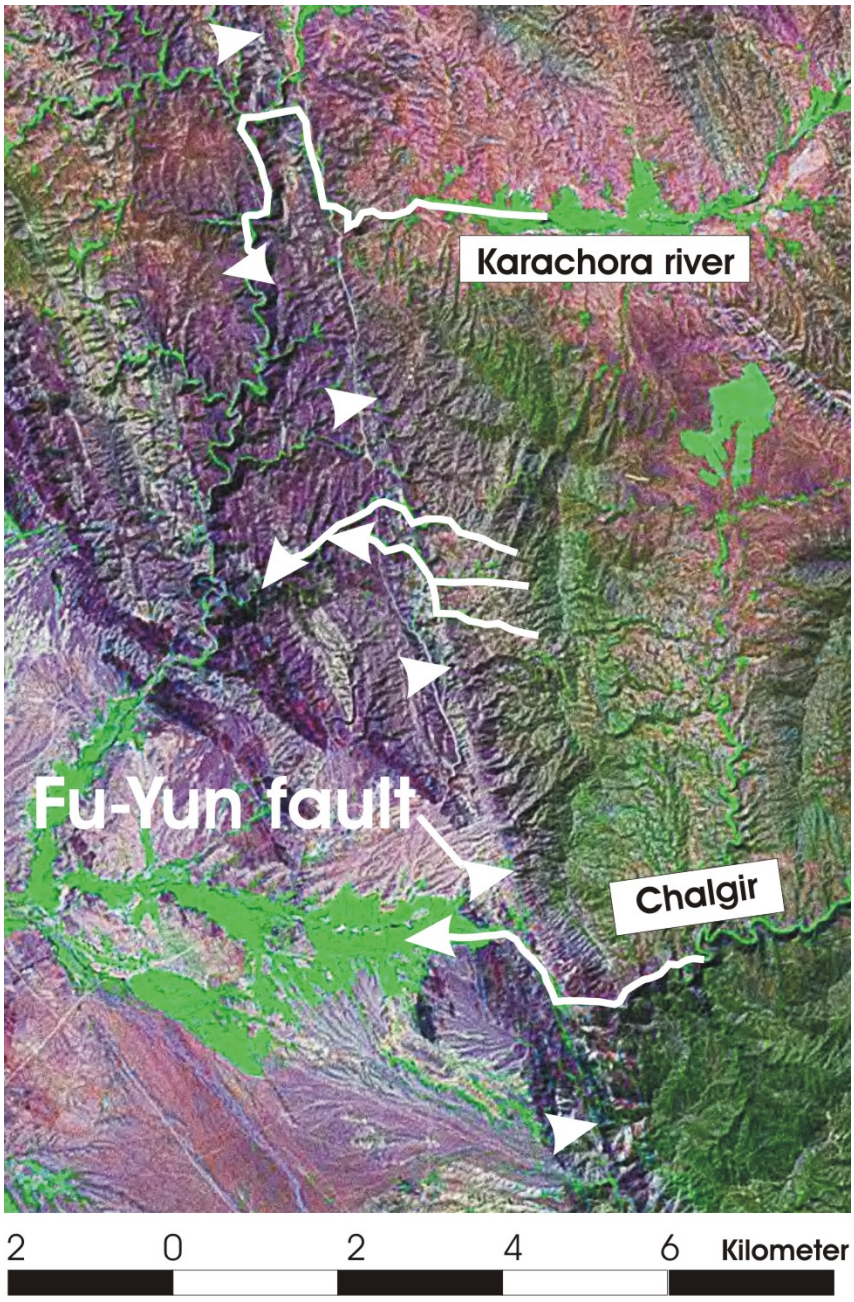

Figure I.22: Zoom on the northern part of Fu Yun fault activated during the magnitude 8.0 August 1931 earthquake. Fault is underlined with white arrows; rivers across the fault zone are underlined with white lines. Between the Karachora and Chalgir rivers we observed on Landsat images four stream cumulated offsets; from North to South: 1.6 km; 1.5 km; 1.5 km and 1.3 km respectively. See location on Fig.I.21.

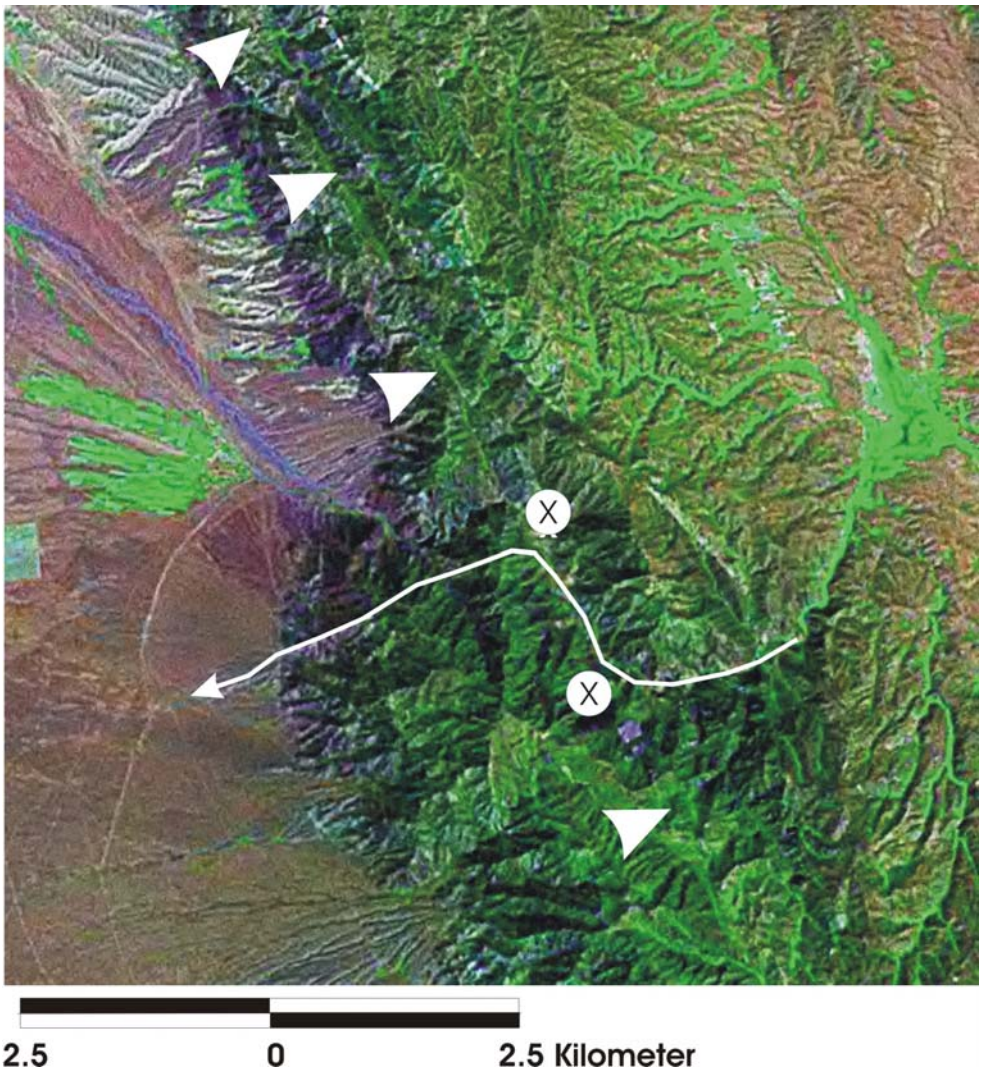

Figure I.23: Zoom on the southern part of the Fu Yun fault activated during the magnitude 8.0 August 1931 earthquake. White arrows underline fault, white line underline a river stream on where a cumulative right-lateral offset of 2.4 km can be measured. See location on Fig.I.21.

I.4.5 Left-lateral faults at the southern extremity of the region

I.4.5.1 The Bulgan fault

The Bulgan fault, oriented N90, is located at the southwestern end of Mongolian Altay where it joins large intermountain basin as Baruun Huurai, controlled by the EW Bulgan Cenozoic active faults (Fig.I.24 and I.5). The Baruun Huurai basin lies on the border between Southwestern Mongolia and Northwestern China.

The geomorphology of the region is characterized by the Bulgan River basin, at a mean altitude of 1000 - 1200 m, bounded by mountains with altitudes between 1500 - 2100 m. The Northern part is higher and on the foot of the mountains are large alluvial fan deposits (fig I.4).

The fault starts near the village Bulgan and continue to the West, along the river Bulgan and the Zuun-Haz Mountain. Khilko *et al.* (1985) mapped a surface rupture for 30 to 32 km from

the border with China to about 46.2°N, 91.4°E. They noticed that the length could be longer if it continues far into China. On the Landsat image, we can follow clear continuous scarps. The Bulgan fault has a total length of about 50 km (Fig.I.24) mostly in Mongolia. Its Mongolian part is about 32 km long and the Chinese part is about 18 km. A vertical displacement is observed when it crosses quaternary alluvial sediments from 90°46'E up to the 91°10'E. Vertical movement is about 2 – 3 m along Bulgan River and 1.5 - 2.0 m in front of Zuun-Haz and Utan-har mountains. Khilko *et al*. (1985) listed average horizontal and vertical displacement of 2 m and 1 m, respectively, and assigned a tentative age of 500 yr to 1000 yr to the last surface faulting (Baljinnyam *et al.*, 1993). Generally the scarp is interpreted as the result of oblique thrust faulting with small left lateral horizontal displacement which corresponds to regional stress oriented SW-NE (Khilko *et al*., 1977). Further to the west, it connects with the Fu-Yun great right-lateral strike-slip fault structures (Fig.I.5 and I.26).

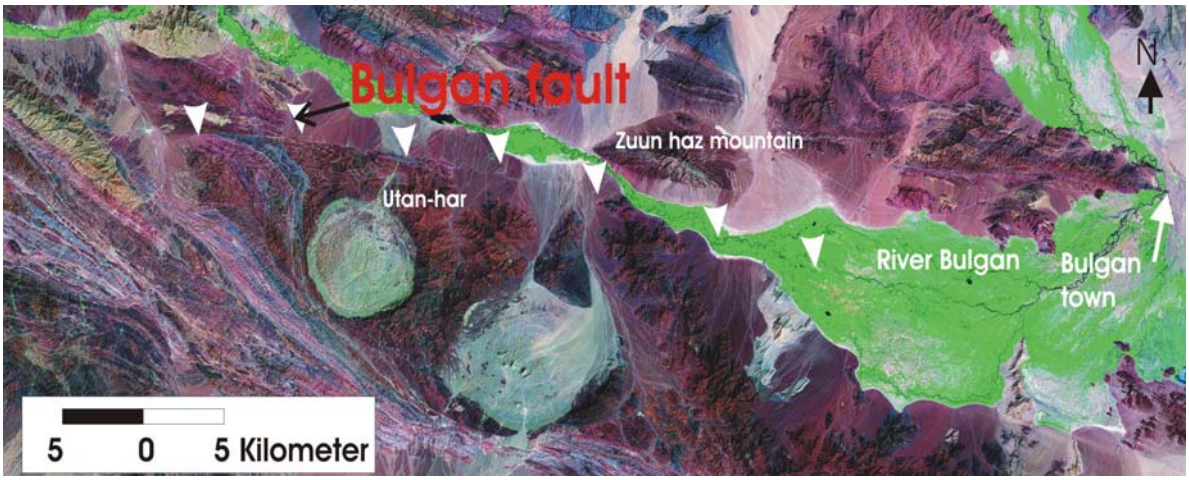

Figure I.24: The Bulgan fault (white arrows) located at the southwestern end of the Mongolian Altay observed on Landsat ETM+ image (see Fig.I.6 for location).

I.4.5.2 The Baruun Huurai fault

The Baruun Huurai fault trends east-northeast and intersects the Bulgan fault east of the town of Bulgan (Fig. I.5). Its northern continuation defined by a series of sub parallel splays with a cumulative offset of 7 to 8 km (Tikhonov, 1974; Baljinnyam *et al.*, 1993).

I.4.5.3 The Tahiin-Shar fault

The Tahiin-Shar fault is associated with an earthquake which occurred on 04th July 1974, in southwestern Mongolia (45.14°N, 94.03°E, M = 7.0). It provides a second example of left-lateral slip near the southern extremity of the Altay range. The fault plane solution for this event show nearly pure left lateral strike-slip faulting on a plane striking N78° (Baljinnyam *et al.*, 1993). The fault consists on a zone of tension cracks and compressive mole tracks extending in an east-northeast direction for 17 km. The width of the zone reaches 15 m, and some crack opened as much as 0.5 m. From the orientations and dimensions of these cracks and mole tracks, the rupture has been interpreting as a left-lateral slip of 0.3-0.4 m (Khilko *et al.*, 1985; Baljinnyam *et al.*, 1993). These authors also reported a maximum vertical slip of 0.4 m but with an average of 0.1 m.

I4.5.4 The Sharga fault

The Sharga fault is a left-lateral strike-slip along the southeastern extremity of the Altay range, where it makes the junction with the Goby-Altay range. A clear scarp can be delineated from Landsat-7 + ETM images over 55 km. From approximately 30 km east of Tajgar-Bulag up to Hoit-Shargin River (Fig.I.25), the scarp is facing north and is crossing young alluvial deposits. At some places, the height of the scarp reaches 2 to 2.5 m, however along much of this segment, its height is only between 1.0 to 1.5 m (Baljinnyam *et al.*, 1993). Left-lateral offsets were measured on dry streambeds on the north side of Buural mountain. Large ridges oriented NW-SE between Tajgar-Bulag and village of Sonduultay appears to be pressure ridges and indicate left lateral slip (Baljinnyam *et al.*, 1993).

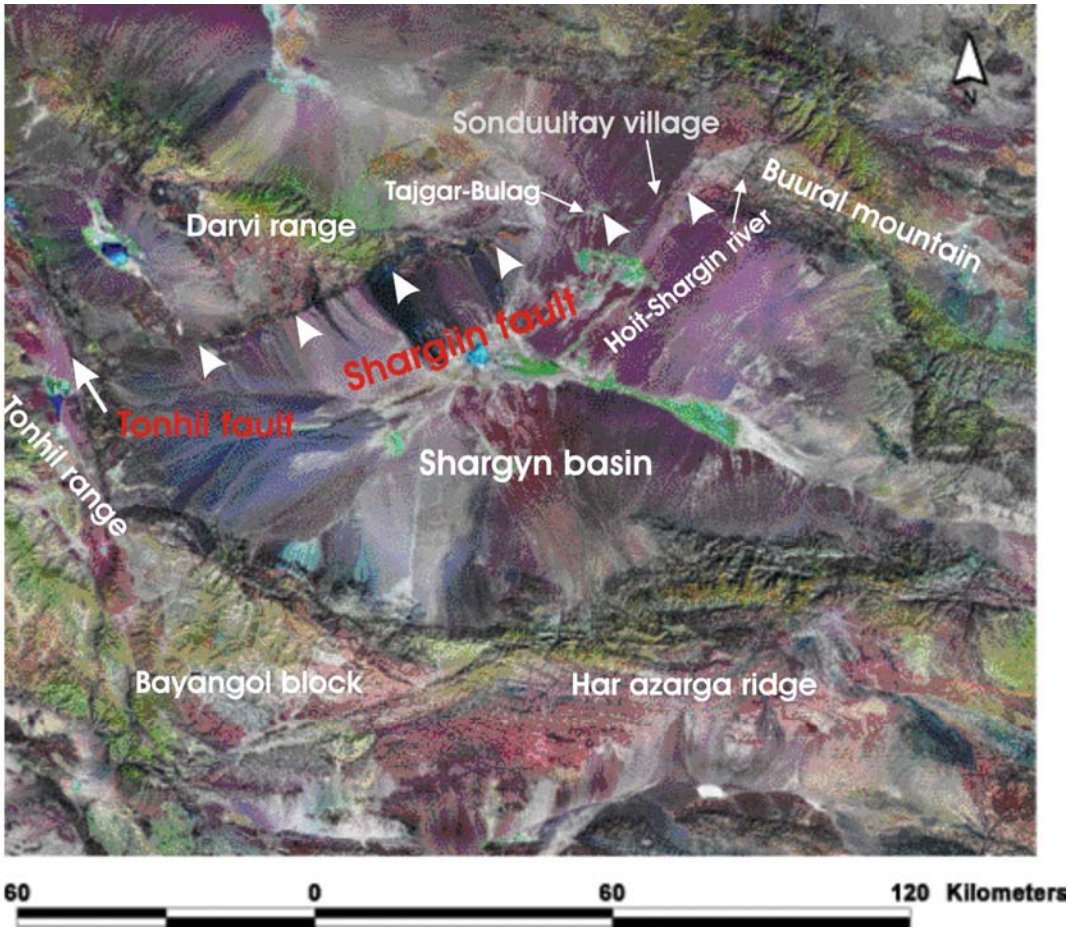

Figure I.25: The Sharga (Shargiin) fault is a left-lateral strike-slip fault that makes the junction between the Altay and the Goby-Altay range (see Fig. I.6 for location). A clear scarp can be delineating from Landsat-7 + ETM images for a total distance of 55 km (white arrows).

I.5 Model of deformation in Altay range

Active crustal deformation in Central Asia affects a wide region between the Himalayas and Siberian craton. Since the beginning of the India-Eurasian collision in the Eocene, stress led to the northward propagation of the deformation, which reached the Tien Shan in Late Oligocene

and the Altay region in the Pliocene (Dobretsov *et al*., 1996; Dehandschutter *et al*., 2002). Our estimation using cumulative rivers displacement confirms that proposition. Indeed, we deduced a **beginning of the deformation in Altay one to four millions years ago.**

The Altay domain is a mobile zone bounded by the Junggar depression to the west and the Valley of Great Lakes to the east. Inside the blocks are expressed **right-lateral displacements along major fault zones.** The satellite images analysis shows **four major fault zones** cutting the Altay block and consisting of several segments. The figure I.26 shows our proposed active fault zones model and the observed cumulative offsets.

The Khovd fault zone is the eastern extremity of Altay block, which is very clear on the satellite image along the whole length of fault. Khilko *et al.* (1985) reported recent surface ruptures on the three segments of this fault (Chihtei, Ar-Hotol, Bidj). Along the Khovd fault, we revealed cumulative offset of six rivers drainage. The reconstruction of these drainage systems displaced by the fault implies a cumulative right-lateral strike-slip between 3.5 and 4.8 km.

At the west of the Khovd fault zone is located **the Tolbo fault zone**. The Tolbo fault can be followed relatively continuously on the satellite image and is one of the zones where we succeed to measure cumulative offsets. These offsets are constant along all segments and are evaluated between 1.3 - 1.5 km with a right-lateral movement.

The third zone is **Sagsai fault system**, which was poorly traced from the satellite image. We can propose a continuity of the structure but no displacement evaluation has been possible using satellite images.

At the western extremity of the Altay domain is the **Fu-Yun fault zone** that marks a sharp boundary between the Junggar and Altay blocks. There are several clear evidences of right-lateral cumulative offsets along the Fu-Yun rupture, with stream channel offsets between 1.5 km and 2.4 km.

The above summarize demonstrates that the cumulative offsets are different between the Khovd structure and the others. They are constant along a selected fault, particularly on the Tolbo fault zone. Without dating, we can only propose **two hypotheses. Either the rates are constant but the rivers have different ages, or the Khovd fault is two times faster that the other ones showing then a partitioning of the deformation over the Altay.**

However, this second proposition is up to now not confirmed by the recent GPS observations. Indeed, GPS shows N-S shortening with respect to Siberian craton with the same velocity for the ULGI and HOVD points, ~ 4 mm / year, despite they are separated by the Khovd fault.

Recent studies of active deformation of Altay range propose or show **counter clockwise rotations** about a vertical axis for the Altay range (Schlupp, 1996; Bayasgalan *et al*., 1999; Thomas *et al*., 2002; Bayasgalan *et al*., 2005). Detail kinematics studies of the Mongolian Altay faults (Bayasgalan *et al*., 1999), based on field and earthquake data, show that **right-lateral strike-slip faults** oriented NW-SE are **ending to the northwest on thrust faults oriented E-W** to N100°. The displacement along these faults decrease away from SE to NW. This style of faulting implies counter clockwise rotation about a vertical axis. Thomas et al. (2002) did a paleomagnetic study on the Chuya basin in the northern Altay. They found a Tertiary counterclockwise rotation of 39° ± 8° relative to stable Asia on the Chuya depression. This is the region where the NW-SE trending right-lateral strike-slip faulting changes to E-W thrusting (Bayasgalan *et al*., 2005) as mentioned above.

Recent GPS measurements of crustal velocities in Northern Asia (Baikal rift zone and Mongolia) relative to Siberian craton show **N-S shortening in westernmost Mongolia** but eastward to southeastward motion associated with left-lateral shear for central and eastern Mongolia (Calais *et al*., 2003). For Altay, they calculated velocities relative to a stable Siberian

block, and find a decrease of velocity amplitude from south to north: **from 10 mm/yr at Urumqi south of the Altay to about 4 mm/yr in NE Altay**.

Bayasgalan *et al*. (2005) used source parameters of earthquakes to constrain slip vector azimuths in Altay. They found that the **slip vectors are mostly in the NNW direction** when the GPS motions are NNE. They conclude that the discrepancy between slip vectors and GPS vectors may also suggest a counterclockwise rotation of Altay range.

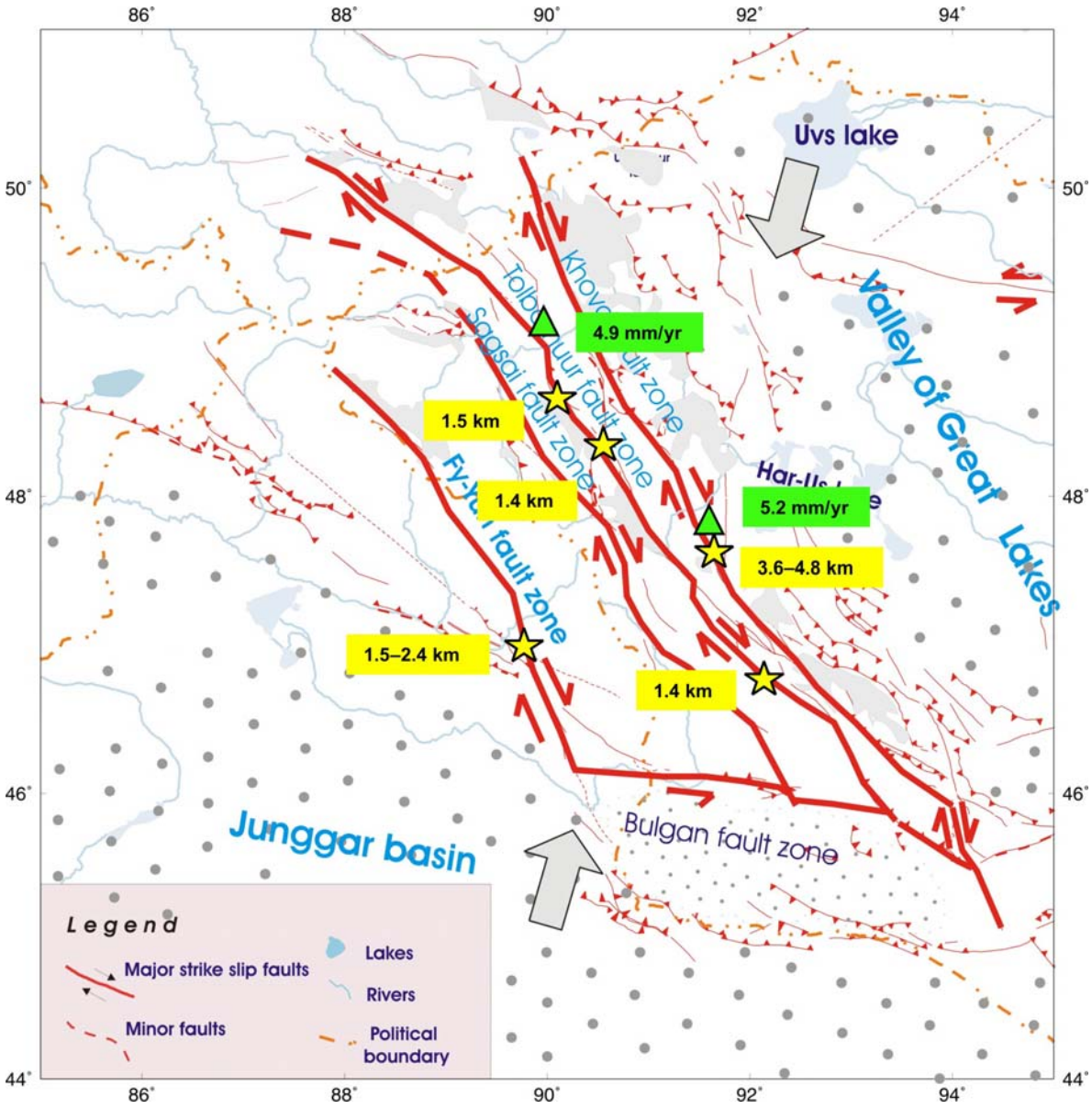

Figure I.26: Simplified tectonic behavior of the region. The values highlighted in yellow are cumulative horizontal offsets in km; yellow stars are placed where they were measured on satellite images. Green triangles show GPS measurements relative to Siberian craton. Large grey arrows show the orientation of the main horizontal stress in the region.

Following these observations, we believe that, as a whole, Altay range is rotating in a counterclockwise direction. It is difficult to conclude and to compare our measurements, over long period of time, with very short time GPS observations. In addition, we do not have observed cumulative offsets along of all fault traces. For example, we could not find any information in Sagsai zone and also the two extreme sites (Fu-Yun and Khovd fault zone) are based just on one fault segment. Also the lack of Mesozoic and Tertiary rock within the Mongolian Altay is likely to make it difficult to distinguish amounts of Cenozoic and older displacements.

I.6 Conclusion

The right-lateral strike-slip faults are particularly clear on the Landsat-7 image. We have interpreted most of the active strike-slip faults to constrain their characteristics, quaternary activity and the cumulative stream offsets. Also we included observations which have been done previously (Baljinnyam *et al*., 1995, Khilko *et al*., 1985, Bayasgalan, 1996) for the surface ruptures over the Altay ranges.

We constrained possible offsets distributions along these zones. Finally, we have defined four micro-blocks that are moving along the fault zones. We have observed several clear stream offsets along these zones and the reconstruction of river streams gives consistent results for all the observations.

The offsets of river drainages and streams suggest some partitioning along the different fault zones. Active fault zones that have been underlined inside the Altay zone seem to move at different rates. It seems that horizontal movements along the major faults are more intense at the border of the range, Khovd and Fu Yun structures, than in the middle part of Altay block, Tolbo and Sagsai structures.

The GPS study shows a global 4.9-5.2 mm/year NS directed motion of the east Altay. Two GPS points are separated by Ar-Hotol fault but give about the same value. Therefore, it seems, from the GPS data, that there were no motions across Ar-Hotol fault during the period of GPS measurements. The apparent contradiction between the morphology and GPS should be interpreted. We think that the deformation expressed on images, which cover a longer period, is more reliable to explain Altay tectonics. A denser GPS network should be installed on the blocks to clarify that question.

Chapter II

Seismic activity and surface ruptures of western Mongolia during the last century

II.1 Introduction

Mongolia is one of the high seismic active areas of the Central-Asian belts and was exposing to frequent strong earthquakes. During the last century occurred four large earthquakes with magnitude $M \geq 8.0$ and several earthquakes with magnitude $M \geq 7$. These destructive earthquakes produced surface ruptures of several hundreds kilometers.

The Research Center of Astronomy and Geophysics (RCAG) is the Mongolian organization who is monitoring the seismic activity of Mongolia. RCAG was established few months before the large Gobi-Altay earthquake (December 1957, Mw=8.1) and then we started the monitoring of the seismicity in Mongolia using at first two seismic stations. The network increased, time-to-time and today we manage more than 40 seismic stations including seismic mini array. Nevertheless, the RCAG upgraded his technologies strongly since 1994 and reached then the level of developed countries, using modern seismic stations and routine tools. This development was possible thanks to the collaboration with DASE (Departement Analyse Surveillance Environnement, CEA, France).

One important product of the seismic monitoring is to produce an earthquake bulletin. For each shock, the catalogue includes the origin time of the event, the geographical coordinates of the epicenters and the magnitudes. RCAG seismic database consists now of several tens of thousand earthquakes which occurred from 1964 up to now. We have recently published a map "One century of seismicity in Mongolia 1900-2000" (Fig.II.1) which shows the result of the seismic monitoring done by the RCAG during the last 40 years and the knowledge about the largest historical events in Mongolia (Adija *et al.*, 2003).

In this chapter, we will describe the seismic network of Mongolia and its instrumentation, discuss the accuracy of the seismic data and analyze the seismicity of Mongolia at a large scale. Finally, we will zoom on the Altay range area.

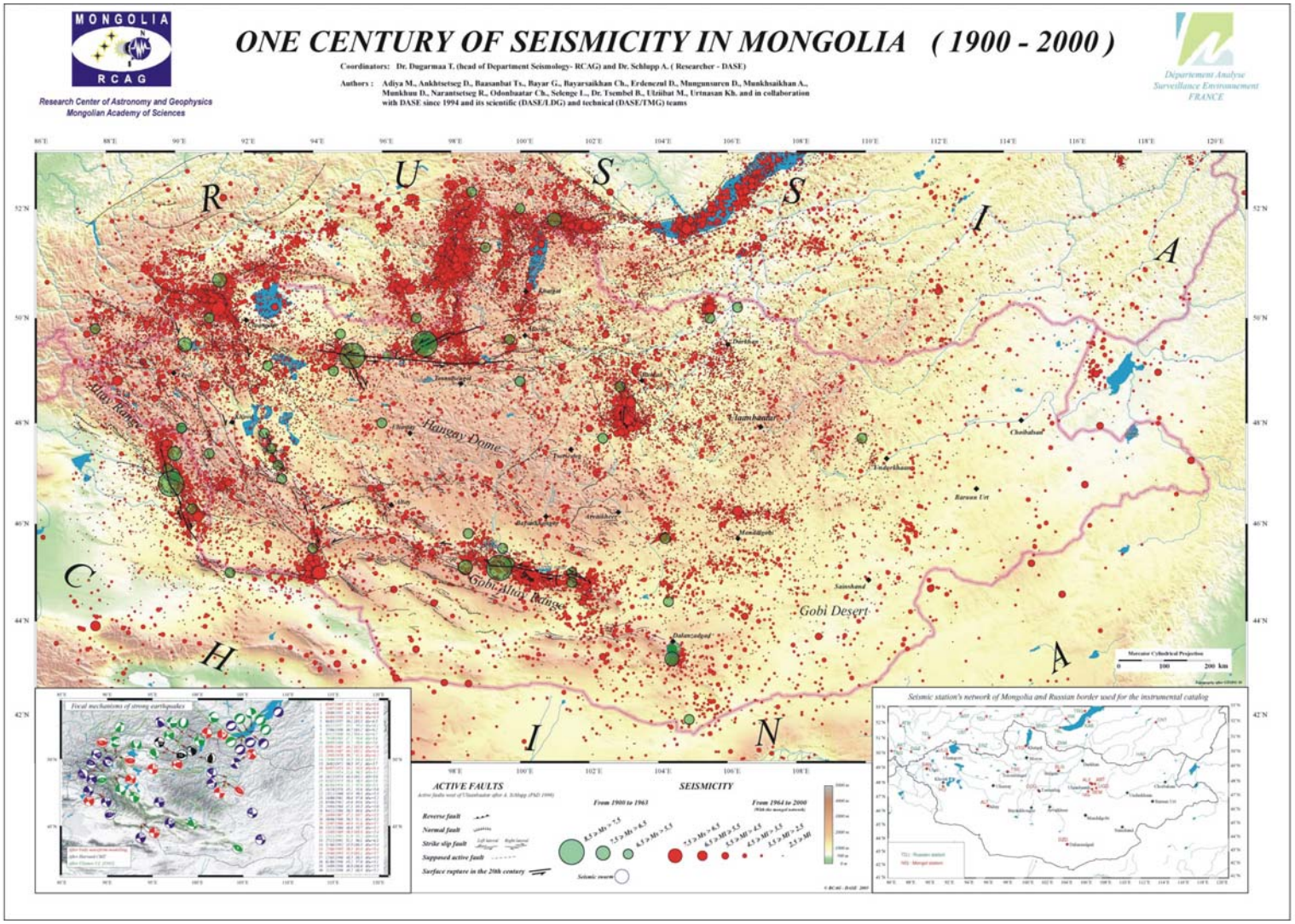

Fig.II.1. Map of "One century of seismicity in Mongolia 1900-2000" which shows the event observed by the RCAG during the last 40 years and the knowledge about the largest historical events in Mongolia (Adija *et al.*, 2003).

II.2 Seismic network of Mongolia

The instrumental seismological study of Mongolia started in 1957, just before the large Gobi-Altay earthquake (December 4, 1957, Mw = 8.1). At the beginning, it was installed two permanent stations, one at the capital Ulaanbaatar (1957) and the other at the Altay city (1958), west of Mongolia. In years 1960th, four new stations were installed (Tsetserleg and Tosontsengel in 1964, Khovd in 1965, Dalanzadgad in 1969) and later the network was increased by another four stations until 1988 (Bulgan in 1973, Hatgal in 1975, Ulaangom in 1987, Ulgii in 1988) (Fig.II.2). The seismic stations have been located1 in region with high seismic activity. Nevertheless, we will see that the map presented on Fig.II.1 is biased, for the small events, due to the detection level of the seismic network and its geometry.

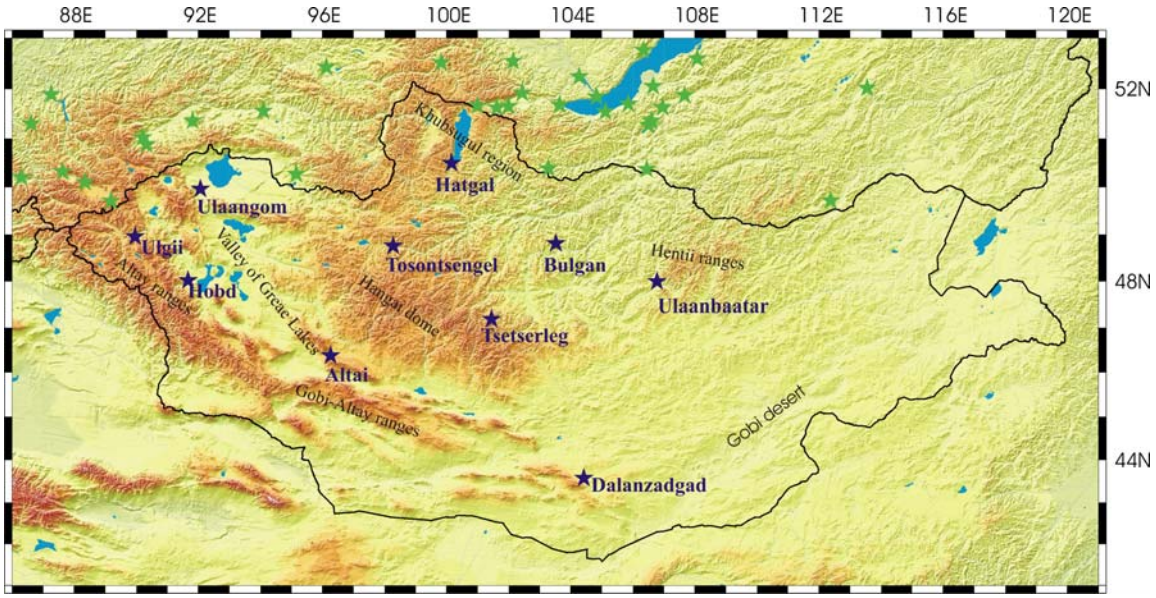

Fig.II.2. Map of the seismic network of Mongolia (1957 – 1993) (blue stars for stations from Mongolia, green stars for stations from Russia on which data are exchanged with RCAG)

All stations were equipped with SKM-3, three component short period seismometers with natural frequency 1 Hz produced in Russia. The acquisition system was analog with a galvanometric (optic) recording system; therefore, the seismic signal was recorded on photo paper. For the time recording, it was used an analog clock at the beginning called 'Khoronometer'. Later, it was changed to an electric clock PVU Russian series product. In the recent time, all recorders are using a common time provided every hour by the national radio, on which the electric PVU clock is synchronized.

First digital seismic stations have been installed end of 1994 through collaboration with France and USA. In collaboration with DASE/LDG, five vertical short periods telemetric digital seismic stations were established around Ulaanbaatar, within a distance range of 30-80 km (Fig.II.3). The aim of this local network was to monitor in detail the seismic activities near Ulaanbaatar, notably for seismic hazard purpose. The DASE instrumentation consists of ZM500 short period vertical component and ZM500H three components short and long period sensors. For data acquisition, we use real time radio telemetric transmission systems until

RCAG office with a PC control station. The data is storage with 50 samples / s for each channel. The network around Ulaanbaatar has been upgraded regularly since. One three component broadband station (6 sensors = 3 short period and 3 long period) and two new stations that replace two closed or stolen stations near Ulaanbaatar. One renewed station at western with first a vertical component and since 2005 with a broadband sensor.

Another seismic station was installed in 1994, 20 km to the southeast of Ulaanbaatar in collaboration with IRIS - USA (Fig.II.3; ULN). IRIS system consists of a three components broadband seismometer connected to a 21 bits "Quanterra" acquisition system. The channels 20pts/sec and 1pts/sec are continuously recorded. Data are distributed at IRIS DMC but also available at RCAG, Ulaanbaatar.

In 2000, in the frame of the CTBTO (Comprehensive Treaty of Ban Nuclear Test Organization) and within DASE cooperation, the seismic network increased by two mini array stations, 40 km south-west of Ulaanbaatar have been installed and included in the RCAG network. The first one is made of 11 high sensitive telemetric digital seismic stations (ten vertical short period stations, one 3 components broadband station) and the second one is made of four infrasound stations.

Later, three short period REFTEK digital stations were used to replace 3 of the old analog stations (Tsetserleg in 2002, Ulgii in 2003, Hatgal in 2003), obtained through the cooperation with International Institute of Seismology and Earthquake Engineering (IISEE), Japan (Fig.II.3). The REFTEK stations consists of three components geophones with natural frequency of 1 Hz and REFTEK DAS acquisition system with PC based modules storing data at 50 samples/s per channels.

Now in Mongolia, more than 40 digital modern stations are recording the seismicity. There are still four analog stations, which are planning to be replaced by digital seismic stations in 2006. Digital seismic stations have been calibrate, so that digital records can be convert in ground velocities and amplitudes comparable from one station to the other. This step is important in the constitution of the seismic catalogue with a common magnitude determination. We show the present seismic network of Mongolia as well as the Russian seismic stations installed in Siberia (Fig.II.3).

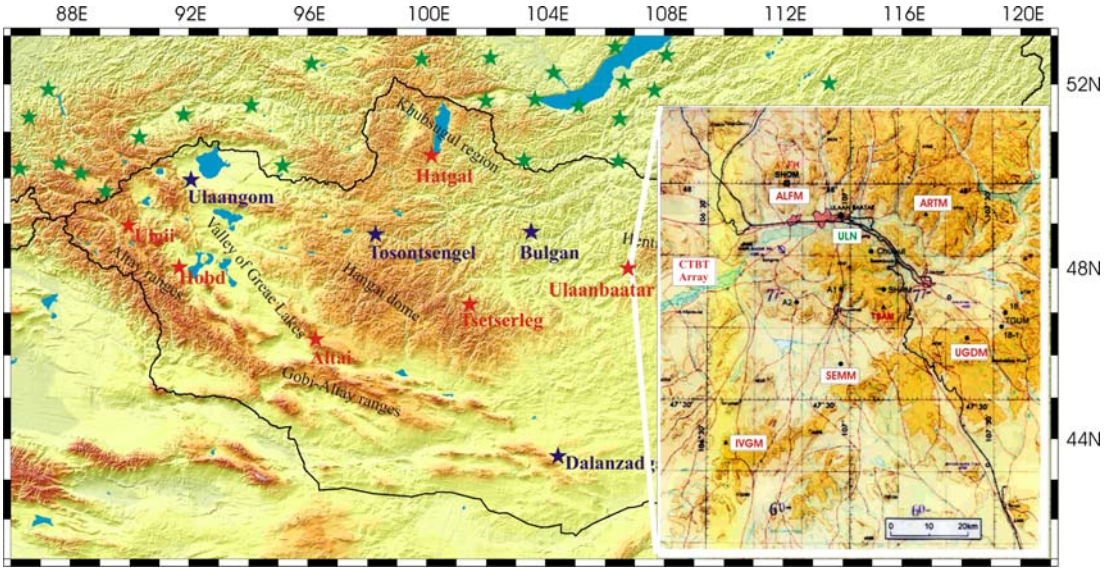

Figure II.3: Present seismic network of Mongolia (red stars - digital, blue stars = analog station) as well as the seismic stations of Siberia (green stars) which data are available for RCAG. No known seismic stations are installed in China nearby Mongolian borders. The zoomed map shows the network around Ulaanbaatar.

II.3 Earthquake processing

II.3.1 Event location

Before the installation of the digital recording in 1994, all data were interpreted manually and processed by "EPIC" software that has been developed by G. Bayar from RCAG. Using EPIC program, we estimated event origin times, location of epicenters, earthquake sizes and calculations errors. For the main events, a 24 hours duty allowed us to localize the main events in the region, the arrivals time where then collected by phone calm to the others stations. The estimation of the depth is difficult, because of the large distance between permanent seismic stations (a mean distance of about 250 km). Therefore, we were not available to determine the depth of most of the events.

Since 1994, all telemetric data are daily interpreted and the main events are localized in real time at the National Data Center of Mongolia at RCAG, Ulaanbaatar, thanks to a 24 hours duty. Non-telemetric data, digital or analog records, are received by post mail after 1-2 weeks and are then added to the other data. The event characteristics are then upgraded.

At the beginning of digital recordings, in 1994, the system recorded only triggered events with DOS based systems and the continuous signal was recorded on SEFRAM paper recorder. The digital acquisition system, upgraded in 1998, allows us now to work with continuous recorded data and with a Windows based system.

Now all data are analyzed using ONYX program that is the actual data processing tools of LDG (France). Onyx is a powerful program for the real time data processing and analyzing with many interpretation tools available such as cross correlation, master event, spectral analysis and which are easy for the operational interpretation.

All data are stored in a "Mongolia" database that is based online with a Oracle database system. The database consists of origin time, phases, location and depth of events, magnitude, errors associated to these parameters and related digital signal.

Unfortunately, it is still difficult to estimate the focal depth over the whole Mongolia, but we started recently to estimate precise earthquakes depths near the mini array stations.

In addition, we have an important cooperation with seismological centers of surrounding countries. RCAG has since long time cooperation with Irkutsk and Novosibirsk Seismological Centers (Russia) and they exchange data for the events of the frontline regions. Fig.II.4 shows the zones (square) for which we exchange data with these centers; red square with the Institute of Earth Crust at Irkutsk and blue square with the Novosibirsk seismological center. It gives us the opportunity to detect and localize more precisely the events of the northern part of the country. More recently, due to Internet facilities, we are able to use worldwide data from different national data centers.

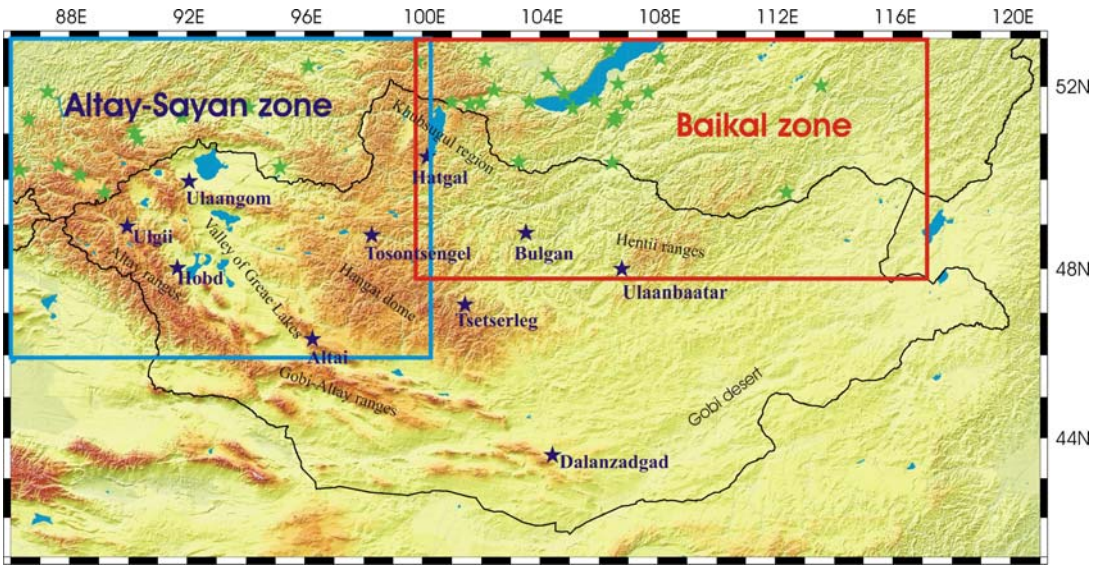

Fig.II.4. Zone for which we exchange data with Irkutsk (red square) and Novosibirsk (blue square) seismological centers (Russia).

This recent improvement of the seismological network of RCAG allowed us to better characterize the earthquakes than before, and to increase the earthquakes detection level. Specially, it is the case around Ulaanbaatar and in the eastern part of Mongolia, where the level of detection was sensitively increased. One clear example is the seismic activity at the south of Ulaanbaatar (Fig II.5).

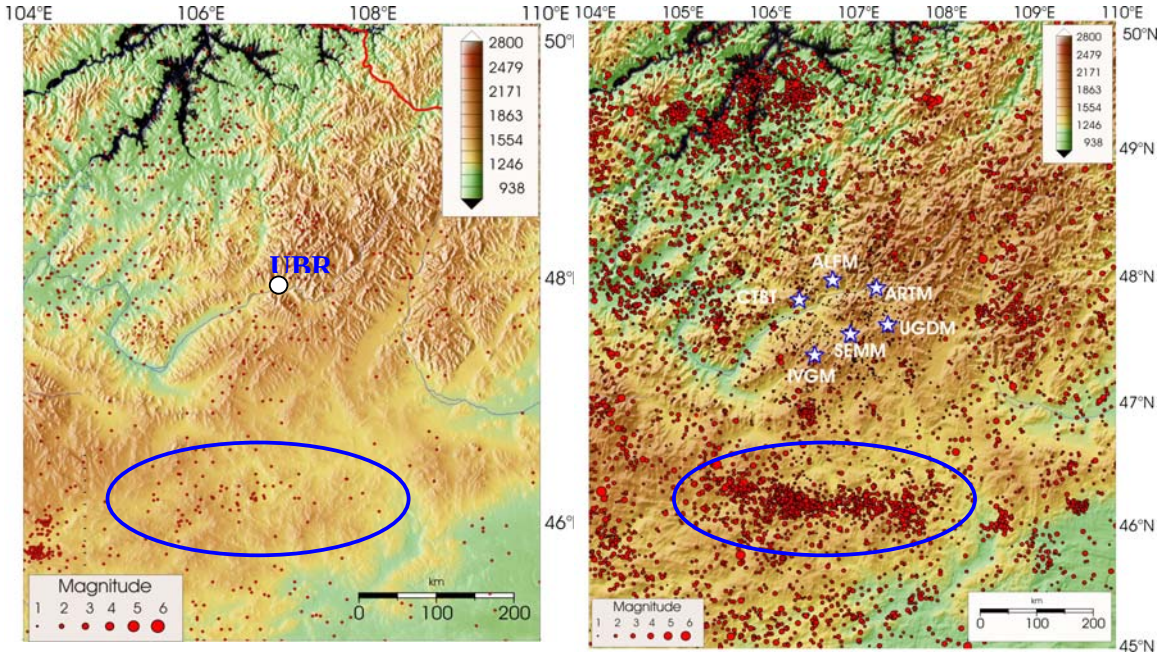

Figure II.5: Comparison of the recorded seismicity south of Ulaanbaatar detected with only the analog network, from 1964 to 1994 (left picture, UBR being our previous station) and with the new digital stations around Ulaanbaatar, from 1994 to 2002 (right picture with the today Ulaanbaatar network). The blue ellipse shows the Deren region, 180 km south of Ulaanbaatar.

II.3.2 Depth estimation

As mentioned before it is difficult to estimate precise depth of earthquakes by using Mongolian network. This is due to the large distance between permanent seismic stations (a mean distance of about 250 km). The lacks of data with focal depth estimation and the low accuracy of their determination do not allow us to analyze the depth distribution of earthquakes in Mongolia. In 1994, we started to use LDG (France) system to determine earthquake source parameters using modern and use friendly routine software, nevertheless, always do to our network, we consider most of time only depth fixed by the data analyzer according to velocity and crustal models.

II.3.3 Magnitude

During most of our seismic observations (since 1957), we used a Russian scale to determine the earthquake size. Worldwide standard is the magnitude scale "***M"*** that derived from amplitude of the ground motion measured at the station whereas the Russian consider an energy scale "***Kl"*** that is deriving from the estimation of the seismic energy released by the earthquake.

We calculated energy class as;

$$Kl = Log(E) \quad \text{(II.1)}$$

It is included a normalization for the distance developed by Rautian (Rautian 1964; Khilko *et al*., 1985), "E" is the seismic energy in joules and "***Kl"*** the energy class. Some special palette's, which is called "Rautian's palette", allows to used determine the energy class function of the distance from epicenter and the amplitude of records in mm. This provides an easy use for the operators which are in charge of the earthquake processing.

The energy classes is still in use over the Russian territory, so it is still important for RCAG to continue the "***Kl"*** evaluation, at least on events occurring near the frontline to insure well understanding in the collaboration with Russian teams.

Nevertheless, since few years, to homogenize the earthquakes parameters provided by RCAG, we determined a magnitude ***M*** and have worked on relations to convert energy class to magnitude (Khilko *et al.*, 1985). Two different relations depending of the magnitude range are used:

$$Kl = 4.0 + 1.8 * M \quad \text{(II.2)}$$

$$Kl = 8.0 + 1.1 * M \quad \text{(II.3)}$$

The first relation (II.2), considered for magnitude less than 5.5, seems to provide a good conversion but the other one (II.3), considered for magnitude greater than 5.5, gives some biases for large magnitudes, the linear expression seems then to be inadequate.

Since the installation of digital modern stations (1994), it was necessary to obtain our local magnitude scales.

The formula used in routine software at RCAG for the estimation of the local magnitude is:

$$Ml = Log\left(\frac{A}{T}\right) + 0.816 * Log(\Delta) + 0.00045 * \Delta - 1.22 \quad \text{(II.4)}$$

Where ***A*** is the maximum amplitude, measured for the ***T*** period of wave, Δ is the epicentral distance. This formula was defined using the numerous new records since 1994 from digital stations (Ulziibat et al., 2000).

II.3.4 Completeness

Because of limited sensitivity and low coverage of seismic networks, small events are generally uncompleted detected overall Mongolia and are missed in the seismic catalogues. Thus, we need to determine magnitude thresholds, above which catalog can be considered reasonably completed. To study catalogue completeness we used the Gutenberg-Richter (G-R) law for the cutoff magnitude and time dependent completeness.

Fig.II.6 shows the number of detected earthquakes per year for various magnitudes. The annual numbers of events were stable starting from 1971 and increased since 1995, which is connected with the installation of high sensitive digital stations end of 1994. This increase is related to small events and we can consider that our catalogue started to be relatively complete since 1971 for magnitude larger than 3 to 3.5.

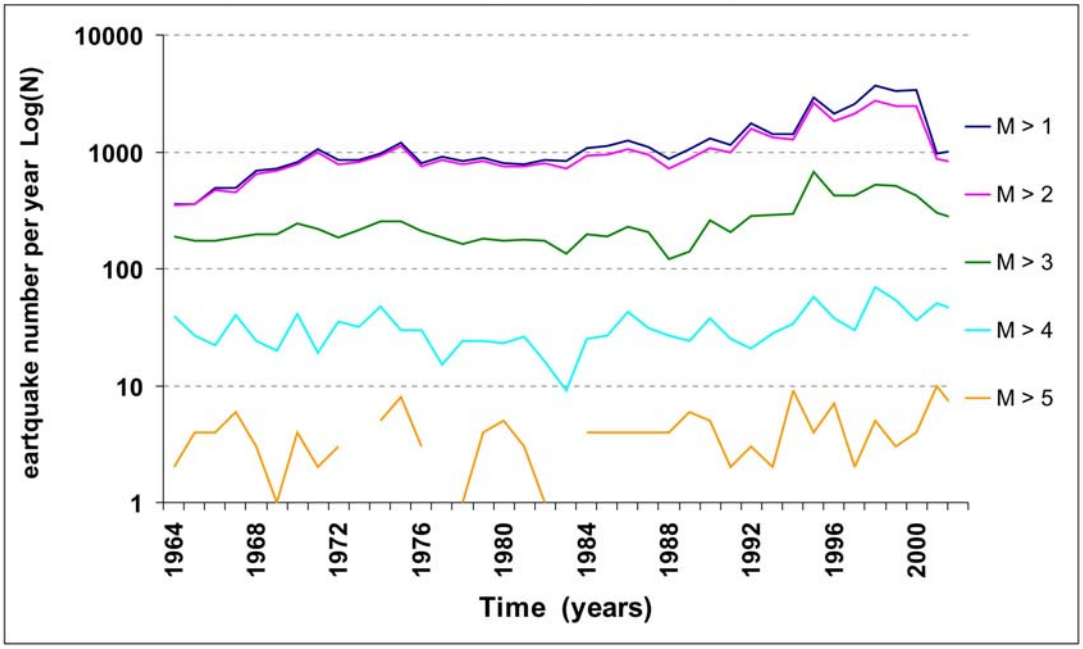

Figure II.6: Number of detected earthquakes per year for various magnitudes.

We tested also magnitude completeness using G-R relation from 1971 to 2002. Magnitudes where binned in interval of 0.1.

The G-R curve, for the time interval from 1971 to 2002, is shown in Fig.II.7. It seems that the cutoff magnitude of our catalogue is Mc ~ 2.5 over this period. Nevertheless, the Fig II.6 shows a clear increasing in the detection of the events of magnitude 2 since 1995 and at a lower scale of magnitude 3. In reality, the detection increasing of small event, very high over a period of 8 years (1995 to 2002) is smoothed by the logarithm scale of the G-R law then it does not allows to detect this particularity. The graph in figure II.6 is more adapted to detect the cutoff magnitude, which is more about magnitude 3 in our case for the period 1971 to 2002.

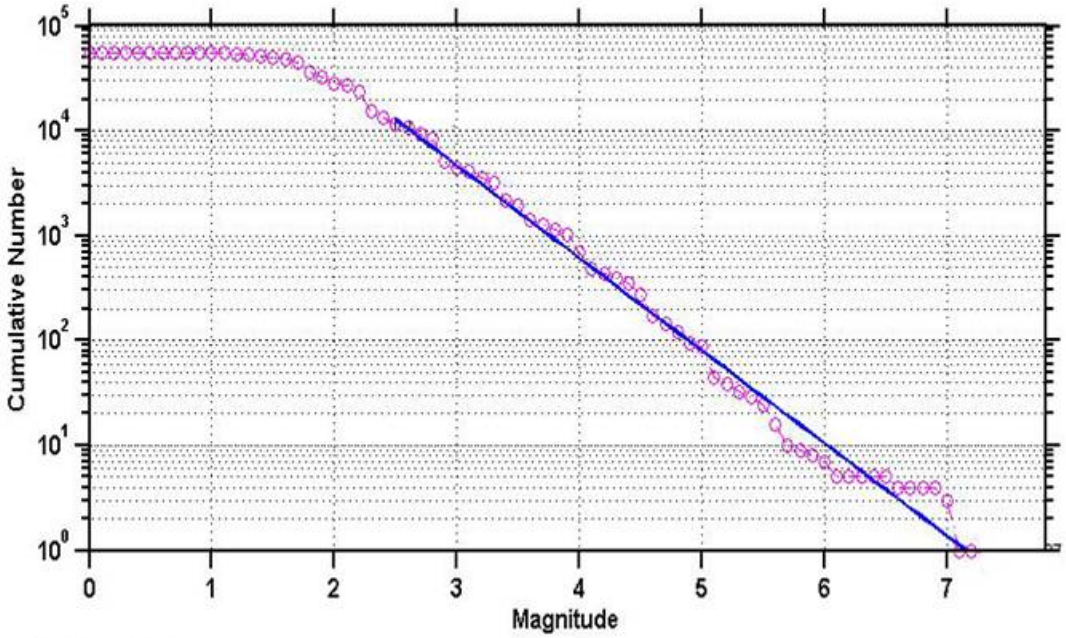

Figure II.7. Gutenberg - Richter law (frequency-magnitude distribution) for the period of 1971 to 2002. The apparent cut off magnitude appears to be Mc = 2.5

II.3.5 Human activity

On the other hand, we must take care to distinguish man made events such as quarry blasts. Possible combination of seismic bulletins with quarry blast is a common problem that all local network operators must deal with. It starts to be more important as the detection level of the seismic network increase that allows us to detect and localize quarry blast as earthquakes, especially explosions at large distances. We separated the quarry blasts and earthquakes using waveform characteristics that are different and recognizable by experienced analysts. This work improved largely the seismic database in which were removed all recognized quarry blasts. Since the installation of infrasound network in Mongolia (2003), it gives us a great chance to discriminate signal of quarry blasts by combining the study of acoustic and seismic signals. The Fig.II.8 shows for example the concentration of quarry blasts (red dots) detected and localized only with the Ulaanbaatar seismic networks.

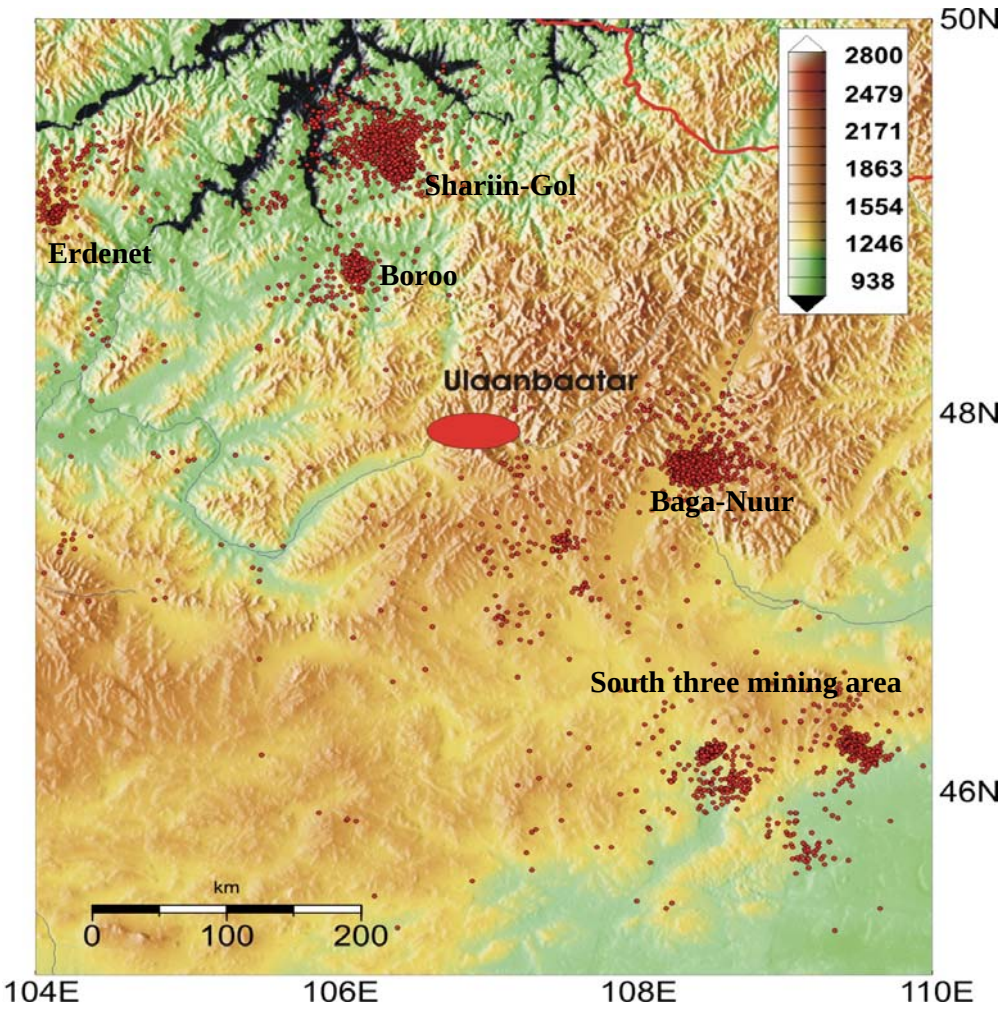

Figure II.8: Map of quarry blasts detected and localized only with the Ulaanbaatar seismic networks. Ulaanbaatar – capital city Mongolia, other names are mining places. The special extension of the quarry blast shows the accuracy of location using the Ulaanbaatar network.

II.3.6 Clustering

The study of the time evolution and the spatial distribution of the seismicity are important to identify and remove aftershocks. If we will not separate the aftershock from the other seismicity, the catalogue will be dominating by main shocks, which produced a large number of aftershocks.

One method is to use time-distance based for aftershock clustering algorithm, which takes into account the fact that duration and spatial distribution of aftershock sequence varies largely for different events (Braitenberg, 2000).

To characterize the aftershocks we used the Reasenberg algorithm (Cluster, 2000). The method of Reasenberg uses a physical approach for the identification of aftershock, which states that each earthquake generates an alteration of the surrounding stress field that may trigger a further seismic event. Depending on a time parameter, this event is associated with the previous event and nucleates in its surroundings a modified stress field. The area and time

extent for which the event is available to trigger a following event is called the interaction zone of the event. The distance for modeling the interaction zone is proportional to the source dimension, scaled by a parameter ***Q***. The source dimensions are modeling from existing empirical scaling relations (Reasenberg, 2000). The temporal extent of the interaction zone is determined with a probabilistic model based on Omori's law, which models the expected rate of aftershocks. The parameter that governs the temporal extent is the confidence level ***P*** (Braitenberg, 2000).

For the clustering in our catalogue, we choose the following parameters:

Mmin = 1.0; ***Q*** = 10; ***P*** = 0.99.

The Fig.II.9 shows the result of the clustering procedure. Here is plotted the number of events per year for the full catalogue (blue line) and aftershock depleted catalogues identified by clustering algorithms (red line). The arrows show the main earthquakes and their date. The correction seems reasonable except for the 04-07-1974 event.

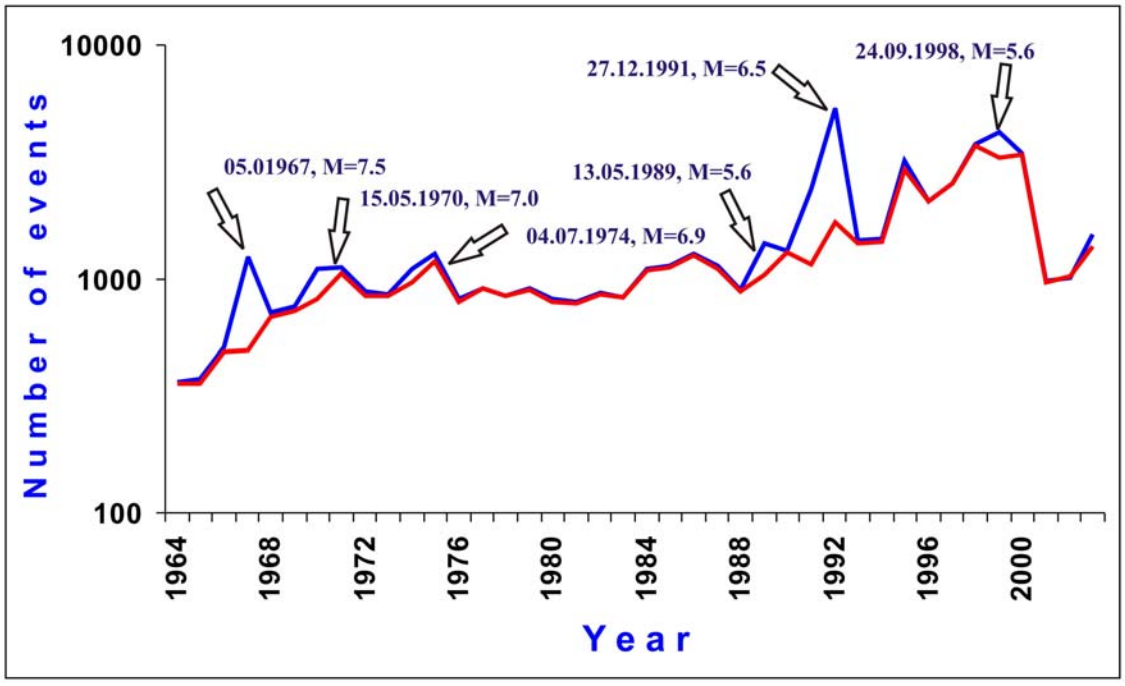

Fig.II.9. The result of the clustering procedure. Here is plotted the number of events per year for the full catalogue (blue line) and for the catalogue when the aftershocks have been removed (red line). The arrows show the main earthquakes and their date.

II.4 The RCAG seismic catalogue

The seismic catalog contains primary data sources for inferring earthquake behavior, testing hypotheses, understanding geodynamic process associated with earthquakes, and many other endeavors (Kagan, 2002). The RCAG seismic catalog contains several thousand events covering whole area of Mongolia and frontline of surrounding countries, from 1902 to present. The time of occurrence, geographical coordinates of the epicenters, the class of accuracy of determination, and the magnitudes are giving in this catalogue.

They are several criteria important for statistical and time evolution study of the seismicity. First, the seismic catalogue should contain homogeneous magnitude determination. As early mentioned, we have reevaluated all local magnitudes using a single homogenous local magnitude law. Secondly, human made activity should be removing from catalogue. Mostly quarry blasts from coal and copper mining could have been included as seismic events in the database. This also has been correct. Third, we have applied some algorithms to characterize aftershocks clusters that do not represent the background activity.

Three periods clearly can be identified in the seismic catalogue of RCAG: historical, early instrumental and instrumental periods.

II.4.1 Historical period

The historical part of the catalogue covers the period from 500 until 1900. The historical data are constrained mostly from paleoseismic structures (active quaternary faults) and macro seismic data. The Russian and Mongolian scientists have done special studies to estimate the parameters using recent surface ruptures of large earthquakes and macro seismic reports. Unfortunately, time and size of earthquakes reported are approximate for these earthquakes. In addition, they were determined using field observations but without using the various modern method to date the age of these events. Not all large active faults have been detected, some have been hided by the erosion and on most of them the last event is unknown. Therefore, we need still to conduct many detailed study of these paleodislocations, to determine age and size of historical earthquakes.

They are 18 paleo earthquakes reported in the historical catalogue of Mongolia from 500 until 1900. Twelve were deduced from paleodislocation and six were constrained from macro seismic observations (Khilko *et al.*, 1985).

II.4.2 Early instrumental catalogue

The early instrumental period consists of data from 1902 to 1964. Between 1957 and 1964, despite 2 stations were installed, the data in the catalogue were insufficient for the analysis. In addition, most of data are coming from different International Seismological Data centers. Therefore, we called this period as "early instrumental". During this period occurred a very high seismic activity in Mongolia. During 1900-1963, occurred four large earthquakes with magnitude 8 and more and also 12 events with magnitude of about 7 (Khilko *et al.*

1985). I have listed the largest and the better characterized events in Table.II.1. That is the case mostly for the to Bolnay earthquake. Schlupp (1996) did a source modeling of Bulnay earthquake and a detailed study of the surface ruptures. That allows us to renew or increase the accuracy of our early instrumental catalogue. He found for Bolnay 455 km long surface ruptures and a magnitude of Mw = 8.3 to 8.5. In addition, he constrained the epicentral position at the junction between the main fault and the Teregtiin fault, a western secondary branch.

Other noticeable information in our data set in comparison to the World data set is the Unegtei earthquake occurred the 1 February 1903 at 09:34. Richter using world seismic network has estimated the Unegtei earthquake with magnitude of 7.5. He located the event in the middle of Hangai dome with a location error of about 500 km. Nevertheless, after it has been displacing by Khilko *et al.* (1985) to the southeast, more than 400 km away, by using macroseismic information. This event is still today wrongly localized in the other published world seismic catalogues.

Table II.1 List of earthquakes occurred in instrumental time.

Date	Magnitude	Length of faults (km)	Vertical displacement (m)	Horizontal displacement (m)
01.II.1903	7.5	-	-	-
09.VII.1905	8.0	190 (160)	(2.0)	(2.5)
23.VII.1905	8.5 (8.3)	455 (455)	2.5 locally	10 (6.5)
10.VIII.1931	8.0	180	3.6	6.5
04.IV.1950	7.0	(2.5)	0.8	-
04.XII.1957	8.1	270	4.0	6.0
07.IV.1958	6.9	(7)	1.0	-
03.XII.1960	6.7	18	0.3	0.1

II.4.3 Instrumental catalogue

A nationwide seismic network, able to localize regional earthquakes, was operating only since 1964 in Mongolia. Since, a relatively complete database was established. Also at this time started intensive exchange of data with Russian seismological centers for local events. The instrumental data base consist of 3 large event with magnitudes more than 7; several large events with magnitude 6 or more and a large amount of moderate and small size earthquakes. At the beginning of the seismological instrumental time, all procedure of interpretation and localization where done manually. Notice that at the beginning of 1991, when informatics and electronic system was intensively developed and used in the world, started at the RCAG the first, and unique, computer for localization. Using this new tool, all seismic data from our database were relocated and reviewed, in the aim to obtain a homogeneous database.

Since the improvement of our seismic network and analyzing system in 1994, we again reviewed all data and the catalogue. At this time, the biggest study was to convert the sizes scale of the earthquakes from energy class to magnitude scale. Other important work we did is the separation between quarry blasts and earthquakes in the database.

After all these modifications, we published a seismic map called "One century of seismicity in Mongolia" with all reviewed data. The seismic map is available at RCAG for

everybody and presents a unique view of the seismicity of the area. I was one main author of this map and managed mostly the correction of our database. Soon we will prepare a publication related to the seismic data of this map and their associated characteristics.

To check the quality of our catalogue, like location and magnitude estimation, we compared them with worldwide earthquake catalogues. The Fig.II.10 shows the comparison between local magnitude Ml used at RCAG and the Mb magnitude published in the NEIC catalogue for seismic events in Mongolia. The difference in magnitude is less than 0.3, which shows the homogeneity of our data and its small difference with the Mb. The Fig.II.11 presents our event localization in comparison with the NEIC localization for teleseismic events. The differences are small so our database does not contain particular wrong epicenter location.

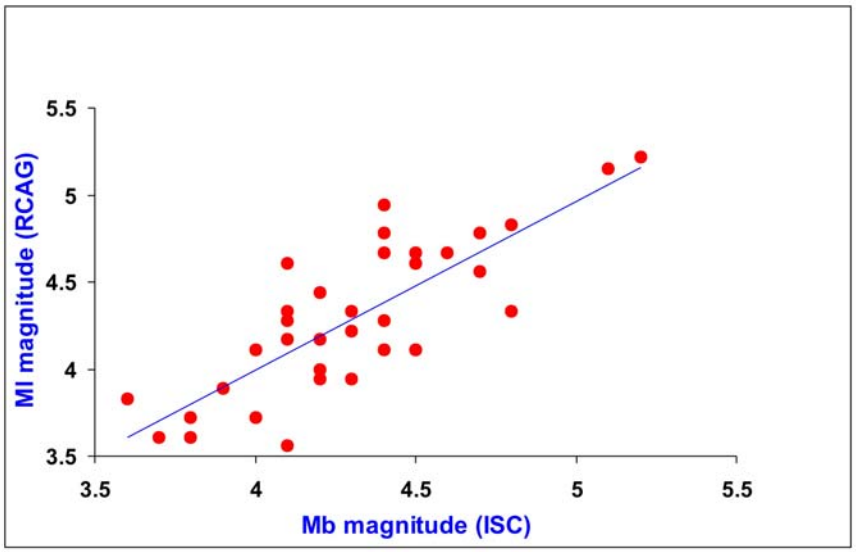

Figure II.10: Comparison between local magnitude Ml used at RCAG and the Mb magnitude published in the NEIC catalogue for seismic events in Mongolia.

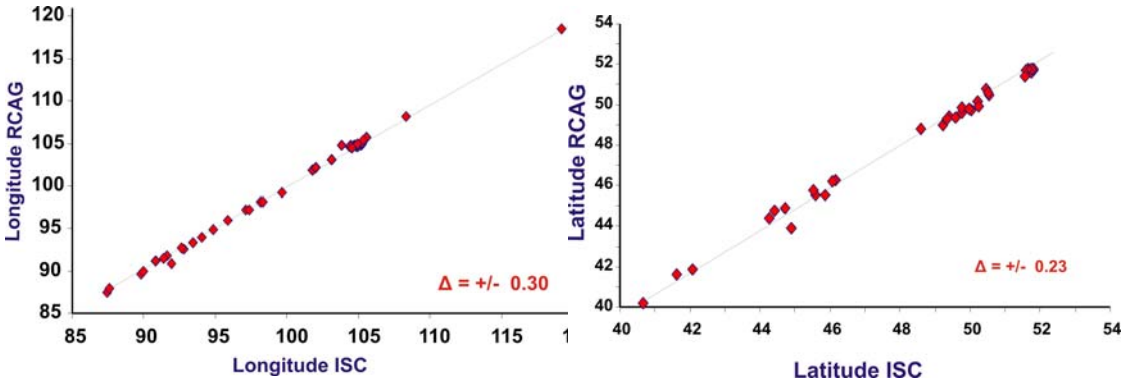

Figure II.11: Comparison of RCAG event localization in comparison with the NEIC localization for Mongolian earthquakes. The scales are in geographical degrees and concern the region of Mongolia

II.5. The seismicity in Mongolia

II.5.1 Global overview

During last century, Mongolia has been one of the most seismic active intracontinental regions in the world with several very large earthquakes. Since 1900, occurred thirty earthquakes with magnitude M≥7, four of them with magnitude M≥8: Tsetserleg 1905, 190 km of surface rupture; Bolnay 1905, 455 km; Fu-Yun 1931, 180 km; Gobi-Altay 1957, 270 km.

The map 'One century of seismicity in Mongolia' (Figure II.1) published by RCAG and DASE, illustrate the earthquakes that occurred between 1900 and 2000. We plotted all known earthquakes including aftershocks. For early instrumental data, before 1964, we included only events with magnitude more than 6.5 detected by the various World Data Centers. The magnitude of each event was recalculated using the new attenuation law recently determined for Mongolia. We did not included historical data on this map because the accuracy on parameters, as location and magnitude, is very low and not comparable to the information that we have on the instrumental data.

From 1900 to 1963 are reported more than 300 earthquakes, with magnitude between 3.5 and 8.2 including the four large events. The figure II.12 shows the maximum magnitude distribution with time. We can observe the occurrence of the largest earthquakes; four earthquakes with magnitude M≥8, eight events with M≥7.0 and several tens earthquakes with magnitude M≥5.5. Fig.II.13 shows G-R relation calculated with magnitudes M > 5 between 1902 and 2002. We can observe two different slopes that illustrate the anomalous occurrence of magnitude M≥8. We obtained ***a*** = 6.3 and ***b*** = 0.8 for magnitudes between 5 and 7 (Fig.II.13a) and ***a*** = 5.1 and ***b*** = 0.6 for magnitude including M=8 (Fig.II.13b). This low value of ***b*** is consistent with a relatively high number of large earthquakes and parameter "***a***" characterizes the number of events.

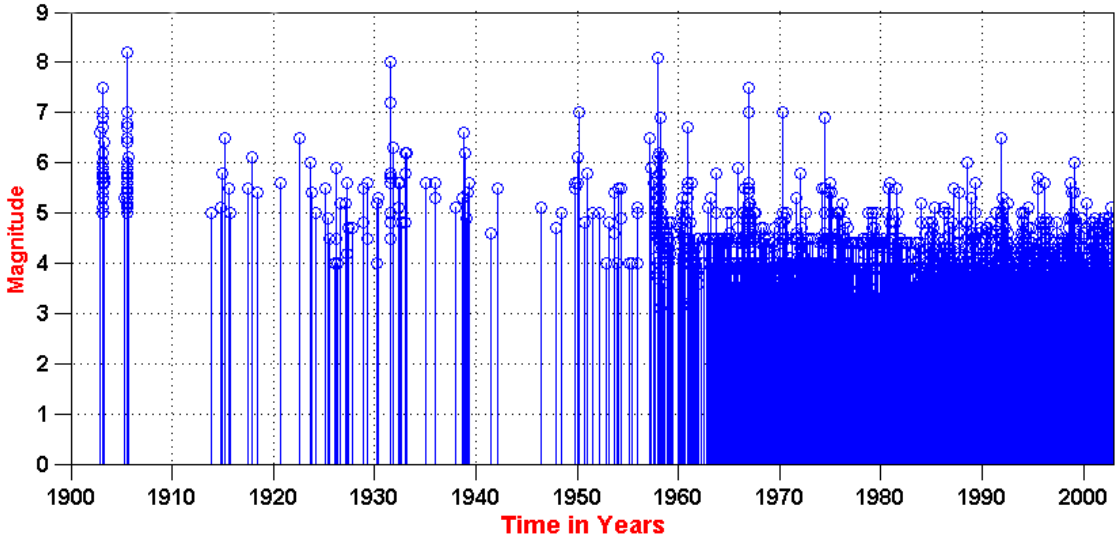

Figure II.12: Distribution of the maximum magnitude observed in Mongolia function of time.

.

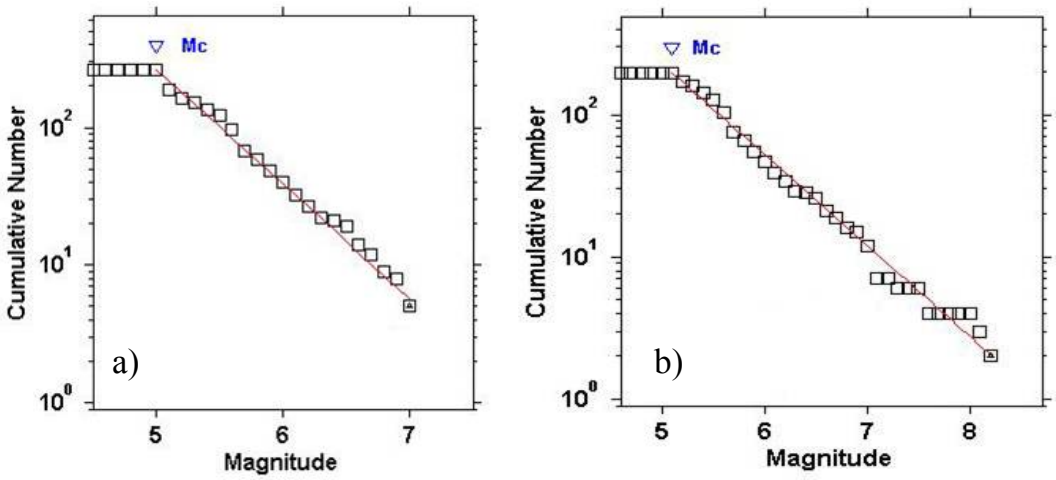

Fig.II.13: Gutenberg-Richter relation using magnitudes M > 5 between 1902 and 2002. We can observe two different slopes, which illustrate the anomalous occurrence of magnitude M≥8.

Since 1964, our seismic network recorded more than 50 000 earthquakes with magnitude between 1.5 and 7.5. Most of the events with magnitude below 2.5 were recorded recently or locally in favor of good station coverage. The Fig.II.14 shows the cumulative number of events function of time. We can see the increasing of detected events starting from 1994, when our network was upgraded. The increasing in 1991 is related to the numerous aftershock related to the M=6.5 event.

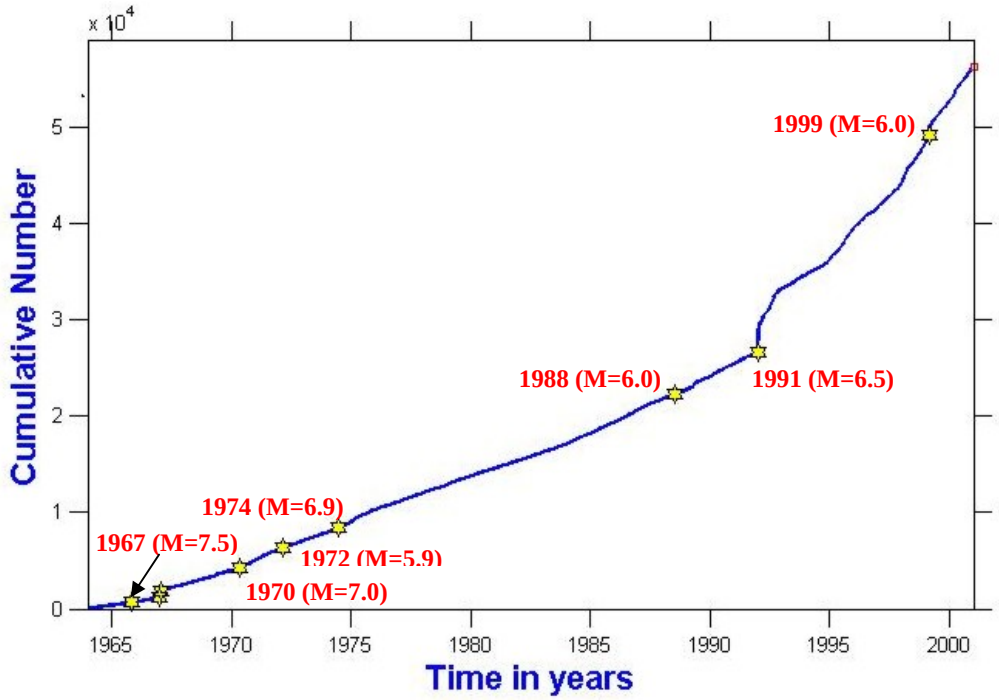

Figure II.14: Cumulative number of events versus time. We can see the increases of detected events starting from 1994 when our network has been upgrade.

Seismic activity of the Mongolia is highly controlled by active tectonic structures (Fig II.1). The concentration of earthquakes is often related to the active faults. Some of these structures where described in the previous chapter. On the other hand, high seismic activity is clearly associated with the fault on which occurred the large earthquakes during the last century. The relationship between aftershocks, produced by large earthquakes, and latter seismic activities along these zones are interesting. It is well known that large earthquakes of Mongolia and surrounding areas produce large number of aftershocks. For example, Busiin-gol earthquake (27th December 1991) produced several thousand aftershocks and also the Chuya earthquake, 23 September 2003, where we can still observe, two years after the main shock, many aftershocks. Chuya earthquake will be discussed later in details.

The seismicity itself helps us to detect some active tectonic structures not visible at the surface. Of course, it will depend of the accuracy of epicenter locations and the delectability of our seismic network. However, the general view of the distribution of the seismicity in Mongolia follows and traces several important active structures. For that purpose, it would be very useful to increase the density of our network to get a more precise image of the seismic activity and the active tectonic structures.

Most of events are located in the west and the north Mongolia as the Khubsugul active rifting zone and the Altay transpression zones. In the south Mongolia, the activity is concentrated near the Gobi-Altay and Gurvan-Saikhan zones. The center of Mongolia, the Hangai dome, looks relatively aseismic and we can clearly track the boundary of the dome by its seismic activity as at the north and east border of Hangai dome where are active Bolnay and Mogod zone. South of Ulaanbaatar, at around 180-250 km, is a clear EW seismic elongated zone near the Deren city (fig II.5). In the eastern part of Mongolia, the seismic activity is low.

II.5.2 Regional description

Before zooming on the Altay area, I will shortly describe the main seismic zones of Mongolia. After, I will discuss spatio-temporal variations of the seismicity and the radiated energy. The Fig.II.15 presents the location of the main seismic active zones.

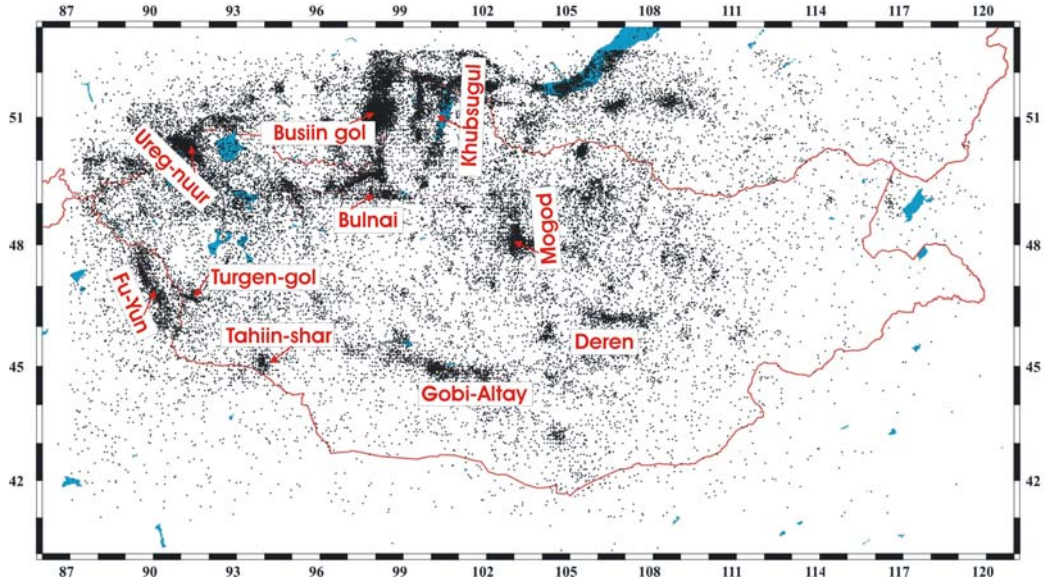

Fig.II.15. The location and names of the main seismic active zones.

Gobi-Altay zone is oriented EW and is associated to left-lateral displacements. An earthquake with magnitude of 8.1 occurred 4 December 1957 and produced about 270 km long surface rupture (Khilko *et al.*, 1985; Ritz *et al.*, 2003). A concentration of earthquake or aftershocks is along this fault.

Khubsugul and Busiin-Gol zone is one of extension zone. The area produces high seismic activity and the largest earthquake occurred on 27th December, 1991, called Busiin-Gol, with a magnitude of Mw = 6.5. The seismicity of Khubsugul zone is complex. There are three seismic NS basins: Busiin-Gol, Darhad and Khubsugul lake area. Most of epicenters are concentrated in the Busiin-gol zone connected with the Sayan active zone to the west and the Baikal active rifting zone to the NE.

Bulnay zone lies between Hangai Dome and Khubsugul extensional zone. From geological and seismotectonic data, the left lateral strike-slip fault is predominant. In this zone occurred two large earthquakes, Tsetserleg earthquake (July 9, 1905) with Mw = 8.0 and 190 km of surface ruptures and the Bolnay earthquake with Mw = 8.3 to 8.5 and 455 km of surface ruptures (Schlupp, 1996). The seismicity seems connect the Tsetserleg fault with the Busiin-Gol rifting. The seismicity recorded along Bolnay fault is more concentrated in the middle of the structure. Notice that they are still aftershocks detected one century after the main event. Near the western end of Bolnay fault, the seismicity is concentrated at the junction with the Teregtiin fault.

Mogod zone is oriented N-S with right lateral active faulting. On the 5th January, 1967 a large earthquake occurred with a magnitude of Mw=7.2 and produced more than 45 km of surface rupture (Bayasgalan, 1999). Mogod zone shows a local high concentration of earthquakes.

Deren zone. The zone is located around 180 km south from Ulaanbaatar city. The largest earthquake in this region was the "Deren" event which occurred the 24th September, 1998 with a magnitude Mw = 5.6 (NEIC) and a strike slip mechanism on an EW or NS unknown fault. This earthquake strongly felt by the population of Ulaanbaatar city. The seismic activity of Deren zone is oriented EW. Nevertheless, this direction is not consistent with the observed surface ruptures of the area. Indeed, the Deren reverse fault strikes in NW-SE direction along more than 30 km.

II.5.3 Normalized energy release

To study the evolution with time of the seismic activity, and how the energy is released, we consider the quantity E, deduced from the magnitude and normalized by the smallest magnitude considered, according the formula:

$$E = 10^{d(M - M\,\min)}$$

E represents the energy released by each event and is normalized to the energy of the smallest event considered in the analysis. In our case we choose Mc = Mmin = 2.5.

d is an empirical parameter of the energy-magnitude relation. We used ***d*** = 1.5 as given by Gutenberg and Richter (1956).

The Fig.II.16 presents curves of the monthly energy release E (t). The energy release exhibits mostly constant background rate which is between $1*10^{14}$ – $5*10^{14}$ J until 1990. It increased slightly after 1991. In addition, they are sporadic periods of strong energy release. The pick of seismic energy release is mainly due to the occurrence of large earthquakes as Mogod earthquake 1967, M=7.2; Tsagaan-Shiveet 1970, M=7.0, Tahiin-Shar 1974, M=6.7; Buteel 1989, M=5.6; Busiin-Gol 1991, M=6.5 or unnamed earthquake 1999, M=6.0. The highest seismic energy released in Mongolian since 1964 is related to Mogod, Tsagaan-Shiveet, Tahiin-Shar and Busiin-Gol earthquakes.

Since 1992, just after the main Busiin-gol aftershock sequence, occurred a slightly increasing of released energy. This increasing cannot be connected to the network evolution or the delectability increase as we normalized to the Mmin = 2.5 which mean that the increase of the delectability of small events will have no impact. It could be connected to the Busiin-gol large earthquake (M= 6.5) followed by many aftershocks still up to now on this extensional region. Other possibility is that Busiin-Gol earthquake triggers other seismic active zones. In that case, we should observe an increase of energy release somewhere else. Therefore, we estimated the energy release at several seismic zones (Fig.II.17). The average annual energy releases estimated in Gobi-Altay and Busiin-Gol zones were about $5*10^{15}$ – $8*10^{15}$ J/year. Others are generally lower and vary between $1*10^{15}$ to $3*10^{15}$ J/year. The periods, when energy release increases strongly, are clearly connected with large earthquakes and the general increase of energy release since 1992 is mainly related to the Busiin-Gol area.

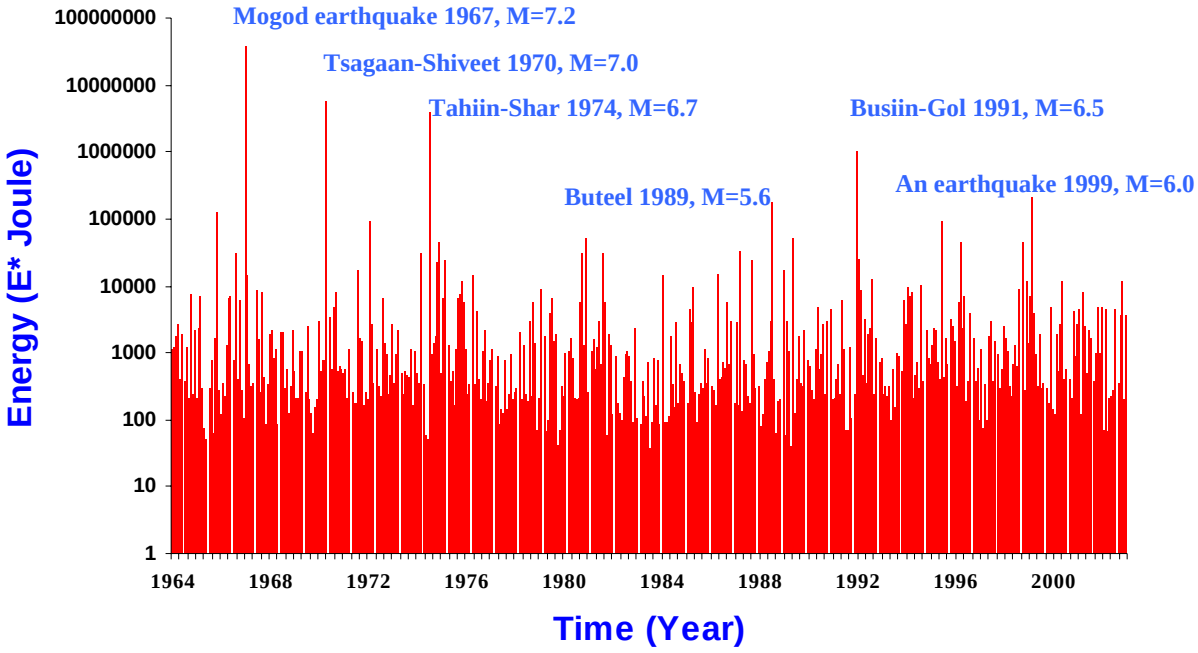

Figure II.16 Histogram of the monthly energy release E* (t). The unit of energy scale is E = E* x $10^{11.7}$ Joule

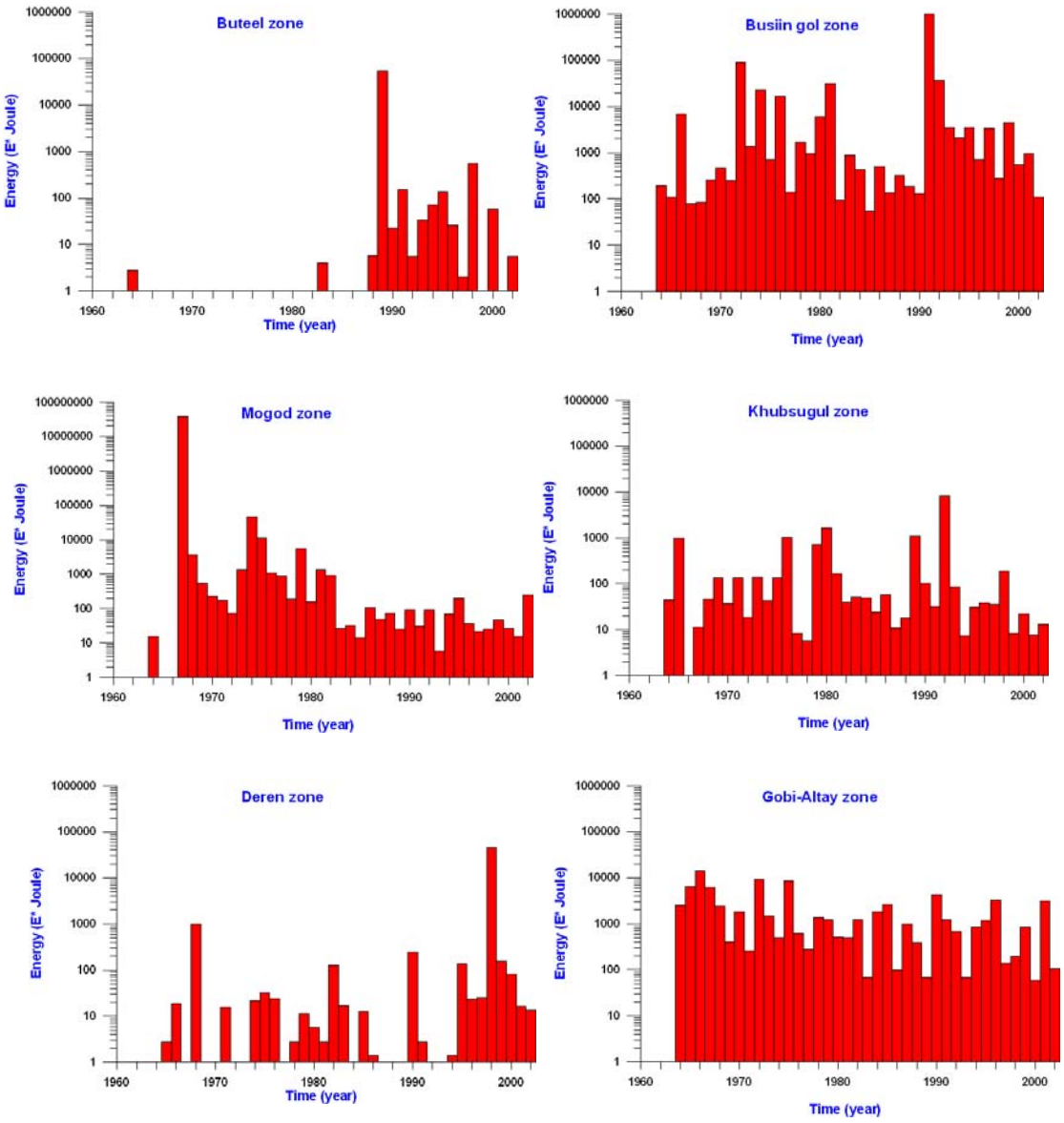

Figure II.17 Energy release E* (t) per year for each active zone in Mongolia. The unit of energy scale is $E = E^* \times 10^{11.7}$ Joule

One interesting question is: Are these dense seismic activities only after the main shocks (aftershocks) or are they continuous (background activity). To test this idea we will work on clustered events. It is true that strong earthquakes in Mongolia produce large number of aftershocks. Busiin-gol earthquake in 1991 produced more than 4000 aftershocks; Mogod earthquake in 1967 more than 700 aftershocks, that represent just a part of the aftershocks because of the lack of stations available for a detailed local survey. Fig.II.18 shows the histogram of these clustered events in comparison to the regional seismicity from aftershock depleted catalogue between 1964 and 2002. For the events that occurred in Mogod region, 36% consist of aftershocks and for Busiin-Gol region the aftershocks percentage reach 69%. For Ureg-nuur only 5 % and for the Deren active region only 7 % consist of aftershocks.

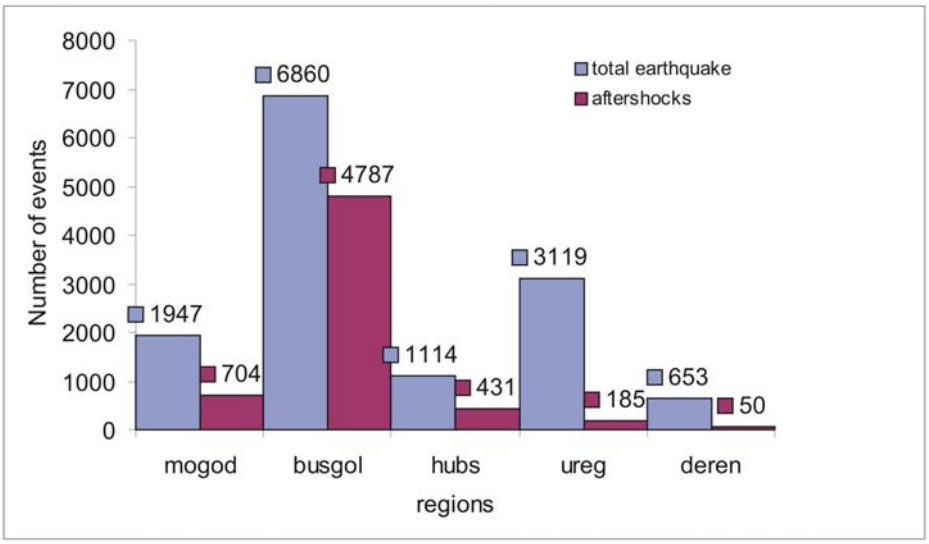

Figure II.18 Histogram of the events related to 5 earthquakes (aftershocks) in comparison to the whole seismicity recorded on the same area.

II.5.4 B value

An important way to understand the time evolution of the seismicity in various regions is to test the variation of b and a value of G-R law at the scale of whole Mongolia and for specific regions (local areas).

To analyze the seismic activity, we used the Gutenberg Richter relation:

$$Log(N) = a + bM$$

Where: M is the minimum magnitude in the data sample. N cumulative number of events in a time intervals with magnitude larger than or equal $\boldsymbol{M}$; "b" and "a" are constants (Gutenberg and Richter 1944).

Generally, the b value will show how the stress changes relative to the tectonic behavior of the region. Scholz (1968) and Wyss (1973) indicated that an increase in stress induces a decrease of the b value. Richter-Gutenberg mentioned that the b value more related to the tectonic behavior rather than to the seismic level. Generally, at the world scale, b value is stable and is around 1.

The a value characterizes the level of seismicity in a region. In contrast to the b value, a value can vary strongly spatially since it depends more on the density of the seismicity than on the tectonic behavior.

Two main methods are used to estimate the b value, which are the least square estimation and the maximum likelihood methods. The method used in this study is Utsu's maximum likelihood methods, which maximize the number of events, used.

$$Log(N) = \frac{Log(e)}{Md - Mc}$$

Figure II.19 shows magnitude - frequency relation. We used all data with magnitude more than 2.0 recorded between 1964 and 2002. Magnitude interval was choose as Md = 0.1. Data completeness is at magnitude Mc = 2.5. At the scale of whole Mongolia, we estimated a rather low b = 0.80 value and high seismic activity a = 6.1. This low b value shows the frequently occurrence of large earthquakes in Mongolia, even since 1964.

Now we test the yearly variation of these values. The Fig.II.20 presents annual variation of a and b value. The b value is most of time constant at b = 0.8 and its variation is less than 0.1. The a value varies in two stages. From 1971 until 1990, average a value was relatively constant with = 4.0 but after 1990, it clearly increased between 4.5 and 5.0. This high value can be correlated to the seismic activity which started in 1991 when numerous events with magnitude 5 and more occurred on the territory (and their related aftershocks), particularly in the Busiin-Gol area.

Then we applied this calculation for each active zone with the same magnitude and time range of data set. Table II.2 and Fig.II.21 show estimated b and a values for the various seismic active regions characterized by different tectonic behaviors.

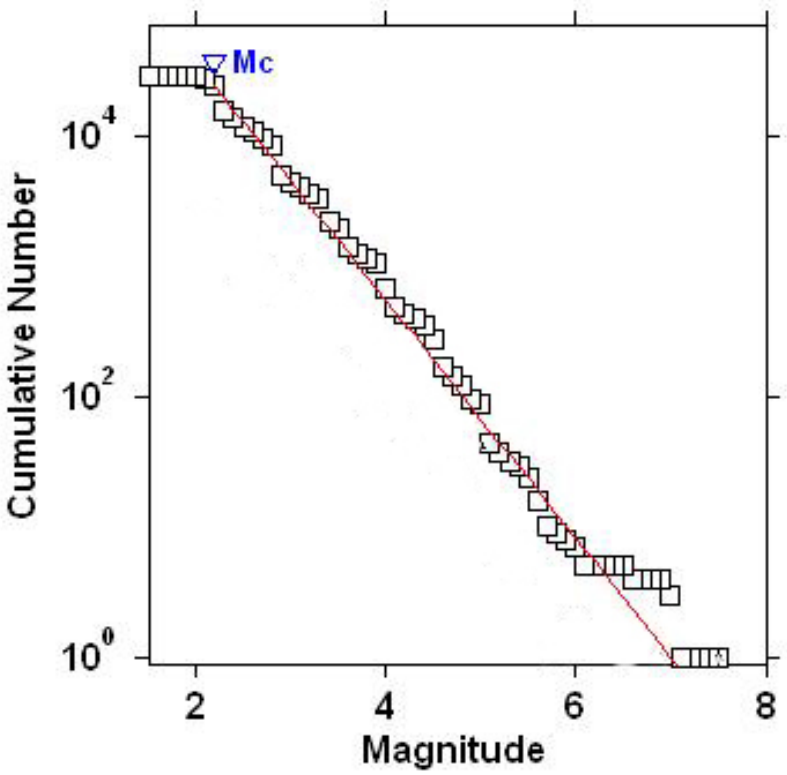

Figure II.19 Magnitude– frequency relation. We used all data with magnitude more than 2.0 recorded between 1964 and 2002. Magnitude interval was choose to Md = 0.1. Data completeness is at magnitude Mc = 2.5.

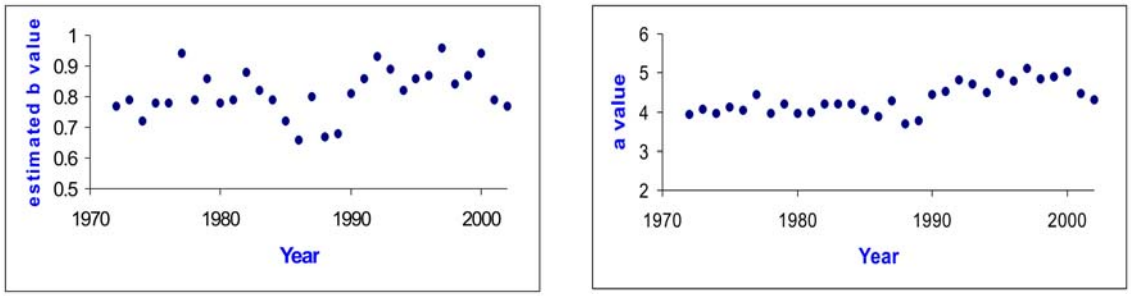

Figure II.20 Annual variation of b and a value for the whole Mongolia. Parameters are the same than in Figure II.19.

Table II.2. b and a values obtained in the different seismic active zones

Zone name	b value	a value
Whole Mongolia	0.8	6.1
Busiin gol	0.9	5.3
Buteel	0.7	3.3
Deren	1.0	4.6
Gobi-Altay	0.8	5.0
Khubsugul	0.95	5.1

Estimated a and b value show that the dense seismic activity is concentrated in the northern part of Mongolia in connection with the Busiin-Gol and Khubsugul regions. These zones are characterized by very high seismic activity and low stress accumulation. This could be the reason why did not occurred large earthquakes in these zones until now; the maximum magnitude being 6.5. For the Deren region, we estimated a higher "b" value (1.0) than for the whole dataset of Mongolia. For the other zones, the average b value is 0.8 that is the same than for whole Mongolia.

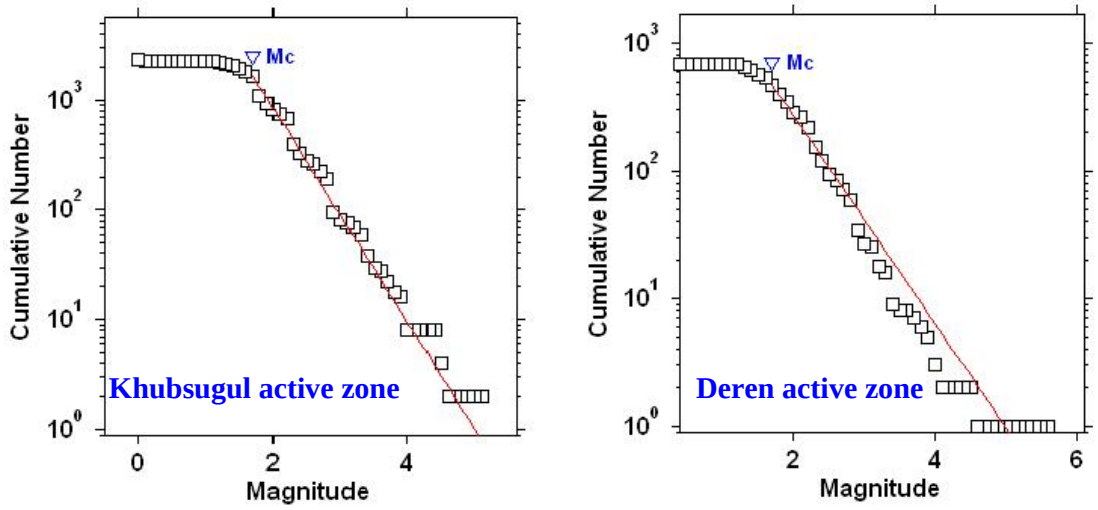

Figure II.21: Estimated b and a value for the various seismic active regions with different tectonic behaviors. Name of active zones are given on each graph.

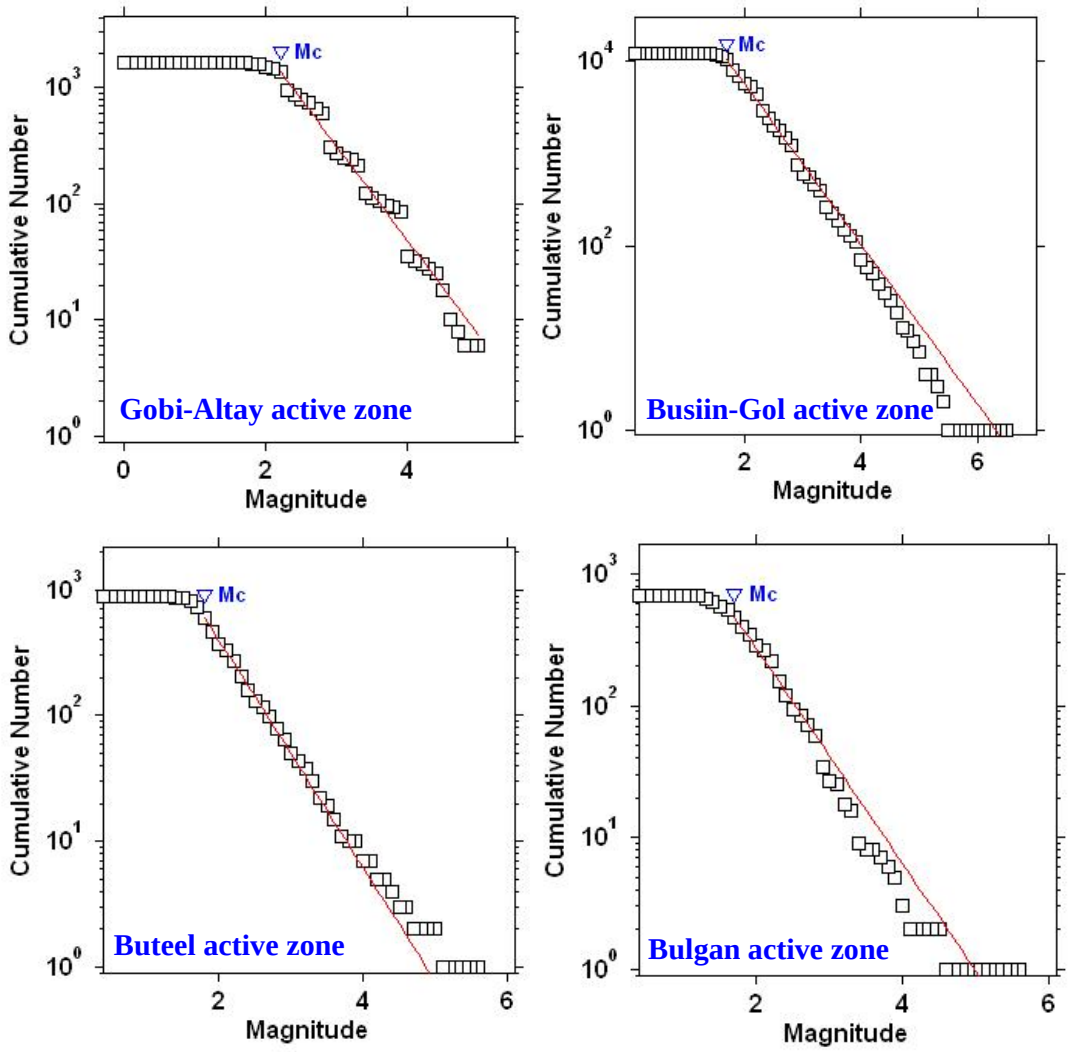

Figure II.21: Continued

II.6 Seismicity of the Altay region

The Altay region is one of the seismic active regions of Central Asia. Since 1903 occurred in the region 60 earthquakes with magnitude more than 5.5 and several earthquakes produced surface ruptures and landslides such as during Fun-Yun, Ureg-Nuur, Tahiin-Shar and Chuya earthquakes (Fig.I.22a)

Between 1964 and 2002, about 30% of known earthquakes in Mongolia occurred in Altay region including two events with magnitude 7 and three with magnitude 6. The numbers of focal solutions are relatively poor, except for the Chuya region (Fig. II.22b). Focal solutions are mainly showing right lateral deformation, but some complexities appear with reverse faulting in some parts.

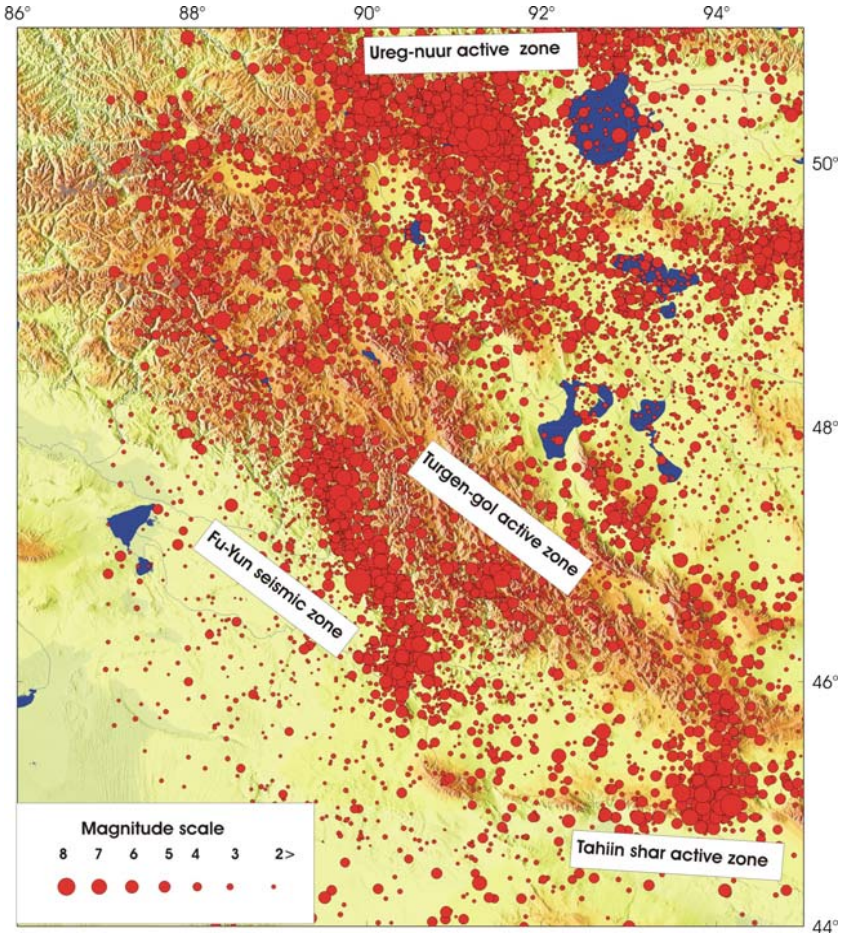

Figure II.22a. Seismic map of the Altay range extract from Fig II.1.

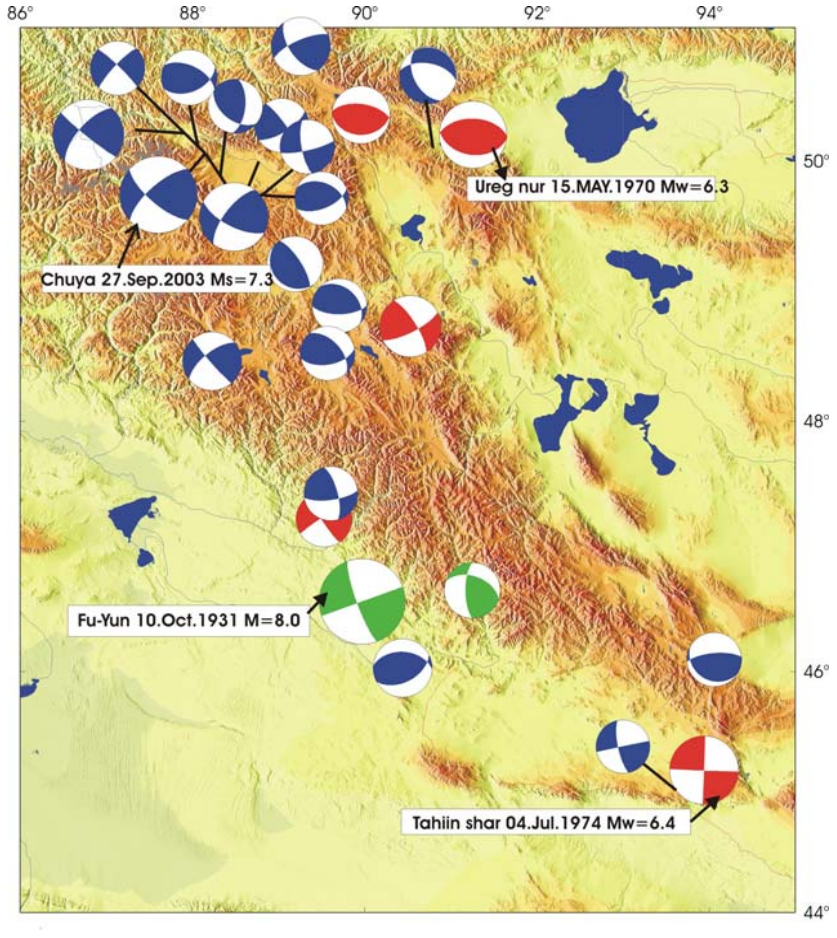

Figure II.22b. Fault plane solutions of earthquakes in the Altay range. The colors show origins: red - body wave modeling, blue - HRV CMT, green - first motion solutions

Figure II.23a shows cumulative number of detected events with time in Altay region. Annual number of events in Altay is mostly constant until 1998. After 1998 and the installation of new modern seismic stations, we could increase the number of detected events. Figure II.23b shows Gutenberg-Richter relation for Altay zone. Data used consists of events with M ≥ 2.0 recorded between 1964 and 2002 in the Altay. The magnitudes are binned Md =1. Data follows a G-R linear law except magnitude M=6, which are too few. It means that earthquake with magnitude M=6 were less than expected. We can not consider that we missed some of them as event of magnitude M=6 must be detected by our network or the world seismic network. The estimated b value for Altay is $b = 0.7$ and $a = 5.2$. This shows that Altay zone is associated with high seismic activity and is the place of frequently big earthquakes.

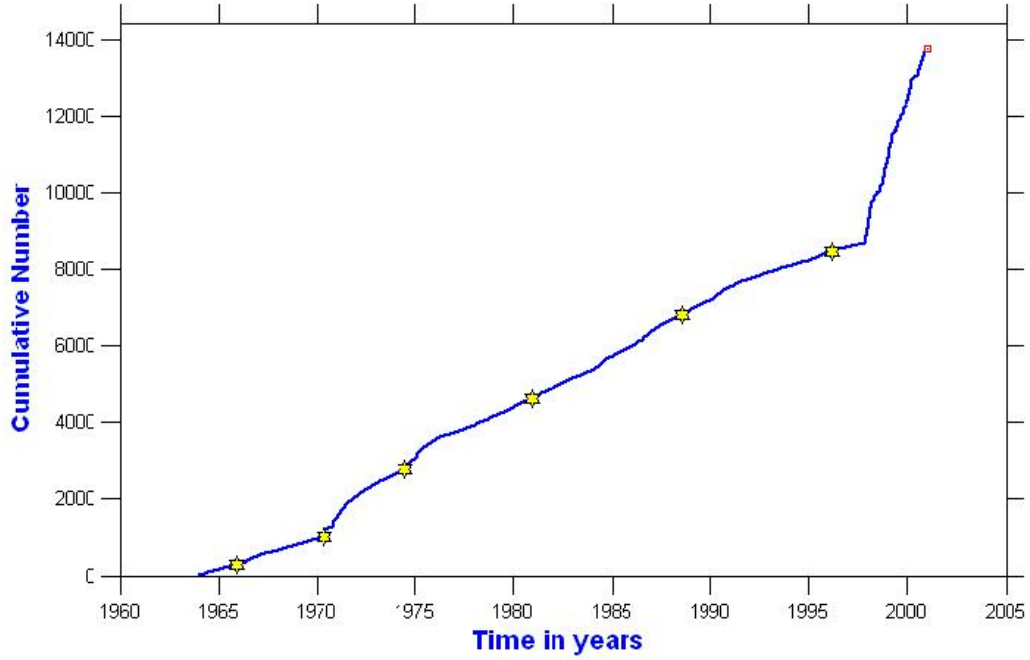

Figure II.23a Cumulative number of detected events with time in Altay region.

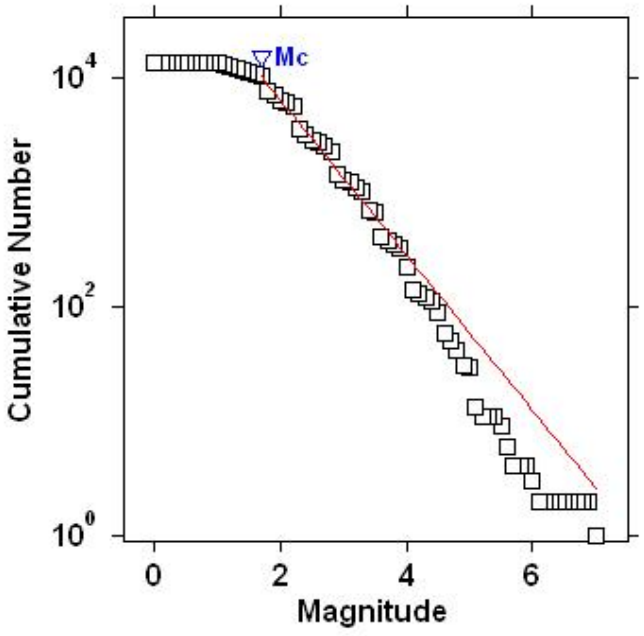

Figure II.23b: Gutenber-Richter relation for Altay zone. Data used consists of events with M ≥2.0 recorded between 1964 and 2002 in the Altay.

II.6.1 Fu-Yun zone

Fu-Yun zone, located at the southwestern end of Altay range, is associated to the great Fu-Yun earthquake with a magnitude of 8, 1931. Details about tectonic characteristics are described in Chapter I. The region is dominated by right lateral strike slip faults that are due to compressional tectonic regime. Since the Fu-Yun large earthquake, we observe high seismic activity following the surface ruptures produced by the 1931 earthquake (Fig.II.24). General trend of seismic activity is oriented NW-SE, except near latitude 46.5°N where it changes to NS. The larger earthquakes occurred at the northern end of the rupture. It could be connected to the prolongation of the fault to the north.

The energy release along the Fu-Yun zone, between 1964 and 2002, is shown in Fig.II.27. At the beginning of this period, the energy released deduced from the detected events is rather stable in time with value of about $3*10^{14}$ J/year. Sharply it increased in 1989, correlated to new moderate earthquake in the range. Then the increase is again significant in 1998, but then mostly due to the improvement of the seismic detectability. Data of Fu-Yun zone is considered to be complete over this region for magnitude larger than 2.5. By using MLE *(Maximum Likehood Estimation)* calculation, we estimated for the Fu-Yun zone b=0.8 and a = 4.4 (Fig.II.28).

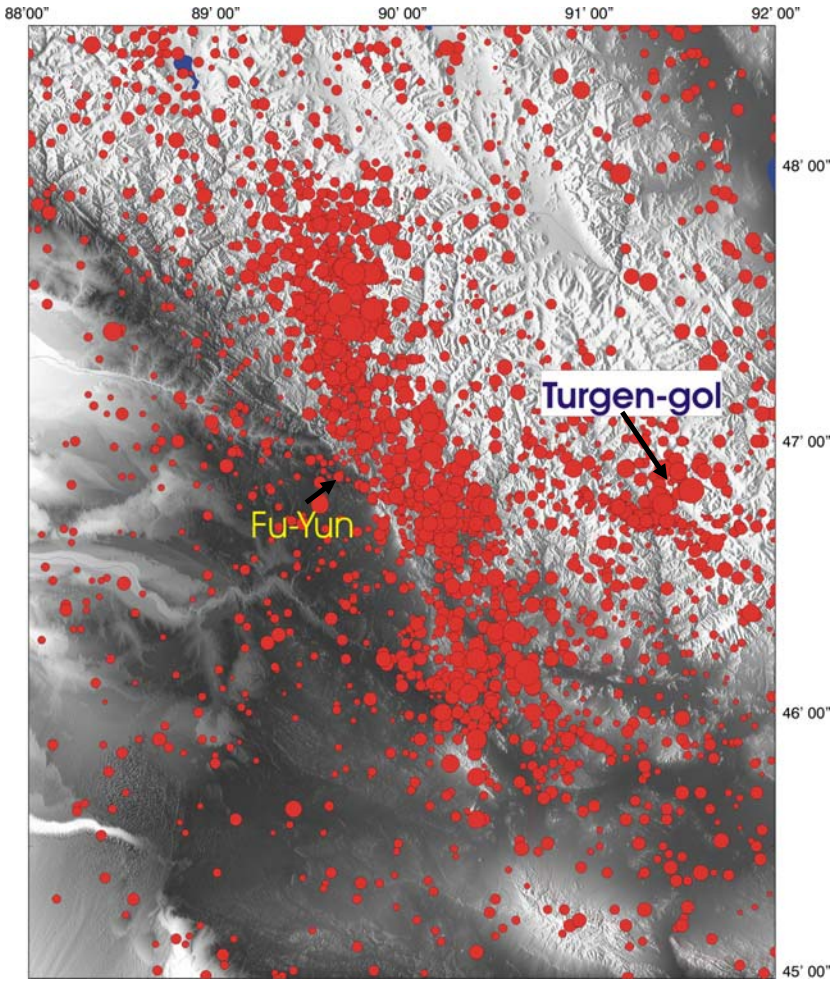

Fig.II.24 Known seismicity of the Fu Yun and Turgen-gol active zones

II.6.2 Ureg-nuur zone

Ureg-nuur zone is located at the Northern end of Altay range where it borders the Sayan Mountains. The zone expresses dominantly compression structures. The 15th May, 1970 an earthquake (50.17°N, 91.25°E) occurred on this zone with a magnitude M=7.0. Khilko *et al.* (1985) reported a short surface rupture associated to the earthquake. The ruptures consist of a zone of cracks striking EW over a distance of 6-8 km (Baljinnyam *et al.* 1993). Bayasgalan *et al.*, (2005) reported that main thrust fault did not reach the surface or maybe has not been found, because the area is very remote from main cities. The Fig.II.25 presents the seismicity of the region. The epicenters are following active structures and they are mostly concentrated along thrust faulting.

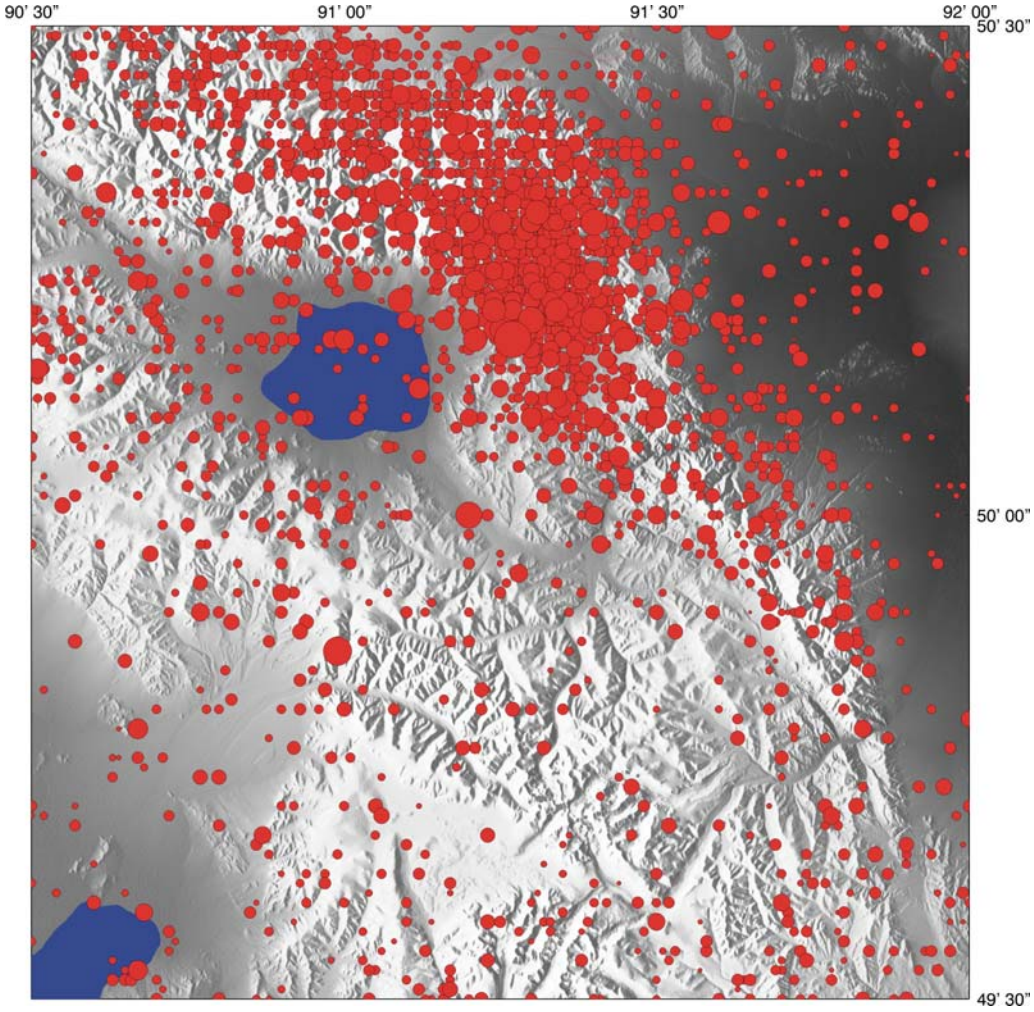

Fig.II.25. The seismicity of the Ureg-nuur region. The earthquake epicenters are following active structures and they are mostly concentrated along thrust faulting.

Seismic radiated energy releases are shown in Fig II.27. The histogram shows two significant earthquakes: Ureg-Nuur with magnitude 7.0 and other one occurred in 1976. After

these two events, rate of energy release is more or less stable and average value does not differs from others zone with E = $3*10^{14}$ – $4*10^{14}$ J/year. The catalogue is almost complete for M > 3 for Ureg-Nuur region. We estimated the G-R values as $b = 0.8$, $a = 4.6$ (Fig.II.28).

II.6.3 Tahiin-Shar active zone

Tahiin-Shar active zone is located south end of Altay range. Khilko *et al.*, (1985) described the coseismic ruptures as a system of ENE ruptures with an overall length of more than 17 km. The general forms of en-echelon mole tacks and tension cracks show left-lateral strike-slip displacement up to 0.4-0.5 m. Along the base of a hill were observed vertical displacements up to 0.4-0.5 m.

The Fig.II.26 shows observed seismicity of the region. Most of events are concentrated next to the epicenter of Tahiin-Shar large earthquakes.

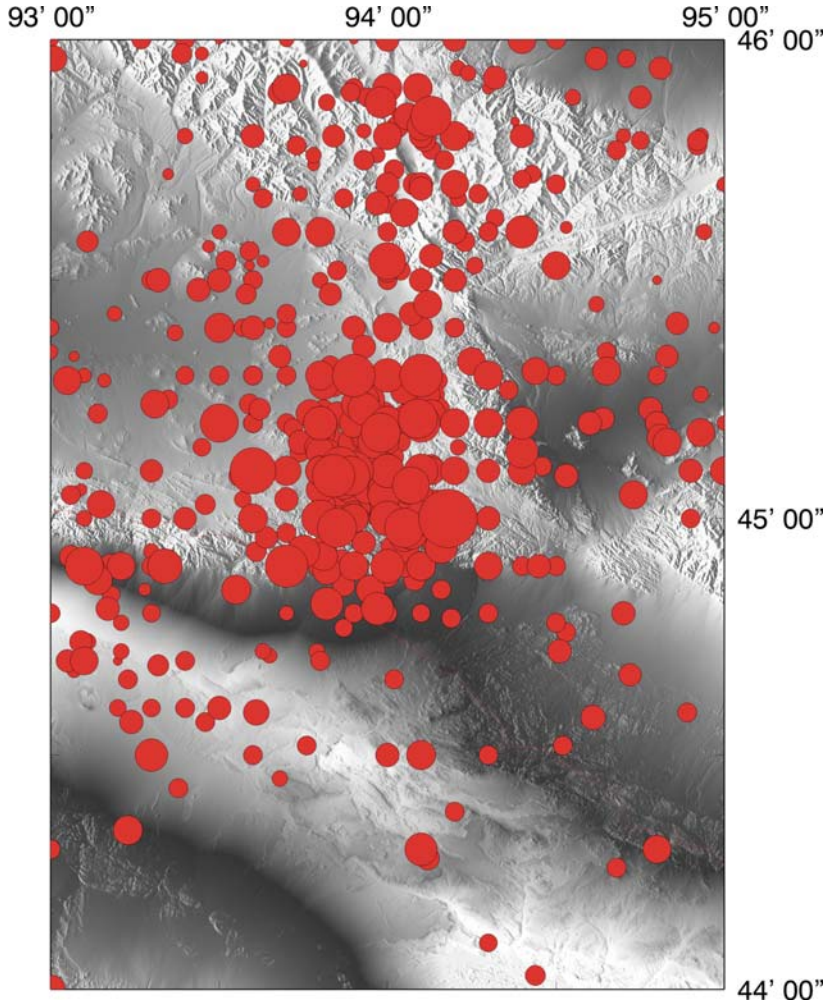

Figure II.26 Seismicity of the Tahiin-Shar region.

Our data set of this region is complete, as for the whole Mongolia, for magnitude more than 3.0. Energy releases are shown in Fig.II.27. The yearly energy release is low except between 1974 and 1976 which is connected to the large earthquake with magnitude M = 6.7.

We estimated b = 0.8 and a = 4.9, which is consistent with the normal average value of Mongolia (FigII.28). Notice that the RCAG has no available station at the south of the area, therefore, the accuracy of the epicenters are lower than for the other actives zones.

II.6.4 Turgen-gol active zone

This area is one of less studied region of Altay. The Turgen-gol fault, oriented NW-SE, is clearly visible on the satellite image. The seismic map (Fig.II.24) shows a linear concentration of earthquake along the main direction of the structures but also some activity is observable at the NE where relatively large earthquakes occurred. Notice that the accuracy of the localization is still limited because the area is outside of our seismic network.

The energy releases (Figure II.27) shows three clear pick in 1975, 1995 and between 1998 -2000. The third pick is connected to the evolution of the network but the other two are correlated with moderate size earthquakes. The event of 3 March 1975, magnitude M=5.4 is the largest event recorded in this area. The G-R relation shows that magnitude M < 3.0 are not completely detected for this region (Figure II.3.28). So we used a cutoff magnitude Mc=3.0. We obtained b = 0.8 and a = 4.0. Relatively, Turgen-gol zone is less active than other zones.

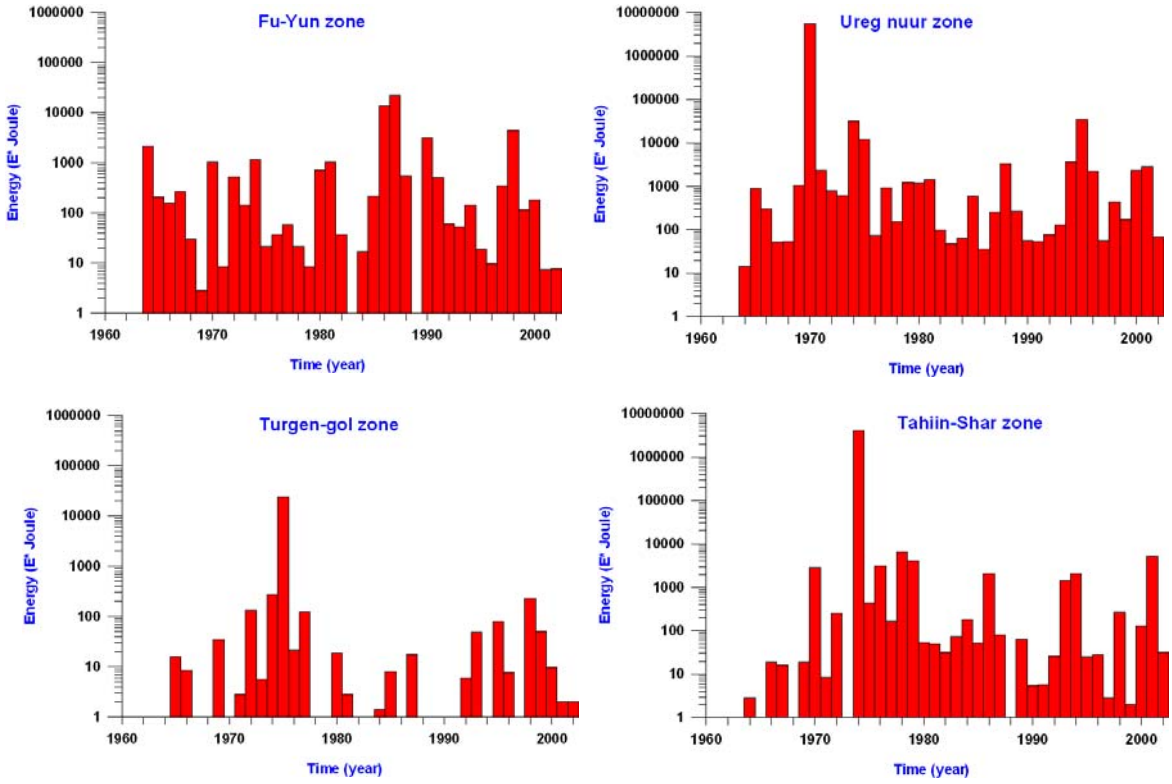

Figure II.27: Energy releases between 1964 and 2002: Fu-Yun, Ureg-nuur, Tahiin-Shar and Turgen-gol active zones. Where E is E=E* x $10^{11.7}$

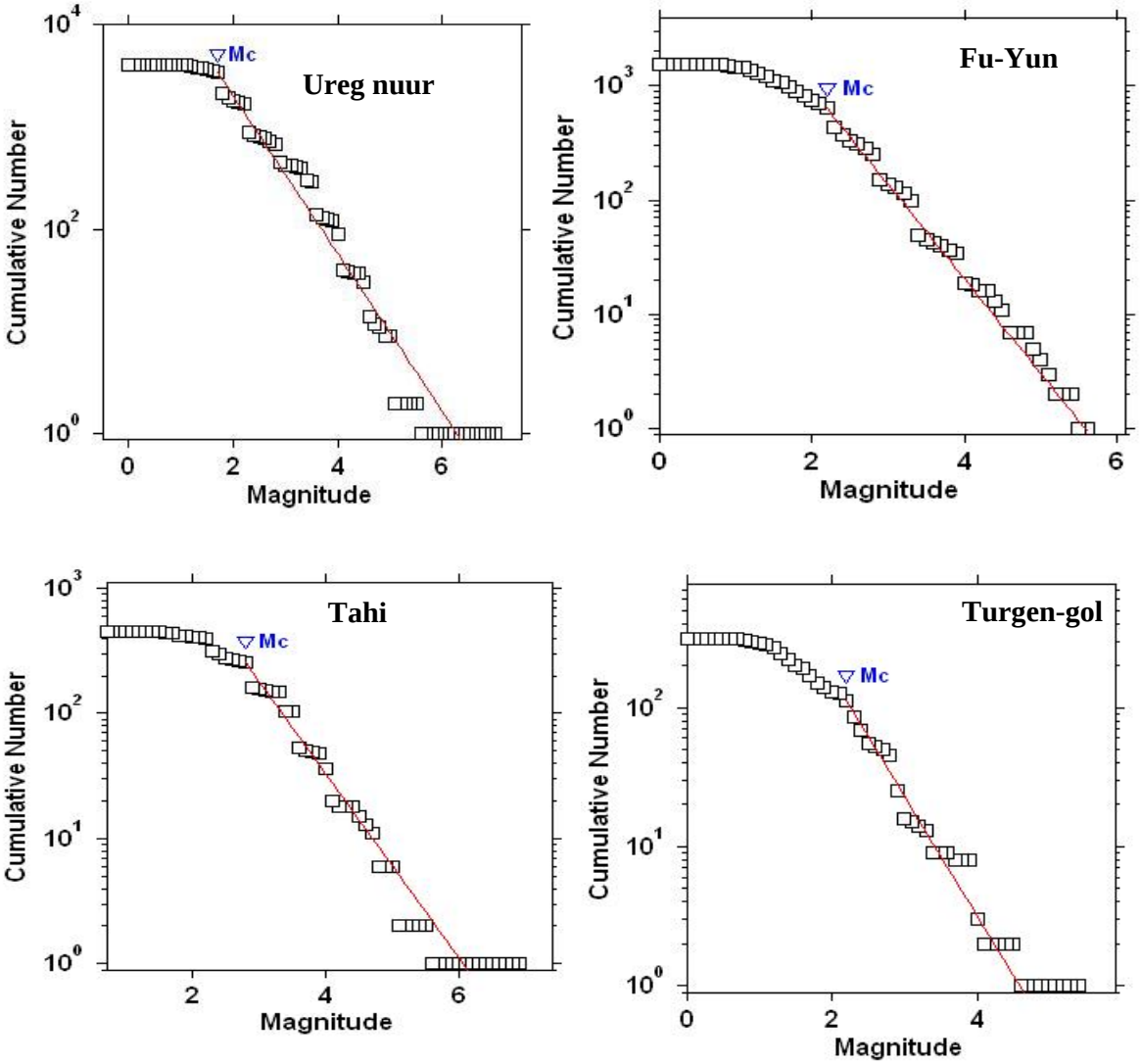

Figure II.28 G-R law using known events from 1964 and 2002: Fu-Yun, Ureg-nuur, Tahiin-Shar and Turgen-gol areas

II.7. Discussion and Conclusion

The seismicity in Mongolia is fairly high and complicated. This is due to the complex tectonic regime of the area that connected to the collision between Asian and Indian plate. Most western and southwest parts of Mongolia are affected by transpressional and compressional tectonic regimes. In the north of the territory, around Khubsugul region, is an extensional regime like in Baikal. In the N and E of Hangai are the active zones of Mogod and Bolnay. Inside Hangai dome, the known seismicity is low, but all around the dome are active seismic areas.

The statistical distribution of earthquakes in time and space give us a first view of the tectonic and geodynamic conditions of the region. The earthquakes of Mongolia are not evenly distributed over the region, but rather good correlated to the major active structures. Most high seismic activity occurred in Khubsugul and Altay region.

We analyzed the seismic catalogue covering the period from 1964 to 2002 with about 50 000 events. Altay region is the most active zone with 30% of earthquakes of whole Mongolia followed by Khubsugul zone with 20%. In addition, we see that the aftershocks and the seismicity associated to the main events or along the activated tectonic structures are dominant. By using clustering event, we identified 629 clusters that include 9040-clustered events. They concern about 20 % of the events in our database. Annually, the seismic energy released in Mongolia is between $5*10^{14}$ – $10*10^{14}$ J/year, and the main part of it is released in Gobi-Altay and Busiin-Gol active zones. Other specific characteristics of the seismicity in Mongolia is anomalous occurrence of large earthquakes. In Tahiin-Shar occurred event with magnitude nearly 7.0 and there are no events with magnitude between 5.5 and 6.5. It is also the same for the Ureg-Nuur and Deren zone.

Many scientists have pointed out that the seismic activity in specific region follows the Gutenberg Richter relation. By using Utsu's maximum likelihood method, we estimated a, b value for whole range of Mongolia and some specific seismic active zones. General seismic activity of Mongolia is high where a =6.2 and b= 0.8. For smaller zones, b value is varying between 0.4 and 0.8, a value 4.5 - 5.0. The Khubsugul region becomes the most active region of Mongolia. For this area we estimated a = 5.3 and b =0.9. Nevertheless, it is also the region where stresses are less accumulated and thus which has less "chance" to produce a large earthquake. Up to now, the largest one recorded there was with magnitude 6.5 in 1991. If we compare Khubsugul zone with Altay region, they have the same seismic activity but lower b value for Altay, which mean that he can accumulate more stress.

Chapter III

The 2003 Chuya earthquake context

III.1 Introduction

On 27th September 2003, a large intercontinental earthquake (NEIC gave origin time: 11:33:23.6 UTC, epicentral coordinates: 50.04°N, 87.04°E, depth~8 km and surface magnitude Ms = 7.3 occurred at the southeastern extremity of Gorny-Altay range along the Chuya and Kurai depressions (Fig III.1). This was the largest earthquake occurring in Gorny-Altay region for instrumental observation time. Its epicenter was 200 km to the west of the main recent event in Altay range, the Ureg-nuur earthquake (15th May 1970, M=7.0,) which occurred near the northwestern boundary of Mongolia (Fig III.1).

Macroseismic observations showed that intensity VIII, MSK-78 scale, was reached in the epicentral area, (Goldin *et al.*, 2003) and the earthquake was felt with intensity VI at Ulgii and Khovd city in western Mongolia, some 300 km far from the epicenter (Ankhtsetseg *et al.*, 2003). The earthquake has caused damages on buildings and constructions in towns of Chuya and Kurai depressions and landslides occurred in the Kosh-Agach and Ust-Ulagan area. Significant damages were also reported in Ongudai and Shebalino (Fig III.2).

The field investigations were carried out rapidly in the epicentral region by Russian researchers, just after the earthquake with some difficulties because of winter conditions (low temperature and snow). Geological team from Institute of Physics of RAS performed field observations of the surface ruptures. They mapped out fault trace along the southern margin of Chuya and Kurai depression. The earthquake produced up to 60 km of predominantly NNW-SSE right-lateral strike slip surface ruptures with an average displacement of 0.5-1.5 m (Geodakov *et al.*, 2003 and 2004).

Two teams (a team of Novosibirsk Seismological Center and a French-Russian-Mongolian team working on the MOBAL'03 project - Mongolia Baikal lithospheric transect) deployed temporary seismic stations in the epicentral area few days after main shock to control the aftershocks sequence. Our team (French-Russian-Mongolian) deployed 8 seismic stations starting four days after the main shock and the last stations have been removed on 19th November 2003.

The Chuya earthquake produced a rich aftershock sequence and within the first month after the main shock, several thousand aftershocks were record nearby the rupture area. A detailed study will be present in Chapter IV. Among these aftershocks, two significant events occurred seven hours (Ms=6.6) and four days (Ms=7.0) after the main shock.

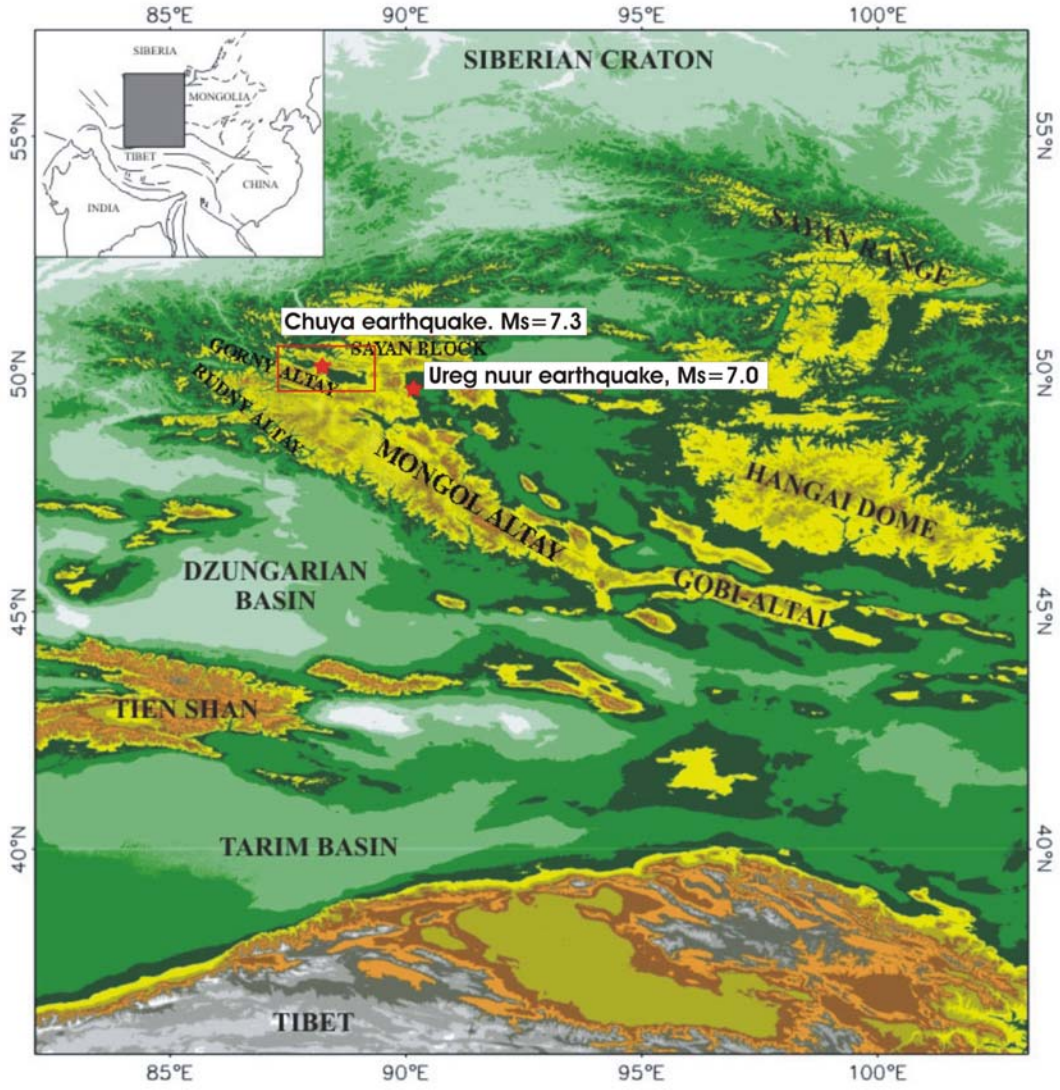

Figure III.1: General topography of central Asia and locations of the Chuya (2003) and Ureg-Nuur (1970) earthquakes. It shows the morphology central Asia affected by the Indian - Asia collision. The Chuya earthquake region is underlined with the red rectangle. Topographic data restored from the GTOPO30 DEM.

In summer 2005, about one year after the earthquake, several seismological centers deployed again portable seismic stations to precise the study of the activated area and they effectively recorded still several thousands aftershocks. The epicenter area is still active at the end of 2005.

The Chuya earthquake was a complex event composed by several subevents, with different focal solutions, on fault planes with almost the same strike. We have performed a detailed study to constrain the source time history and focal solutions of the Chuya earthquake and the two large aftershocks. We used teleseismic body-wave modeling which will be discussed in details in Chapter V. This chapter presents general information on the sequence, which will help us to constrain starting parameters of the inversion.

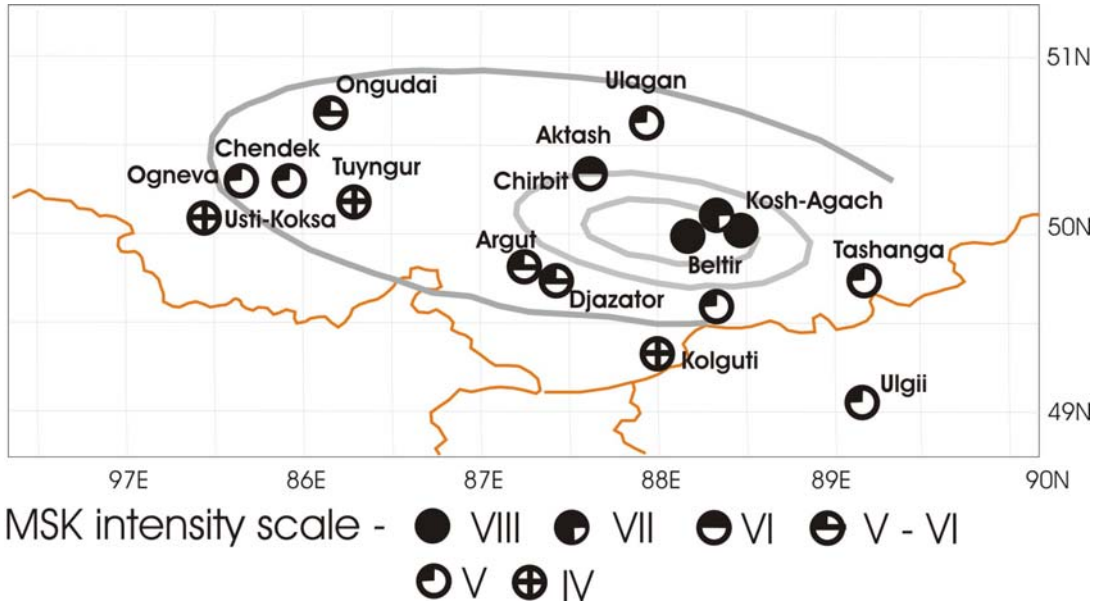

Figure III.2. The intensity map of the Chuya earthquake (redrawn after Goldin *et al.*, 2003). Maximum shaking at the epicentral area reached intensity of VIII. However, the result of Goldin *et al.*, (2003) is a partial result, as it does not include all data observed in surrounding countries. Taking into account all-available data an extension of area of intensity of V and VI will be observe.

A correlation measurement using two SPOT5 images (09th September 2003 and 26th June 2004) has been done by Remi Michel and Renaud Binet (DASE - Département d'Analyse et de Surveillance de l'Environnement, CEA, France). With this process, we can trace horizontal surface deformation and then estimate the slip along the fault and the location of the deformations. Unfortunately, for the northwestern end of the surface ruptures, no image was available before the Chuya earthquakes. Therefore this area remains described only by the field observations.

In the following, we describe the geographical, geological and tectonic setting of the Chuya earthquake associated to the coseismic surface faulting reported by Rogojin (Geodakov *et al*, 2003 and 2004). Then we discuss the results of subpixel correlation of SPOT images (5 m resolution) before and after earthquakes. Finally we include very brief information of GPS measurement available on the area of the Chuya earthquake and obtained by Russian researchers.

III.2 Location and topography of the region

The Gorny-Altay region is a northwestern part of Altay range which consists of a system of NW trending mountain ranges and intermountain basins. It is bounded on the north by the Siberian craton, on the south and southwest by Rudny-Altay range and Mongol Altay and on the east by the Sayan block (Fig III.1). The Chuya-Kurai region is located at the southeastern extremity of the Gorny-Altay accretion wedge. The Fig.III.3 shows the major topographical elements of the studied region. Local physiographic in the Chuya-Kurai region consists of a succession of high ranges with intermountain depressions. The main structural

directions trend WNW-ESE. At the center are located two large depressions, Chuya and Kurai, which are surrounded by high mountain ranges: Kurai, North and South Chuya, Sallyngem, Kyzylchin and Kubadru (Fig III.3).

The morphology of the region is well illustrated by topographic profiles extracted from SRTM data (3 arc seconds resolution = about 90 meters). The profiles outline the different segments and morphological units located in the study area (Fig III.4.a).

The Chuya depression is one of largest intermountain depression in the Gorny-Altay region. It extends along a sub latitudinal direction up to 90 km long and 60 km wide decreasing to 30 km at the west and 12 km at the east. The depression has weakly concave form with an altitude between 1750 m and 1850 m at the bottom located at its central part, and between 2000 m and 2150 m at its periphery (Novikov, 2004). The Kurai depression, smaller and located at the west of the Chuya depression, has diamond-shaped form. The depression is 30 km long and 20 km wide, and it has an altitude of 1550 m. The Chuya and Kurai depression, drained by the Chuya River, developed in the zone of dislocation between Kurai and Charysh-Terekta fault zones (Fig III.5). They are separated by the Chagan-Uzun horst (tilted block) with summit at 2900 m. The Chagan-Uzun horst has a progressive slope to the Chuya basin, at east, but has a steep scarp at the west with the Kurai basin (Fig III.4.b). The NW-SE trending profile 1 (Fig III.4.b) runs through the Kurai and Chuya basins and Chagan-Uzun horst.

The recent geometry of Kurai and Chuya basins looks like lozenge-shaped half-graben, but Kurai basin and western part of Chuya basin Quaternary structure is closer to half ramp basin. The lozenge-shaped geometry mainly is inherited from the Tertiary structure, which is itself controlled by the pre-Cenozoic fault pattern (Delvaux *et al.*, 1995).

Profiles II, III and IV (Fig III.4 c, d and e) show the junction between basins and ranges of studied area.

On the north of the Kurai and Chuya basins, the Kurai range, with a maximum altitude of 3400 m, is characterized by steep southern slopes and is bordered by a system of parallel thrust and reverse faults (Fig III.4c). The major geomorphic feature of the range is its northern and southern slopes shaped-up by the deformation of the primary pre-orogenic peneplain. The southern slope of the Kurai range has a clearly terraced structure and fault scarps (Novikov, 1998). In the central part of the range is a lens-like northwesterly trending block bordered, at the west and east, by intricate wrench fault zones (Novikov, 1998). Along these zones, the block borders the Kubadru and Bashkaus massifs, which are isometric uplifted blocks. On the north of Kurai WNW trending range and separated by the Bashkaus river basin is the Chulyshman range with a maximum altitude of 2500 m.

The Chuya river valley makes a deep separation between the Chagan-Uzun tilted block and the Kurai range. It is more than 1000 m deep and only 5 km apart from the highest part of the 2 massifs. The vertical deformation of the region contributes probably to a part of this deep incision.

At the south of Chuya and Kurai depressions the Chuya range is divided into two parts: the North Chuya range, with a maximum elevation of 4176 m, limits the south of the Kurai basin and the Chagan-Uzun horst is the northeastern extremity of the North Chuya range. The South Chuya range, with a maximum elevation of 3936 m, bounds the south of the Chuya basin. The Salyugem plateau limits the southeast of the Chuya basin, with a maximum elevation of ~3100 m. The northern slopes of Chuya ranges (South and North Chuya) are gentler towards the Kurai and Chuya basins (Fig III.4d and e).

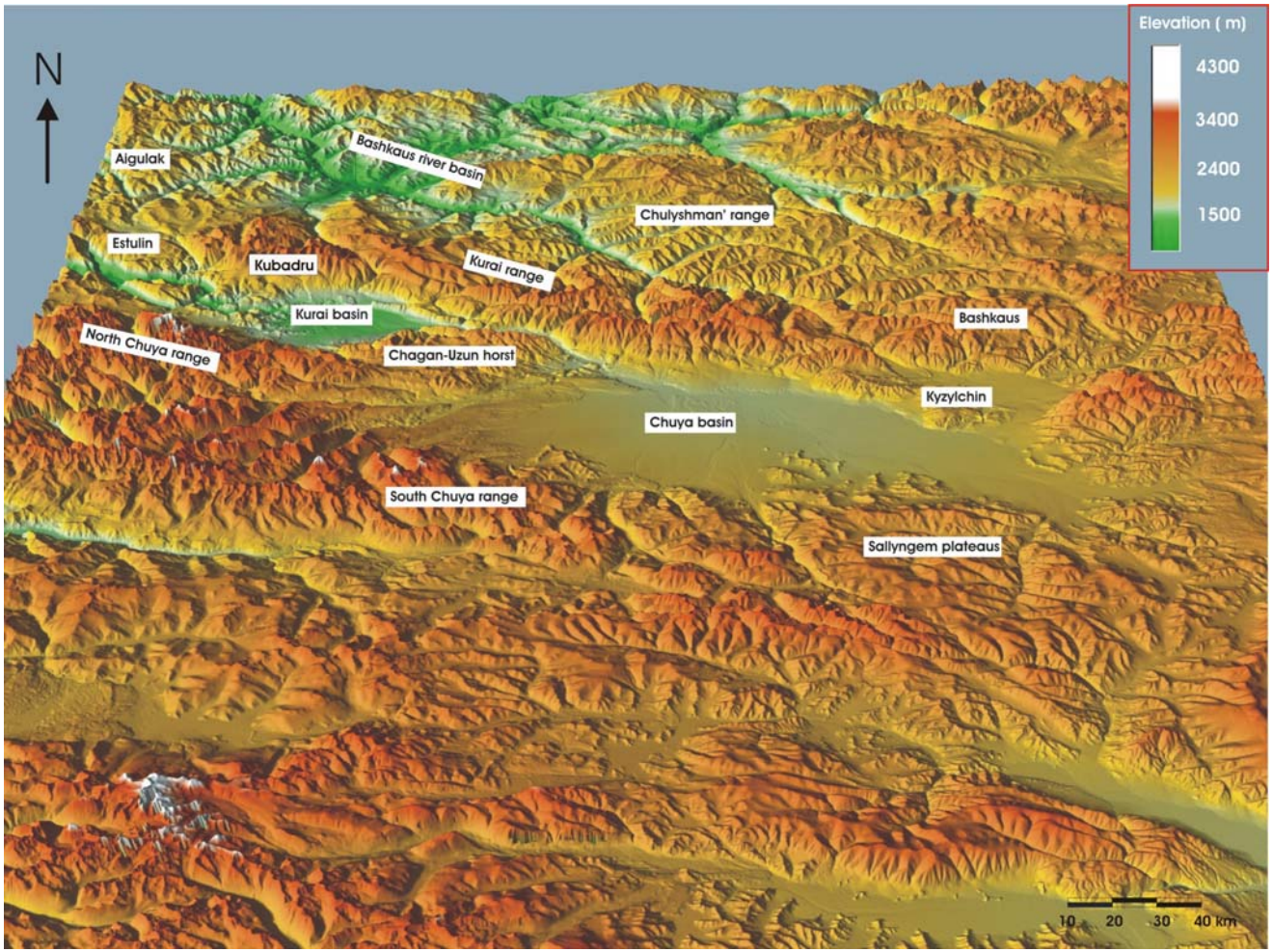

Figure III.3 Morphology with geographic names of the Chuya region (red square in Fig III.1 is represented). Topography from SRTM with 90 meters resolution.

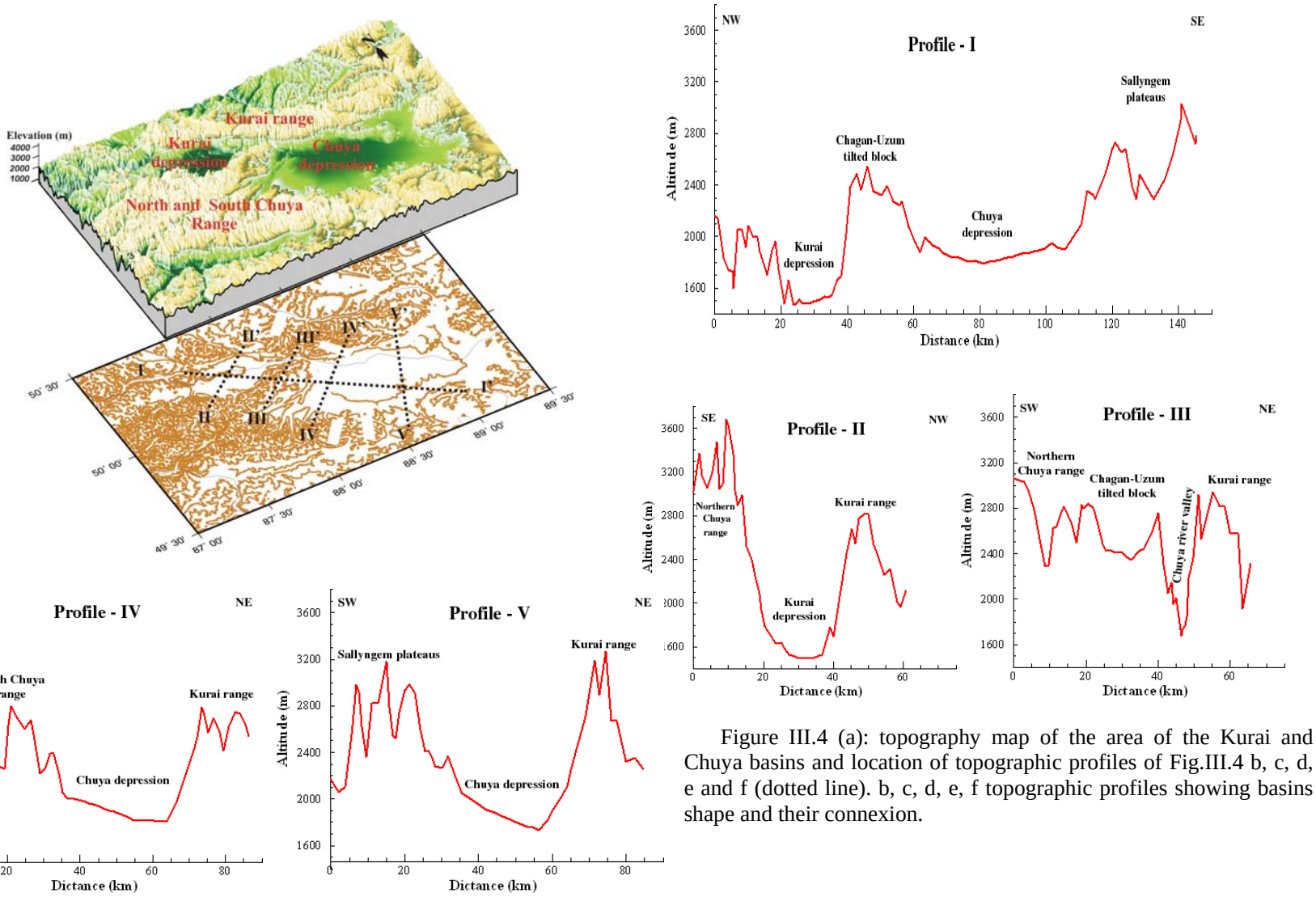

Figure III.4 (a): topography map of the area of the Kurai and Chuya basins and location of topographic profiles of Fig.III.4 b, c, d, e and f (dotted line). b, c, d, e, f topographic profiles showing basins shape and their connexion.

III.3 Geology and tectonic setting of the region

The Gorny-Altay region, in southern Siberia, corresponds to the western part of Altay-Sayan fold belt, formed in the stage of Paleozoic accretion-collisional tectonics. It is a complex elevated zone, where thrust and high-angle reverse faults are present, as well as normal faults (Delvaux *et al.*, 1995). The neotectonic structure of Gorny-Altay is partly controlled by Cenozoic reactivation of major fault zones, which often correspond to the Paleozoic suture lines and major strike-slip faults (Dergunov, 1967). These faults were reactivated several times, as showed by the frequent occurrence of Cambrian peridotite-serpentinite ophiolite fragments and Middle-Late Devonian, Late Carboniferous and Jurassic sedimentary lenses along them (Delvaux *et al.*, 1995).

The epicentral region of the Chuya earthquake lies on the southeastern extremity of the Gorny-Altay accretion wedge. The main geological and tectonic features of the Chuya earthquake region are Kurai and Chuya depressions, Charysh-Terekta and the Kurai fault zones; Kurai and Chuya (South and North) ranges and Chagan-Uzun tilted blocks (Fig.III.5). The following geological and structural description is a synthesis of the studies that have been done by Devyatkin (1981), Bogachin (1981), Luzgin *et al.* (1992), Delvaux *et al.* (1995) and Novikov (1998). The geology and tectono-stratigraphic evolution of the region is extensively discussed in these papers. The Fig III.5, modified from Delvaux *et al.* (1995), shows simplified quaternary structures map of Chuya earthquake region.

III.3.1. The Kurai - Chuya depressions:

The Chuya-Kurai depressions developed under the complex interaction of tectonic, sedimentary and climatic process. The Chuya depression contains the best sections of Cenozoic deposits for the Gorny-Altay region. Thanks to the work performed for the mineral and coal exploration in the year 60's, several drillings have been conducted in the area. The drillings reach a maximum depth of 671 m. These several boreholes in both basins allowed constraining detailed structure and stratigraphy of the region. The Chuya and Kurai depressions contain respectively up to 1200 m and 525 m of Cenozoic sediments (Delvaux *et al.*, 1995; Thomas *et al.*, 2002).

We describe the deposit from bottom to top. The period of the Late Cretaceos-early Paleogene, the stable tectonic conditions under humid tropical climate caused the development of an extensive peneplain over the region. The basin subsidence and sedimentation in the area of Chuya and Kurai depressions started in the Late Eocene-Oligocene. On the basement of Chuya and Kurai depressions lies 40 m thick of middle-upper Oligocene deposits consisting of sub aerials kaolin clays, with color brown to red. This overlaid by 250 m thick early and middle Miocene deposit. They are composed of brown, green and dark clays, aleurites and fine-grained sands with lenses of coal. It covered by about 150 m of green-gray colored, fine lacustrine middle-upper Miocene clays. Over that, the late Miocene to early Pliocene deposits is composed of yellow to brown sands with level of stromatolite limestone. These sediments, deposited in a long-lived deep lake, have a total thickness is about 100 m. The lower Pliocene deposit is made of green muds and fine sandstones with lenses of coarse and poorly sorted gravel, which point the beginning of the main uplift phase (Thomas *et al.*, 2002).

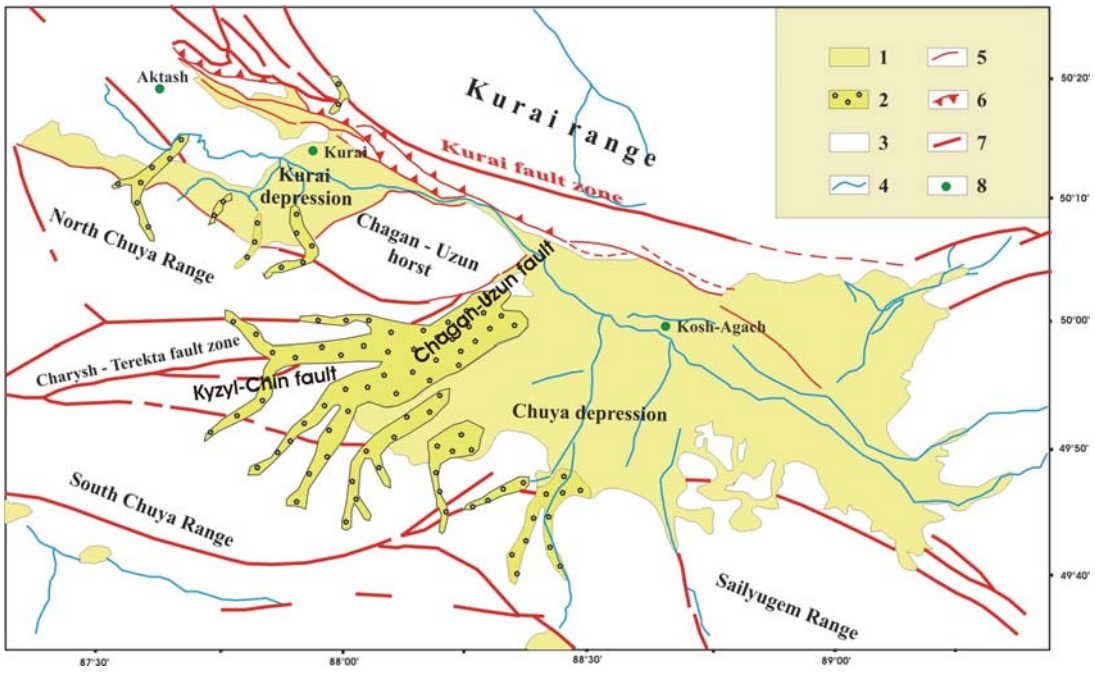

Figure III.5. Simplified quaternary structures map of the Chuya and Kurai basins (redrawn after Delvaux *et al.*, 1995). 1- Depressions, 2- Glacial moren sediments, 3- Ranges, 4- Rivers, 5- Active faults, 6- Major trust or reverse faults, 7- Major fault zones, 8- Cities.

The Kurai and Chuya depression developed in a zone of intense dislocation between the Kurai and Charysh-Terekta fault zones. To the north of the depressions, Kurai fault zone separate the no metamorphic Early Cambrian and Devonian basement from Late Precambrian metamorphic gneiss and to south Charysh-Terekta fault zone separating large lenses of metamorphosed Cambrian (Gorny-Altay series).

Their basement consists dominantly of Vendian-Cambrian and Devonian volcano-sedimentary sequences. Structural analysis reveals that post-Devonian structuring of basement occurred under the Chuya and Kurai depressions in response to two successive compressive tectonic stages. The first stage caused general folding of the Devonian along a broad E-W axial trend, and reverse to thrust faulting in the pre-Devonian basement. The second stage corresponds to large-scale left-lateral strike-slip movements, reactivating the previous thrust and affecting the folded Devonian. The Major Late Paleozoic faults control the basin structure and the distribution of Devonian basement rocks and Paleogene-Neogene sediments (Fig III.5).

Up to middle Pliocene, the two depressions formed probably a single strike-slip basin and a large, long-lived lake persisted during this period. In the Late Pliocene, a strong tectonic pulse caused the splitting of the former unique depression into two subsiding blocks (Kurai and Chuya), separated by a rising block (Chagan-Uzun). The Kurai depression evolved as a full ramp basin and Chuya depression as half-ramp, owing to thrust reactivation of the border faults. During the strong tectonic activity, the molassic-type sediments with sandstones levels were deposed (Thomas *et al.*, 2002).

III.3.2 The Kurai fault zone:

The Kurai fault zone is the active northern margin of both Kurai and Chuya depression. The Kurai fault zone is particularly complex in the Aktash area, with three separated north-dipping thrusts inducing the superposition of early-Middle Cambrian, Late Cambrian-Ordovician, Devonian-Carboniferous and Tertiary-Quaternary: the Aktash faults, Meridionally and Quaternary, are recognized from north to south (Delvaux *et al.*, 1995). At the northern margin of the Chuya depression, the structure of the Kurai fault zone is simpler (Fig III.5). The major fault trace passes in the Kurai range, 5-6 km to the north, separating the Late Proterozoic basement (West Sayan block) from lenses of Cambrian and Devonian rocks. The Cambrian and Devonian rocks overthrusted Tertiary and Quaternary rocks by several closely spaced faults.

The neotectonic structure of Kurai range is not uniform. The central part occupied by a lens-like northwesterly trending block. They are borders in the west and east formed by intricately fault zones associated with nearly horizontal displacement. In the southwest, the Kurai range bordered by a system of reverse faults typical of the boundaries of "rose" structures. Similar topography in the northeastern boundary of the Kurai range suggests the presence of an equivalent symmetric feature there. Therefore, the Kurai block could be a typical neotectonic "rose" structure developing under regional-scale compression, similar to those west and east of Altay (Novikov, 1998). This shows a general NS compressive context of the region.

On the western half of the Kurai depression, along the first fault line, the basement is up over-thrusting the Tertiary rocks and corresponds to a relatively degraded morphological scarp, which does not seem to be active in the Quaternary (Delvaux et al, 1995). Quaternary movements occurred along a new fault, 1-2 km toward the center of basins, and affected directly the Neogene sediments. It corresponds to a fresh morphological scarp, 200-300 m high, along several large landslides which occurred after the disappearance of the Late Pleistocene glacial lake. Toward the center of the depression, several minor normal faults affect the Quaternary sediments and control the location of the Chuya River and associated swampy plain. They induced the development of a small graben in the footwall of the main thrust zone (the Ortolyk graben), as in the Aktash region (Delvaux *et al.*, 1995).

III.3.3 The Kyzyl-Chin and Chagan-Uzun fault zone:

The Kyzyl-Chin and Chagan-Uzun fault zones trend northeastward, about parallel to the orientation determined for the Kurai fault zone (Fig III.5). These NW-dipping faults separate the Chagan-Uzun tilted block from Chuya depression and a Quaternary normal movement is confirmed by field data (Delvaux *et al.*, 1995) on it.

III.3.4.The North and South Chuya range:

The North and South Chuya ranges are less studied compare to Kurai range. As reported by Delvaux *et al.* (1995,), in the Chuya range no evidence was found for recent or active tectonics, even at the margin of the Chuya depression. The general morphology shows clearly that the boundary between North-Chuya range and Kurai depression is a tectonic scarp, although degraded by important glacial process during the late Pleistocene glaciations. We will see that this structure was probably reactivated during the 2003 earthquakes.

The Late Pleistocene glacial period had a strong effect on present day surface geology and morphology (Fig III.5). Glacial moraines cover an important part of the depression and important glaciers even caused the damming of the Chuya River at the outlet of the Kurai depression (dotted areas on fig III.5) and the creation of giant Late Pleistocene lake in both Kurai and Chuya depression

III.4 Coseismic surface ruptures

The Chuya earthquake produced surface ruptures oriented NW-SE along the southern end of the Chuya and Kurai depressions. Few days after the main shock Russian scientists visited the area and they published a preliminary map of observed surface ruptures. With the beginning of the very cold winter season and the difficulties to access to high Altay Mountains, they were unable to observe the details of all surface ruptures during their first site visit. They came back to the epicentral area during summer of 2004 and produced at that time a more detailed study on the area. As we did not reach the epicentral area, the following description of the surface rupturing based on the two reports of Geodakov *et al.* (2003 and 2004) and discussions with E. Rogojin, one of the co-authors. The preliminary map showed only 25 km of length of surface rupture (Geodakov *et al.*, 2003). After the second site visit, it has been modified and the observed surface rupture due to the Chuya earthquake was increased up to 60 km (Geodakov *et al.*, 2004) (Fig III.6). Notice that the first site survey was after the three main events and that it is unknown which were the surface ruptures associated with the main event and with the two large aftershocks. During the field survey, Geodakov *et al* observed also induced features due to gravitational slumping or vibration effects.

The surface ruptures were predominantly right lateral strike slip with a general strike of 300-350°, which intersect the morenas, the proluvium of the foothills, and the alluvial and glacial deposits of rivers valleys. The surface ruptures expressed as either zone up to 0.1-10 m wide, 30 m deep, 500 m long containing distributed tension cracks or shorter mole tracks (< 50 m), often displaying strike-slip motion. These features were in "en echelon" patterns as a set of left-stepping tension cracks oriented 320-340° N and occasional mole tracks oriented 40°-60° N, which show right lateral strike-slip.

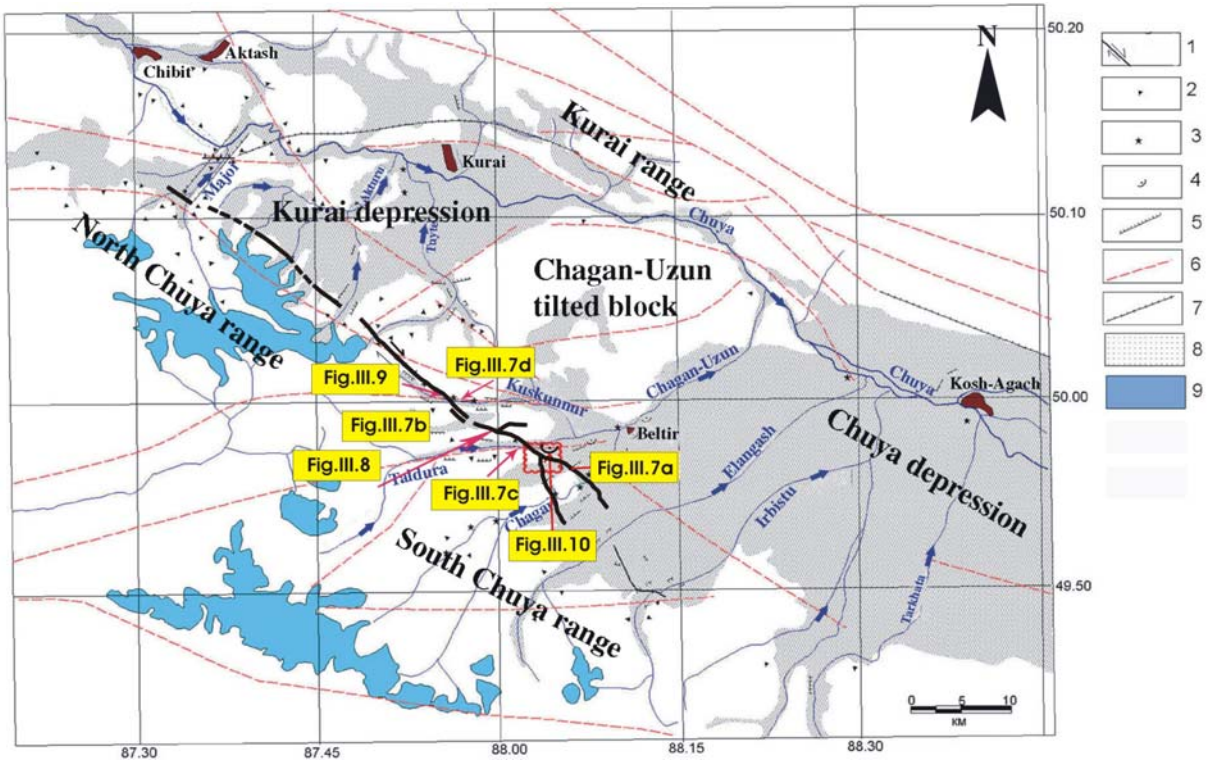

Figure III.6. Map of surface ruptures observed on the field and associated to the Chuya earthquakes (redrawn after Geodakov *et al.*, 2004). The red lines show potential active faults. 1 - seismic faults (dextral strike-slips); 2-5 - secondary seismic ruptures: 2 - rock-falls, 3 - marks of liquefaction, 4 - landslides, 5 - seismic gravitation fissures and slope displacement; 6 - neotectonic faults (Devyatkin, 2000); 7 - faults, reactivated during Altay earthquake due to resonance shaking; 8 - Quaternary lacustrine, alluvial and glacial deposits; 9 - mountain glaciers.

I describe now the field observations from the southeast to the northwest. At the southeastern end, on the flat top of a deposit between the Chagan and Taldura rivers, the rupture split into two branches with a maximum distance around 5 km. On one of this branches, the orientation of the rupture turned to the southeast direction (red square on Fig III.6). The two branches consisted of several en-echelon tension cracks oriented N340° to N350° and mole tracks with small vertical offsets of about 30 cm.

The surface ruptures crossed small valleys of rivers Chagan and Taldura. In the valley of Chagan the surface rupture expressed as a system of open cracks 1.5 m wide (Fig III.7a) and continued, in the direction of the Taldura valley, with series of "en echelon" stepping segments of tension cracks oriented N 320°, 1 to 3 m wide and 100 m long. Between the open cracks were several parallel faults with right lateral displacements of about 0.5 m on each segment. Evidence of right-lateral strike-slip also found along the displaced road, were displacement between 0.1 to 0.2 m on individual segments.

In the valley of river Taldura, the surface rupture formed a zone with a general orientation of N 290° to N 300°. It was locally associated with "en echelon" tension cracks with strike of N 320° to N 330° (2 m wide, up to 50 m long) and small overthrusts or mole tracks trended N 40° to N 60° (Fig III.7b and Fig III.6 for the location). These shear features were all developed in soft alluvial deposits of valleys and in moraine sediments of early and

middle Pleistocene. The tension cracks and mole tracks were very common along the Bolnay surface ruptures (left lateral strike slip at North Mongolia, magnitude 8.3 ± 0.2 on the 23th July 1905).

Most obvious surface breaks are observed at a wide saddle between the rivers Taldura and Kuskunnur. On both side of the saddle, the surface ruptures clearly expressed like form of scarps. Geodakov *et al.*, (2003) consider that these scarps represent partially paleodislocations and that the Chuya earthquake only reactivated them. The saddle, about 4 km wide, is bounded by Devonian slates hills with flattop. At the saddle, where sediments consist of moraine of the middle Pleistocene, the surface ruptures separate into two branches. On the eastern border of the saddle, the width of such micrograben is less than 50 m and vertical component is about 0.5 m (Fig III.7c and Fig III.6 for the location). On the western slope of saddle, the micrograben is larger with a width up to 500 m and a vertical offset up to 2.5 m (Fig III.7d). The coseismic ruptures expressed on the saddle, consisting in en-echelon systems of open cracks oriented NS and closed by linear zones of compression. Open cracks are large, characterized by width up to 10 m, length up to 300 m and depth measured down to 30 m (Fig III.7c). Zones of compression represent mole tracks with height up to 2 m and length up to 50 m with border like as small thrusting.

Evidence of right-lateral strike-slip was observed along these ruptures, such as a road displaced by several ruptures oriented N300° to N320° (Fig III.8) were the slip is about 0.5 m on each segments with a total displacement of about 1.5 m.

Further to the west, the surface ruptures continue only along the northern branch, through a steep rocky slope following the western riverbank of Kuskunnur (Fig III.9). The surface ruptures cut the alluvial sediments of this valley and built S-shape system of faults. Again, it has been observing a system of surface ruptures formed by open crack and mole tracks (length of 40m to 600 m, width of about 1 m and deep up to 3 m). The right lateral displacement observed here 0.3-0.5 m, measured on displaced road. Lengths of compression and dilation features are about identical and do not exceed 50 m. Surface rupture cross through whole valley and continue the opposite border of mountain.

The Chuya earthquake induced many secondary effects as landslides and collapses. The largest landslide occurred on the right-bank of the river Taldura (Fig III.11). The completely apparent thickness of the landslide is about 150 m and moved to the valley over a distance of more than 100 m. The Fig III.10 shows a general view of the landslide as observed by the satellite SPOT5 (panchromatic channel with 5 m resolution) before and after the earthquake. Several other smaller induced landslides has observed and mapped (see locations on Fig III.6).

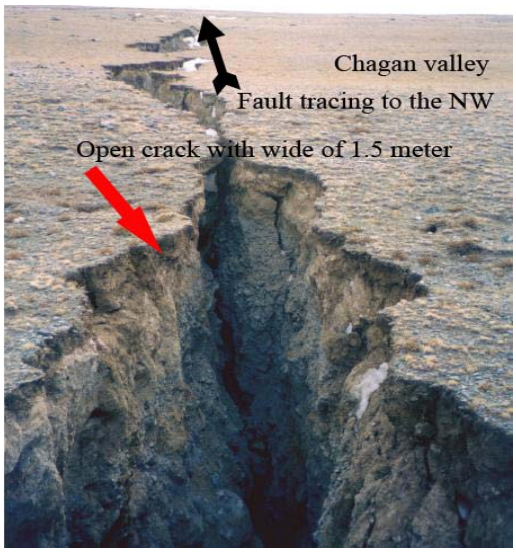

a

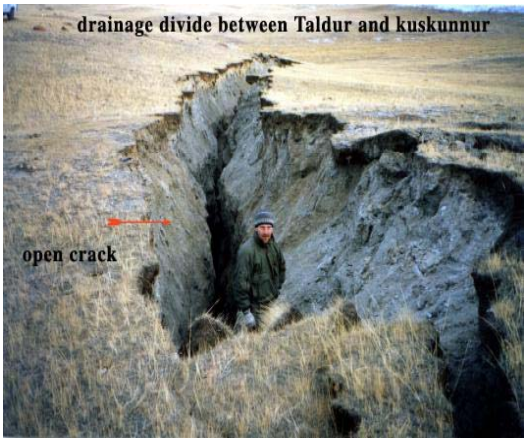

b

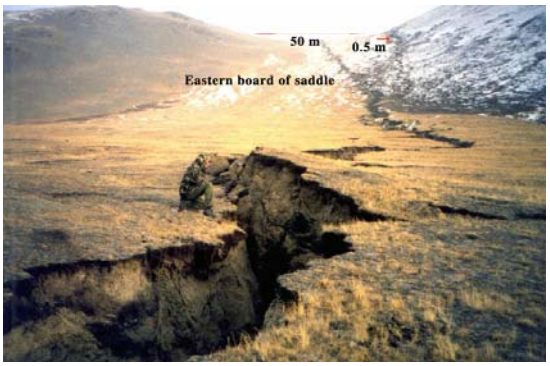

c

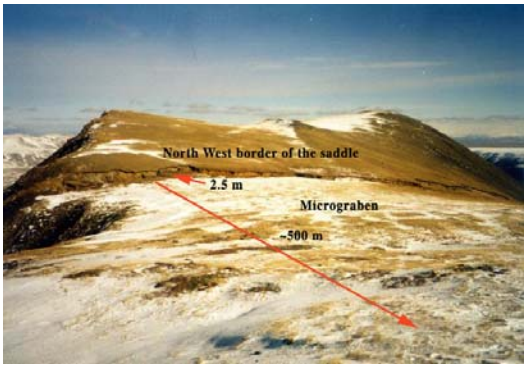

d

Figure III.7a: Photo of surface rupture (for location, see Fig III.6). a) Open cracks with right lateral strike slip observed in Chagan valley, b) Open cracks between Taldura and Kuskunnur rivers, c) Open cracks associate to right lateral strike slip. Notice the vertical deformation due to a horizontal slip on a curved surface rupture. At the saddle can be seen the split of the surface rupture in two structures with small vertical components, d) micrograben with a cumulated vertical slip of 2.5 m.

Figure III.8: Photo of surface rupture (for location, see Fig III.6). Road displaced with a right lateral strike slip. The displacement is 0.5 m on the first segment. If we add all segments, the total horizontal displacement is about 1.5 m.

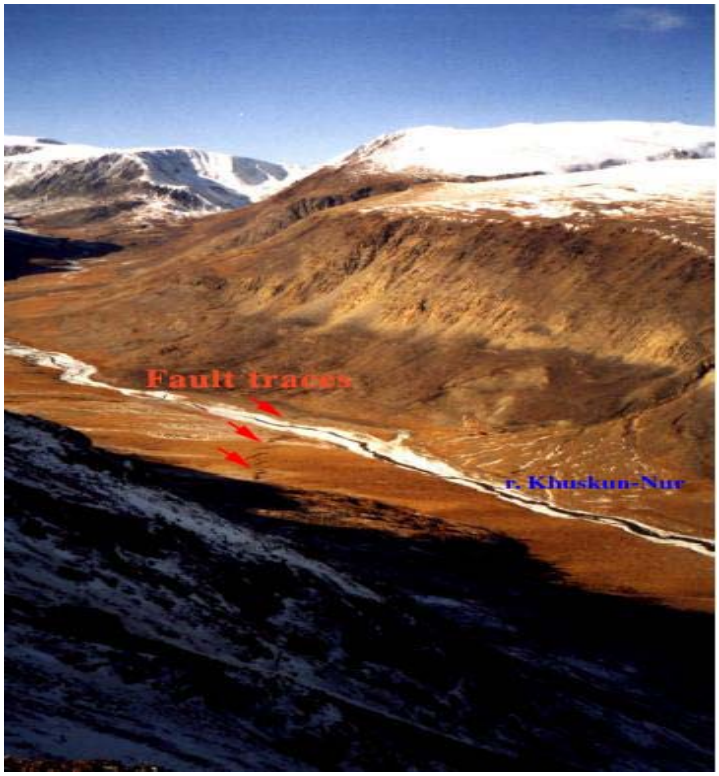

Figure III.9: Photo of surface rupture (for location, see Fig III.6). "En echelon" fault traces in the Kuskunnur river valley. They show a right lateral strike slip in the area.

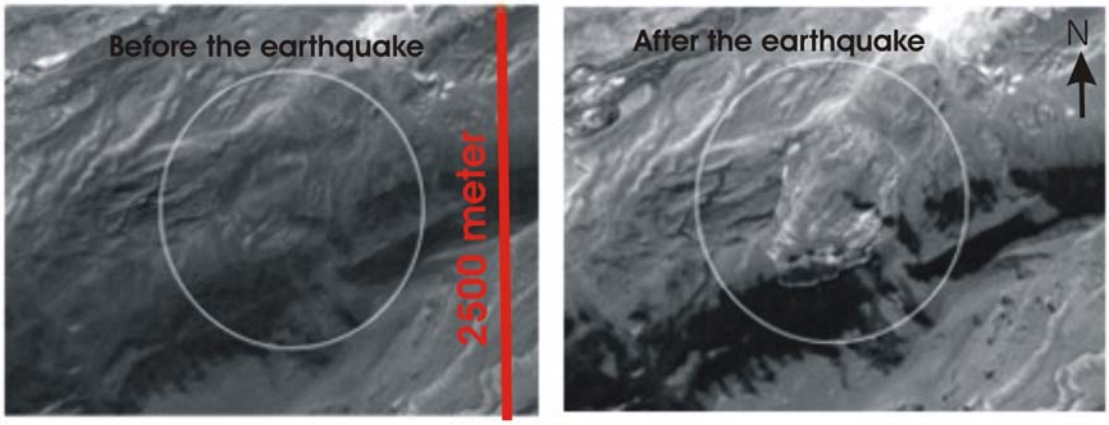

Figure III.10: Photo from satellite SPOT5 (5 metres resolution), area of the large landslide (Fig III.11), before and after the 2003 events (for location, see Fig III.6).

Figure III.11: Photo of secondary effects of earthquakes (for location, see Fig III.10 on Fig III.6). Large landslide induced by the Chuya 2003 earthquakes. At the left part of the picture can be seen a probable previous landslide.

III.5 Result of GPS measurement in the Altay region before Chuya earthquake.

In the region of Altay developed a project to estimate horizontal and vertical velocities of the crustal deformation in Altay-Sayan area using GPS space geodesy and gravimetry applied by Timofeev *et al.* (2003). The project started in 2000: GPS temporary points established over the north Altay and one permanent station at Novosibirsk. First campaign started with 12 points over north Altay region and the summer of 2001, it increased to 17 points. As explained by Timofeev *et al.* (2003), each site was observed between 2 and 5 days, in each summer. The summer 2001-2002 GPS network included the measurements at 17 points of Altay network (Timofeev *et al.*, 2003). Fig III.12 shows the location of these points and Novosibirsk permanent GPS station (NVSK).

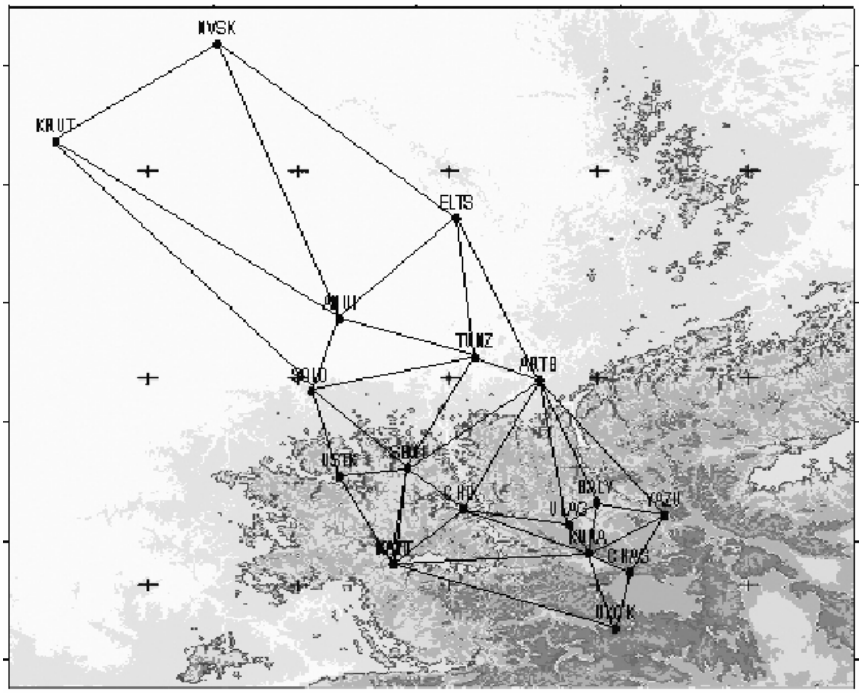

Figure III.12 Map of the Altay GPS reference points derived from Seredovich *et al.*, 2004. NVSK- Novosibirsk GPS station is the reference permanent station used for the study.

The preliminary results on summer 2001-2002 campaigns, were published by Timofeev *et al.* (2003). These authors determined a velocity up to 10 mm per year in the north direction for the horizontal component in northeastern Altay region compared to Novosibirsk (stable Siberia). This velocity is higher than what is expected in Altay region by Calais *et al.* (2003) who found velocities directed northward relative to stable Siberian platform. They give rates, decreasing from south to north, of 10 mm yr^{-1} south of Altay at Urumqi and of about 4 mm yr^{-1} in Altay.

III.6 Detection of Surface ruptures and slips by subpixel correlation of SPOT images.

Horizontal surface coseismic displacement can also measured using a subpixel correlation of SPOT satellite panchromatic images acquired before and after an earthquake (Micheal *et al.*, 2002; Dominguez *et al.*, 2003). The two images are first resample in the same cartographic projection using a digital elevation model (DEM), a physical model of image acquisition and an accurate interpolator. During that initial processing, some artifacts due to SPOT push-broom system corrected together with misregistrations due to the changing attitude of SPOT during the acquisition of each image. Next, residual offsets are computing from the phase shift of the Fourier transform of a sliding window. Spatial sampling and accuracy of measurement mainly depend on the local level of correlation of the images (Van Puymbroeck *et al.*, 2000). Offset also includes residual artifact due to errors and under sampling of the roll, pitch and yaw characterizing SPOT attitude. This latter source of error may introduce a significant apparent warping at spatial wavelengths larger than a few kilometers (Micheal *et al.*, 2002).

In this study, two panchromatic SPOT images has been used with pixel size of 5 m, which covers the southeastern part of the surface rupture, acquired on 09th September 2003 (Fig III.13a), 18 days before the main earthquake, and on 26th June 2004 (Fig III.13b), 9 months after the three large events. Notice that the difference between these two images does not show only the deformation at surface due to 27th September earthquake but also the whole sequence of aftershocks during 9 months including the two large events which occurred within four days after the main event. The 5 meters resolution allows having a more precise result useful in our case because of the small amount of horizontal slip expected. The results are averaging on a window of 80x80 pixels. Therefore, it takes into account not only a deformation on a specific surface rupture or fault but also the permanent deformations near the fault.

The SPOT image processed at DASE (France), in the frame of collaboration between DASE and RCAG, by Remi Michel and Renaud Binet who have developed the technique and the software for subpixel correlation. As no SPOT5 data are available before the earthquake for the area of the northwestern surface ruptures, we obtained the information only along the two third (about 40 km) of the surface ruptures at the southeastern part.

Fig III.14 (b) shows the map of surface ruptures observed on the field and location of the spot scene (common part of the two available images) used for the subpixel correlation. Fig III.14 shows (d) E-W and (e) N-S horizontal offsets respectively, obtained from the correlation between the two SPOT images. On both components (E-W and N-S), the offset field clearly reveals a strong discontinuity along an ESE-WNW direction and allows a detailed mapping of the southern end of surface deformations due to the Chuya earthquake sequence. Generally, the cartography of the surface rupture determined from SPOT satellite offsets in good agreement with the one observed on the field. Nevertheless, as the image covers a large area, it helps to detect other potential surface deformation that has not observed on the field (large area with difficult access).

The geometry of the surface ruptures and deformation of the area, detected from SPOT5 correlation, show the complex ruptures of the Chuya earthquake with 2 segments and slightly different trends (Fig III.14a and b). As observed on the field, fault trace is changing clearly to the SE, between Taldura and Elangash rivers (Fig III.14d and e).

To investigate ground deformation in the fault zone, we have drawn profiles perpendicular to the fault strike, by stacking all data along 3 km wide swaths. Fig III.15 shows horizontal offset determined from the profiles (see location of profiles on Fig III.14a). We have search a line which follows the averaged displacement on each side of the fault mapped using the SPOT correlation (solid red lines). Notice that evens on the SPOT 5 original image, the surface ruptures were not detectable using visual image interpretation. This shows the power of the correlation method to detect the horizontal surface deformation.

Some of profiles (profile between 0-2) give high uncertainties with errors up to 2 and 20 m (Fig III.15_1 and 2). This is probably due to uncertainty associated with the interpolation of offsets across river valley of the Kuskunnur or Tuyte rivers. Then we did not consider the results of these profiles to determine the average horizontal slip along the faults. The dashed line on Fig III.14f shows a stack of the 10 profiles along the southeastern surface rupture trace of the Chuya earthquake, retrieved from the two pairs of SPOT images. SPOT offset suggest that the Chuya earthquake produced an average horizontal displacement between 2.5-3.5 m with an uncertainty of 0.1 m (Fig III.14i). Fig III.16 show variation of the average offsets measured on each profile (location of profiles are in top image). We find a mean slip of 3.5-3.8 m along the NW segment of surface rupture, decreasing eastwards, and of 2.2-2.6 m along the SE segment (profiles 11 and 12). On profile 13, almost no slip is observed, so we can consider that surface rupture is finishing around this area.

The fault traces obtained from image processing is well correlated to what is observed during field survey. Fault displacement determined by SPOT correlation shows larger slips (2.5-3.5 m) than those observed during field investigation of surface rupture (1.5 m). However, it is in good agreement with our teleseismic body-wave inversion results that we will discuss in details in the chapter V.

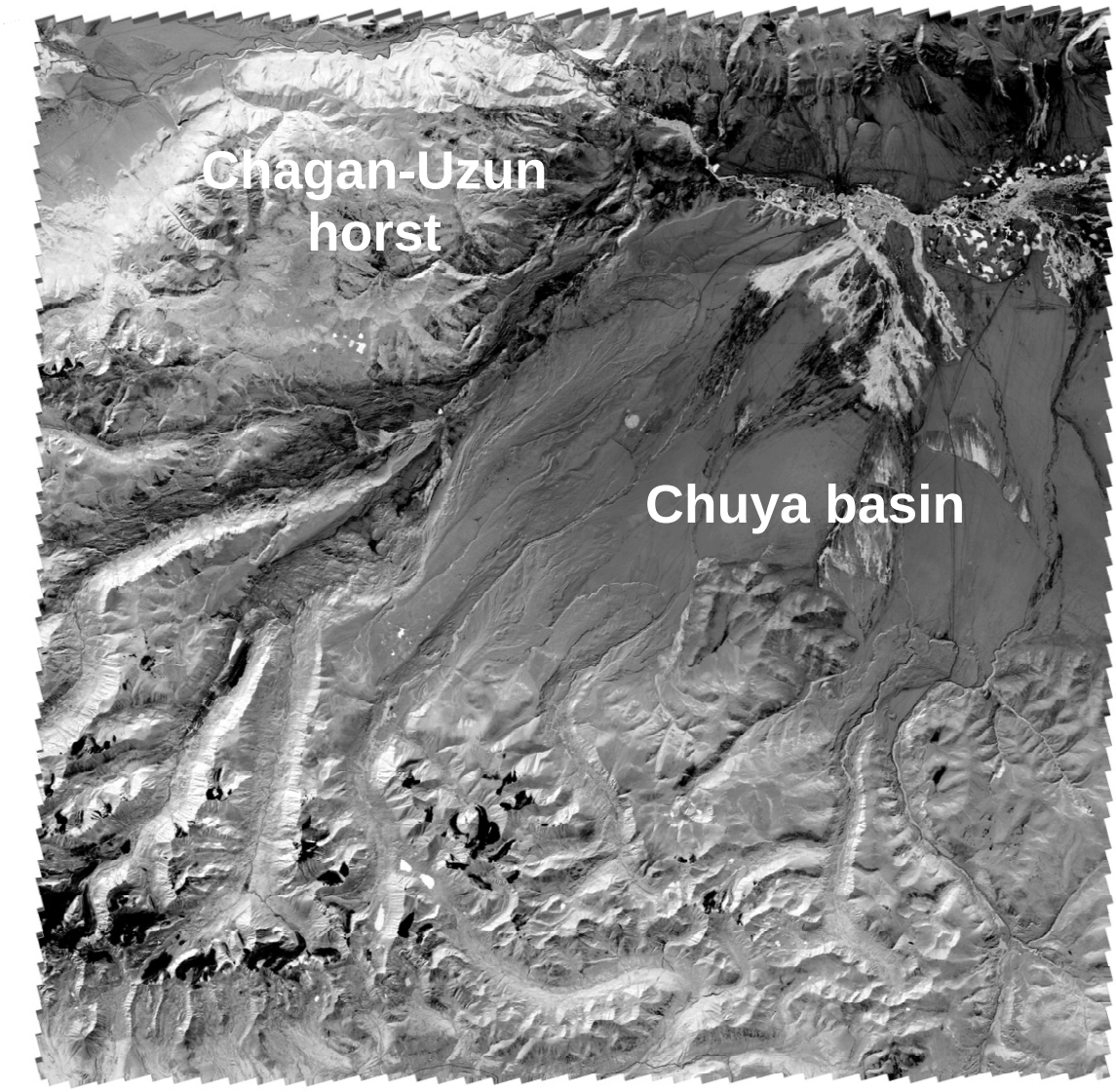

Figure III.13a: Spot5 Panchromatic image (ground resolution = 5m) before the Chuya earthquakes (09th September 2003). The colour code has been inverted (negative). The image size is 60x60 km and has been corrected geometrically. Image used for the SPOT correlation.

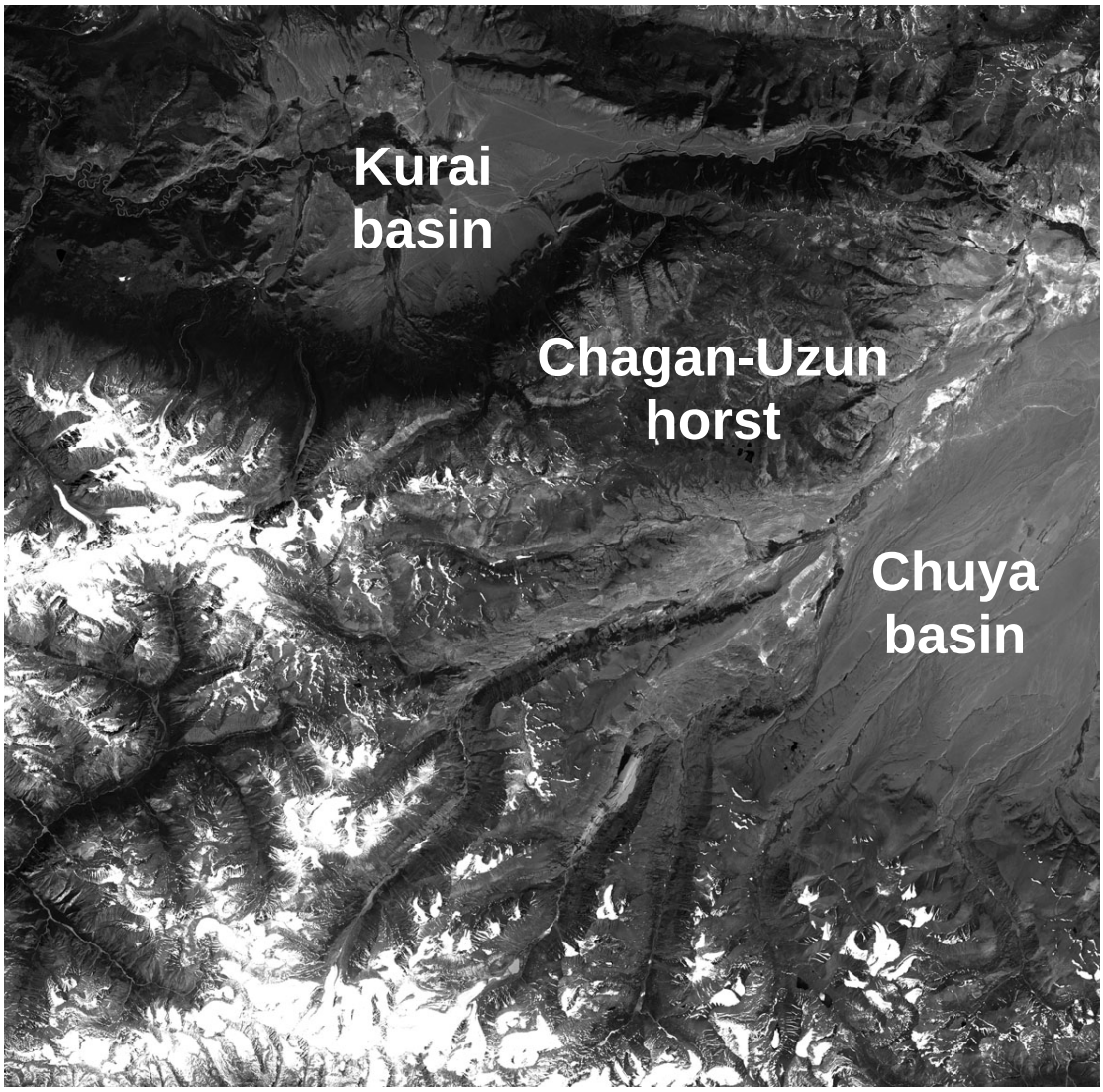

Figure III.13b. Spot5 Panchromatic image (ground resolution = 5m) after the Chuya earthquakes (26th June, 2004). The image size is 60x60 km. Image used for the SPOT correlation. The surface ruptures of the 2003 events are not visible except the large landslides (presented on Fig III.11).

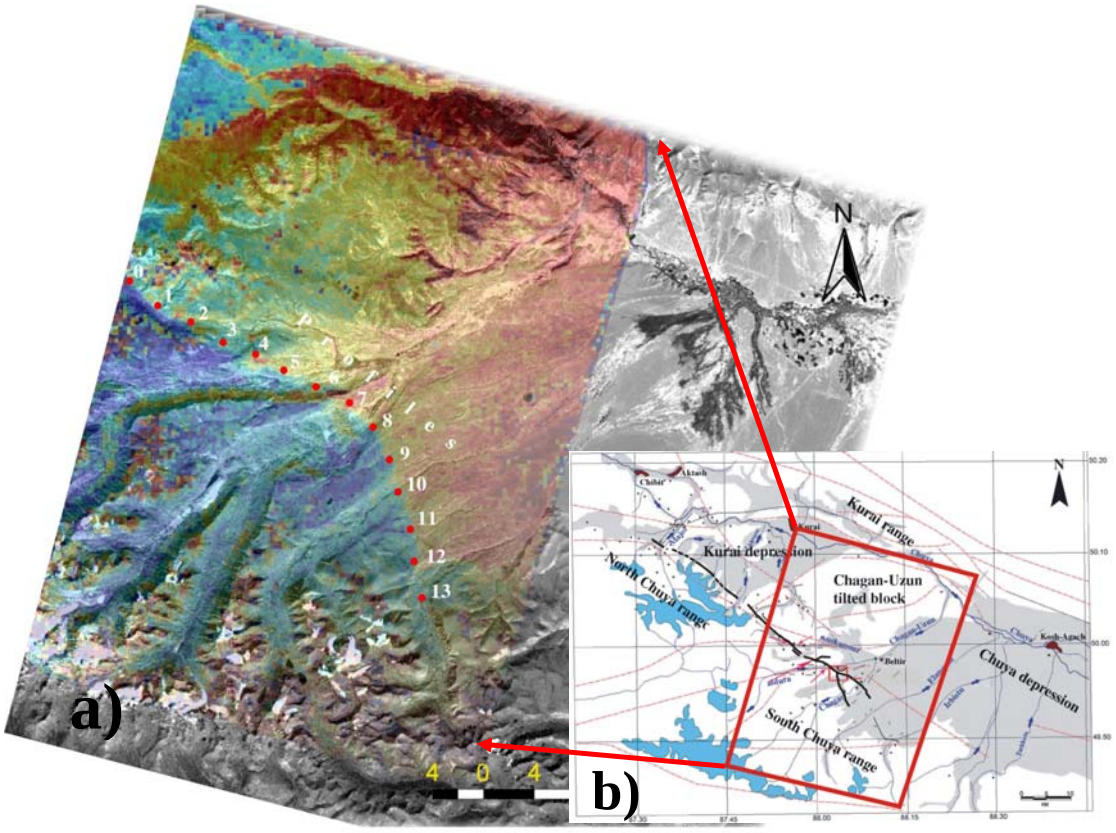

Figure III.14: The horizontal displacement along the fault as calculated from SPOT5 correlation.

a) Calculation of the correlation between SPOT5 images from the 09th September, 2003 and 26th June, 2004 overlaying a panchromatic scene. The numbers show the position of the profiles of Fig III.15.

b) Map of observed surface rupture on the field (after Geodakov *et al.*, 2004)*

c) Overlaying area of the two SPOT images

d) Correlation in the EW direction. The fault branches are clearly detectable and slips in NS direction are more important along the eastern branch.

e) Correlation in the NS direction. The fault branches are clearly detectable and slips in EW direction are more important along the western branch.

f) Profiles 4 to 13 on the same picture. The position "0" is at the fault. The red line shows the average horizontal displacement along the fault (right lateral strike slip)

i) Profiles 4 to 13 on the same picture. The position "0" is at the fault. The vertical red line shows the uncertainty on the horizontal displacement

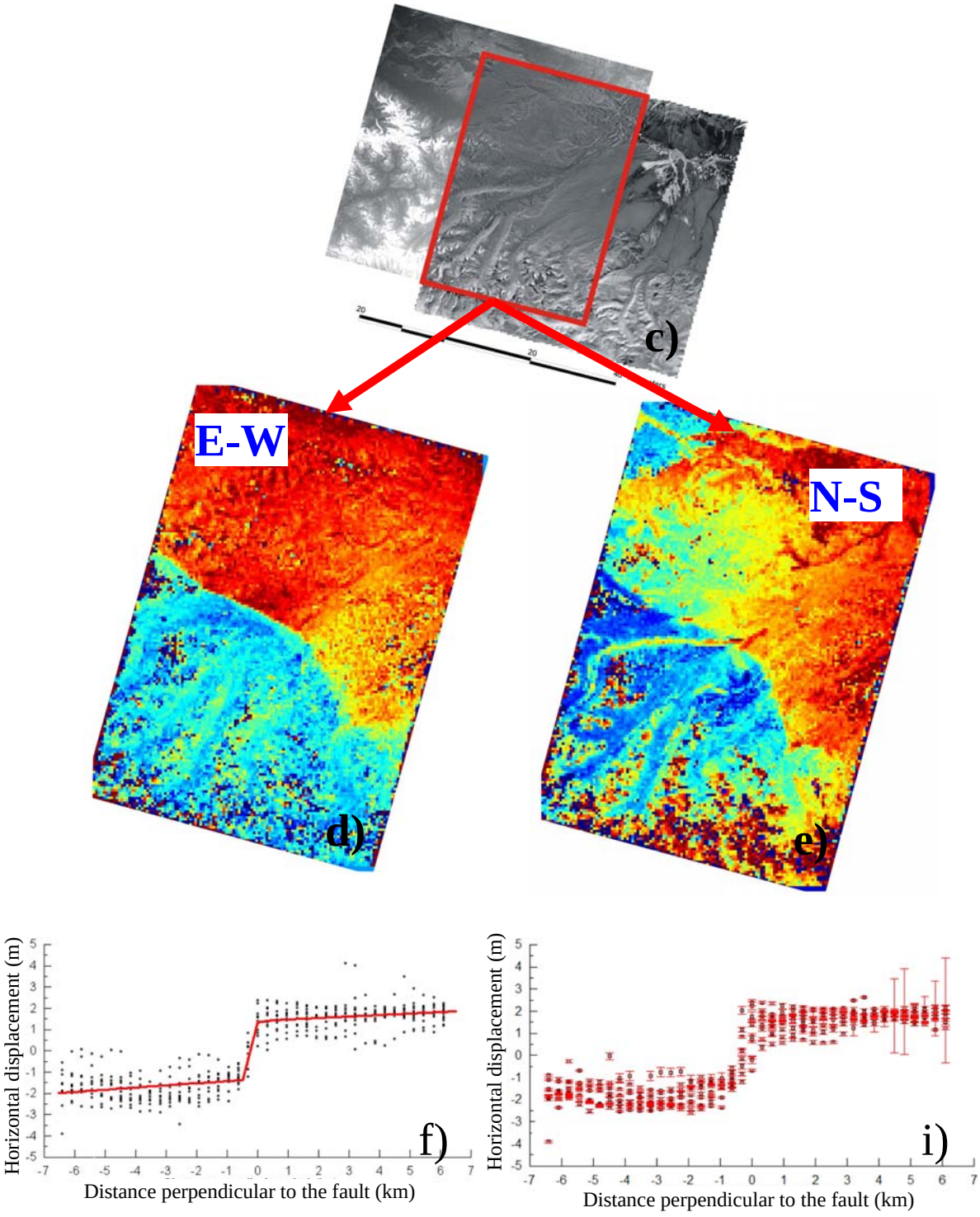

Figure III.14 Continued

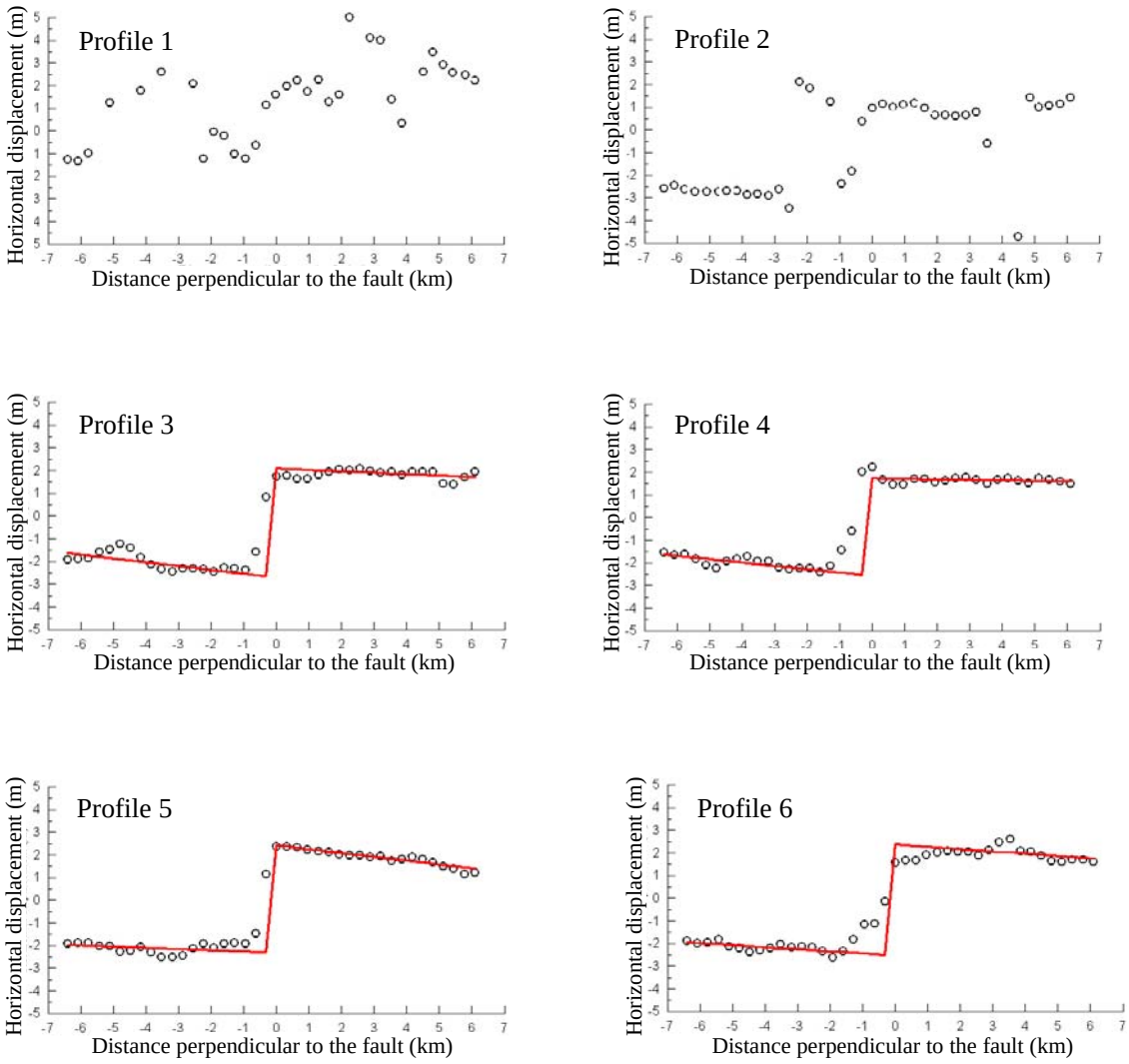

Figure III.15 The horizontal displacement along the fault as calculated from SPOT5 correlation at profiles between 1 and 13. The origin " 0" is at the fault and the location for each profile is represented as red points on fig III.14a. To decrease the noise, each point represents the horizontal slip averaged along 3 km. The red line shows the average horizontal displacement at each side along the fault (right lateral strike slip). The slip values of profile between 0 and 2 are largely dispersed and not represented here. This is probably due to uncertainty associated with the interpolation of offsets across river valleys. Other noticeable information is that, starting from profile 11 and 12, horizontal displacements significantly decrease which can be related to the presence of two branches of surface ruptures. On the profile 13 almost no displacement is observed compare to others.

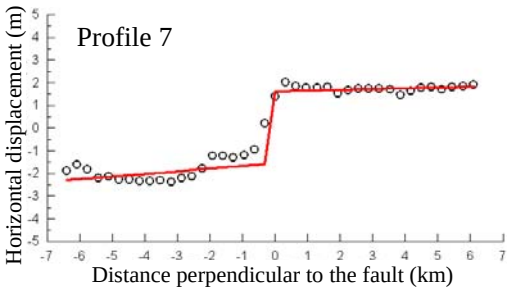

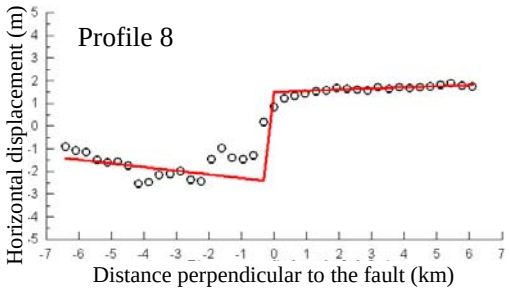

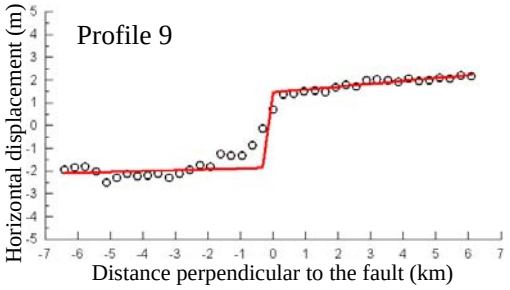

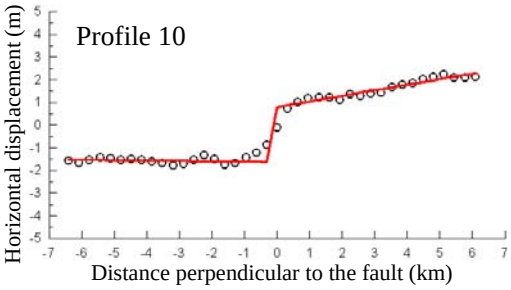

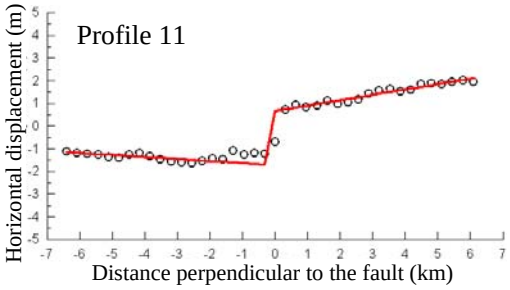

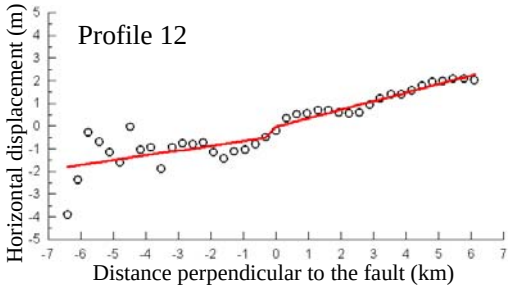

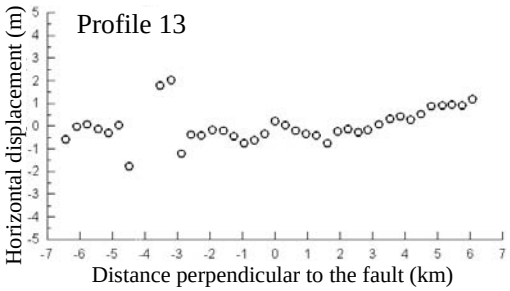

Figure III.15 Continued

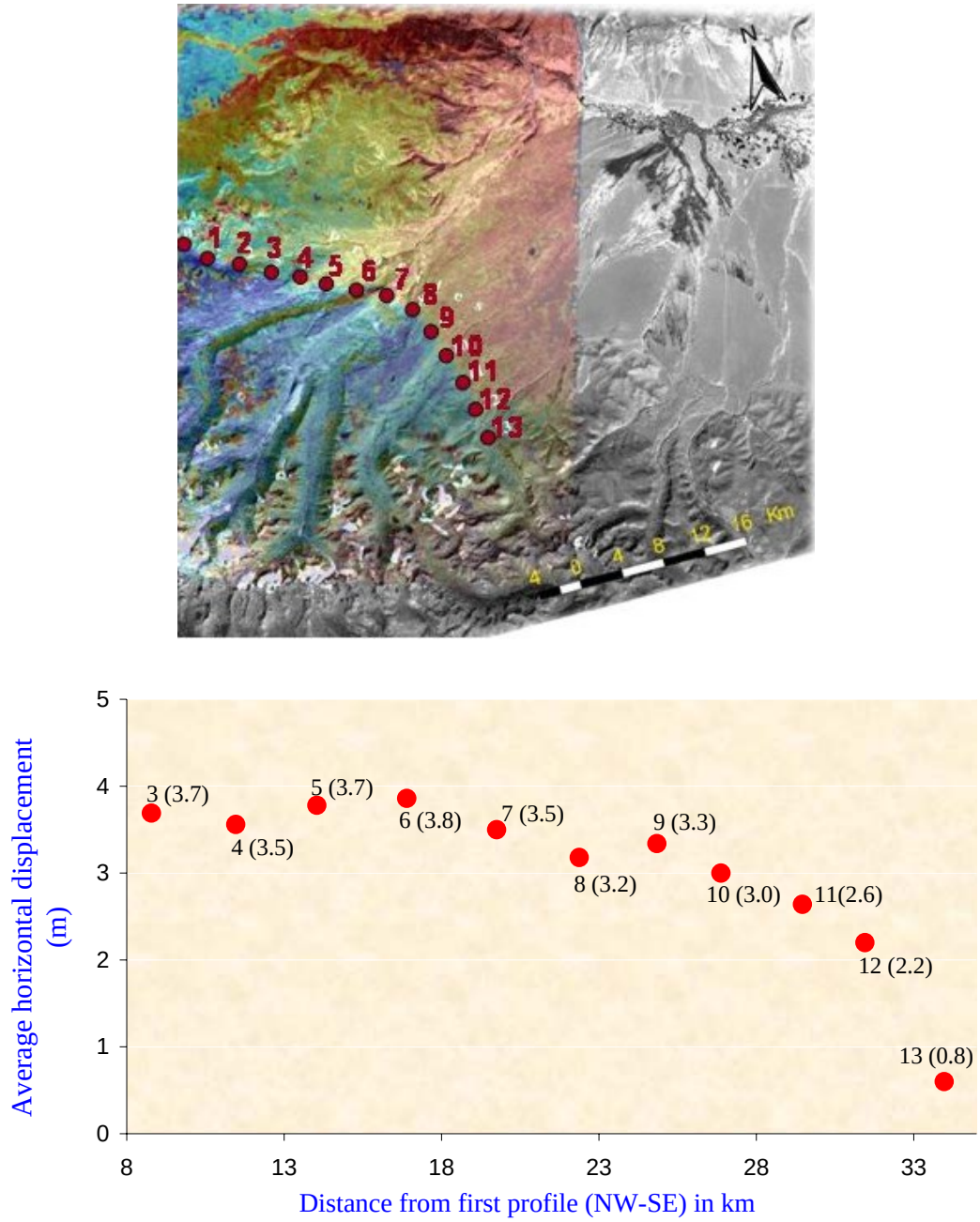

Figure III.16: Horizontal displacement along the fault as calculated from SPOT5 correlation at point 3 to 13 (see location on top image). In order to decrease the noise, each point represents the horizontal slip averaged along 3 km.

III.7 Discussion and Conclusion

The tectonic and fault geometry show that neotectonic activity in the Chuya-Kurai zone controlled by N-S horizontal compression expressed in active faulting and block tilting. The previous study of the region and the existing geological literature shows that the Chuya-Kurai depression was developing under complex interaction of tectonics, sedimentary and climatic processes. The structure of the depression is controlled by reactivation of pre-existing Late Paleozoic fault systems (Delvaux *et al*, 1995). The northern margin of these two depressions is the most active zone in the region where are expressed clear strike-slip and thrusting or high angle reverse fault. Comparing to this active zone, the southern margin of the depression shows less active structures. Because of the absence of clear active faults along the southern border of these depressions, previous study done by Delvaux *et al.* (1995) started to reject the pure strike-slip model considering that the basin was developed between two major WNW trending strike-slip faults. However, since this proposition, the Chuya earthquake occurred at the southern margin of Chuya and Kurai depression and was associated on its main part with right-lateral strike slip ruptures.

The large Chuya sequence (Ms = 7.3 and Ms = 7.0) produced 60 km long right-lateral strike-slip surface ruptures along the southern margin of Chuya and Kurai depression. The field information about the surface rupture and demonstrated rupture photos of the Chuya earthquake described section III.4 of this chapter was based on the report of field investigation have done by Geodakov *et al.* (2003).

The southeastern part of the surface rupture is clearly visible on the field and described in details. The northwestern part of the rupture is not describing in details in the report; the authors just noted that the ruptures continue until valley of Majoi river (Fig. III.6), observing average right lateral offset of 0.5-1.5 m. Unfortunately no SPOT image was available in this northwestern part of the area before the events and we could not obtain complementary information. The result of subpixel correlation of SPOT image shows us clear surface rupture trace in the southern part of Chuya basin and with a clear change in strike to the south. That result is very well consistent with the field observations which are also related to the global sequence (main shock and strong aftershocks).

On the field a small surface offset (maximum 1.5 m) was measured if we compare with the length of fault and the estimated magnitude (Ms = 7.3). If we refer to the usual scaling laws relating coseismic slip, moment magnitude and fault dimensions (Wells and Coppersmith, 1994), more than 2 m of average coseismic slip would be consistent with fault rupture of 60 km length and moment magnitudes of order of Ms=7,3. In addition, for a magnitude 7.3 and strike slip fault, Wells & Coppersmith got an average rupture length of 70 km.

The expected surface offsets are proportional to the length of the activated fault. For intracontinental earthquakes, the coefficient is typically $\alpha = 5x10^{-5}$ (Scholz *et al.*, 1986). This ratio related to the static stress drop on the fault, and it is equivalent to say that stress drops are typically between 1 and 10 MPa (Berberian *et al.*, 2001). Taking a length of 60 km, the surface offset should be of 3 m.

All these evaluations shows that surface displacement observed on SPOT 5 image correlation is more in agreement with general scaling laws for intracontinental strike-slip events.

Differences between displacement measured on SPOT images correlation and reported directly from field observation can explained by the fact that the first is a global measure 3 km wide, when the second is obtained on individuals cracks. The presence of parallel cracks makes the global evaluation, more difficult.

The presence of thick quaternary deposits may also have absorbed a part of the on depth displacement, which was not able to reach the surface. The fact that the measure on SPOT image correlation is similar to the expected values deduced from magnitude shows that this absorption is only superficial and that this event should be considering as an event, which breaks the whole upper crust.

We can consider that each local observation on the field was precise. Nevertheless it is possible that the offsets reported were for a specific segment and did not took into account all offsets of parallel segments of ruptures. This problem is very often encountered when surface ruptures are expressing as pure strike-slip and consist of several en-echelon rupture systems. The other possibility is that there is a part of deformation, which was spread at the surface around the fault without any clear break and thus impossible to observe from the field without previous detailed measurements as a local dense GPS network. This would explain the higher value obtained with SPOT correlation and would not bring into question the field observations. Also we note that, in the report of the field survey, the surface ruptures of the northern part is poorly described probably due to access difficulties.

These studies confirm that SPOT correlation method is a tool that gives a detailed mapping of the fault rupture geometry as well as surface horizontal offsets. These results are important because the area was difficult to access and we could not observe clearly the fault trace on the original SPOT images, despite a ground resolution of 5 m. In addition, despite the field measurements are generally precise, they do not show always all the deformation.

Chapter IV

The 2003 Chuya earthquake sequence: aftershocks study

IV.1. Introduction

Despite a high seismic activity of Mongolian Altay, the Gorny-Altay did not suffer large earthquakes during instrumental observation period, before the Chuya large earthquake. The largest earthquake was a magnitude 6.0 event which occurred in the region on 21st September 1923 (Novikob, 2004).

At the time of Chuya earthquakes several permanent digital seismic stations (Fig.IV.1) were working close to the region of aftershock activity, operated by Novosibirsk Seismological Centre. The installation of these regional networks started in 2002, increasing significantly the number of seismic stations in the area. The specific aim of this network was to establish a specific seismological experimental zone for the study of seismic activity of Chuya and Kurai region (Goldin *et al*., 2003). Nevertheless data of these stations were not available for this study. Discussions are in progress to find an agreement for a joint collaborative project among RCAG, Novosibirsk Seismological Centre and Kazakhstan, and specifically dedicated for the Chuya earthquake study.

Even if we will have access to the larger data set which should exist on the sequence, we already know that the study will be limited by the fact that when the large Chuya earthquake occurred the region of Kurai and Chuya, suffered of failure of the connection to electricity supply. This was solved only three days later (Goldin *et al*., 2003) and thus the early part of the sequence are poorly determined.

The Chuya sequence was recorded on the national seismic network of Mongolia. The nearest seismic station was located at a distance of around 150 km to the SW from the aftershock zone; the other stations were at a distance range from 200 to 1500 km to the SW. Because of the position of the seismic stations which imply a large azimuth gap, aftershocks were poorly located and it was impossible to constrain rupture zones only with these data. On Fig.IV.2 are shown locations of the Mongolian permanent network.

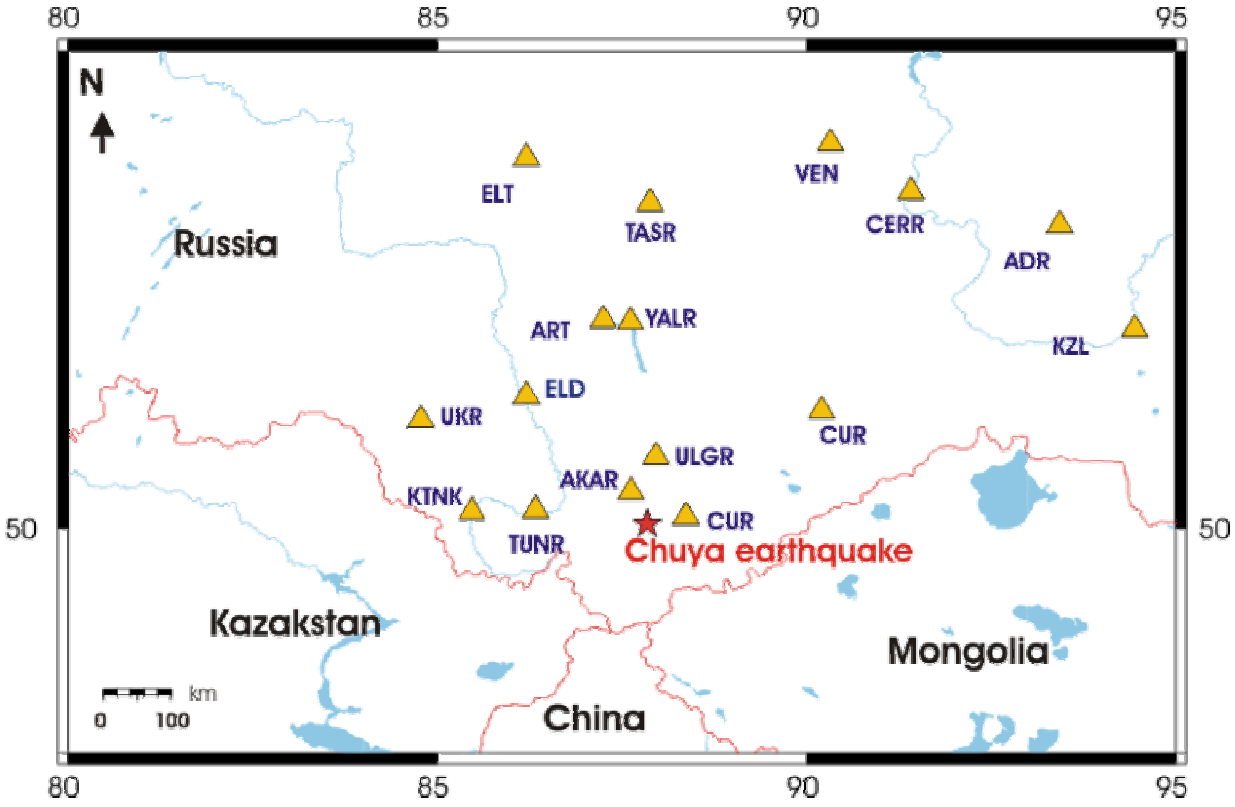

Figure IV.1. The regional seismological network maintained by Novosibirsk Institute in the region of Chuya earthquake.

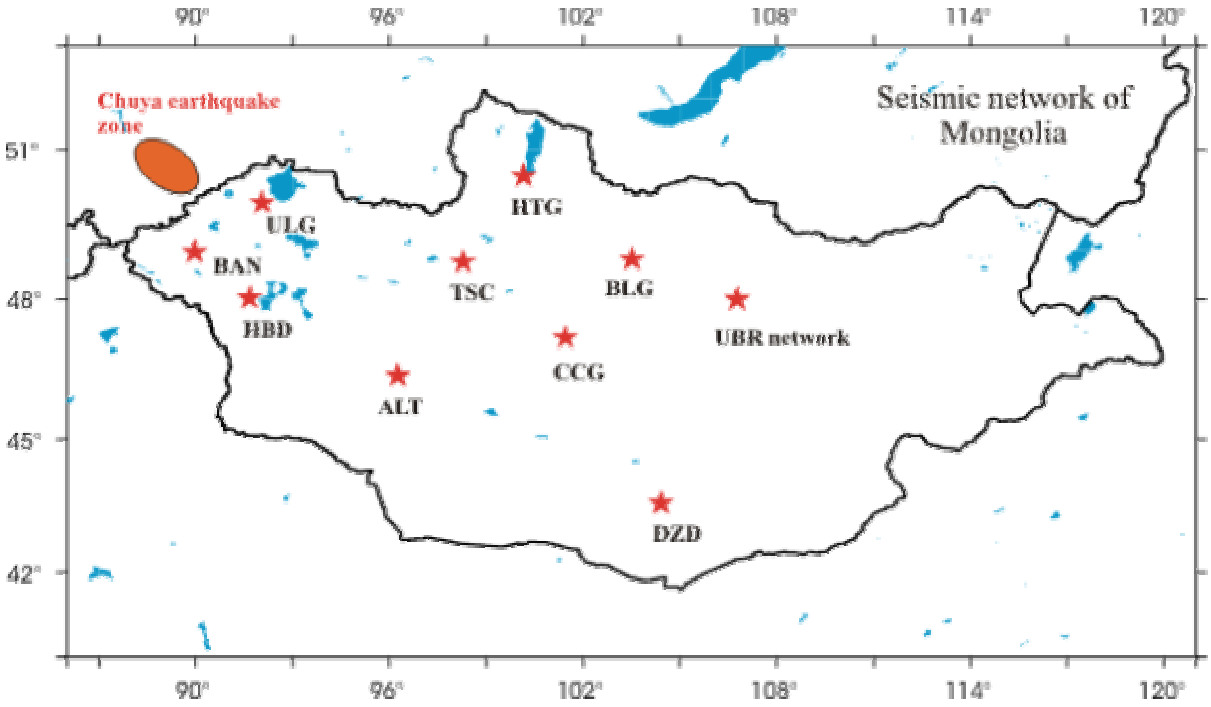

Figure IV.2. The Mongolian permanent seismological network, in operation in September 2003.

After the main shock, eight portable stations were installed along the Mongolian border and in the Chuya basin by a Mongolian-French-Russian collaboration to study aftershock sequence. Stations were operated during around one month and were removed mainly because it was difficult to continue to maintain the instruments in the field a longer time in the winter season. Most of the stations were installed in open wild area, without possibility for low temperature protection and difficult access. The available data set is nevertheless sufficient to show the aftershock area complexity. During the observation period more than 3400 aftershocks were recorded and located. The location was first performed with the standard routine in RCAG in a standard velocity model relevant for whole Mongolia. In order to produce the best aftershock distribution for this study we first determined the 1D velocity model of Altay region. We used VELEST routine on the selected data set of well distributed events of intermediate magnitude; starting from different model we were able to propose an *ad hoc* velocity model which allows reducing the errors of location as the RMS errors. The corresponding model is almost a 2 layers model with a Moho discontinuity at 50 km in agreement with some seismic profiles available in neighbouring regions and Pn/Pg observations on seismograms.

In this chapter, first we will discuss determination of the early aftershock distribution with the relocation of three large events of Chuya sequence. Then we discuss result of aftershock locations observed during survey period.

IV.2 Main shock relocation and early aftershocks activity

The location of the main shock and of the two largest aftershocks given by different seismological institutes varies significantly (Table IV.1). In the Fig IV.3 are shown the locations of the three largest events by different institutions. To discuss the position of these locations, we presented them over the map of aftershock activity as detected by our study and of surface ruptures described by Geodakov *et al*. (2004).

The epicenter locations of the main shock given by IDC and NEIC are very close to the surface rupture presented by Geodakov *et al*. (2004) and of the aftershock distribution zone. The locations of these two centres differ only by few kilometres. Depth of the main shock estimated by NEIC is giving at 16 km, calculated using arrival time difference between P and Pp phases. The other centres did not informed how is performed the depth estimation but 33 km means mainly that it is constrained to be a crustal event. The SSD and ALT epicenter locations of the main shocks are questionable as they feel southwest of the others locations, outside aftershock activity.

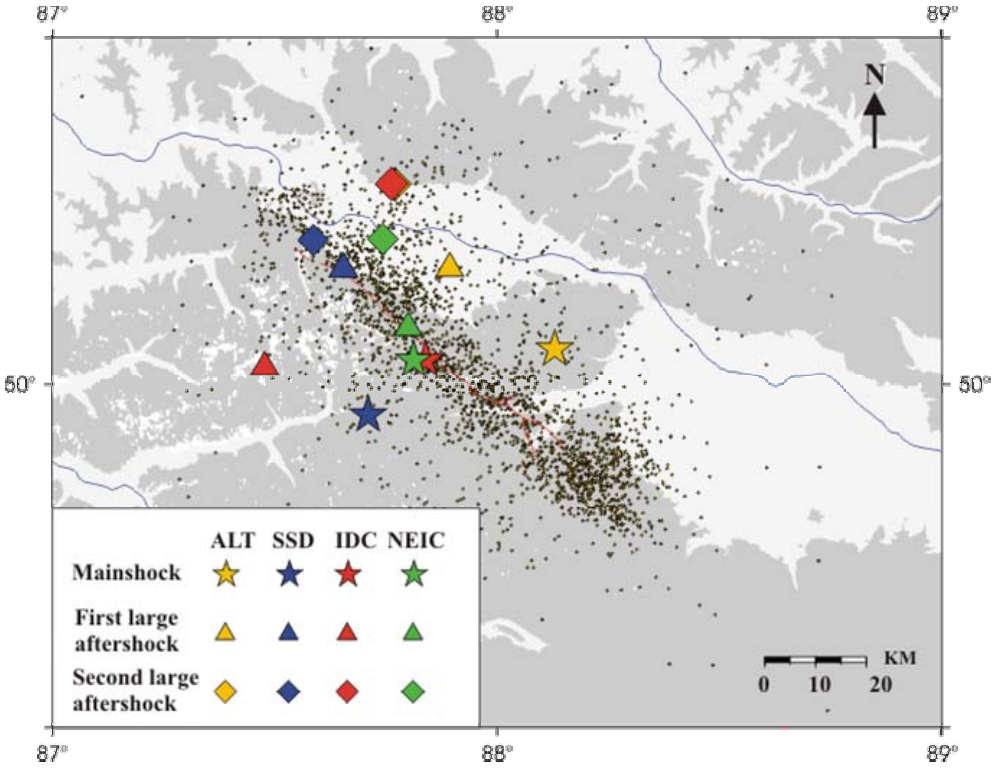

Figure IV.3. Epicenters of 3 main events of the Chuya sequence given by different seismological agencies

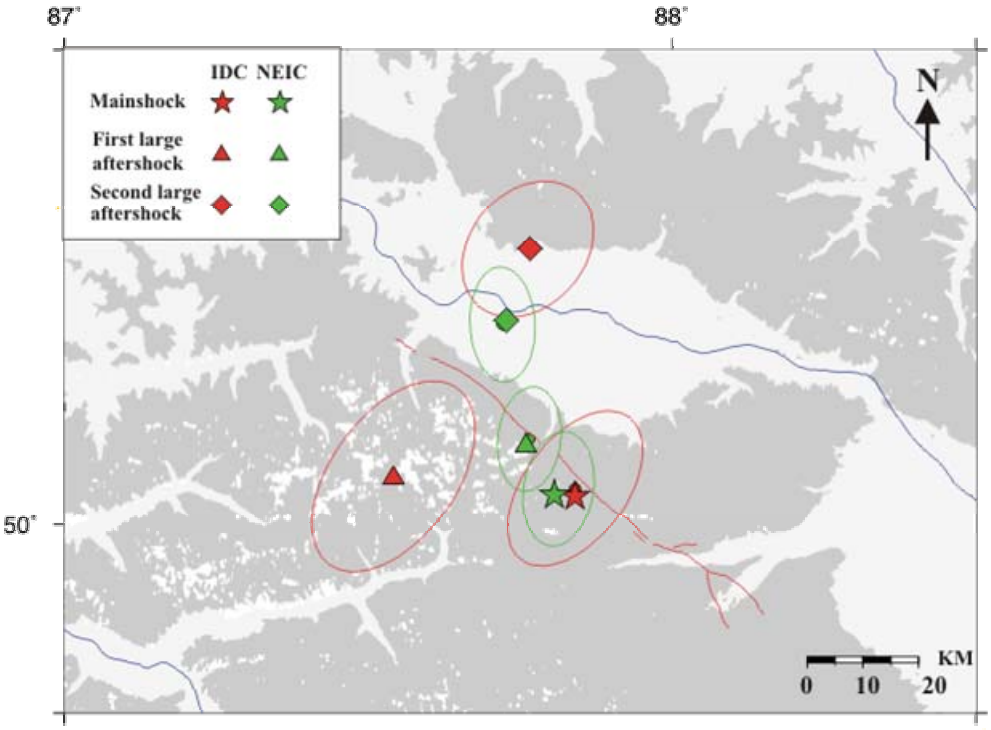

Figure IV.4 Errors in the IDC and NEIC locations of the three main events of Chuya sequence.

For the two large aftershocks with magnitude 6.6 and 7.0 respectively, IDC and NEIC results are different. IDC result propose that the first large aftershock occurred south-westward of the aftershock activity zone and that the second large aftershock occurred northward, near the north-western margin of the Kurai range. These locations seem to be not well constrained as shown by the large errors ellipses and it can explain that they are far from main surface ruptures and aftershock activity. Epicenter positions determined by NEIC for the two large aftershocks are more convenient for explained within the frame of all other available information. The Fig IV.4 shows uncertainties on the locations for the three large events by NEIC and IDC. NEIC location reported smaller error than IDC with an average value of 3.0 km. The IDC calculation for the second large event (27th September, 18:52, Ms=6.6) is poorly constrained with a large uncertainty of 10 km. For this event, the uncertainties ellipses from NEIC and IDC do not have any common part.

In the Russian catalogues, uncertainties of locations are not given; therefore we cannot introduce resolution of this information. There is a generally large difference in the location results from SSD and ALT centres, varying between 10 and 15 km. This can be explained by the fact that on local station records it is difficult to define S waves arrival times for large events as the records are saturated; therefore location of these events is less constrained, mainly in depth. We suppose that it is why locations given by ALT and SSD for these three large earthquakes are far away from worldwide agencies locations.

Date	Origin time	Latitude	longitude	Depth	Ms	Institute
27 /IX/03	**11:33:23.6**	**50.038**	**87.840**	**0.0**	**7.3**	**IDC**
	11:33:25.1	**50.038**	**87.813**	**16.0**	**7.3**	**NEIC**
	11:33:26.7	**49.97**	**87.77**	**33.0**	**7.3**	**SSD**
	11:33:23.3	**50.04**	**88.07**	**0.0**	**7.5**	**ALT**
	11:33:25.0	**50.042**	**87.838**	**9.7**	**7.3**	**HYPODD**
27 / IX/03	**18:52:48.7**	**50.051**	**87.541**	**13.7**	**6.6**	**IDC**
	18:52:46.9	**50.091**	**87.765**	**10.0**	**6.4**	**NEIC**
	18:52:49.7	**50.16**	**87.66**	**33.0**	**6.7**	**SSD**
	18:52:49.1	**50.15**	**87.83**	**0.0**	**6.6**	**ALT**
	18:52:47.0	**50.080**	**87.763**	**16.0**	**6.6**	**HYPODD**
01 / X/03	**01:03:29.3**	**50.29**	**87.76**	**27.2**	**7.0**	**IDC**
	01:03:25.2	**50.21**	**87.72**	**10.0**	**7.0**	**NEIC**
	01:03:27.7	**50.21**	**87.61**	**33.0**	**7.0**	**SSD**
	01:03:27.9	**50.29**	**87.77**	**0.0**	**6.9**	**ALT**
	01:03:25.4	**50.165**	**87.703**	**11.2**	**7.0**	**HYPODD**

Table IV.1 Locations and magnitudes of the main shock and the two large aftershocks of Chuya sequence by different seismological data centres. (IDC - International Data Centre CTBTO; NEIC - National Earthquake Information Centre USGS; SSD - Urgency Reporting Agency of RAS; ALT - Local Centre of Altay-Sayan of RAS ; HYPODD - This study, see later in the text).

Nevertheless the as precise as possible relative locations of the main shock and large aftershocks are necessary for the interpretation of the rupture process proposed in the next chapter. To relocate the main shock and two large aftershocks, we used a double difference method to improve location of these large earthquakes. The double difference technique is thoroughly described by Waldhauser *et al.* (2000) and a discussion of the effect of different initial parameters is proposed by Dunn (2004). The location method incorporates ordinary absolute travel time measurements and P and S and can include differential travel time measurements obtained by wave form cross correlation when available. Residual between observed and theoretical travel time differences (calling double differences) are minimized for pairs of earthquakes at each station linking together all observed event-station pair. The procedure is valid till the residual between observed and differential travel time for two earthquakes are sufficiently close together compared to the event-station travel time.

HYPODD program was used in many areas (Waldhauser *et al.*, 2000) as the code is freely distributed since almost five years. It gives, when the stations distribution is well adapted, impressive results and produces images of active regions, where faults segments and bends could be recognized by some structures of the activity. In the interpretation, it must be taken into account the production of ghost structures in the outer parts of the network, and some possible distortions of the structures dues to the bad knowledge of the velocity models.

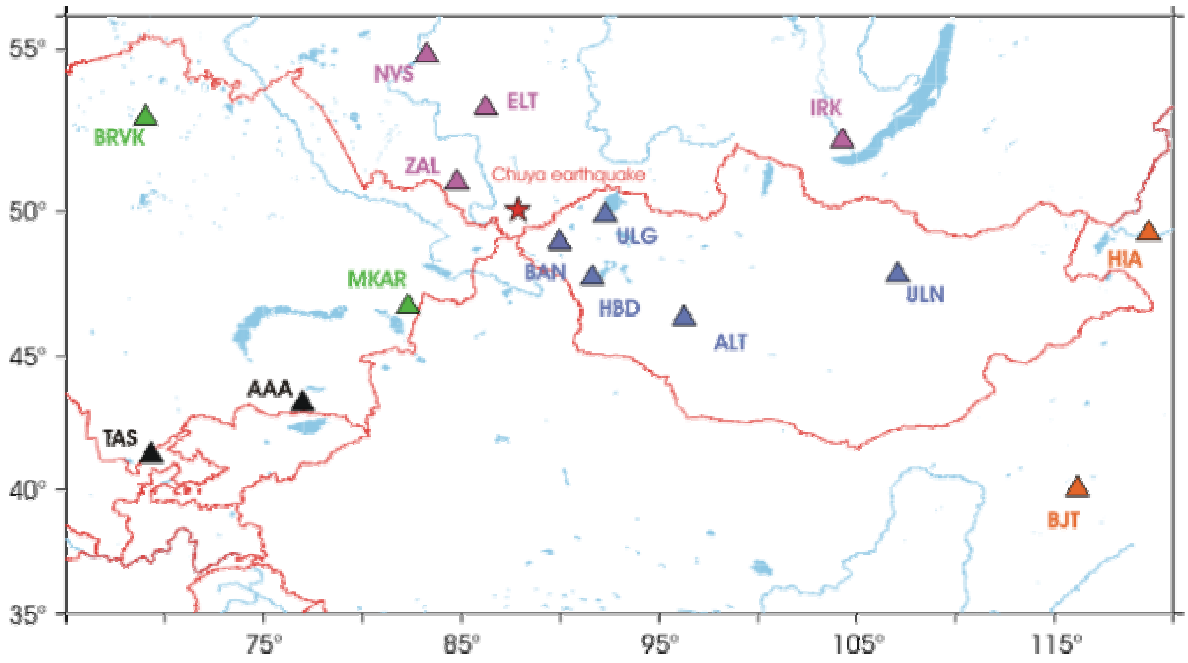

Figure IV.5. Location of stations from which data have been used for the relocation of the main events of Chuya sequence

To compute relative location of these three large earthquakes and other early aftershocks we used HYPODD software. IDC results on the distribution of aftershocks and position of the three large events are shown in Fig IV.6. We used arrival time data reported in IDC and NEIC bulletins, combined with data recorded at RCAG networks. From IDC data we used mostly data from stations at regional distance from the aftershock sequences zone. Fig IV.5 shows distribution of the stations used for the relocation procedure. The stations MKAR, BRVK and ZAL are located at the nearest distance from the aftershock sequence. For most of the events, data of these three stations were combined with RCAG network data for the relocation so that these data composed the data set in a distance range from 300 and 500 km. At larger distance we have chosen mostly stations located at distances smaller than 2500 km, the western are stations of RCAG (HBD, ULG, BAN). These stations are equipped with short period seismometers digital and analogue recording systems. To improve input the data set, we have included some aftershocks recorded during mobile instrumental study period, for which we have records at local distances.

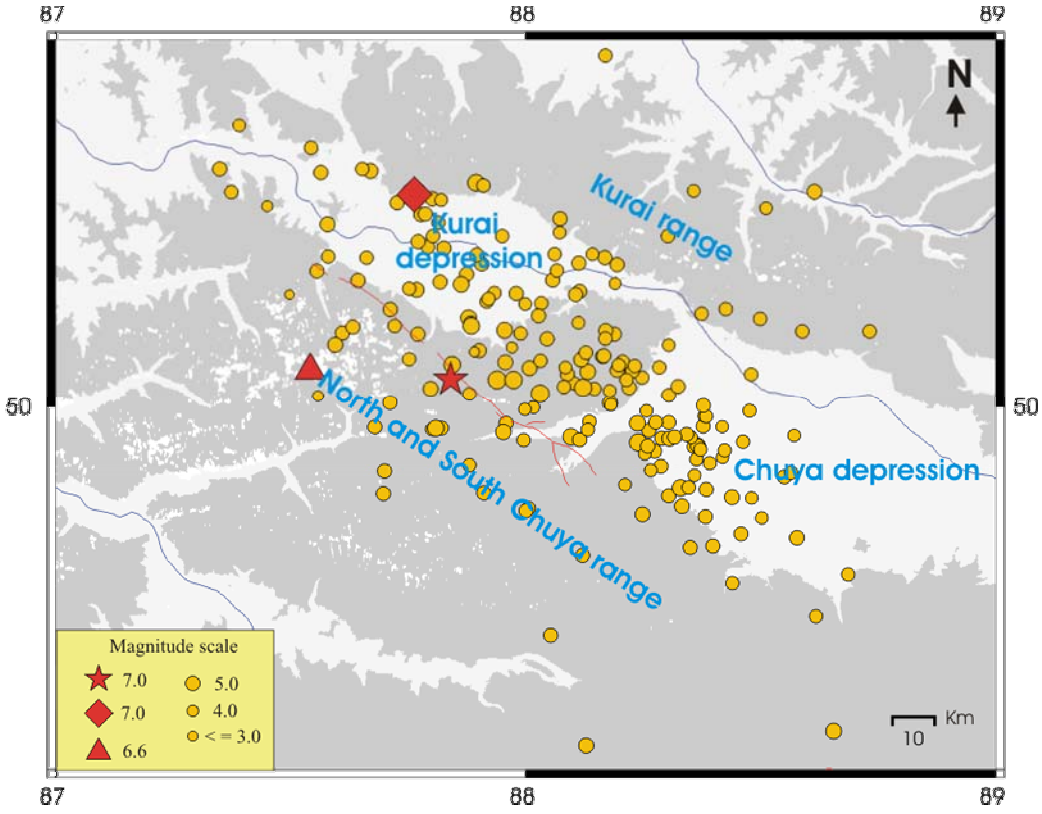

Figure IV.6. IDC locations of the main events of Chuya sequence.

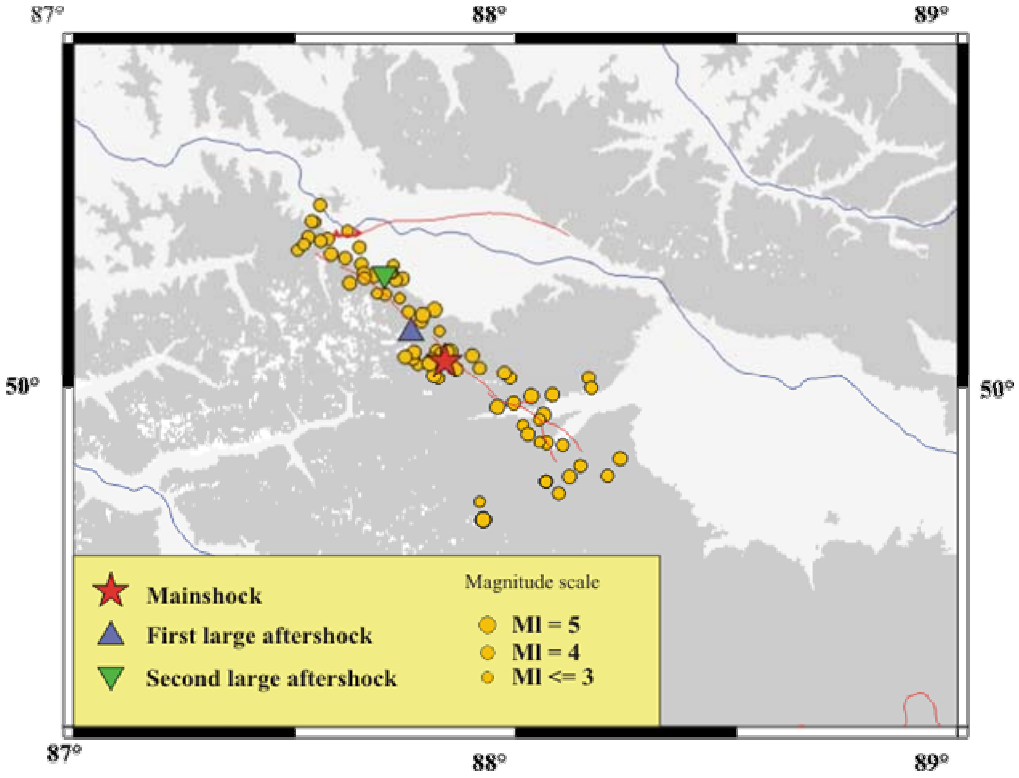

Figure IV.7. Relocations of the main events of Chuya sequence with HYPODD procedure.

These events consist mostly on moderate size events with magnitude more than Ml ≥ 3.0. The numbers of events recorded within both international and local stations are a very small data set compared to earliest aftershock activity. Nevertheless, it is the enough data to fix the locations of main shock and other large aftershocks relatively to the aftershock activity. This procedure was used in different other studies and, when it exists a good network configuration, it can provide a good resolution on the absolute position of main event position compared to some well determined aftershocks.

In the starting step of relocation calculations we used IDC location results which are shown on Fig IV.6; the distribution is quite spread around the aftershock area. To get reasonable event pairs we have tested different maximal separation distances i.e., 5, 10, 15 and 20 km. In our case 15 km was the best choice. It corresponds to the problem geometry, because our data set that consists mostly of larger aftershocks regionally recorded. Distances between stations and events are generally higher than 100 km. We started with an initial data set of 234 events recorded both by international and local seismic networks. From the initial location of these events, the average distance between events was about 13 km. These events are connected through a network of link that consists of 17864 P and 337 S-wave phase pairs. The average number of links per event pair is 5, while the average offset between strongly linked events is 13.5 km. We obtain travel time differences for each event pair with a separation distance less than 15 km for the final relocation.

108 events were successfully relocated by the LSQR method, solving the damped least squares problem. We adopted the typical definition of initial parameters that was reported by Waldhauser *et al*. (2000). The choice of damping factor is rather empirical and depends on the condition of the system to be solved. It can be expressed as the ratio of the largest to the smallest condition number (Dunn, 2004). This ratio is continuously reported during the procedure of the HYPODD program. In our case a damping factor 60 was found to be appropriate. We used different weights for P and S wave observations, 1.0 and 0.5 respectively. Theoretical travel times differences were estimated based on 1D velocity model. We use the model obtained by VELEST (Kissling *et al*., 1995) inversion on data from the 8 mobile stations installed for the aftershock study. More detailed explanations on the procedure to determine the local velocity model will be discussed in a later section.

Mean RMS error for the data set was 0.9 sec. The average uncertainties on the relocated hypocenters are 0.5 along latitude, 0.8 km along longitude and 0.4 km in the vertical direction. These errors represent the statistical errors, and could be an underestimation of the real errors on the hypocenter locations. In particular, in our case, we infer from the station distribution and the fact that we are working on crustal events, that depth cannot be well constrained. We propose and estimation on depth error of 3 km on the base of the results of the different tests that we have performed. Fig IV.7 shows distribution of relocated epicenters of early aftershocks together with main shock and the two largest aftershocks epicenters shown by different symbols. Obtained locations for the main events are given in Tab IV.1 and compared with NEIC and IDC locations on Fig IV.8.

The relocations of these large earthquakes are well correlated with surface ruptures, fault plane dip and aftershock distribution: the main shock is relocated in the middle of surface ruptures, nearby the locations given by international data centres. In details, the HYPODD location of main shock is almost similar to both IDC and NEIC results. The first large aftershock (27th September 2003) is relocated 5 km to the northwest from main shock, in an area where surface ruptures have been reported after the field study; the position given by our study is similar to NEIC location, when the IDC location feel out of the aftershock activity. The largest aftershock (1st October 2003, Ms = 7.0) is relocated at 15 km to the northwest from the main shock; starting from the IDC position in Kurai range, far from the NEIC position, the relocation procedure move the epicenter in the same area than NEIC position. Such result is important for the understanding of the fault system associated to this magnitude 7.0 event. The IDC position has been used to propose that the Kurai active thrust fault system could have been reactivated during this large event. Some field observations were reported to support this assumption (Geodakov *et al*., 2004). However, the lack of aftershock activity in Kurai range (see later), well constrained in the region by two mobile stations, is more compatible with the fact that the whole sequence (main shock and the two large aftershocks) is related to a fault system associated with the south margin of Kurai and Chuya basins.

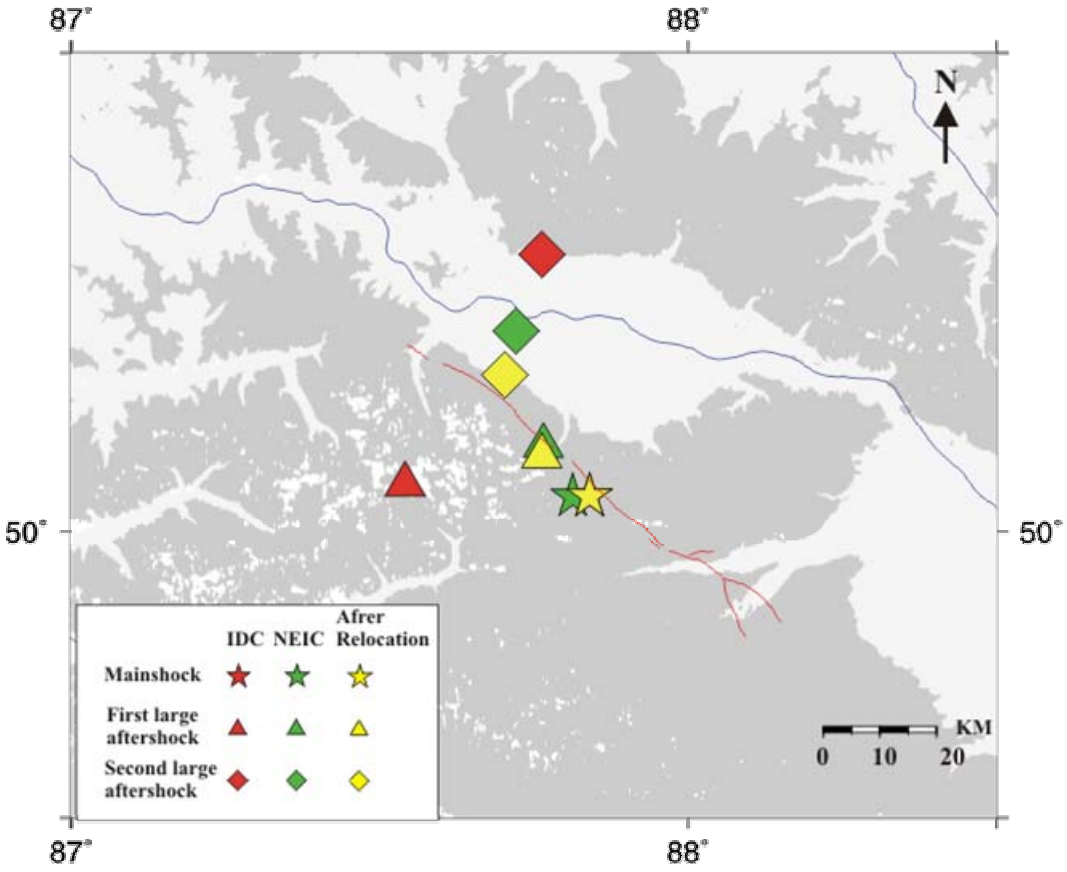

Figure IV.8. The relocation results of the Main shock and two large aftershocks.

The distribution of relocated early aftershocks (Fig IV.7) shows a clear compact feature elongated along the southwestern border of Kurai and across Chuya range. The direction of this feature is compatible with the strike of one of the fault planes of available focal solutions. The south-eastern seismicity pattern almost disappears, and seismicity stopped not far from the northern border of the Chuya basin. From the final image we can propose a global fault length of 90 km which should represent the whole sequence, compatible with empirical laws between magnitude and fault length (Wells and Coppersmith, 1994). The rupture seems to extend bidirectionaly from the first epicentral area, but only the individual study of the major events can be used to propose rupture process.

Depth distribution obtained by HYPODD relocation for these early aftershocks is poorly constrained and do not present any clear structure. Nevertheless, hypocentral depths of the 3 main events seem to be reliable. The main shocks of Chuya earthquake nucleated at a depth of 9.6 km. The first and second large aftershocks occurred at a depth of 13 km and 9 km, respectively. The depth estimations from our relocation is shallower than NEIC result but are consistent with our body wave inversion, result which we are going to discuss in the next chapter. This shallow depth is also confirmed by Novosibirsk team result which has been presented in a workshop in Novosibirsk (Goldin *et al.*, 2004): a depth of 8 km was determined using local seismic network.

IV.3. Aftershock investigation

IV.3.1 Temporary network installation

As expected for a shallow Ms = 7.3 event, Chuya earthquake was followed by many aftershocks. The epicenter area is located near the Chuya and Kurai basins which belong to southern part of Novosibirsk region in Russia and a large part of this region was very difficult to access.

As the event was not far from the Mongolian border and few was known on the possible faults related to the event, monitor the aftershock distribution was of great interest for the Mongolian institute. From preliminary locations, a southward extension of the activated area was proposed as far as on the Mongolian border. At that time French broad-band portable seismic stations from the Lithoscope pool, were just in the process to be removed from the MoBal transect profile (PICS collaborative experiment, Deschamps *et al*., 2004) and almost available in Ulaanbaatar and Irkutsk were researchers were also able to manage installation and operation of these stations. A collaborative effort to monitor aftershocks of Chuya earthquake was then decided between Research Center of Astronomy and Geophysics (RCAG), Mongolia, Institute of Earth Crust (IZK), Russia, Geosciences Azur, France and Department of Analysis and Surveillance of Environnement (DASE), France. Financial support was found from DASE, IZK and Geoazur.

Geometry controls of the temporary network was difficult because of the problems to cross Mongolia-Russia border, but also because of bad accessibility conditions of high relief of Altay Mountains and need of secure places for stations. As it was impossible to install portable seismic stations on the rupture zone of Chuya earthquake for the RCAG team, three stations were installed at the NW limit of Mongolian border and other two stations was installed more south to monitor at the same time possible seismic activity in other active region of Altay. IZK team, thanks to collaboration with Novosibirsk team, installed three stations on the area of aftershock sequences (Fig IV.9). Therefore, station distribution of the temporary network is not the best to obtain a precise location of the aftershock sequence during the observation period; mainly there is a large azimuthal gap due to a lack of instruments in the western and southwestern areas of the activated zone.

Of course, installation of portable stations was a little late and therefore the main crisis between main event and magnitude 7.0 event on 01st October was lost. On 04th October, eight days after the Chuya earthquake, two short period seismic stations (TE07 and TE08) have been installed near the north-west border of Mongolia, 100-120 km away from main shock area. A few days later, three more broadband stations (DAYN, CHIK and KHOH) were installed in Mongolian side by RCAG team. DAYN, the nearest station from the Mongolian site was located 60 km away from main shock. The distances from epicentral area of the two other stations are important, around 190 - 300 km.

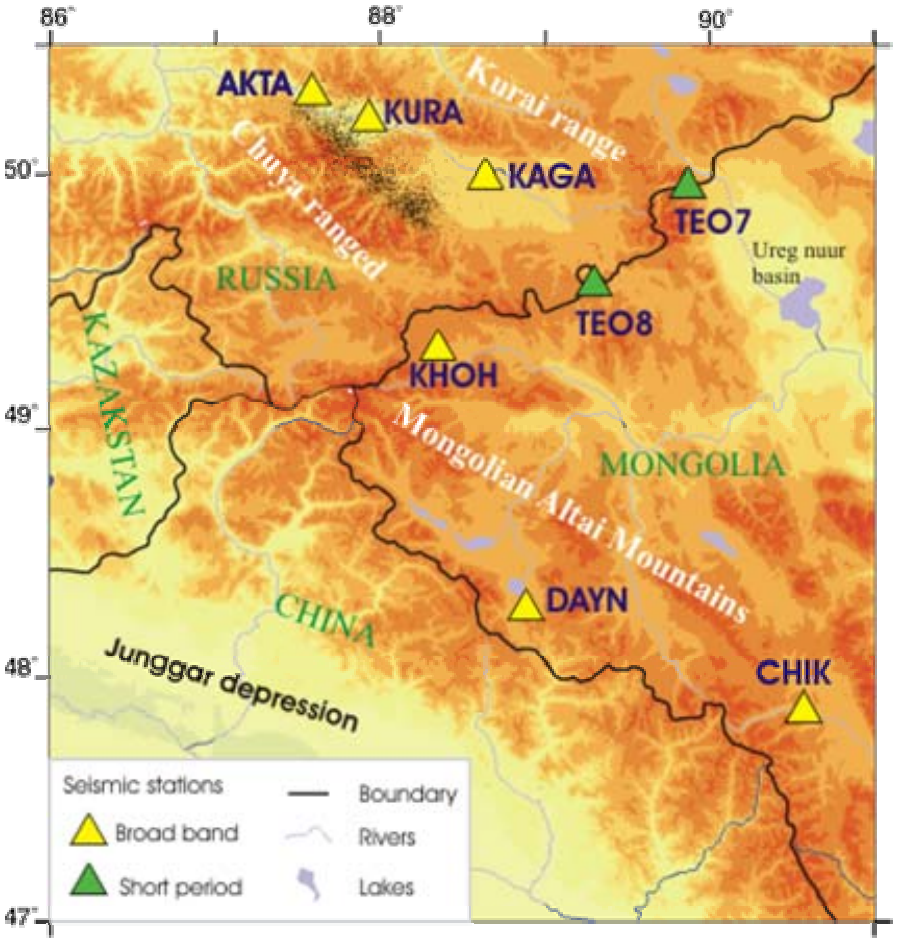

Figure IV.9. Position of the temporary network which was operated during a period of one month (09th October to 19th November).

Russian team installed three broadband stations (KAGA, KURA and AKTA) which are located directly on the epicentral area. Stations started from 08th November. Stations KAGA and KURA are located in the north-western part, near the Kurai basin and AKTA station covered the north-eastern part, in the Chuya basin. Locations of the 8 portable stations are shown in Fig IV.9 together with observed aftershocks and the location of observed surface ruptures.

All stations were installed on bedrock basis to minimize effect of local soil condition. The seismic background noise of the region was low and that gave opportunity to record high quality signal which allows generally a good picking of first arrivals.

Fig IV.10a and IV.10b shows examples of recorded vertical signals of Chuya aftershocks. We can observe that the signal to noise ratio at all stations for a Ml = 3.6 event on 18th October and a Ml = 2.4 event on 21st October is good and that arrival time of P and S phases are easy to pick.

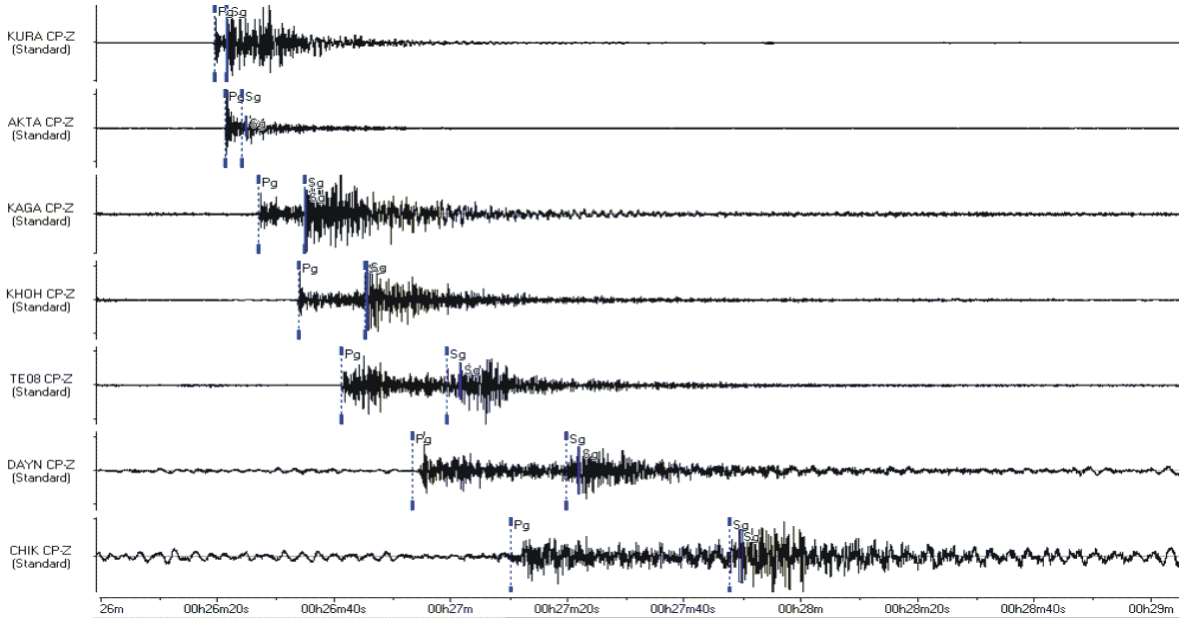

Figure IV.10a. Example of recorded events on the temporary network on 18th October; Ml = 3.6

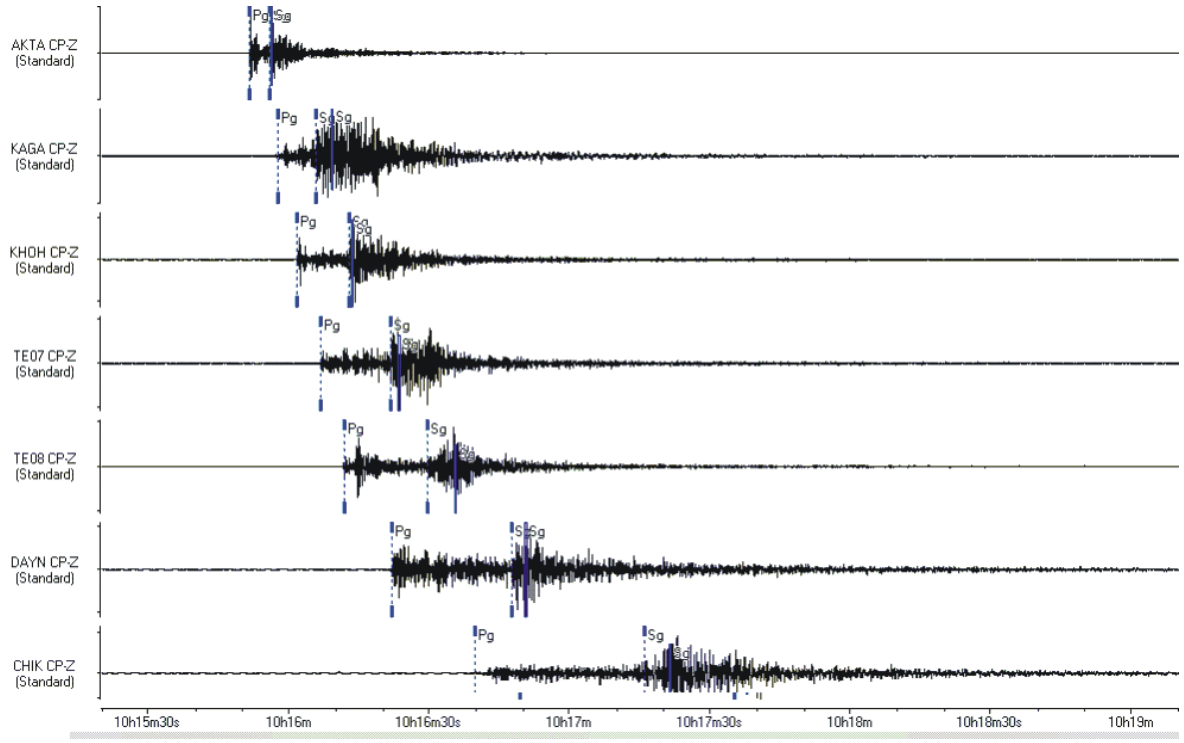

Figure IV.10b. Example of recorded events on the temporary network on 21st October , Ml = 2.4

The portable network remained in operation for a period of one month near the aftershock zone. It was removed mainly because of the difficulties of the operation during wintertime: instruments were not conditioned to support the very low temperatures, batteries

and solar panels were not adapted for wintertime during which the sun is very low, and access to sites was uncertain. We decided that it was not scientifically useful to make the necessary effort to insure reliability of the recording as one month recording time period is sufficient to describe the aftershocks spatial distribution of a magnitude 7.3 event. Latter on, we could observe from worldwide data available for this sequence that no large event occurred after we removed the instruments.

Operation of temporary stations was satisfactory and all recording period corresponds to available data. Fig IV.11 presents the data availability from each site and colours show sensor type. The recording period of stations near the aftershocks zone, the Russian ones, was a little shifted, compare to that of stations installed in Mongolia. Stations in Mongolian sites started one week after the main shock but must be removed earlier than in the Russian part.

The team in charge of station installation in Mongolia has worked on the field to collect information from inhabitants on shaking and damage effect on buildings due to the main shocks. It is important to do this immediately after a large earthquake, because in time the information is going to be forgotten and, if it is performed later, the data set is either not fully complete, either biased by loss of memory. That information will be used to build complete isoseismic map of this large event in collaboration with Novosibirsk scientists. During the study of macro seismic observation we found a maximum intensity of VI in the Mongolian side. We provide a macro-seismic report from different places, to build intensity distribution of Mongolian side (Fig IV.12).

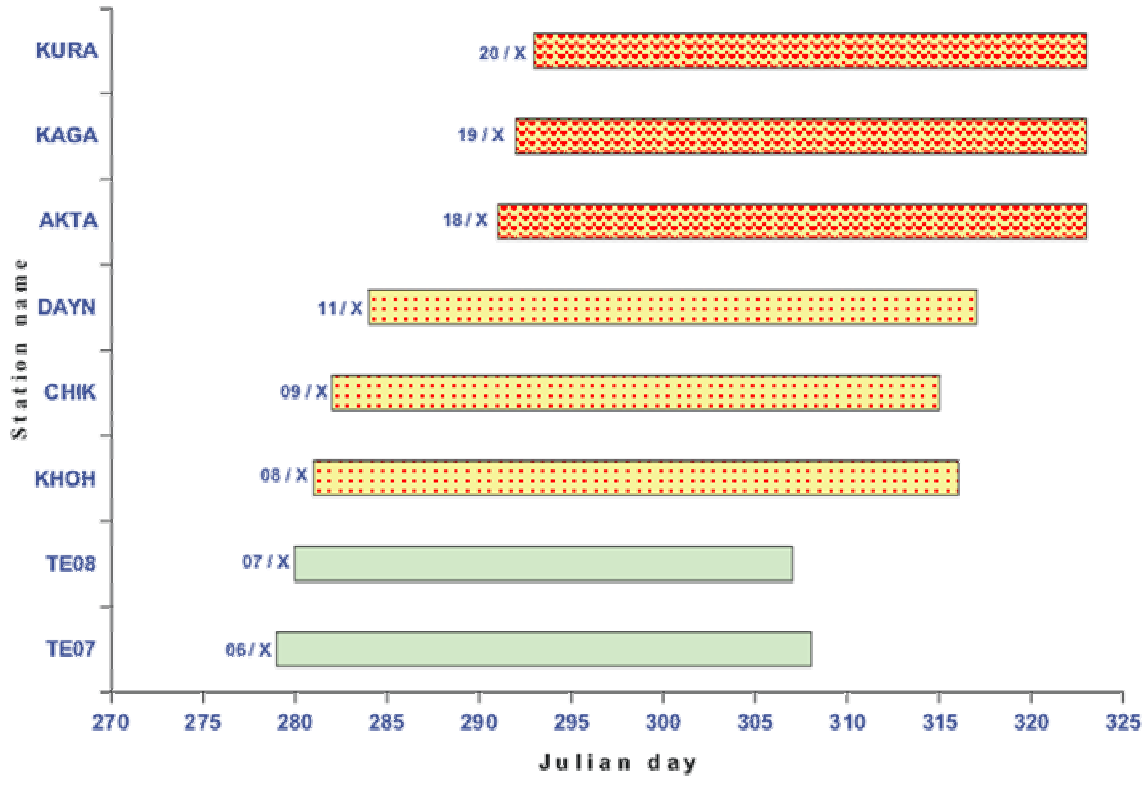

Figure IV.11. The operate period of each temporary station. Note that the instruments installed in Russia were installed a little later than the ones in Mongolia

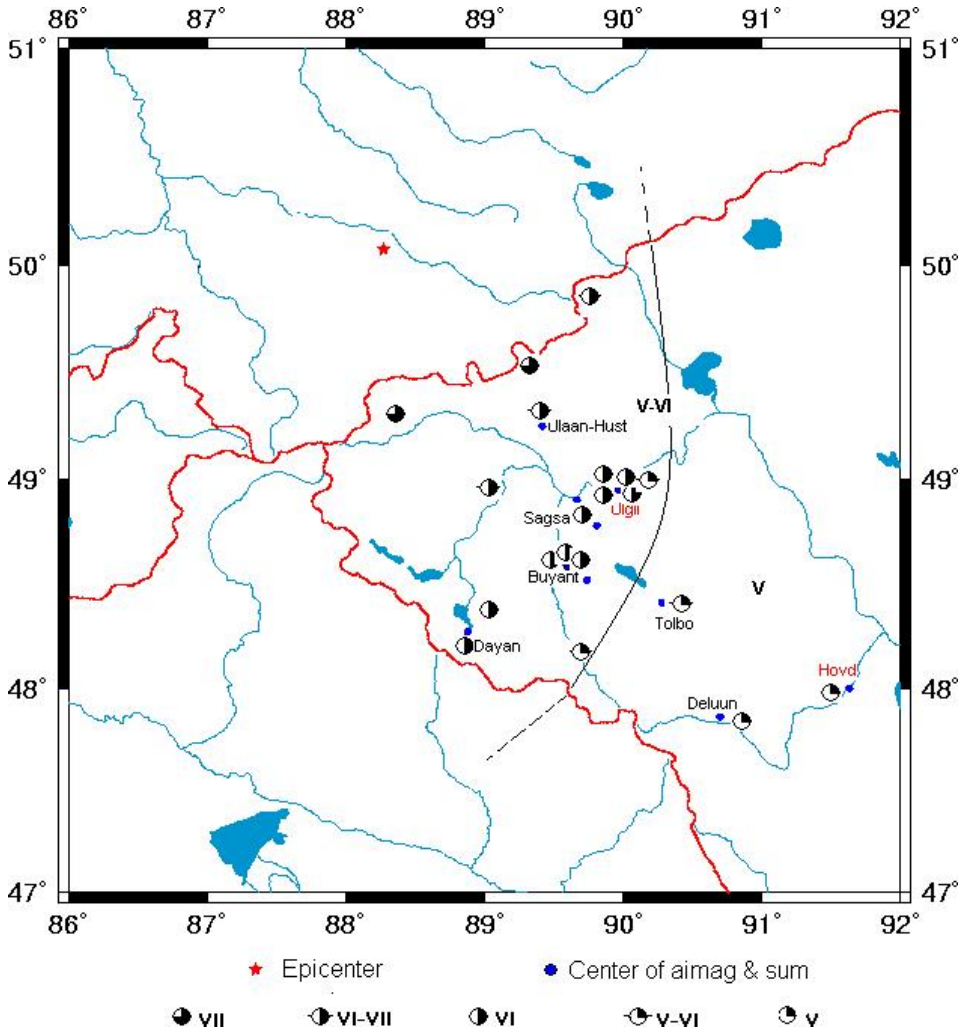

Figure IV.12. Map presenting the macroseismic information collected during the survey in Mongolia. This must be related to the results obtained in Russia and presented in the chapter III

IV.3.2. Instrumentation.

There were two different types of seismic instrumentation used during the aftershock deployment: six three component broad band and two three components short period stations.

Broadband stations were portable stations from the French Lithoscope pool composed of Guralp CMG-40T velocity sensors (response flat between 50 Hz and 60 sec, sensitivity of 400 V/m/sec or 800 V/m/sec depending of the serial number) and Titan3XT 24 bits (true 21 bits) recorders. Data are stored directly to high capacity SCSI hard disks allowing a long autonomy. A 125 samples/sec sampling rate per channel was chosen.

Short period three component stations were composed of short period geophone sensors and the AIRAO recording system developed by DASE. This recorder is less adapted to such long term recording as data are stored on a 64 MBytes flash memory card. It is while a 50 Hz sampling rate was used; data should be transferred every two days to the data storage computer.

On each station, power was provided by 12 Volts battery, charged with solar panels. Time was controlled by GPS clock, continuously synchronized for the AIRAO station and every hour for the Titan recorder to minimize power consumption. All stations were recording ground motion in continuous mode and had the possibility of online control of noise to signal ratio directly on the site. Fig IV.13 shows some installation of the portable stations.

Figure IV.13 Images from the installation of the temporary network. The CMG40 sensor is installed on a concrete base. Two solar panels provide the alimentation.

IV.3.3 Data control and processing, raw location

The completed data set of Chuya aftershock consists of almost about 10 GB of continuous record of the ground motion collected on eight portable stations and the RCAG permanents stations. A backup of the raw data are available on CD-ROM and USB hard disk.

Raw data collected from the temporary deployment were in two types of format. The six broad band stations provided data in titan format; conversion software is provided by the French seismological community to SAC, ASCII or MSEED. The other two stations provide data in a format which is easily converted in FONYX format, the format used by the permanent stations of RCAG and the picking and location software routinely used in Ulaanbaatar. We decided to convert all raw data to this FONYX format to be able to add all data from temporary network to the Mongolian permanent data. The first step was to organize all data by station and time, and to convert it to FONYX format. I developed special routine to make automatic procedure to transfer data between the different formats.

First I converted all titan data to the SAC format, after a careful analyze of the internal clock time drift and including the time correction; then I used SAC2FONYX software has written at DASE, to convert SAC to FONYX.

The final data set was analyzed using the routine software with which national seismicity is analyzed in RCAG: continuous recordings are simultaneously processed, an event triggering is applied, and then the picking is proposed to the analyst. All the data set, was processed at RCAG with the participation of different analysts who participate to the national seismological centre and have already defined common definition of phases and picking weights.

There is no published velocity model available for the Altay region. A single layer crustal velocity model, currently using in routine hypocenter location for Mongolia, appears to be too simplistic because it is a very general model for a broad region with large varying crustal thickness. It was developed by Baljinnyam (Baljinnyam *et al.*, 1975) using data from local earthquakes on the territory of Mongolia. The model is essentially a half space with a P wave velocity of 6.17 km/sec and an S wave velocity of 3.56 km/sec with average Moho depth at 45 km.

However, two deep seismic sounding studies have been carried out in the Altay region. One is the 3850 km long seismic profile QUARTZ-4 (Russia): it goes from Baltic shield until north of Altay folded belt (Fig IV.14a). Results were obtained using the complete Quartz data set and suggest that crustal velocity structure under the Altay Mountains can be modelled using four layers with seismic velocity varying between 5.5 km/sec and 6.9 km/sec (Morozova *et al.*, 2000)

Another seismic refraction profile was studied across Western China. The profile crosses the southern margin of the Altay Mountains, the Junggar Basin, the Tianshan mountains and the Tarim basin (Fig IV.14b). Mooney *et al.* (2000) found a large difference in crustal thickness at the northern end of profile, where, over distance of less than 400 km, it varies from 54 km thick under Altay Mountains to 46 km thick under Junggar basin. As mean value, this study proposed that the crustal structure under the Altay can be modelled using three layers with seismic velocities of 6.1 km/sec, 6.6 km/sec and 6.9 km/sec.

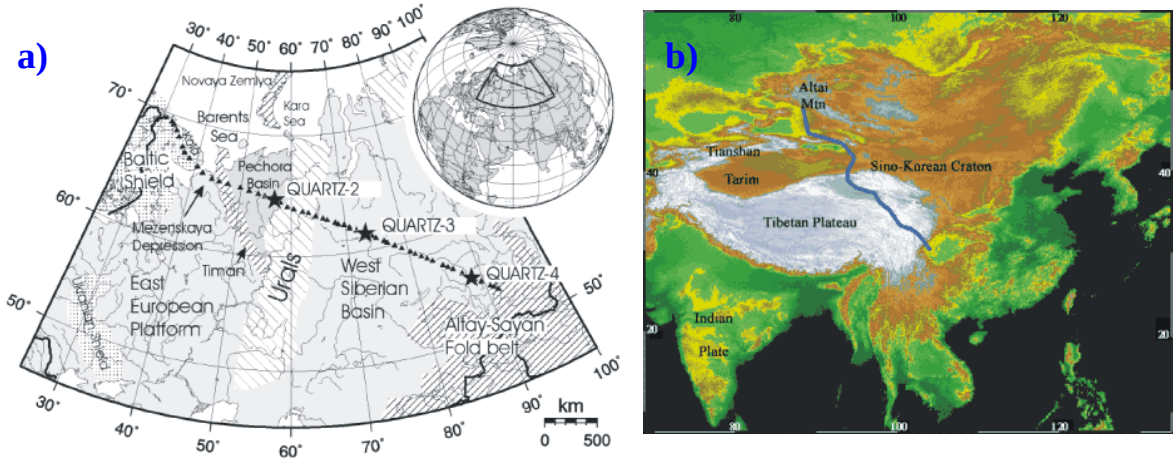

Figure IV.14. Geographic position of 2 large profiles (a- seismic profile QUARTZ-4; b-profile crosses the southern margin of the Altay Mountains) which provided information on crustal structure in the area.

IV.4 1-D model estimation by VELEST

As shown above, the available seismic profiles were located far from our study area. Thus we thought necessary to get a better velocity model for Chuya earthquake region mainly adapted for the aftershock location. To accomplish this, a schema of simultaneously inversion for the hypocentral and velocity parameters from the travel time data was used. The algorithm VELEST developed by Roecker and Ellsworth (Kissling *et al*., 1995) was used to get 1-D initial velocity model for region. Program VELEST has been designed to derive 1-D velocity models for earthquake location procedures and as initial reference models for seismic tomography. This simultaneous inversion procedure is a damped least squares inversion with individual damping parameters for each independent parameter such as origin time, earthquake epicenter and depth and velocity of the model layers.

As the process is highly non linear, to determine a velocity model several inversions run that must be made with velocity interface depths varying between runs. Because VELEST does not automatically adjust layer thickness, these have to be determined by a trial-and-error process. Thus the inversion of velocity model must start with finding an appropriate model layering. Following Kissling suggestion (Kissling *et al*., 1995), we start with a model which covers the assumed regional crustal thickness (50 km) and in which the layer thickness increases with depth (trial layer thickness of 2 km for shallow crustal levels and increased layer thickness with increasing depth till about 5 km for lower crust). As very few information on velocity model for the Chuya aftershock area is known, we started with five different initial velocity models as proposed in user's guide of VELEST program (Kissling *et al*., 2000): starting from a model with low crustal velocities (from nearly 2 km/sec near the surface to possible Moho velocity) and increasing the velocity values in the next models until an extremely high velocity crustal model (6.5 km/sec at the surface).

We selected 584 events (Fig IV.15) from the whole aftershocks data set, recorded at minimum six stations and with observation of both P and S phases. To get velocity of Pn phases (velocity beneath the Moho) we included data from permanent stations of RCAG at distances larger than 200 km from Chuya area. A total of 3590 arrival times of P and S phases (1794 direct and 1796 refracted rays) were selected and used with VELEST to determine a crust velocity structure.

After selection of the data set, we localized the corresponding events with routine VELEST using, damping coefficient of 0.01 for the hypocentral parameters and the station delays and 0.1 for the velocity parameters as suggested. In most of the inversion run we used a maximum of 9 iterations to get minimum RMS value. The input parameters are not changed during the first step iterations to allow comparison between different initial models. We repeated inversion procedure several times with new updated velocities and new hypocenters. To regularize the inversion problem, neighbouring layers with differences between velocity values smaller than 0.15 km/sec were merged into thicker layers and inversion was performed again using the modified model as initial model. This procedure is repeated until when we get reasonable stabilized mean RMS value.

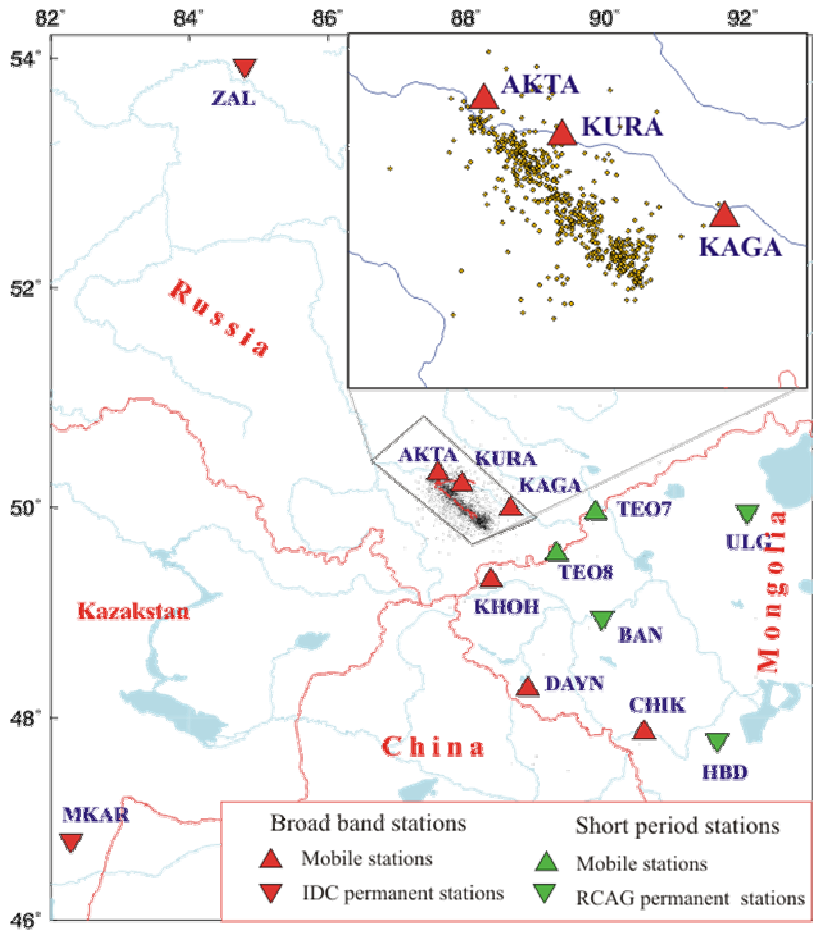

Fig IV.15 Map of the stations from which the data have been collected to run VELEST and inverse travel time in order to deduce the velocity model.

As explained above, we started with different velocity models which are varying from extremely low velocity model until to extremely high velocity model. We classified them within five types:

L ***Extremely low velocity model with a velocity varying between 2.0 km/sec at the near surface and 6.0 km/sec at bottom of the crust.***

M ***Lower intermediate velocity model with a velocity varying between 3.2 km/sec at the near surface and 6.4 km/sec at bottom of the crust.***

M1 ***Intermediate velocity model with a velocity varying between 4.2 km/sec at the near surface and 6.9 km/sec at bottom of the crust.***

H ***High velocity model with a velocity varying between 5.4 km/sec at the near surface and 7.4 km/sec at bottom of the crust.***

H1 ***Extremely high velocity model with a velocity varying between 6.4 km/sec at the near surface and 7.9 km/sec at bottom of the crust.***

The purpose of the first step is to infer from the inversion the thickness of the crustal layers: we start from an initial model which simulates a linear variation of the velocities between the two extreme velocity values with a lot of almost same thickness layers. With the first runs thickness and velocities of the different layers are obtained. We verify that the procedure converges to almost identical results for the different initial models. After some probes of the inversions we succeed to get meaningful results.

Fig.IV.16 shows different velocity models obtained from VELEST inversions starting from models as classified above. The colours of lines are correlated to the different types of models and will not be changed for the all the following figures. Results obtained in the first step presented on Fig IV.16a, emphasis that determination of layers depths was difficult. Even after some iterations, no layers with similar velocities are clearly identified except for the higher velocity model for which a lower crust seems to be identified between 30 and 50 km. We notice that for all the obtained models, a low velocity superficial layer can explain well the data and that the Moho depth is always proposed at depths between 50 and 55 km.

On Fig IV.17 are presented the RMS estimation corresponding to the best model obtained during these inversions. RMS remains higher for the models deduced from models L, M, M1. In the second step, we began to merge layers with similar velocities in the lower crust to reduce the parameters number. After few runs of the inversion procedure, we noticed that our data set is better explained with higher velocity model.

Whatever is the starting model, the results converge to similar estimation of the velocity model presented on Fig IV.16b and the corresponding best RMS estimation (Fig IV.17) is very similar and confirm this observation. The lower crust velocities are very well constrained. Only the model deduced from starting model L (low velocities) present major differences in the upper part of the crust. The proposed low velocities are clearly not compatible with the inverted data set as the RMS corresponding to this model remains important (Fig IV.17).

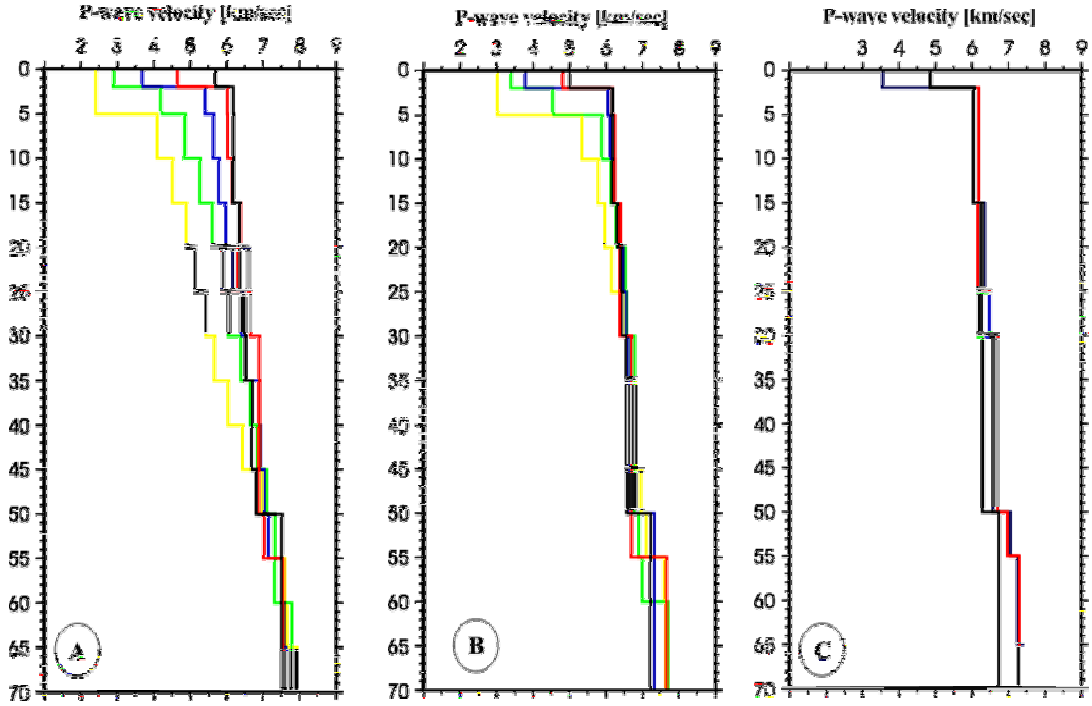

Figure IV.16 Velocity models obtained at different stages of the VELEST procedure as explain in text. The colours represent the starting model from which the presented solution has been obtained from a low velocity model in yellow to a high velocity model in black. A, B, C are explained in text.

Next we keep only models deduced from models M1, H and H1 and continued inversion procedure, to test the depth of Moho and a possible intermediate layer around 30 km depth, which is poorly constrained. The Fig IV.16c shows the inversion result for these three models after joining thin layers of only slightly different velocities into thicker layers. The model deduced from H1 (extremely high velocity model) starts to have unrealistic low velocities in the upper mantle. We eliminated these solutions and constrained one initial model for the last inversion, comparing M1 and H. Models deduced from these two models were almost identical and in good agreement with general velocity from other information. However the lower limit of the crust was still not clear and we focus some more runs on the determination of that parameter. To fix Moho depth we increased damping of the sub-Moho velocities as noted in VELEST users guide (Kissling *et al.*, 2000). After several inversions velocity models are stabilized and we found smaller RMS value. Fig IV.17 presents minimum RMS values from different solutions. We select a final solution presented in Table IV.2, with three layers in the crustal thickness. The upper and lower crustal layer velocities, with an error of two standard deviation are 4.35 km/s (± 0.013 km/sec) and 6.47 km/sec (± 0.043 km/sec) respectively with a total crustal thickness of 50 km.

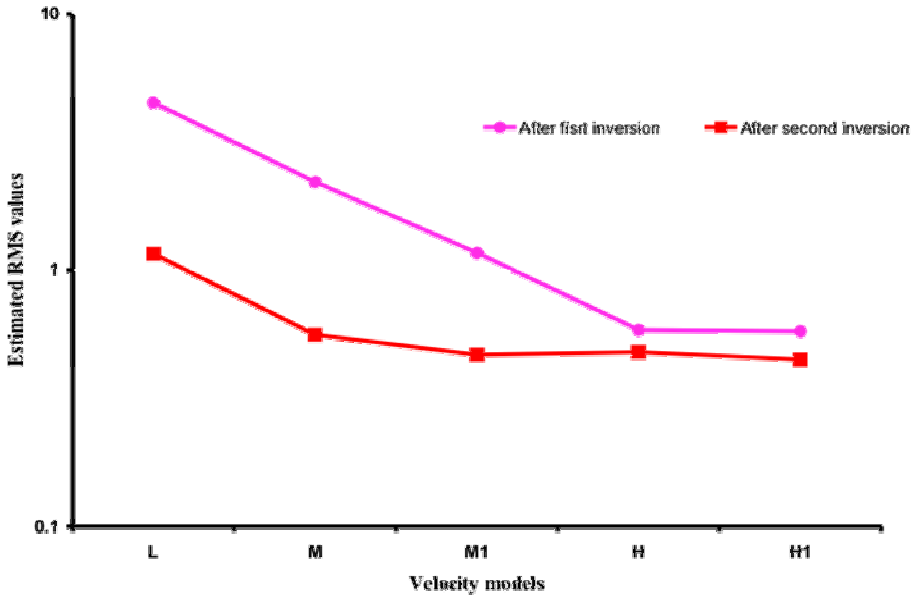

Figure IV.17. Evolution of the RMS for two starting models during the inversion procedure.

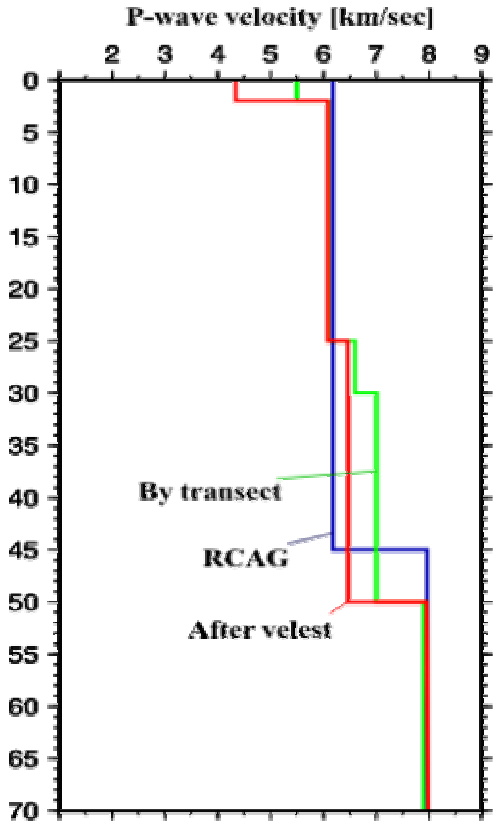

Figure IV.18. The final selected model compared to other information available. A clear improvement in the velocity model was not possible with our data set.

This solution is the best one-dimensional model we obtained by VELEST. It corresponds to lowest RMS error of 0.2 sec in the inversion procedure of the selection of 584 aftershocks, and this after many trials and error steps.

Layer	*Velocity (km/sec)*	*Starting depth (km)*
1	***4.35***	***0***
2	***6.08***	***2***
3	***6.47***	***25***
5	***7.96***	***50***

Table IV.2 The selected crustal model obtained by different runs of VELEST

The final model obtained by VELEST and the velocity information obtained from seismic profiling are shown in Fig IV.18. Our model 1D which derived from inversion of travel time of the aftershock sequences at temporary and permanent stations do not much differ from observed result of seismic sounding studies. It is the 1D model which explains the best the travel time of our data set.

IV.5 Location of aftershocks and analysis of the distribution in time and space

IV.5.1 Aftershock localizations

We interpreted about 3268 events from the records of the 8 portable and 3 permanent stations. We added readings of two ISC stations, if available. Reason to include ISC station data was to try to complete azimuth coverage of stations. Mostly data from stations BRVK, MKAR and ZAL have been included in our data set. These stations are located in south-west and north-west directions from the aftershock area at distance range between 300 and 500 km (Fig IV.19).

The P and S wave arrivals are picked manually by analysis at RCAG during the initial process of data. The resolution of reading P and S phases of closest broadband stations was excellent and all recorded phases are fully weighted (1.0). Readings of S waves deteriorate with increasing epicentral distance, mostly for the short period vertical component stations. S waves arrival time is easier to pick on three component records of the mobile instrumentation, and even more on the broad-band record. For stations located far away from aftershock zone, P and S phases are weighted separately; P wave readings are fully weighted (1.0), S-waves are weighted by half (0.5). Average of the number of S to P picks ratio is 60% for the entire data set, but it is only 50% for closest stations.

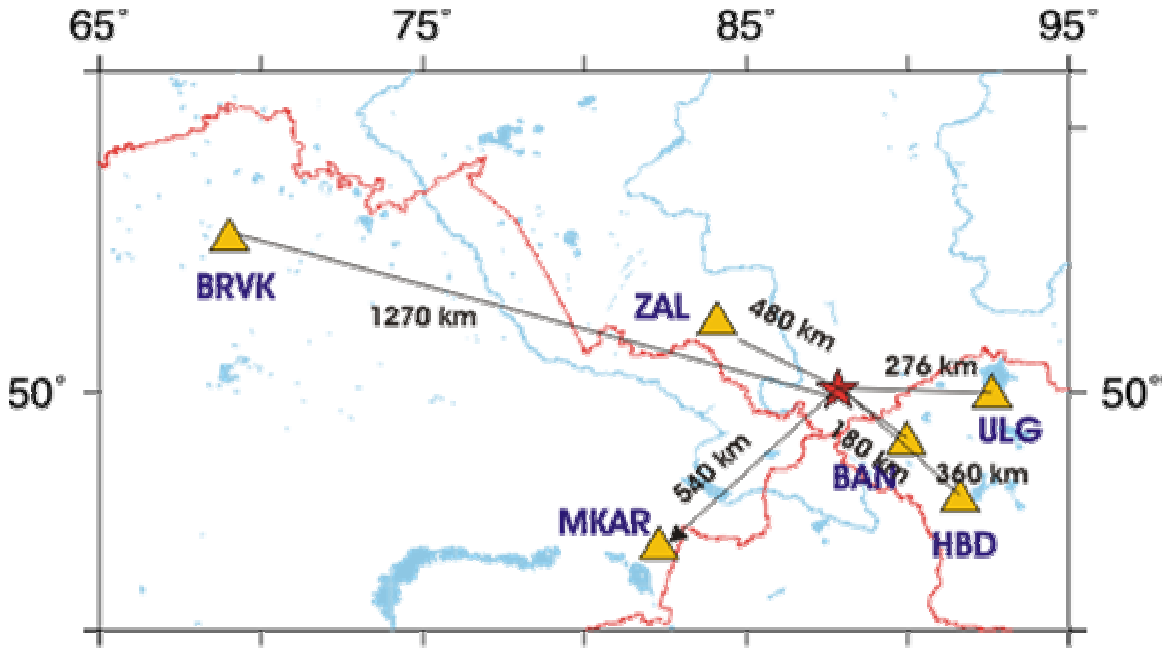

Figure IV.19. Stations from which arrival times were used, when possible, to complete the temporary network data set.

The Fig IV.20 shows travel time versus distance on the aftershock data set. We see that arrival times correspond to direct phases (Pg and Sg) travel time recorded in a distance range between 5 and 700 km and to Pn and Sn phases travel time in a distance range from 300 to 700 km. Between 150 and 250 km, some Pg waves have been interpreted as Pn, because the separation in time is weak. There is a gap of data around 275 km and almost no

information for distances larger than 550 km which is related to the selection of stations that we choose to include in the data set.

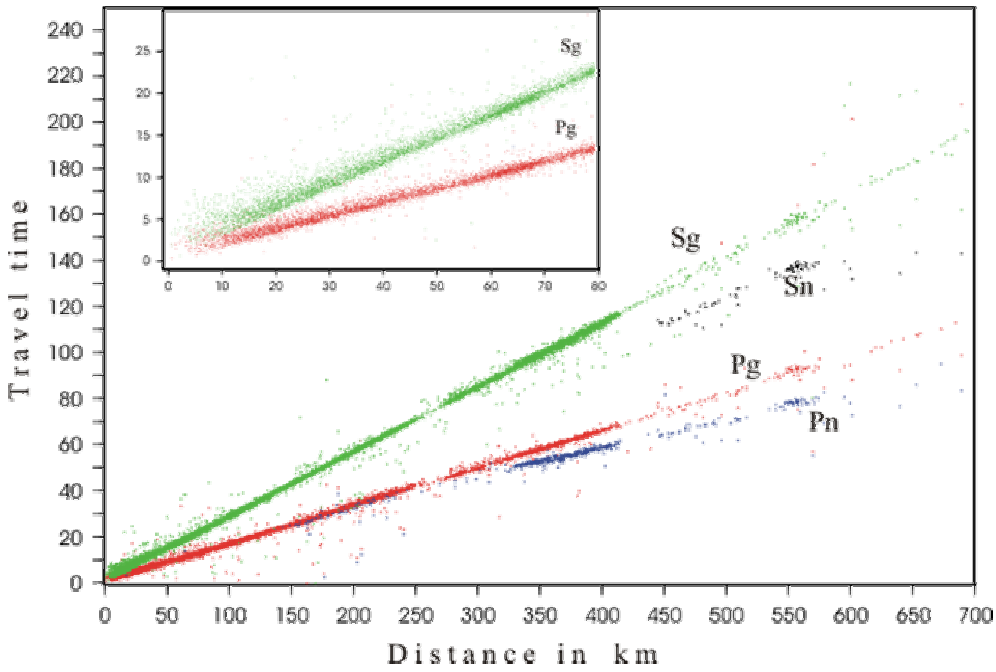

Figure IV.20 Travel time versus distance curves which can be deduced from our data set after preliminary location with FONYX standard program. Pn and Pg are clearly identified.

The dispersion is large at small distances as it can be expected on such plot which uses the event location and does not take into account depth of events. Preliminary estimates of the hypocenters for Chuya aftershocks are calculated using the program FONYX using a half space model proposed by Baljinnyam *et al*. (1975). These locations do not have the accuracy necessary to conduct the studies of the spatial and temporal correlation aftershocks, mostly because of poorly constrain on depth. To improve these earthquake locations was necessary to use improved velocity model and many trial and error tests. FONYX program is not compatible with relocation of large number of data same time, because it is designed for the operational interpretation of seismic data. Therefore, it was impossible to relocate all events with different starting configurations using FONYX program.

Finally, the locations of aftershock hypocenters were determined using the program HYPOCENTER 3.2 developed by Lienert *et al*. (1994) with the velocity model (Table IV.2) derived in this study. HYPOCENTER is a program to locate seismic events at local and global distances. It is developed under different operating systems. We used it under Windows on PC. The program has the possibility to process a large number of data: the number of arrivals and stations is only limited by the hard disk space available. For a layered model, it is possible to input complete name of the phase as Pg, Pn, Pb, Sg, Sn, and Sb to specify the refraction or reflection interface. Non precise phases could be also used, with label P and S; the program use then the fastest P or S arrivals (Lienert *et al*., 1994). Is also allowed for users to start location with different configuration, stations corrections and to choose phase weights which can solves miss reading of arrival time or phase association. The different starting parameters are controlled by minimizing the average residuals of all events after different runs. Other capability of the program is that some parameters, suspected by the user to be less solved by the data set, can be fixed as the depth.

As the starting parameters of hypocenter localization procedure, we have chosen events with a minimum of 4P and 4 S arrival times. At all station located close to aftershock zone, we have used full weight of all available arrival times, at other stations only to the first arrival time was affected a full weight. For the readings of Sg and Sn phases recorded at long distance, weight is decreased until half weight of P phases.

For the starting depth, we tested several values starting from hypocentral depth at 5 km to 20 km, increasing by 5 km. Average error of these tests did not differ so much which shows that the depth of most of these events are poorly constrained. However depth determination is also strongly dependent on the relation between Vp and Vs velocity models. As HYPOCENTER program is using Vp/Vs ratio to deduce S wave velocities from the P wave velocity model, we should define this parameter before beginning the final location procedure. To get an estimation of this parameter we repeated the location procedure with different values of Vp/Vs between 1.69 and 1.76. Two graphics illustrated in Fig IV.21a and Fig.IV.21b shows result of estimation minimum RMS value for the average initial depth and Vp/Vs ratio respectively. After several calculations, we considered that a starting depth at 10 km with Vp/Vs ratio of 1.71 is the best initial parameters for the data set.

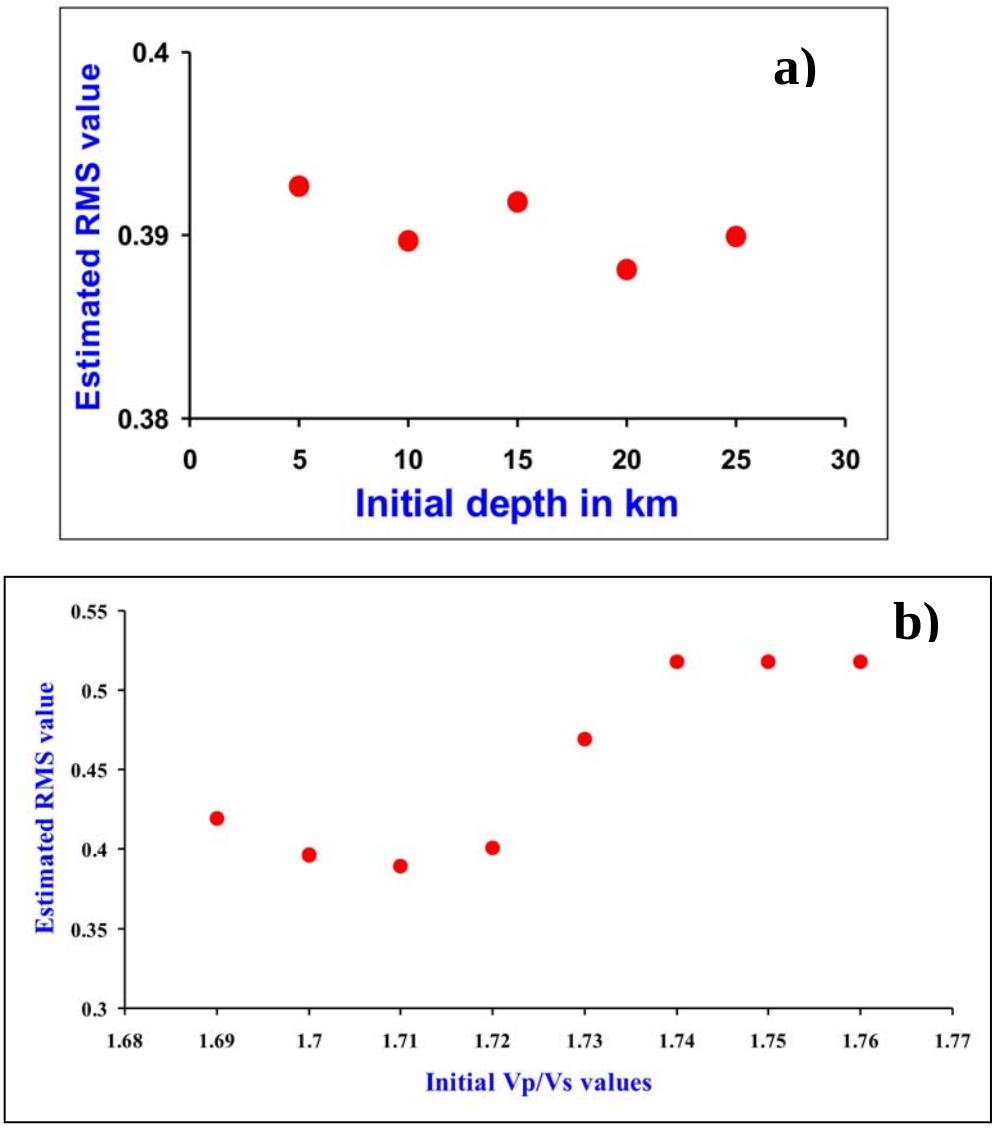

Figure IV.21. Variation of the global RMS with (a) starting depth and (b) Vp/Vs ratio.

Magnitude of aftershocks is determined using local magnitude formula in use at RCAG and which was developed taking account of local wave attenuation. Measurements of Sg-phase amplitude at station with distances larger than 100 km are used to calculate Ml magnitudes. We prefer to use of this scale of magnitude, to keep homogeneity with what is done within the permanent network of Mongolia.

RCAG never established the formula for duration magnitude estimation which is used in most of the aftershock studies. In case of large aftershocks we used record on low gain station at the shortest distance possible without saturation of records. For 20 aftershocks that were worldwide recorded, we have compared our estimated magnitudes with IDC and NEIC Mb magnitudes determined using teleseismic phases (Fig IV.22). The difference between the three evaluations of magnitude is large only for some events. We estimate a mean difference of respectively 0.3 and 0.4 between RCAG and IDC, NEIC magnitudes. This justifies us to use the magnitude evaluation that we made for the whole aftershock data set.

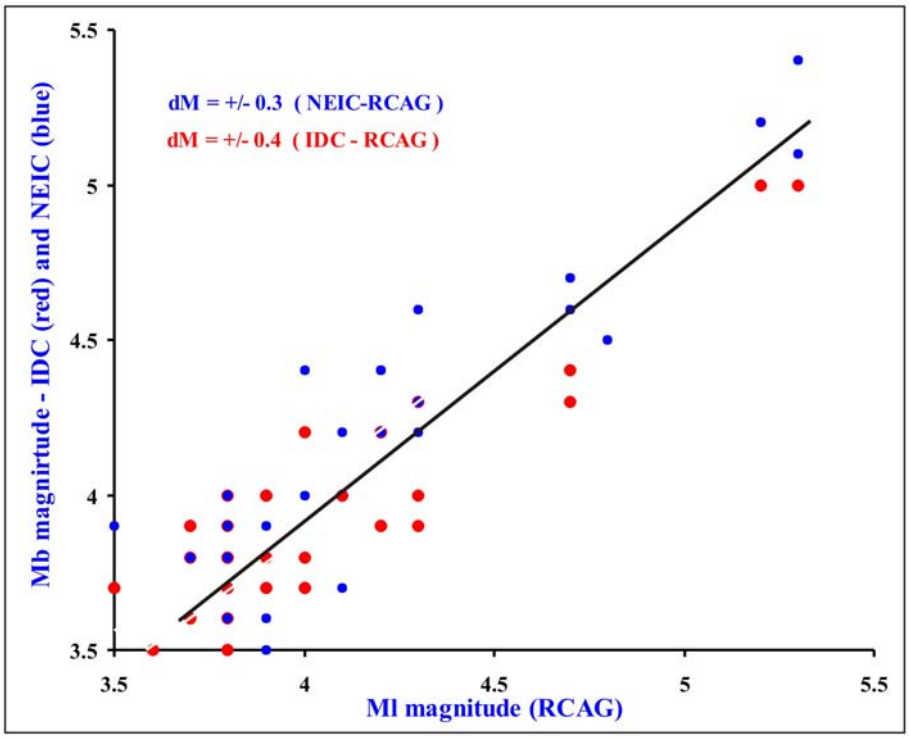

Figure IV.22. Magnitude comparison: our results are compared for 20 events with NEIC results in blue and IDC results in red. The dispersion is relatively large but a systematic bias is not observed.

A selection of 3268 events was available to be included in the process of aftershock location. Fig IV.23 shows the epicentral distribution of these aftershocks. The star shows the main shock epicenter as determined by the relocation. The average RMS time residual for this subset of events is 0.39 sec with horizontal errors of respectively 4.65 km and 3.25 km along latitude and longitude. Most of aftershocks are located with RMS value varying between 0.1 and 0.3 sec (Fig IV.24a) and the horizontal errors are mostly concentrated around a value of 2 km which is much lower than average errors (Fig IV.24b and Fig IV.24c). It shows that, in the data set, there are some events with large error for which the location is very unprecise. To remove these extreme values which are not significant, we

have chosen events with horizontal errors smaller than 5 km. With these criteria we obtained a subset of 2640 aftershocks on which the average RMS residual decreased to 0.26 sec and horizontal errors to .83 km and 1.33 km respectively along latitude and longitude. On the Fig IV.25a is presented epicentral distribution of these selected events.

Finally, we selected data set on depth determination: keeping events with an error on depth smaller than 2.5 km we obtain the 1315 events plotted on Fig IV.25b. The corresponding mean horizontal errors for these selected events are reduced to respectively 1.45 km and 1.00 km along latitude and longitude.

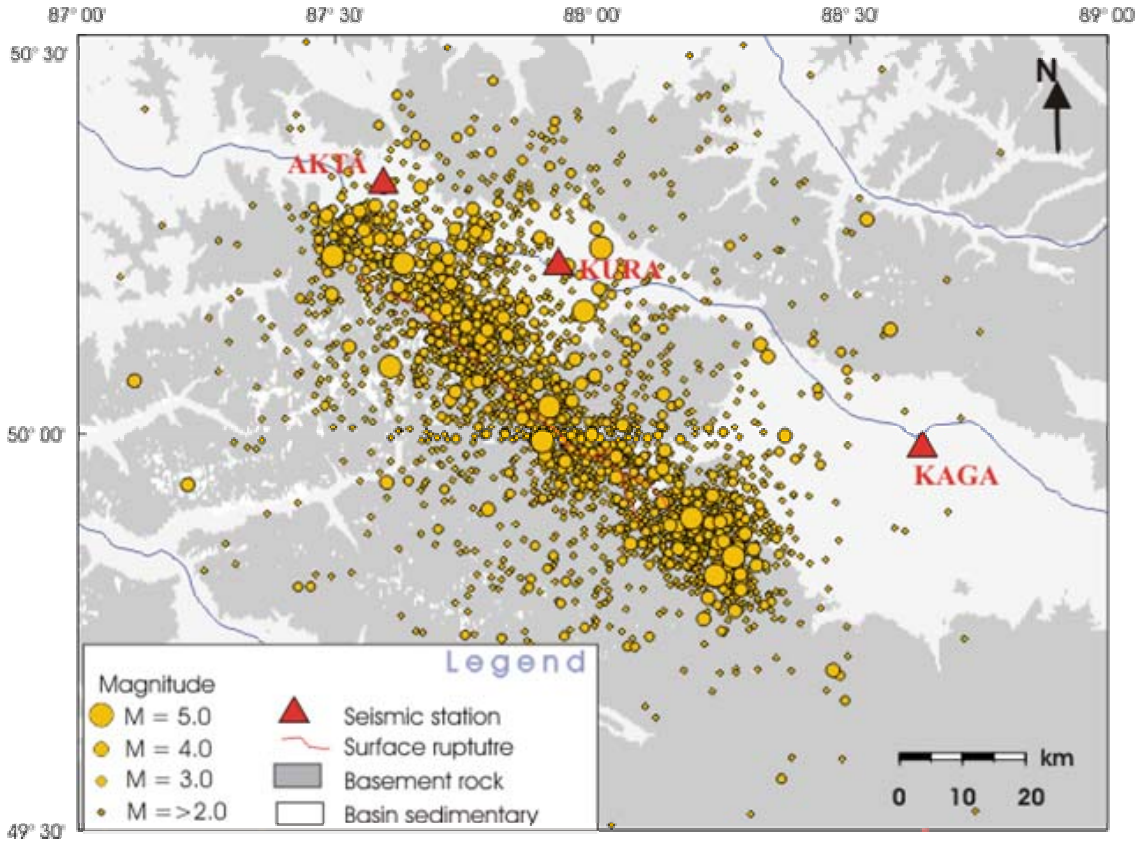

Figure IV.23 Epicentral location obtained for all the data set recorded by the temporary network

All these selections provide a very similar image of the epicentral distribution of seismic activity. Activity is distributed on an elongated zone oriented along 90 km in 310°N direction; this direction does not present any strong variation from NW to SW. The width of the active zone is more or less broad, depending of the selection criteria apply on events. This distribution can be easily related to an almost vertical fault plane as the focal mechanisms proposed it determined by world wide agencies.

The estimated dimension of this aftershock area agrees to what is commonly found for event of this magnitude or a little larger. For example, Chi-chi earthquake (Taiwan, Mw = 7.7) had an aftershock area of about 40 x 100 km^2 (Hirata *et al.*, 2000). We will consider that, despite the relatively poor station coverage, this data set a good image of the activity. Of course errors on locations (horizontally as in depth) are relatively important, surely larger than the statistical errors given by the location procedure.

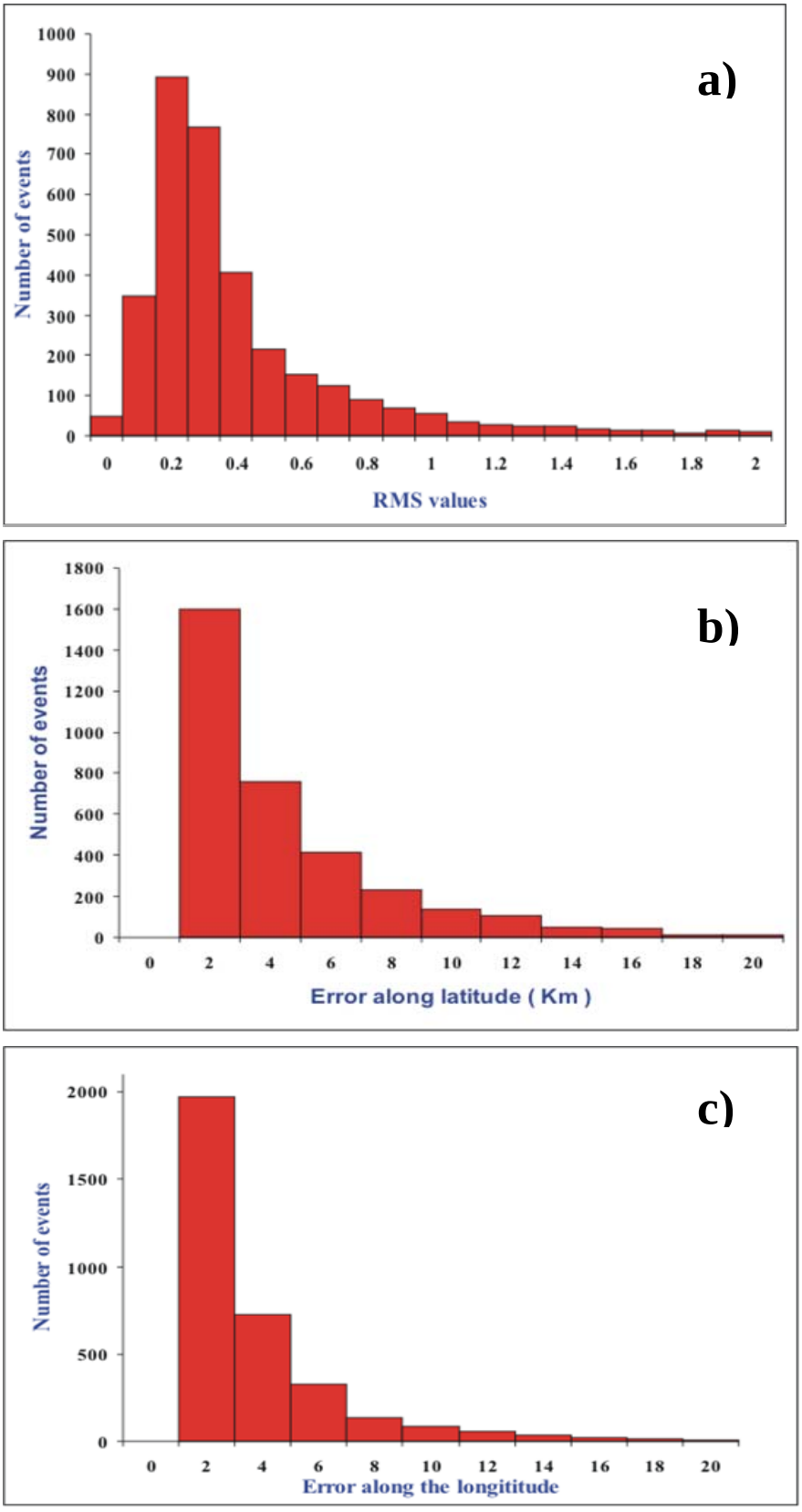

Figure IV.24. Distribution of RMS values (a), error in latitude (b) and longitude (c) overall aftershock data set. Some very large values show that the data set, contain events with very poor location.

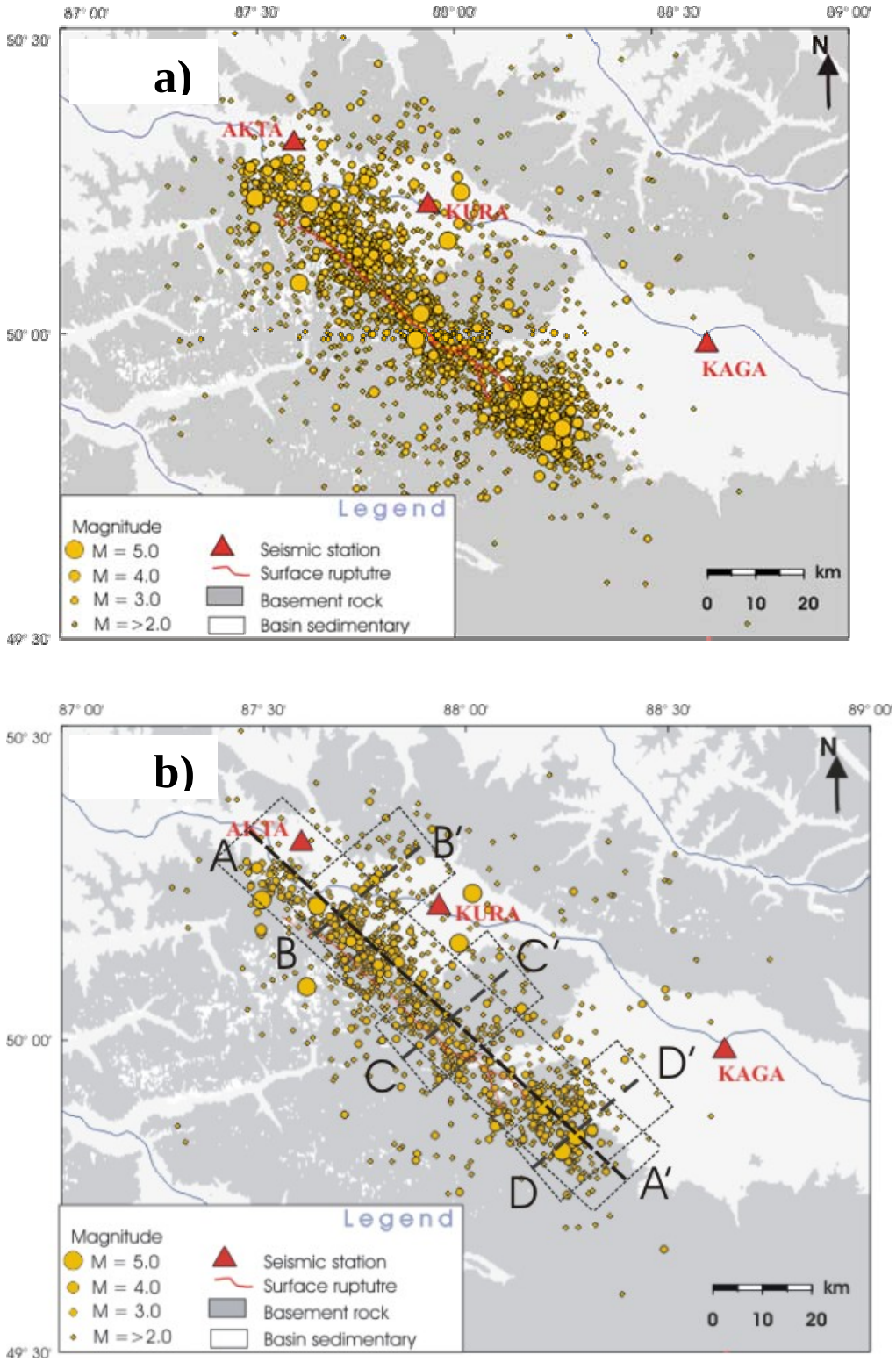

Figure IV.25 Subsets of the whole aftershock data set. (a) Events selected with location error in latitude and longitude smaller then 5 km, (b) events selected between the previous and with depth error smaller than 2.5 km. On this second map is reported the traces of cross-sections Fig IV.30.

In the next step, we try relative relocation with HYPODD procedure. We tested the inversion process with several initial parameters and the procedures suggested by Waldhauser (2001) and Dunn (2004). Nevertheless the result was strongly dependent of these initial parameters. In the proposed best solution, many of events are not localized and all the founded epicenters collapse in the central area, near the main shock epicenter. This feature is clearly an artefact of the procedure which can be explained by the small number of local data, and therefore the small number of pairs in the double difference estimation. Such artefact was already observed even in case of a better station distribution (Got *et al*., 2002). This application, show once again, that relocation procedure like HYPODD can be, and should be, used with caution with a good control of the effect of relative ponder of the travel time and difference on travel time. Generally epicenters features can be improved in regions were the recording network is homogeneously distributed around the epicentral zone. The relatively sparse and very heterogeneous in distance distribution of station of the temporary network which was installed, is clearly not sufficient to improve the aftershock distribution image with double difference relocation.

IV.5.2 Distribution in time

To analyze the distribution in time, we decided to work on the data set of 2640 events selected on the criteria of horizontal errors less than 2.0 km which is a good compromise between the global data set in which very poorly events are present and the final data set were a large number of smaller events are disappearing. Fig IV.26 shows the time distribution of the aftershock sequence from 09th October through 19th November. The activity of aftershocks varies sharply during observation period. Between 11th October (day 284) and 19th October (day 292) the detection threshold changes clearly with the installation of the stations in Russia. After that first period, the number of events per day decreased as expected, almost exponentially. Some picks and holes are present around the possible mean curve. It does not seems that picks of seismic activities are related to the larger aftershocks except for events on day 302 (M = 4.7), and may be event on day 296 (M = 5.2).

We notice particularly the lack of activity after event of magnitude larger than 5 which occurred on days 315 and 321 in the latest period of the temporary network. We know that another temporary array was installed in the epicentral area in summer 2004 to record aftershocks and that, at that time it was still possible to record a high level of seismicity. Nevertheless we think that the data set with which we are working is well representative of the aftershocks distribution. The cumulative energy released in this area during the temporary experiment is plotted versus time by Julian day (Fig IV.27b).

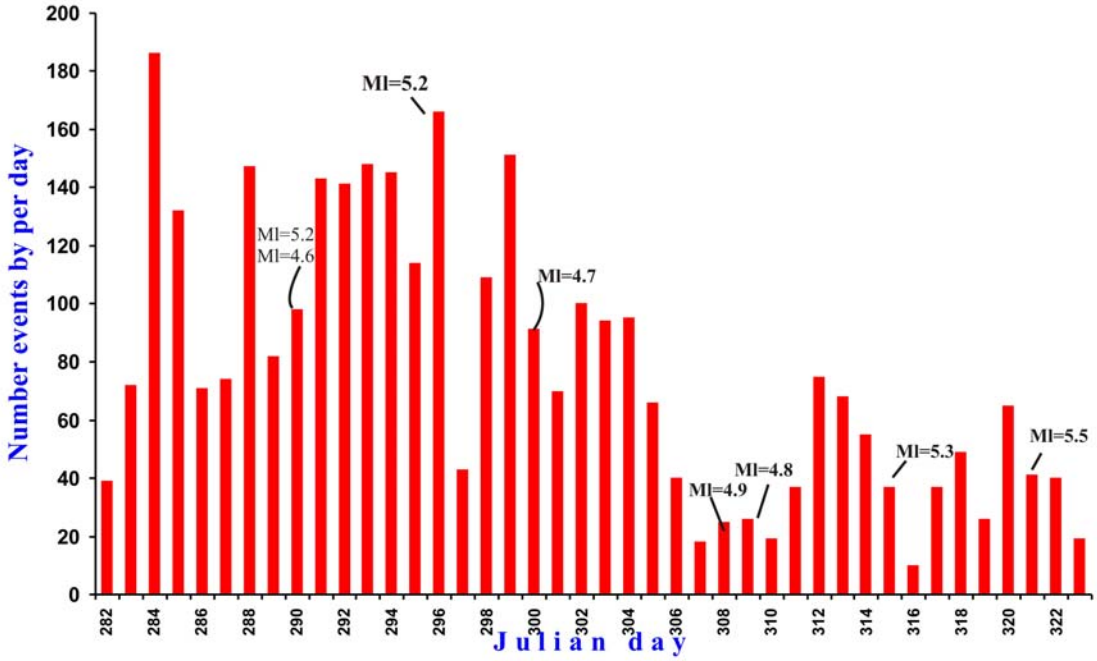

Figure IV.26. Distribution of the daily number of events recorded by the temporary network. It shows that after day 292 the data set that seems to be homogeneous.

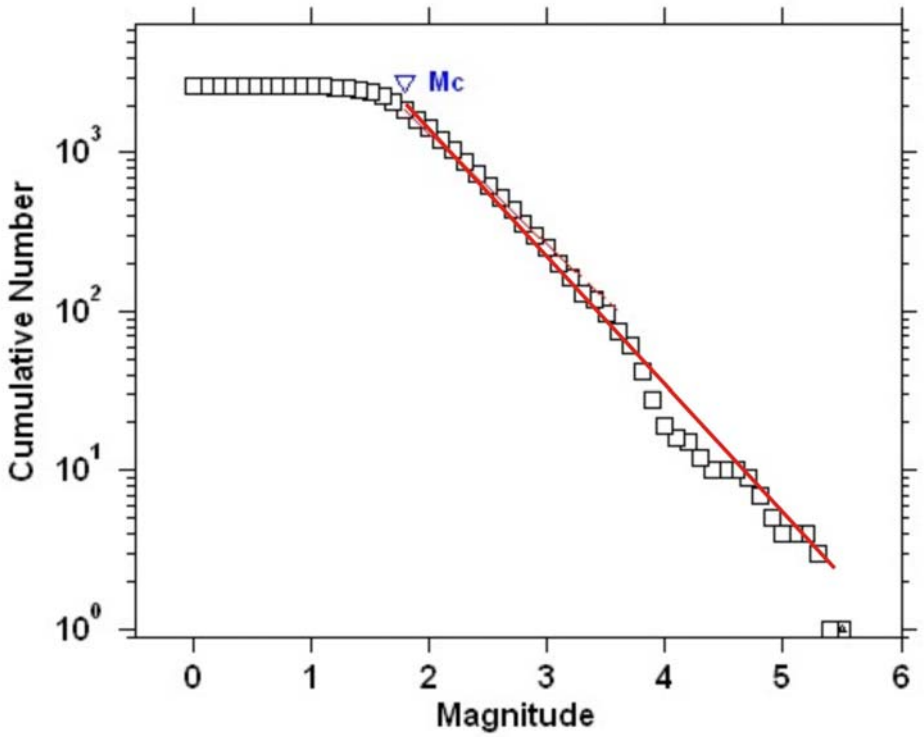

Figure IV.27 (a). Magnitude distribution in the recorded data set.

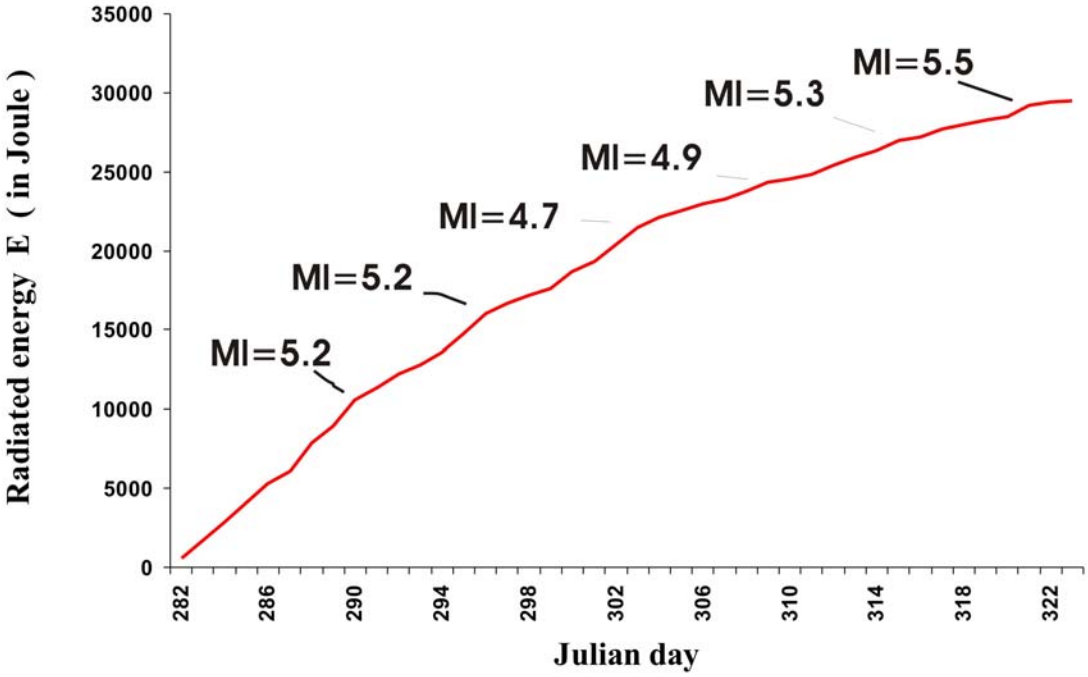

Figure IV.27 (b). Cumulated energy released during the temporary network period.

It shows also that, during the first period covered, the data set is not complete as we observed a quasi linear progression till day 295 and that on the last period, despite several events of magnitude larger that 4.5, the decay of activity is very much similar to the standard.

The magnitude distribution of earthquakes usually is well described by the G-R relation (Gutenberg and Richter, 1944):

$$\mathrm{Log}_{10} N(M) = a - b*M$$

Where N (M) is the cumulative number of earthquakes having magnitude larger than M, ***a*** and ***b*** describe the size distribution of events and their values are characteristic of the seismic area. Previous studies of seismicity parameters in different aftershock zones showed that the estimated coefficient ***b*** vary mostly from 0.6 to 1.4 (Wiemer *et al*., 1999).

Fig. IV.27a shows the magnitude-frequency plot of Chuya aftershock sequence observed during our intervention period and constructed on the data set selected on horizontal errors in location. Several moderate size earthquakes with a magnitude between 4.5 and 5.5 occurred during the survey period and it seems that globally, there is a deficit of events with magnitude around 4.5. This can be due to selection on location errors of the events of the data set with which we are working. The deviation from linearity for magnitude M < 2.2 points out clearly a detection threshold of M = 2.2 for the temporary network, even if the data set of 2640 located aftershocks include 1400 events with magnitudes lower than 2.2. Nevertheless, the relatively large range of magnitude recorded, allows us to define well a ***b*** value of 0.8.

IV.5.3 Distribution in space

All the aftershock figures (Fig IV.7, Fig IV.23, Fig 25a, b) present very similar features. Fig IV.28 proposes our selection of locations to discuss of the whole sequence till Mid-November. We have reported the location of the three main events and the early activity as we obtained it from our relocation as well as the aftershocks data set, provide by the temporary network. Surface ruptures described by the Russian team were also reported (Geodakov *et al*., 2004). The majority of aftershocks occurred along the northern and southern Chuya range margins with the Chuya and Kurai depression. Distribution of Chuya aftershocks are well correlated with main surface breaks. We notice that during the period covered by the temporary network, most of the largest events occurred at both extremities of the activated zone which was not the case during the period just before the installation. There is also some large events less well determined (they did not appear on Fig IV.25b) in central part of the area at the level of the Chagan-Uzun block, a few kilometres southeast of the main shock epicenter.

The aftershock pattern can be described in three parts: the central one, at the level of Chagan-Uzun uplift, from main shock epicenter to the surface breaks bifurcation and one segment on each side which are more active during the recording period.

The aftershock pattern at the north-western end is well correlated to the end of the observations of surface breaks. It can also be observed some complexity. On Fig 25b, we notice the possible activation of a smaller structure, transverse compared to the main directions (Kurai active thrust or reverse zone and North Chuya active zone), well controlled by the presence of AKTA and KURA stations and which could be related to the northern border of Kurai basin. The epicenter of the 01st October aftershock is not far from this structure. Some activity is also present beneath the Kurai Basin.

In the central part, mostly connected directly to the main shock, the activity is less important as if most of the stress release took place during the main shock and the first days of the sequence.

The aftershock activity in the south-eastern part, along southwest margin of Chuya depression, is spread over a larger area than in the others with a large number of events and a concentration of the larger events of our data set (magnitude between 4 and 5). This part of aftershock sequence is obviously observed out of surface breaks described by Geodakov *et al*. (2004). Even if the locations are less precise as the nearest station is KAGA at a distance of more than 30 km, we think that the southeast extension of the seismic activity along Chuya basin should be considered. It corresponds also to the regions were horizontal surface displacement was deduced from the correlation of SPOT images. On the other hand the northeast extension, with activity till beneath the Chuya basin, can be related to this large error on epicenters determination and will not be considered as a main feature.

On Fig.IV.29 are showing different vertical cross sections along rupture direction and perpendicular with the aftershock selection for which we have the best control en depth (1315 events plotted on Fig IV.25b, with depth error less than 2.5 km). The position of cross section is reported on Fig IV.25b. Fig.IV.29a shows the cross-section along a NW-SE direction with a width of 10 km. This cross-section reveals that most of the seismic activity appears to be located within a depth range between 5 and 20 km and mainly concentrated at depth around 13 km.

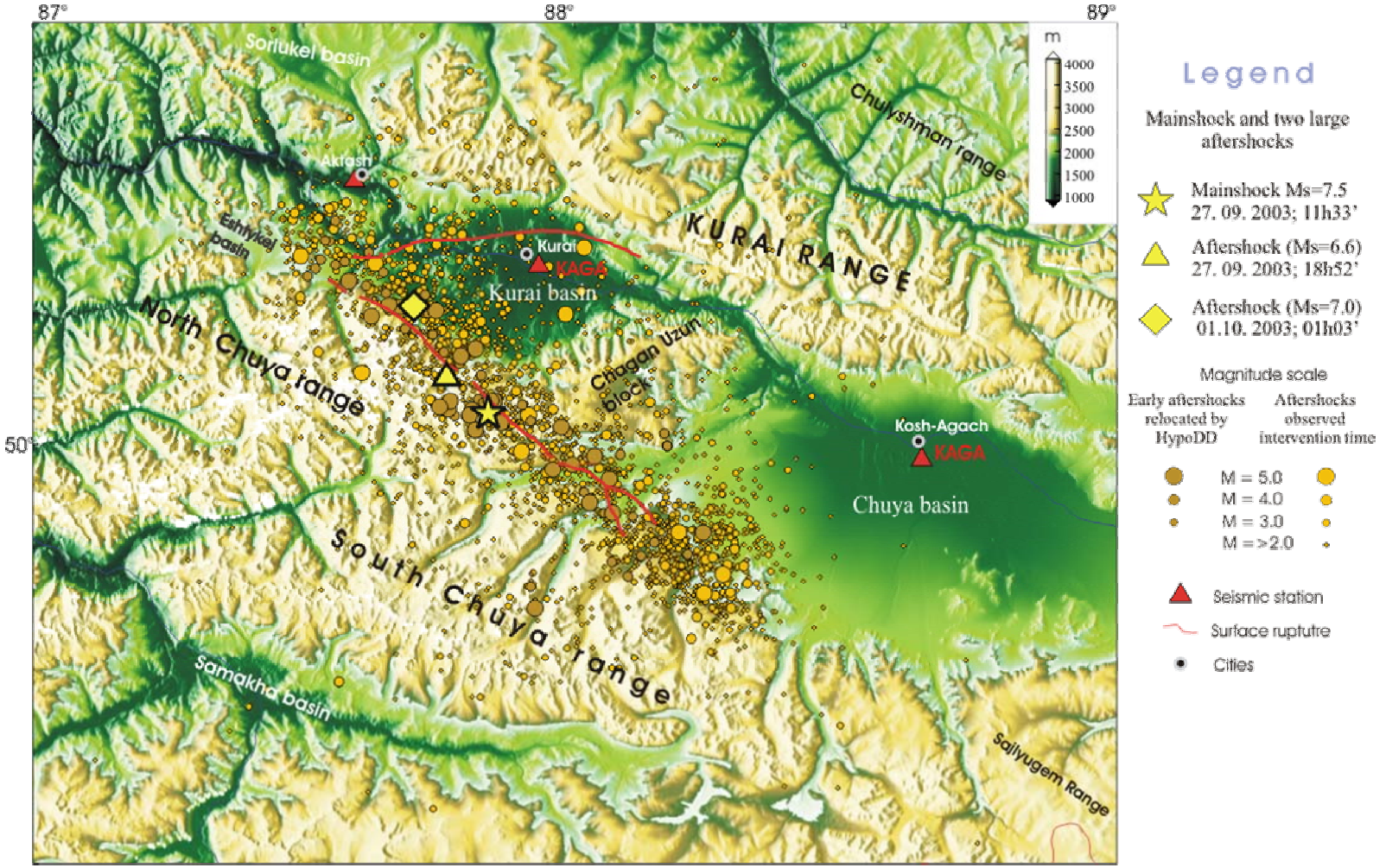

Figure IV.28. Final selected image of the aftershock sequence. The early events relocated and selections of the best aftershocks located with the temporary networks are represented. Main events relocation and surfaces breaks reported by Russian team have been added.

These depths are consistent with depth obtained from relocation of the main events (10 km, 16 km and 11 km respectively for the main shock and the 2 main aftershocks). The increase of events at larger depth in the south-eastern part should be put without doubt on the fact that these locations are less precise. So we will not argue on any variation in depth along the whole segment. However we point out again different level of activity from northwest to southeast. The central region, related to the main shock is less active and a gap could be noticed between central part and south-eastern part. Our network was clearly not adapted to locate the superficial seismicity. The fact that surfaces breaks have been observed in enough to suppose that the displacement reached the surface and that with a denser network activity could have been detected.

The Fig IV.29b, c, d, present cross sections in direction perpendicular to the general strike of the aftershock distribution. None of these section shows an almost vertical distribution which could be related to a fault plane. This could be explained either by the fact that the error on location of these events are considerably larger than what the statistical errors are given, either to the fact that the fault structure is more complex, with variations in strike and in dip. On the northern cross-section, an extension to the northeast could be related to the activity along the northern border of Kurai basin. As mentioned above depth of most aftershocks are poorly constrained.

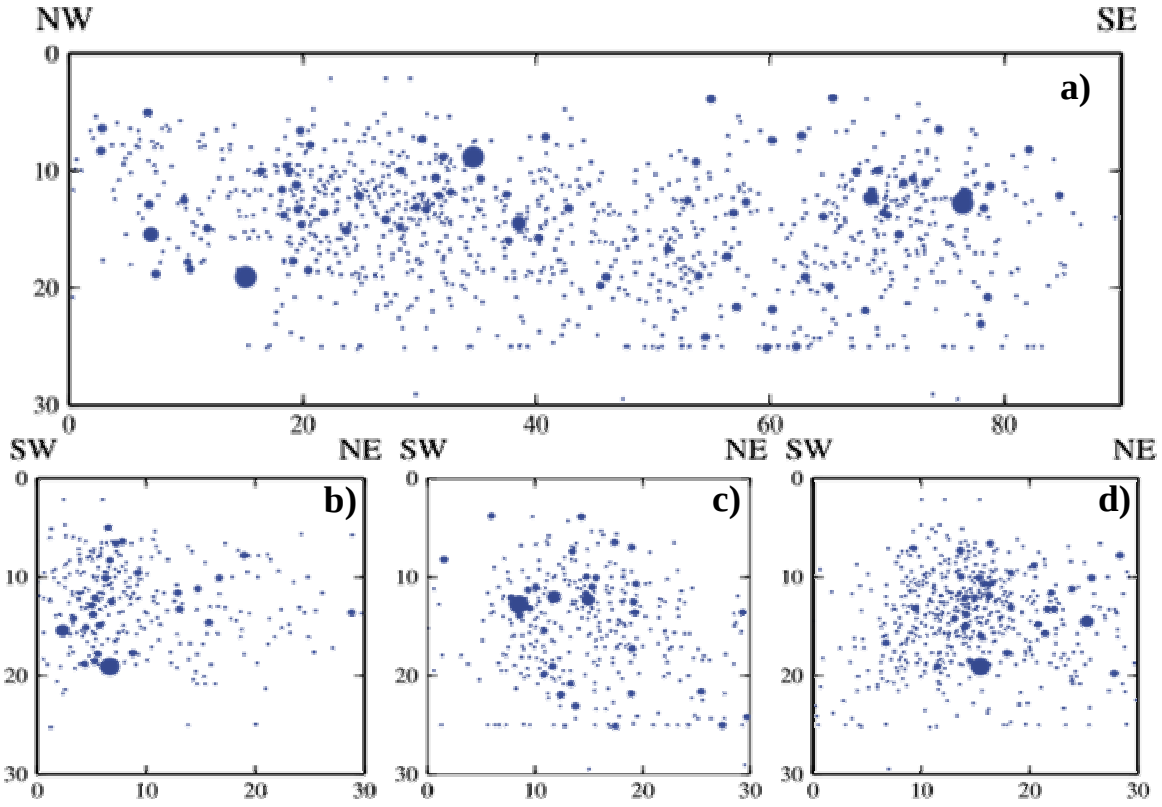

Figure IV.29 Vertical cross sections with a width of 10 km on both sides through hypocentral aftershocks locations as represented on Fig IV.26b. (a) along the strike of the distribution, (b, c, d) along a perpendicular direction from northwest to southeast.

IV.6 Discussion and conclusion

The Chuya earthquake and the following aftershock activity occurred along the south margin of Chuya and Kurai basins which belong to the Gorny-Altay accretion wedge. No local information is available on the aftershock activity before field aftershock survey period during which some large events have occurred. The data recorded by the Mongolian national the networks were not able to produce a precise location of the early aftershock sequence. Therefore we used regional phase data from IDC and NEIC bulletins to relocate mains shock and earliest aftershock activity. Using double differences method (HYPODD) we succeed to relocate main shock and some other moderate size aftershocks. Our relocation result shows that main shock was nucleated almost in the middle of aftershock sequences at depth ~9 km. The early aftershock distribution shows that rupture propagated bilaterally because of activity is increasing in two sides from the main shock. Second large aftershock occurred not far from the main shock, in place were surface rupture segmented into two parts (Geodakov *et al.*, 2004). The largest aftershock occurred north, between Kurai active fault zone and North Chuya range where rupture strike changed slightly to the southwest.

The aftershock data set was obtained by field study from 09th October until 19th November; we propose that it was sufficient to determine geometry of the fault zone. The aftershock activity is extended about 90 km along the NW - SE direction. The general shapes and the position of the aftershock distributions are well correlated to the surface ruptures which have been observed by Russian scientists. On Fig IV.28 is presented a significant image of the whole sequence (larger events and whole aftershock sequence till mid-November). The errors in location are such that too much detail cannot be extracted, but only the main features of the distributions are discussed.

The Chuya and Kurai basins are developed in a zone of intense dislocation between the Kurai and the Charish-Terekta fault zones (Delvaux *et al.*, 1996). In the region the most tectonically active structure is the Kurai fault zone which bounds the northern margin of the Kurai and Chuya basin. It has a typical "rose" structure formed by systems of thrust and reverse faults. Despite this main active structure, Chuya earthquakes occurred on the southern margin of these two basins, along North and South Chuya range. Northern end of aftershock activity is limited near the Eshtykel basin where some complexity seems to take placing. The largest aftershock of Chuya earthquake (Ms = 7.0) occurred in this zone, near a zone where azimuth of the surface breaks are changing. It has also produced a large number of aftershocks, but no important activity seems to be related to the northern segment of the surface breaks reported (Geodakov *et al.*, 2004). Even, if some activity occurred between the two segments, below the northern part of Kurai basin.

The central part of aftershocks is mostly connected to the main shock and first large aftershock. Most of activity of this zone occurred on the southwestern margin of Chagan-Uzun tilted block. The Chagan-Uzun block is tilted to the southwest, towards the Chuya depression, but separated from it by the NE trending Kyzyl-Chin fault. The aftershock activity is crossing this fault zone. The resolution on epicenter location does not allow us to infer any activity on this fault. Several moderate aftershocks have occurred just after the main shock in this central part of the activated area. During the period of the temporary network, the activity was less important that on the two external segments of the area. The release of stress migrated bilaterally from the main shock epicenter towards the north-

western and south-eastern edges of the zone. The southwestern end of aftershock distribution was significantly active during our observation time with the occurrence of several moderate size earthquakes with magnitude between 4 and 5. This activity occurred mostly on the south margin of Chuya basin. According to information on surface rupture, the fault does not reached the surface in this zone.

Majority of earthquakes occurred in a depth range between 5 and 20 km. The activity in north-western and south-eastern zone may be a little shallower than in central part. It is difficult to follow a vertical fault on cross section perpendicular to the general strike of aftershock sequences even if the main activity lies below the surface breaks.

Clearly the temporary network installed for the aftershock study, has allowed us to characterize the general features of the distribution which is well related to the main events location, the focal mechanisms, the tectonic environment, the field observations and the displacements observations from SPOT image. However, apparently such a sparse network cannot solve the details of the post-seismic sequence. The present results could be improved by collaboration with Novosibirsk scientists in which a common data set will be processed including all the local data during the October-November period. Such collaboration is in discussion. Not only better locations should be obtained, but also some focal mechanisms which can help to describe the fault complexity.

Chapter V

Source parameters of Chuya 2003 earthquakes

V.1 Introduction

Continental strike-slip faults are often major sources for seismic hazard, but only few large earthquakes along these faults have been studied with modern instrumentation (Ozacar *et al.*, 2004). Understanding the nature of such large strike-slip earthquakes helps to reveal the underlying mechanics of the rupture process and allows the understanding of faults interaction and, at the end, leads to better strong motion predictions. Most of the large strike-slip earthquakes present a multiple-event nature with complicates the seismic analysis; the proposed space-time functions of slip should accommodate complex sets of crustal faults (Kanamori *et al.*, 1977; Butler *et al.*, 1979; Kikuchi and Kanamori, 1982).

The destructive Chuya earthquake is an important event because it is the first event in northern Altay region large enough to be recorded globally since the development of the worldwide broadband digital seismic networks. These data are well adopted for the study of large events when accelerometric data are not available near the source. Also it is one of important intercontinental strike-slip earthquake which recently occurred - just after Kunlun fault earthquake, 14th November, 2001 - in the region where active deformation is expected from the motion of the Indian plate with respect to Siberia (Fig. V.1). An excellent set of observations from surface faulting, seismic waveforms, image processing and aftershock study is now available for the 27th September, 2003 Chuya earthquake and on the Gorny-Altay region. This allows us to compare results of different techniques to obtain rupture histories of large Chuya earthquake.

In this chapter, we analyze main shock of Chuya earthquake and two important large aftershocks using teleseismic P and SH wave data to derive a rupture history that may help us to understand details on the corresponding fault, one of the major fault in Altay region discussed before but also more generally to add an example of the complex behaviour of large strike-slip earthquakes. In addition, we compare the source parameters obtained with other information derived from geodetic, geological and image processing results. We used an application (bwidc84 modified) of body wave inversion techniques developed by Nàbelek (1984) and special algorithms for the preparation input data of Nàbelek program developed by B.Delouis (2002) to derive source parameters of these three large events. All events were modelled as complex earthquakes, consisting of multiple shocks with fault-planes of different orientations.

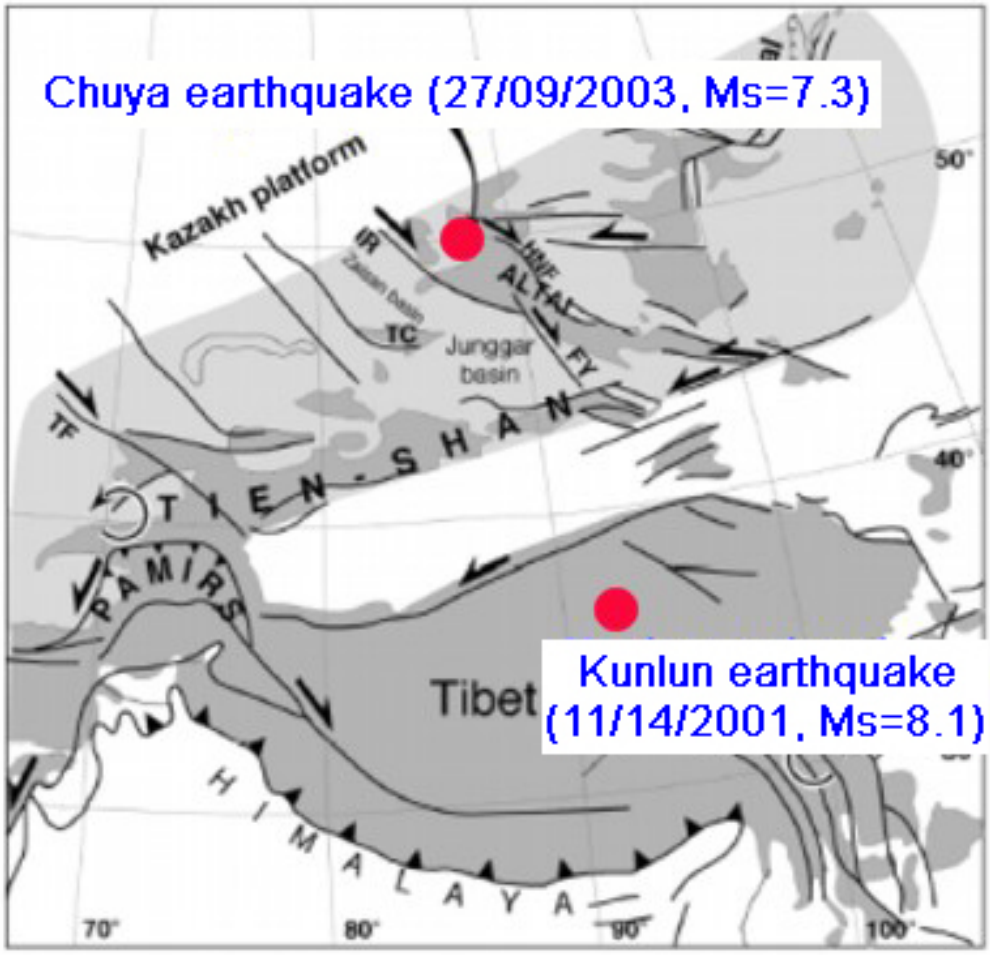

Figure V.1. The location of the two large strike-slip earthquakes which occurred in central Asia beginning of this century.

V.2 Methodology of modelling

Since development of the digital seismic instrumentation, waveform modelling has become one of powerful tools to determine earth structure models and understanding fault rupture process. Waveform modelling and source inversion is an iterative process in which differences between observed and synthetic seismic records are minimized by adjusting the seismic source parameters and earth structure models.

The teleseismic body waveform modelling method was developed by Helmberger (1974), Langston and Helmberger (1975), Burdick and Mellman (1976) and others; Stump and Johnson (1977), Fitch and Ward (1980) made first attempts in applying inverse method to body waves. Their work concentrated mainly on the determination of the source mechanism. Langston (1981) and Kikuchi (1982) developed inversion method by using source time function parameterization. Nàbelek (1984) develops an inversion technique applicable to teleseismic P and S waves from earthquake with a wide range of magnitude and complexity.

Earthquake source parameters in this study are determined using Nàbelek teleseismic body waveform modelling software. The Nàbelek technique enables us to obtain precise estimation of the strike, dip, slip of focal mechanism and its centroid depth, scalar seismic

moment and source time history of large and moderate size earthquakes by using least square method which minimizes the misfit between observed and synthetic P and transverse SH waveforms.

Teleseismic body wave at distance between 30° and 90° is the easiest of all seismic phases to model and invert waveform of these phases are one of the most effective methods to determine source parameters. Because, observations are made at great distance from the source we can consider that these wave packets are approximately characterized by a single ray parameter; the velocity of propagation along the path is the same for the whole packet (Dahlen *et al.*, 1998) so that the shape of the packet does not change. For a shallow source, the wave packet of teleseismic P or S wave is usually composed of at least three energetic rays: the direct and two reflection from free surfaces which calling pP and sP for the P and sS and pS for the S wave packet (Lay and Wallace, 1995). The Fig.V.2 shows general travel path of the different phases.

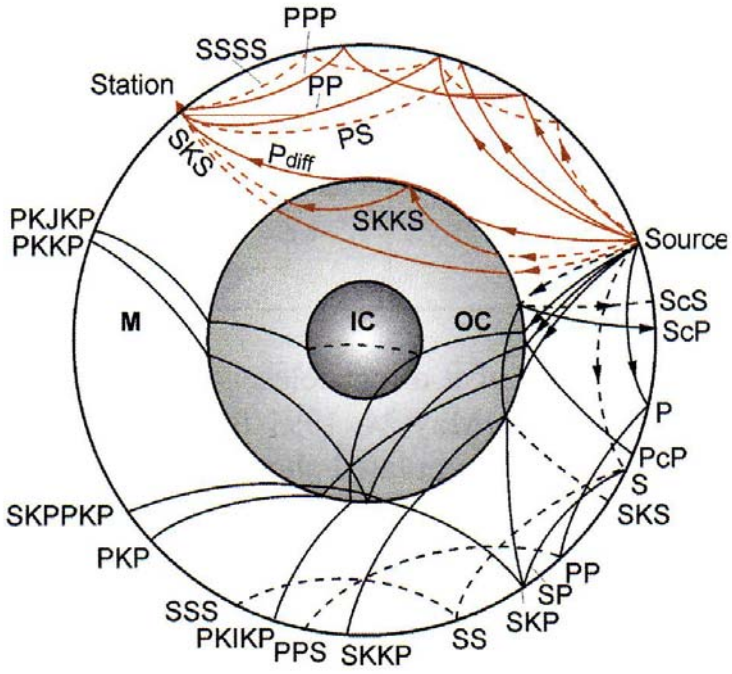

Figure V.2. Global travel paths of P and S waves (after Williams *et al.*, 2004).

The equation for the far-field P and S waves from a point double-couple source with standard fault orientation parameters, δ, λ and ***i*** source takeoff angle can be written as :

$$U_p(r,t) = \frac{1}{4\pi\rho r\alpha^3} R^P \dot{M}\left(t - \frac{r}{\alpha}\right)$$

$$U_{SV}(r,t) = \frac{1}{4\pi\rho r\beta^3} R^{SV} \dot{M}\left(t - \frac{r}{\beta}\right) \qquad \text{(V.1)}$$

$$U_{SH}(r,t) = \frac{1}{4\pi\rho r\beta^3} R^{SH} \dot{M}\left(t - \frac{r}{\beta}\right)$$

Where:

$$R^{P} = \cos\lambda \sin\delta \sin^2 i_h \sin 2\phi - \cos\lambda \cos\delta \sin 2i_h \cos\phi + \sin\lambda \sin 2\delta(\cos^2 i_h - \sin^2 i_h \sin^2 \phi) + \sin\lambda \cos 2\delta \sin 2i_h \sin\phi$$

$$R^{SV} = \sin\lambda \cos 2\delta \cos 2i_h \sin\phi - \cos\lambda \cos\delta \cos 2i_h \cos\phi + \frac{1}{2}\cos\lambda \sin\delta \sin 2i_h \sin 2\phi - \frac{1}{2}\sin\lambda \sin 2\delta \sin 2i_h (1 + \sin^2 \phi)$$

$$R^{SH} = \cos\lambda \cos\delta \sin i_h \sin\phi + \cos\lambda \sin\delta \sin i_h \cos 2\phi + \sin\lambda \cos 2\delta \cos i_h \cos\phi - \frac{1}{2}\sin\lambda \sin 2\delta \sin i_h \sin 2\phi$$

and with the fault strike and the station azimuth. The 1/r term account for geometric spreading in a whole space, and we need to modify this for actual geometric spreading in the Earth (Lay and Wallance, 1995).

The Green's function calculation of teleseismic body wave we can be divided into three parts: the contributions from the crustal and free surface effect in the source and receiver regions and contribution from the mantle (Fig.V.3).

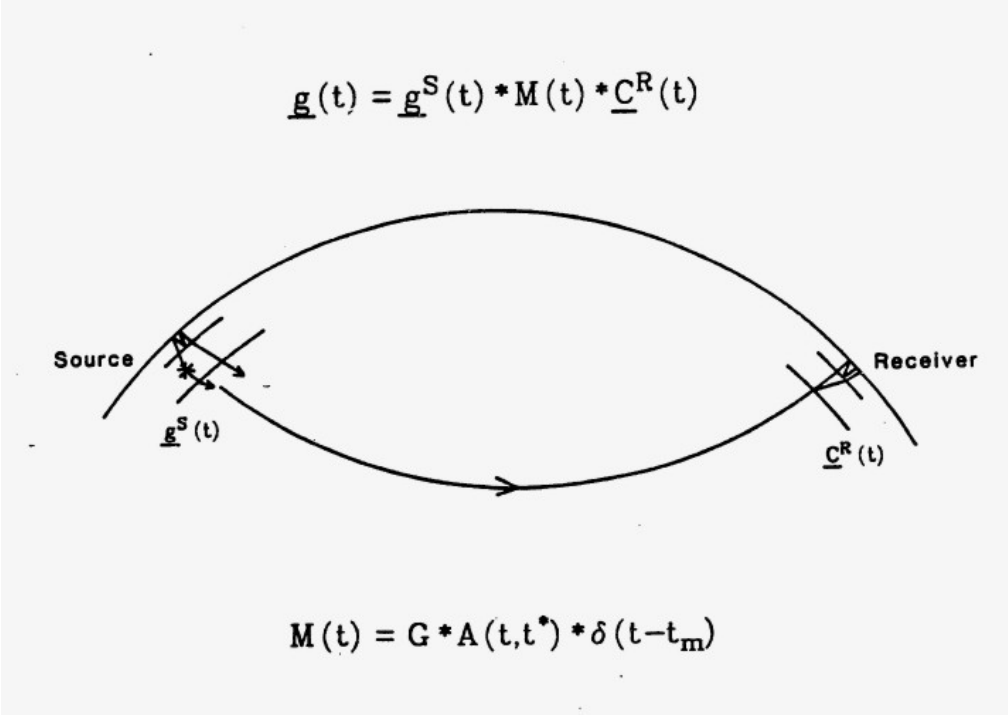

Figure V.3. The problem configuration for the determination of the Green's function of the teleseismic body waves. (after the Nàbelek, 1984)

$g^{S}(t)$- represent the effect of the earth's crust in the source; $C^{R}(t)$ and $M(t)$ are respectively the receiver area and mantle response. $G * A(f, t^{*})$ and $\delta(t - t_m)$ represents the contribution of geometrical spreading, anelastic attenuation and travel time in mantle.

To take into account the third part of the propagation path, it is possible to consider only geometrical spreading, inelastic attenuation and travel time. This standard model is commonly used because it represents well the homogeneity of the mantle.

To model the effect of the crustal structure in the receiver region we can also consider a single average crustal model common to all stations. Because most world wide stations used in this study is located on the hard rock sites, no unusual site effects are expected (Nàbelek, 1984).

The approximations used in Nàbelek technique suppose that the half-space is a good model for modelling the waves which contribute to the P or S waves group. Out of all the rays of up and down going P and S waves which depart from the source in the real earth, only fours are taken into account and contribute to the body wave seismogram at a giving point in the half-space. All correspond to the same ray parameter. The Green's function can be written as equation:

$$g_{ki} = g_{ki}^{\downarrow p} + g_{ki}^{\uparrow p} + g_{ki}^{\downarrow s} + g_{ki}^{\uparrow s} = \sum_{n} g_{ki}^{n} \qquad \text{(V.2)}$$

Where: $g_{ki}^{\downarrow p}$, $g_{ki}^{\uparrow p}$, $g_{ki}^{\downarrow s}$ and $g_{ki}^{\uparrow s}$ are the contributions to the Green's function from the rays which depart from the source downward and upward as P and S waves.

It also implies that for a horizontally layered structure, since the source remains within a given layer, the responses g_{ki}^{n} remain the same (except for the change in travel time to the first interface) regardless of the vertical position of the source. If g_{ki}^{n} are known for one depth **h**: the g_{ki}^{n} for a depth of h+Δh are obtained simply by the appropriate time shift of the originals, i.e.

$$g_{ki}(h+\Delta h) = g_{ki}^{n}(h)\delta(t-\eta^{n}\Delta h) \qquad \text{(V.3)}$$
$$\eta = \left(-\eta_{\alpha}, \eta_{\alpha}, -\eta_{\beta}, \eta_{\beta}\right)$$

Where δ is the delta function and $\eta_{\alpha(\beta)}$ is the vertical slowness, of the P(S) wave ray in the layer in which the source is located. This is a very useful property since the efficiency of iterative inverse procedure depends greatly on how quickly can update the model after each iteration and depth are one of the parameters which we usually want to determine (Nàbelek, 1984).

Of course we usually do not know the source time function or source depth a priori, so we can recast the problem as iterative inversion. Here we discrete the source time function and invert for the time series. The two most common parameterization of the time function are a series of boxcars or overlapping triangles (Husebye *et al.*, 1996). The Nàbelek procedure has chosen triangle function which is more suitable to represent the high frequencies of source process. The time function $\Omega(t)$ is discretized by a series of

overlapping isosceles triangle functions $B_{\Delta\tau}(t)$ of equal duration $\Delta\tau$ with variable amplitude W_k :

$$\Omega(t) = \sum_k W_k T_{\Delta\tau}\left(\tau - \tau_k\right) \qquad \text{(V.4)}$$

$$T_{\Delta\tau}(t) = B_{\Delta\tau}(t) \cdot B_{\Delta\tau} \qquad \text{(V.5)}$$

$$\tau_k = \Delta\tau(k-1) \qquad \text{(V.6)}$$

Amplitudes W_k are determined by the inversion and number of the time function elements and their duration will be chosen a priori (Nàbelek, 1984). Usually inversions begin with a source time function duration that exceeds the expected total duration of the source. The numbers of isosceles triangles are then adjusted until no significant improvement in the seismogram is observed, or until the data are matched to their expected accuracy, or until the amplitudes of the later overlapping isosceles triangles become insignificant. The number of elements of significant amplitude determines the total source duration. In the above parameterization we assume that the observed source time function is entirely due to the time history of the source. The area under the source time function curve is proportional to the scalar seismic moment, Mo.

Complex earthquakes

The seismic source process of some large earthquakes can be thought of as a series of subevents. When source time functions become sufficiently complicated to suggest earthquake multiplicity, the event is known as a complex earthquake (Lay and Wallace, 1995; Scholz, 1990).

The seismogram for a multiple event with n_e subevents delayed with respect to the origin time by a time Δt_e can be written as

$$S(t) = \sum_{e=1}^{n_e} S_e(t - \Delta t_e) \qquad \text{(V.7)}$$

Where $S_e(t - \Delta t_e)$ is the seismogram due to a subevent e with the centeroidal location referenced relative to the nucleation point of the first subevent (Nàbelek, 1984).

Directivity and rupture propagation

In the simple Haskell source model the boxcar associated with the propagation of the rupture had a length τ_c for a station at an azimuth perpendicular to the strike of the ribbon fault. Length of rupture depends on the dimension of the fault and rupture velocity, but also depends on the orientation of the observer relative to the fault. In general, the rupture

velocity is less than the S-wave velocity of the faulted material; the body waves generated from a breaking segment of the fault will arrives at a station before the body waves arrive from a segment that ruptures later. The azimuth dependence due to fault propagation is called directivity. If seismic station is located along the direction of rupture propagation, the trapezoid is very narrow and has the high amplitude.

The effect of a propagating horizontal line source is achieved by varying the duration of one of the box function according to the well known formula (Ben Menahem, 1961)

$$\Delta\tau' = \Delta\tau\left(1 - v_r \rho \cos(\phi - \theta)\right)$$

Where ρ is the ray parameter, v_r is rupture velocity; ϕ is station azimuth and θ is fault strike.

If the seismic station is located such that the fault is rupturing away from it, the source time function will be spread out and have the small amplitude (Lay and Wallace, 1995) as it is shown on Fig.V.4.

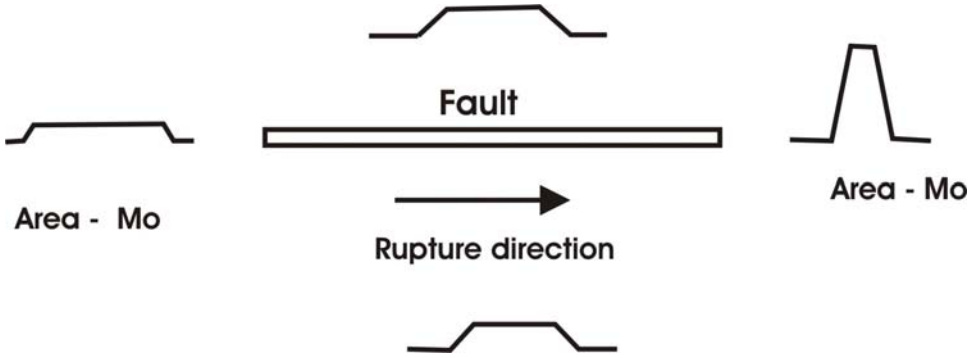

Figure V.4. Azimuth variation of source time function duration and amplitude, in case of unilateral rupture propagation.

There are different rupture propagation types. If rupture propagates in one direction along the fault, propagation is called unilateral rupture. For some earthquakes, unilateral rupture is a sufficient model of the faulting process, but many earthquakes nucleate in the center of a fault segment and spread in both directions. This is known as bilateral rupture. The source time function for the bilateral rupture varies much less with azimuth, and it is often impossible to distinguish bilateral rupture from a point source (Lay and Wallace, 1995). Some faults appear to expand radially, as circular ruptures. However, in some rare cases, the effects of vertical directivity are observed. Directivity can also be detected for complex ruptures with multiple subevents that are spatially and temporally offset.

Earthquake scaling

Earthquakes are often though to follow self-similar scaling in which the source dimensions are scale-invariant, i.e., events of different sizes cannot be distinguished except by a scale factor (Scholz, 1990). Using the relation between seismic moment and source dimensions:

$$Mo = \mu LWD \qquad \text{(V.8)}$$

Where $\boldsymbol{\mu}$ is the rigidity of crustal rock, self-similar scaling predicts $Mo \propto L^{1/3}$, $Mo \propto W^{1/3}$, and $Mo \propto D^{1/3}$. For a uniform stress drop shear crack, the static stress drop, $\Delta\sigma$, is defined as (Aki, 1972)

$$\Delta\sigma = C\mu * \frac{D}{L_C} \qquad \text{(V.9)}$$

Where D is the mean slip, L_C is a characteristic length, the smallest dimension of rupture within the fault plane, and C is a constant of order unity, that depends on rupture geometry. In a real earthquake, for which slip is spatially variable at all resolvable scales, the stress drop will varies strongly with position and will be controlled by length scales much shorter than the length or the width of entire rupture (Vallée, 2004).

V.3 Data preparation and strategy of modelling

The Chuya earthquake was well recorded globally around more than 200 stations. The azimuth coverage was well covered except south east direction. For this direction and correct distance range data of IRIS stations does not exist and we used GEOSCOPE stations to construct well azimuth coverage. To obtain data we used WILBER II IRIS web pages interface which is collecting a triggered event that included data of all stations which recorded this event and for GEOSCOPE data we used NETDC request to GEOSCOPE data base by ROSCOE connection. All signals are converted to the SAC format and for the deconvolution of signals we extracted all stations response files. Hereafter we started to prepare input data for the Nàbelek program by using special procedure developed by B. Delouis.

To avoid problems during the inversion procedure, we examined each signal and remove data which have not good polarization of components which are recognized by the similarity of the waveforms with others stations are the same area, and high noisy signals. From experience, we know that a good qualities single seismogram is better than more noisy signals.

Raw signals of chosen stations are not suitable for use directly in the body waveform inversion procedure (long-period data because these lack sufficient high-frequency content and the broad-band data because these have too much high frequency content). To overpass these problems, P and SH waveforms have been deconvolved to the ground displacement and band-pass filtered at 0.01 - 0.8 Hz. The S wave seismograms were rotated to retrieve the transverse and radial component for the SH analysis.

The P and S arrivals was picked theoretically by using **'ttime'** program and after that resolved by visual picking. After convergence, the assumed onset was allowed to vary by few seconds if a better cross-correlation between the observed and synthetic waveforms was found. The computation was then restarted, until to find the final solution.

The waveform were resample at 0.5s for the P wave and 1s for the SH wave for the analysis. The data window used in the inversion begins with the arrival of the direct P or SH phases and includes the reflected or converted phases (pP, sP or sS). For this we cut signals starting 10 second before of P or S phase arrivals. The length of the signal was chosen for each event individually depending of the duration of the P- and SH-wave groups. We verify

that it always include both the direct and surface reflected phases, which arrive less than 6 seconds after in our case of crustal events.

Amplitudes are corrected for anelastic attenuation using a Q operator with a t^* value of 1.0s for P and 4s for SH waves (Futterman, 1962). Amplitudes were equalized to an instrument magnification of 10000 and a distance of 40° to avoid weight due to amplitude for stations at different epicentral distances. The last procedure in data preparation is to convert SAC binary signals to the SAC ASCII files and create Nàbelek input file.

The P and SH waveform were inverted for the source mechanism, seismic moment, depth and source time function. The source time function is parameterized by a series of overlapping triangles whose relative amplitudes are determined by inversion. The time length of the time function elements should be set to the minimum resolvable interval, which depends on the frequency content of the signal. If the time length chosen is too short, the result is unstable in the estimated amplitudes. If it is too long, the result is a poor description of the source and possible biased estimates of other source parameters, most likely depth. The number of time function elements needed depends on the duration of the source.

The sensitivity of the least square inversion is directly proportional to the power of the signal. A particularly large concentration of stations or signals of some stations which have the largest amplitudes can make bias the estimated parameters. So, to avoid this problem some of the stations are removed from the inversion or down weighted, in particular when stations are at similar distance and azimuth. This decreases the effect of random noise contamination of any given station.

For all events the initial source and receiver structure was specified as a simple half space model. In some additional case we tested layered crustal structure for the modelling, but this did not improve the obtained solution. An initial focal mechanism, depth and scalar moments are needed to generate the first synthetic waveforms. We used parameters of the Harvard CMT solution as starting model.

We began each inversion with simple one point source. Next, one point source is replaced by two or more point sources with bidirectional or unidirectional rupture.

Keeping centroid depth fixed we first inverted for the parameters of the initial focal mechanism, the amplitudes of the source time function elements and scalar moment using the P and SH waveforms. After by fixing estimated parameters of focal mechanism we inverted centroid depth and this procedure was continued until best fit of synthetic and observed seismograms.

Fixing the strike, dip and rake of the fault plane at the values previously determined and allowing the depth and the seismic moment to vary during the inversion, we tested several ranges of centroid depths and rupture velocities until to get the smallest RMS value of the modelling

V.4 Inversion result

V.4.1 Main shock

The Chuya earthquake of 27th September, 2003 is an important event because it is the first event in North West Altay range (Gorny-Altay) large enough to be recorded globally since the installation of the global seismic networks. It gives us opportunity to study ongoing tectonic process of this region.

After the Chuya earthquake, Russian research team inspected the epicentral area. Field surveys for studying aftershock monitoring were conducted by teams from Russia, Mongolia and France, seven day after the main shock. Information of the surface fault break and general tectonic contexts are introduced in Chapter III and study of aftershock distribution in Chapter IV. By preliminary result of field survey, in the epicentral zone was observed up to 60 km length surface rupture with right lateral strike slip displacements. Maximum horizontal displacement observed east part of rupture with around 0.5 -1.5 m slip. Average strike of fault is oriented 320° to the NW direction (Geodakov *et al.*, 2003 and 2004). The intensity of shaking was mapped by Russian scientists and the strongest shaking reached intensity VIII (MMS). Square of contour VIII intensity is about 100 km long and 36 km wide with elongation in the NW direction (Goldin *et al.*, 2003). Most of aftershocks are located east and west side from the main shock and distributed about 100 km long and 30 km wide place that general direction cloud of aftershock is striking 300° to the north-west.

The focal mechanism solutions from different data center are shown in Fig.V.5 and Table V.1. Focal solutions from all data center are very similar and propose right-lateral strike-slip mechanism with a small vertical component. Considering observed direction of aftershock distribution the strike of the NW-ES fault plane was chosen for modelling. Taking into account all that information we have been able to choose the initial parameters of the starting model in the waveform inversion procedures.

SOURCE	TIME (UTC)	EPICENTER		H (KM)	M_W	MOMENT (NM)		NODAL PLANES			
		LAT (DEG)	LON (DEG)			VAL	EX	P1		P2	
								STK	P	STK	P
USGS	11:33:25.1	50.04	87.81	1.0	7.3	1.0	20	38	70	130	85
HRV	11:33:36.2	50.02	87.86	5.0	7.3	9.4	19	228	70	131	71
OBN	11:33:25.1	50.04	87.81	1.0	6.9	2.2	19	33	70	302	84

Table V.1.Location, seismic moment and focal mechanism solution from different data centers: GS – USGS data set, HRV – Harvard Seismology Group, OBN – Obninsk International data center (strike and plunge of the 2 nodal planes are given in degrees).

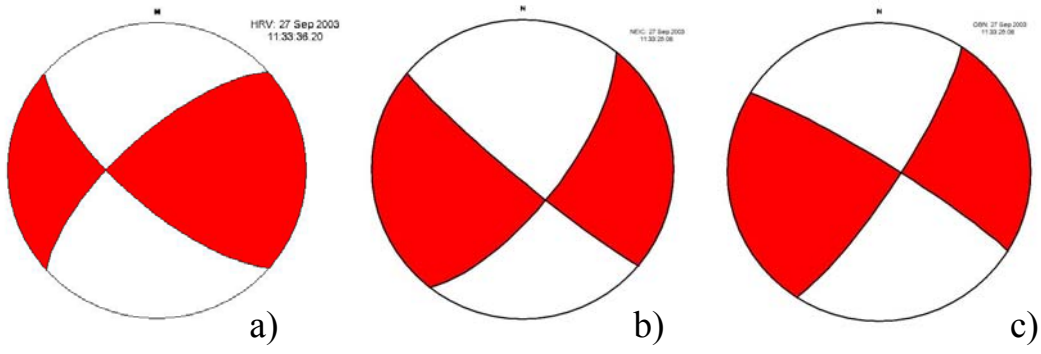

Figure V.5 Focal solutions obtained by different international data centres: a). Harvard CMT solution; b) USGS moment tensor solution; c) Obninsk data source.

For the modelling we choose stations with good quality signals, well above the noise level. Other a criterion is a polarization of horizontal components for SH wave. After

selection we found 19 IRIS and GEOSCOPE stations located at the distance between 30 and 90 degrees, taking care of a good azimuthally coverage (Fig.V.6).

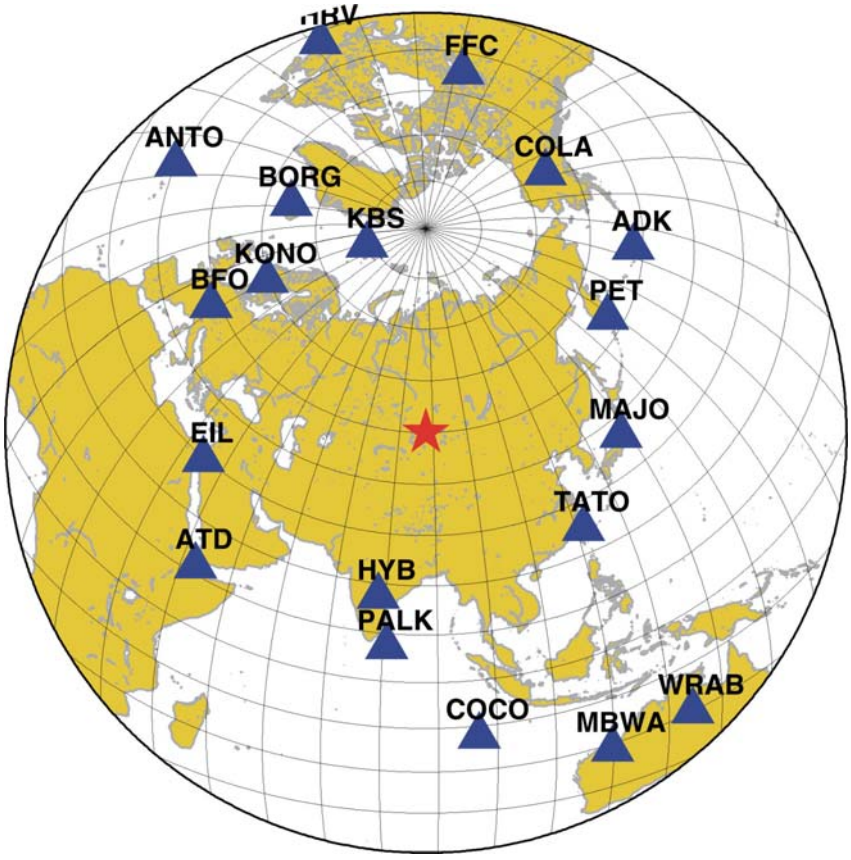

Figure V.6. Locations of seismic stations used P and SH body wave inversion of the main shock of Chuya earthquake. Red star shows epicenter of Chuya earthquake (50.04°N, 87.83°E; To=11:33:25.3) which occurred on 27th September 2003, Ms=7.3.

Azimuth coverage of the stations was sufficient for the modelling. The 19 well recorded seismic stations were choosing for the modelling instead of more than hundred stations. The data set for the inversion of Chuya earthquake consist of P waves from 17 broad band stations and SH waves from 15 long period records. Some examples of raw data in counts are shown in Fig.V.7, for instance to illustrate quality of signals.

The time window for the inversion P wave was chosen 60s after arrival of P wave and for the SH wave 100s which included waveform contained energy. For the inversion source time function is parameterized by a series of overlapping triangles of 1.5s duration.

The duration of the inverted signal depends on the depth of the source but also on the duration of the source. Ten triangle elements of time function were sufficient to determine source duration of this event.

To each P wave is affected a weight of 1. A weight of 0.5 is affected to each SH wave which takes into account the fact that SH waves are generally larger and lower frequencies

than the P waves. For the all inversion procedure we used both broad-band P wave and long-period SH wave modelling.

During the inversion we studied layered crustal models at the source region to test their effect on the inversion. The two crustal models we used for the inversion procedure is presented in Table V.2

	Thickness (km)	Vp (km/sec)	Vs (km/sec)	Density g/cm^3
Source region				
Homogeneous crust	Half space	6.00	3.46	2.75
Layered crust	0	4.35	2.54	2.50
	2	6.08	3.55	2.75
	25	6.47	3.78	2.84
	50	7.96	4.65	2.90
Receiver region				
Homogeneous crust	Half space	6.00	3.46	2.75

Table V.2 Crustal velocity model for the source and receiver region used for this study

Four sets of inversion have been performed for the modelling of Chuya earthquake. Evaluation of the result is based on the fit of the seismograms.

V.4.1.1 Point source model with simple half space crustal model

First we made the analysis considering a single point source. For starting model we have chosen the parameters shown Table V.3.

Here we obtained an almost vertical pure strike slip faulting focal mechanism was the fault plane can be chosen as the 129°N striking and 65° dipping plane (result are summarized in the Table V.3). The centroid depth is ~10.8 km. But even if the strike of the plane selected as the fault plane agrees to the observed information obtained from the aftershock distribution and preliminary result on surface rupture, the misfit between the observed and synthetic seismograms give relatively high rms-error value (RMS = 6 x 10^{-1}).

The most noticeable problem of this first model is a large misfit between synthetic and observed seismograms at the northern stations (Fig.V.8). The inversion processes do not succeed to match the width of the first full cycle of the P waveforms in all the azimuths. We conclude that some additional moment release is required beyond the first 15s of the time function, particularly to match the double upward pulse at all stations to the north such as COLA, HRV, FFC and others (Fig.V.8).

This analysis of the P waveform, and the obtained fit with the one point source model, was sufficient to deduce that the rupture was complicated, involving slip in at least two or more subevents. Before to start more complex model solutions, we have test possible directivity according these northern stations. But none of the founded the solution was sufficient to explain these double upward pulses at the northern stations.

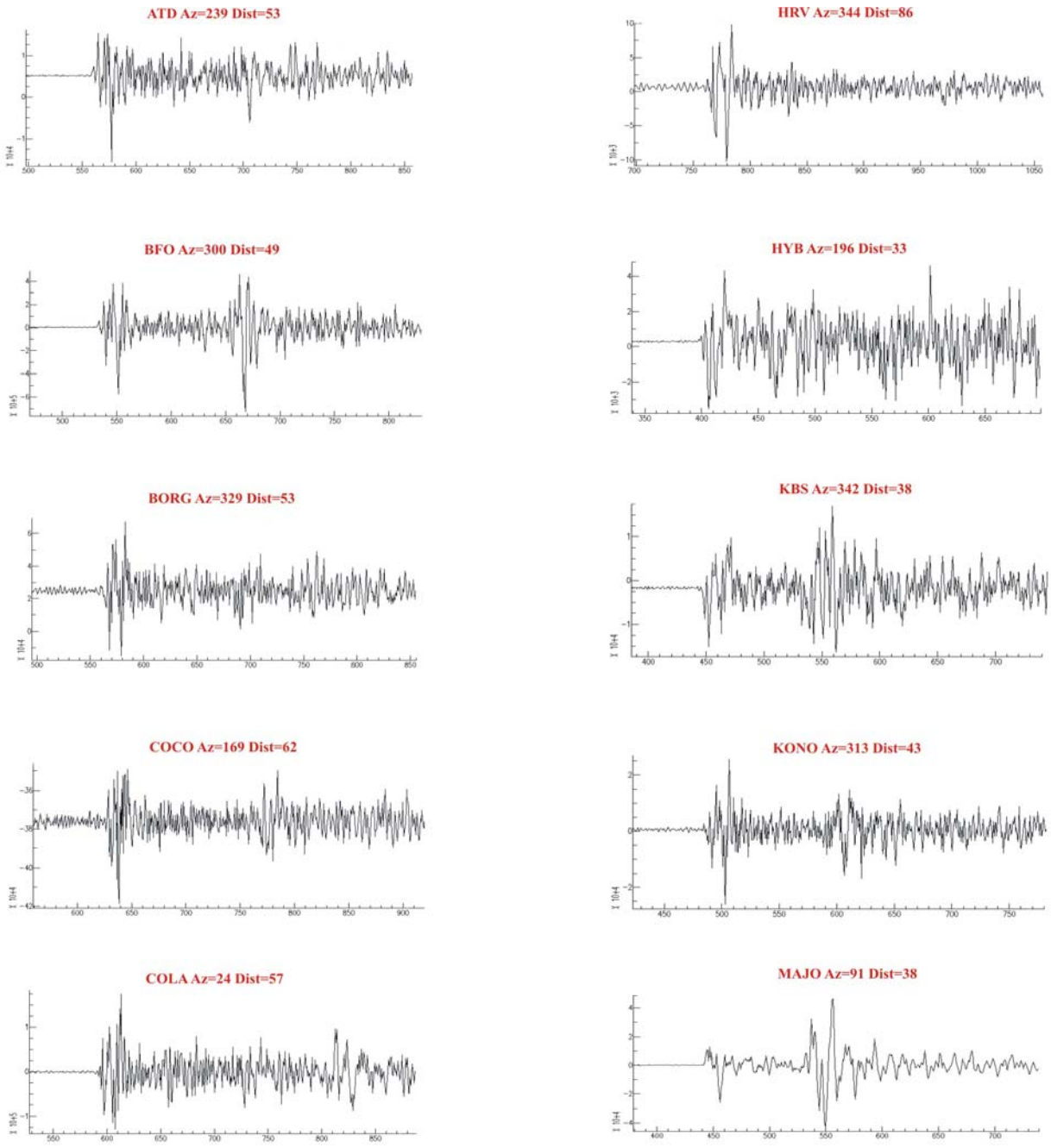

Figure V.7. Examples of broadband ground velocity records of the main shock of Chuya earthquake observed at different azimuth and distance on worldwide seismic stations. Complexity of P motion (and PP when observed) is observed clearly for the all stations. Ten seconds after the first P wave onset, is starting other energy phase which can be related to a second event.

The comparison of synthetic and observed long period SH waveform was correct for all inversion procedure. These waves are not so much sensitive to the different parameters determined by the P waves. This can be explained by the fact that only longer periods are present in the SH due to a larger attenuation of S waves. But it should be also noticed that for strike-slip events, P waves at teleseismic distances are related to rays starting from the source nearby the nodal planes of the radiation diagram, when they are nearby the maximum of radiation of SH waves. Therefore a small variation of focal parameters make a strong perturbation on the Pwave calculated amplitude, when it does not modify strongly SH amplitude.
We present SH waves modelling fit present just for last solutions we obtained in the inversion procedures.

V.4.1.2 Point source model with layered crust

The second inversion performed is identical except that the layered velocity model shown Table V.1 is used near the source. The goal of this inversion is to test the effect of "real" layered crustal model on the source area and to compare results of the previous study. Comparisons of results of inversion using these two models are shown in the Table V.3.

Event	Strike (°)	Dip (°)	Slip (°)	Depth (km)	Mo (Nm)
Starting parameters for the point source model					
Point source	130	70	170	10	1.10x10**19
Result of the inversion for the point source models					
PS halfspace	129	65	162	10.8	7.9 x10**19
PS layered	130	70	170	10.0	7.1 x10**19

Table V.3. Summary of source parameters determined by using two different velocity models at the source (in blue input parameters and in red obtained results: this color code will keep be for all following tables).

The Fig.V.11 shows example of waveforms fitting for these two inversions. Inversion result shows that inversion of this event does not depends too much of the layered crustal model. The two results are very similar and the RMS indicates that there is no significant improvement of waveform modelling using a layered crustal model at the source. Most likely the reason for this result is that the information on the crustal model (thickness and velocity) are not sufficiently precise to improve the modelling. In the next inversions we will use only the simple half space velocity model.

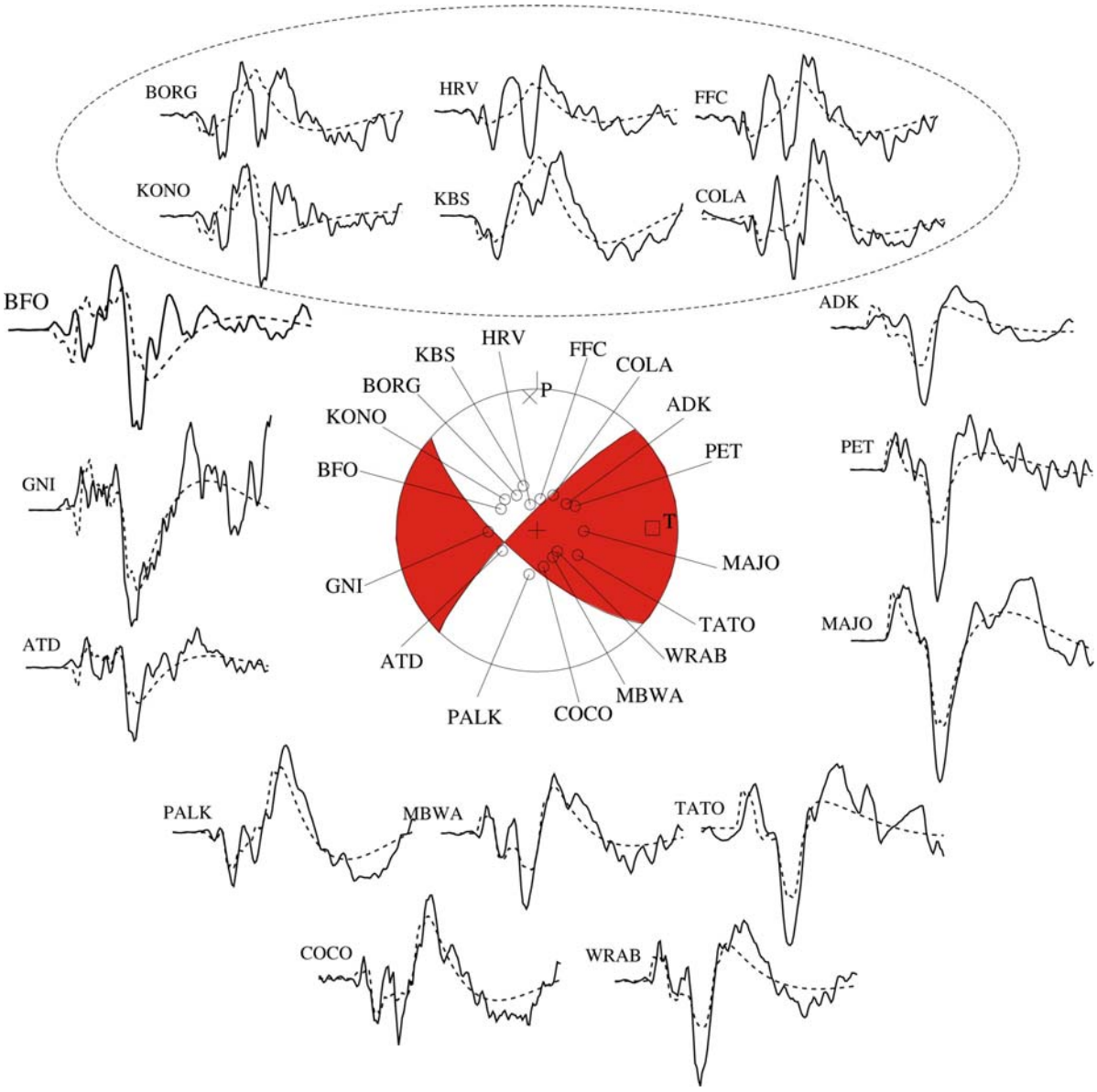

Figure V.8. Comparison between observed (solid line) and synthetic (dashed line) seismograms of the point source model. Modelling of records at the northern stations are not correct with this model. Station's dispositions will be kept in the next illustrations of the different models.

V.4.1.3 Bilateral rupture model

In third model, the point source is replaced by a line source that propagates bilaterally from the nucleation point. If we thrust the epicentral location, bilateral rupture is supported by aftershock distribution and surface ruptures that are almost symmetrically located southeast and northwest of the main shock location.

In this model we assume that during the Chuya earthquake rupture propagated bilaterally about 2.5 km/s from the nucleation point. So we model such event by the superposition of 2 subevents, starting at the same point and propagating in the opposite direction. The starting parameters of the third model are shown Table V.4.

Event	Strike (°)	Dip (°)	Slip (°)	Vr (km/sec)	Depth (km)	Mo (Nm)
Starting parameter of the bilateral rupture model						
Subevent 1	130	70	170	-2.5	10	3 x10**19
Subevent 2	130	70	170	2.5	10	3 x10**19
Result of the inversion for the bilateral rupture model						
Subevent 1	131	81	177	2.5	14	6.9 x10**19
Subevent 2	121	58	109	-1.5	12	1.8 x10**19

Table V.4. Summary of teleseismic body-wave inversion: bilateral rupture model.

The result of this inversion and the estimated focal mechanisms are shown in Table V.4 and Fig.V.9. Result of inversion shows that the seismic moment of the first subevent was 3 times larger than seismic moment of second subevent. The deduced source mechanism of first subevent is a pure strike slip vertical fault with right lateral displacement. According to aftershock distribution the fault plane is striking 131°N (almost NW-SE) and dipping 81°N. The scalar seismic moment is 6.9 x 10^{19} Nm.

Testing several depths ranges, the smallest RMS was found at a focal depth of 14 km and 12 km respectively for the 2 sources (Fig. V.10). Source mechanism of the second subevent modelled is a reverse fault striking 121° NW-SE, and dipping 58° N. The calculated seismic moment is 1.8 x 10^{19} Nm. Estimated source duration and rupture velocity for each subevents are 14s, 2.5 km/s and 9s, 1.5 km/s, respectively.

The total source duration is around 23s and total seismic moment is 9.3 x 10^{19} Nm. Time delay between the two subevents is around 2s. Relative seismic moment of the 2 subevents allows us to propose that the event can be considered mainly as an unilateral rupture 14s long towards NW to which is added, with a small delay in time and at almost the same position, a smaller event with different focal mechanism orientation.

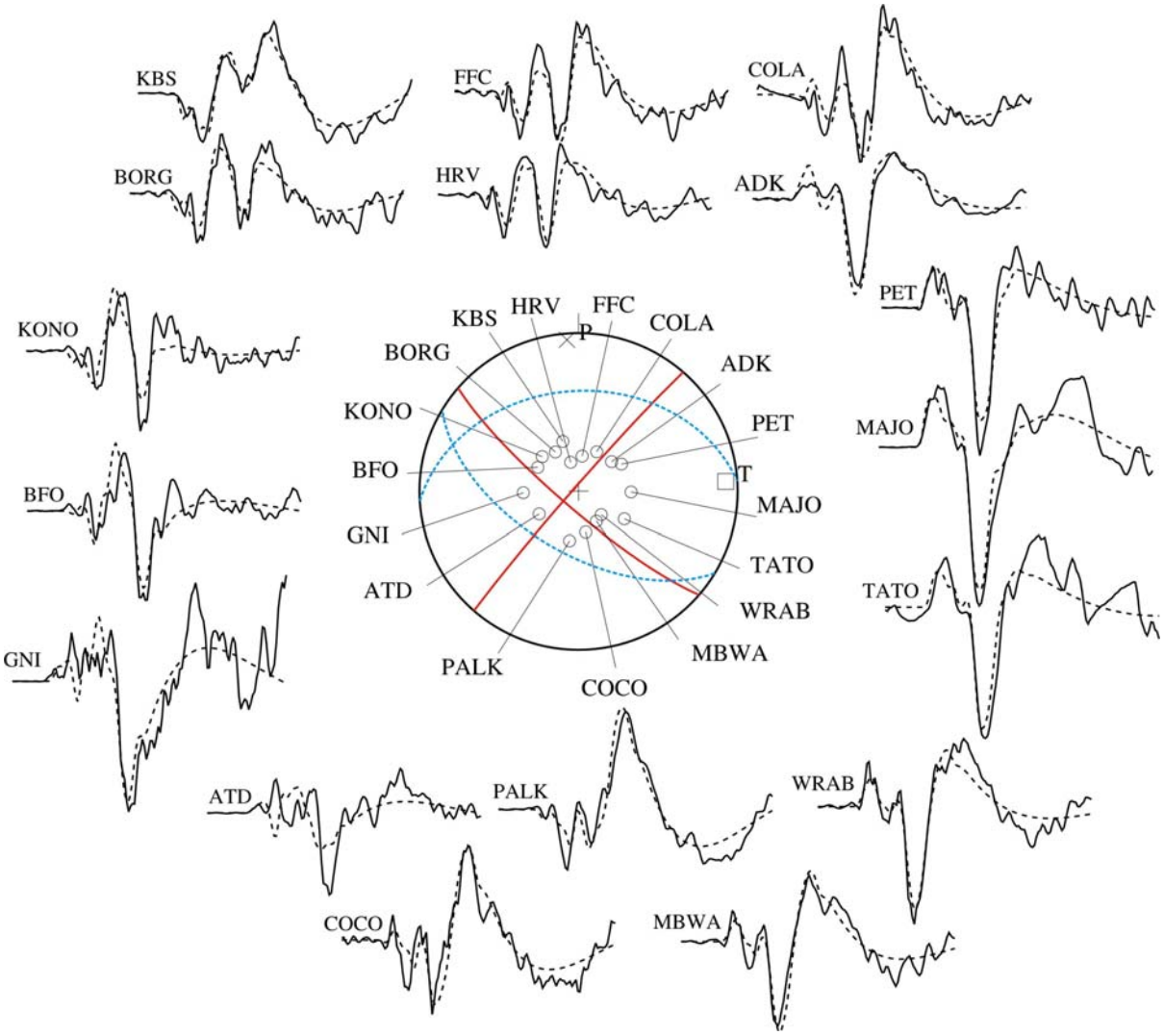

Figure V.9: Comparison between observed (solid line) and synthetic (dashed line) seismograms of the bilateral source model. Modelling of records at all stations are improved, mainly at the northern stations.

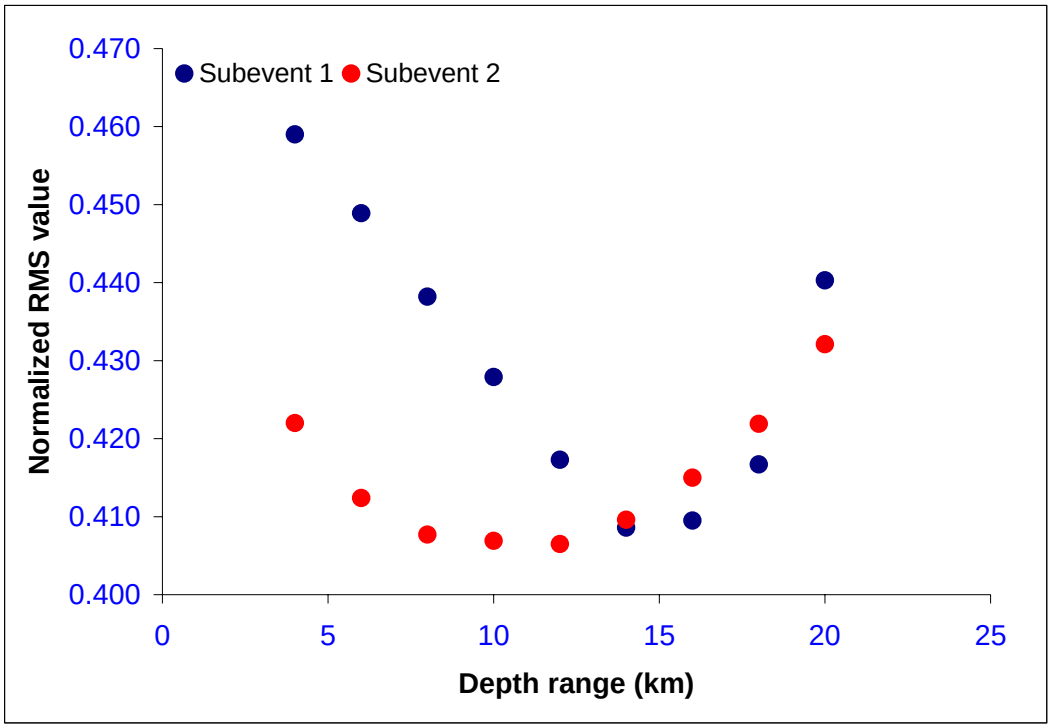

Figure V.10 Variation with depth of RMS for the best solution obtained by inversion at fixed depth.

The fit between observed and synthetic seismograms are much improved compare to the point source modelling, especially the fit to the northern stations. In Fig.V.11 we illustrate the sensitivity of the waveforms to these two models.
Improvement is quantified in the normalized RMS error that decreased to the value of RMS = 0.41. Although some waveform fits were improved, the inversion still not matches the south eastern stations as well as the other ones. It violates the P-wave first motion at the stations ATD, GNI and others (Fig.V.11). We thus tried to improve the fit by representing the source as a three subevents summation, each subevent separated spatially and in time.

V.4.1.4 Multiple subevent model

In the next step we studied a propagating source along the preferred fault azimuth. We parameterized the fault with 3 segments with a rupture velocity of 2.5 km/s, and let vary the following parameters for each of the sources: seismic moment, focal mechanism and centroid depth. In this model we assume that the first subevent nucleated at the location of the Chuya earthquake and propagates towards the northwest direction. The second subevent is located almost at the same position than the first subevent with the same fault strike but is propagating to the southeast. For the last subevent we assume that it is located 15 km further to the SE from the nucleation point of the first subevent. We fixed the depth of all the segments to 10 km. The starting parameters for the inversion of this model is shown in Table V.5

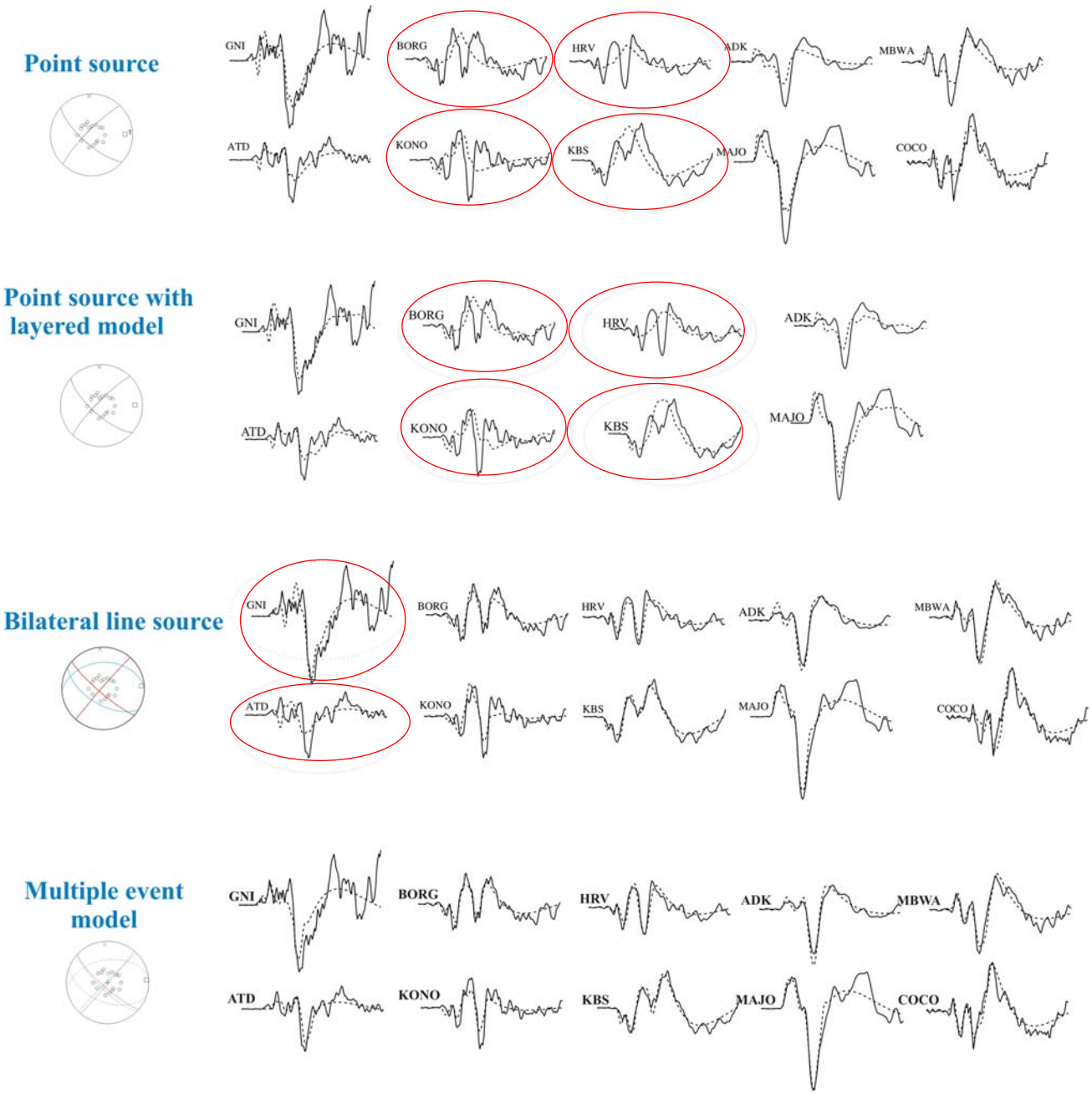

Figure V.11. Comparison of synthetics (dashed lines) and observed seismograms at the most critical stations for the different solutions obtained at different stages of the inversion procedure.

As the number of parameters is larger and we know that the inversion procedure is note able to solve independently all these parameters, we use a step-by-step procedure to control the parameters variation. Therefore we began to invert the first subevent parameters that are seismic moment, focal mechanism and centroid depth keeping fixed parameters of the other two subevents. We then held this first event and the third subevent fixed, and inverted for the second subevent parameters. In the next step we made the same procedure for the third subevent. This procedure was continued until stabilization of our inversion results.
After that, we fixed the focal solution and made the inversion for different rupture velocity in the range 1.0-4.0 km/s; the best match between observed and synthetic waveforms was obtained with a value between 1.5 km/s and 2.5 km/s (Fig.V.12).

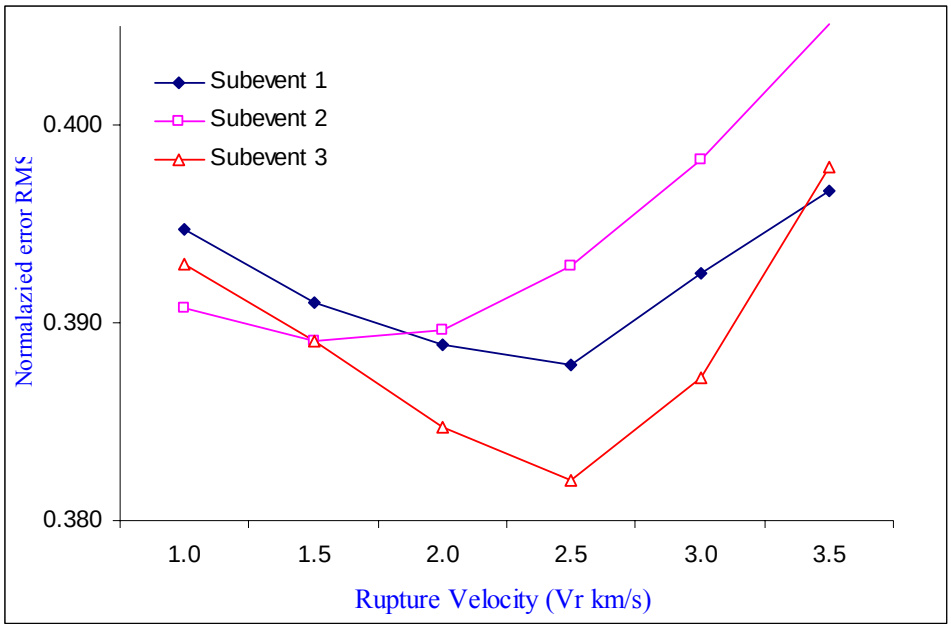

Figure V.12 Variation with the rupture velocity value imposed in the solution of the best solution RMS.

The behaviour is different for the three subevents; for subevent 1 and 3 we observe a clear minimum at 2.5 km/s which shows that the propagation should be considered and is well solved. For sub event 2 the minimum is obtained for a much lower value of the rupture velocity (1.5 km/s). This subevent corresponds to a reverse mechanism and a smaller seismic moment (Table V.5).

Then we examined the rise time: assuming that the source time function consists of ten ramp functions successively with the three rise time values of 1.0s, 1.5s and 2.0s, we found that 1.5s gave a better fit than others.

We also examined the distance and azimuth between these subevents. According to the smallest estimated value of RMS, the second subevent nucleated 0.6 km to the NE and only one second after the first subevent. For the third subevent we found that is nucleated 12 km further to the SE, 1.5s after the first subevent (Fig.V.13).

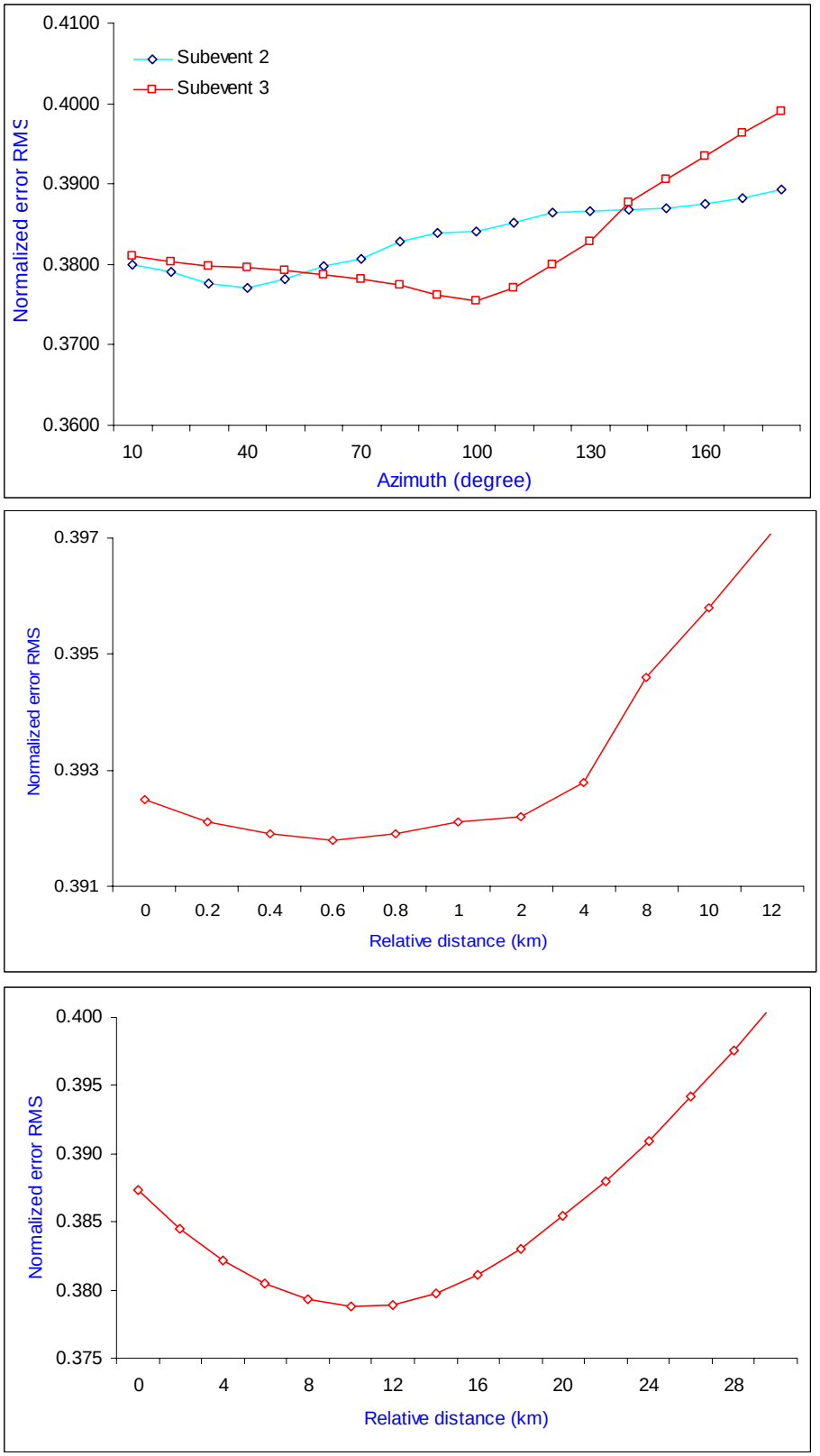

Figure V.13 Determination of the relative positions for second and third subevents: the criteria of the minimum RMS is used (a) variation of best RMS with azimuth of the position of subevents 2 and 3 compare to subevent 1; (b) variation of best RMS with distance of subevent 2 compare to subevent 1; (c) subevent 3 compare to subevent 1.

Inversion result shows a good agreement between the synthetics and the observed recordings with smallest value of RMS = 3.6 x 10^{-1}. The result of this inversion is shown in Fig.V.14 and Table V.5. A lot of different sequences of inversion have been tested. Finally we try to propose a procedure which retrieves first the most sensitive parameters. But we are conceit that the final result can be sensitive to the inversion sequence; some of the parameters are very poorly constrained and there is a trade-off between some others (rupture velocity, maybe position of the subevents).

Event	Strike (°)	Dip (°)	Slip (°)	Vr (km/sec)	STF (sec)	Depth (km)	Mo (nm)
Input parameter for the inversion							
Sub1	130	70	170	2.5		10	1. x10**19
Sub2	130	70	170	2.5		10	1. x10**19
Sub3	130	70	170	2.5		10	1. x10**19
Result of the inversion for the multiple subevent model							
Sub1	131	80	181	2.5	9	8	3.9x10**19
Sub2	111	49	110	1.5	7.5	12	1.8x10**19
Sub3	134	74	177	2.5	7.0	12	2.8x10**19

Table V.5. Summary of source parameters of the main shock Chuya earthquake determined in this study

Compared to previous models, this last model provides the smallest RMS value and leads to good fits to the observation at all stations. The fit of observed seismograms at ATD and GNI are much improved and it is chosen to be the best fitting model of Chuya earthquake. On the Fig.V.11 is illustrated the improvement of fitting between observed and synthetic P for different key stations.

Finally, results of body wave inversion show a complex rupture process: the earthquake was composed of three subevents of 9s, 7.5s and 7s duration respectively. The first subevent released the larger seismic moment with a right lateral strike slip faulting mechanism along a plane striking 311°N and dipping 80°. For the second subevent we deduced reverse faulting double-coupling mechanism striking 111°N. The third subevent is modelled like the first subevent with NW-SE trending strike slip mechanism. Time delay between the first shock and the second and third shock were ~1s and ~1.5s respectively. Relatively to first subevent, the centroid of second and third subevent were located respectively at a distance of 0.6 km and in 40°N azimuth and 12 km and 106°N. The moment released by these three subevents add up to a total seismic moment of 8.5 x 10^{19} Nm. This value is comparable with result of the Harvard CMT (9.4 x 10^{19} Nm).

We can calculate Mw magnitude by Kanamori relation (Kanamori, 1977):

$$Mw = \frac{Log_{10}(M_0)}{1.5} - 10.73 \qquad \text{(V.10)}$$

Using equation (V.10) we obtained *Mw = 7.2,* which is in good agreement with USGS surface magnitude, Ms = 7.3, estimation.

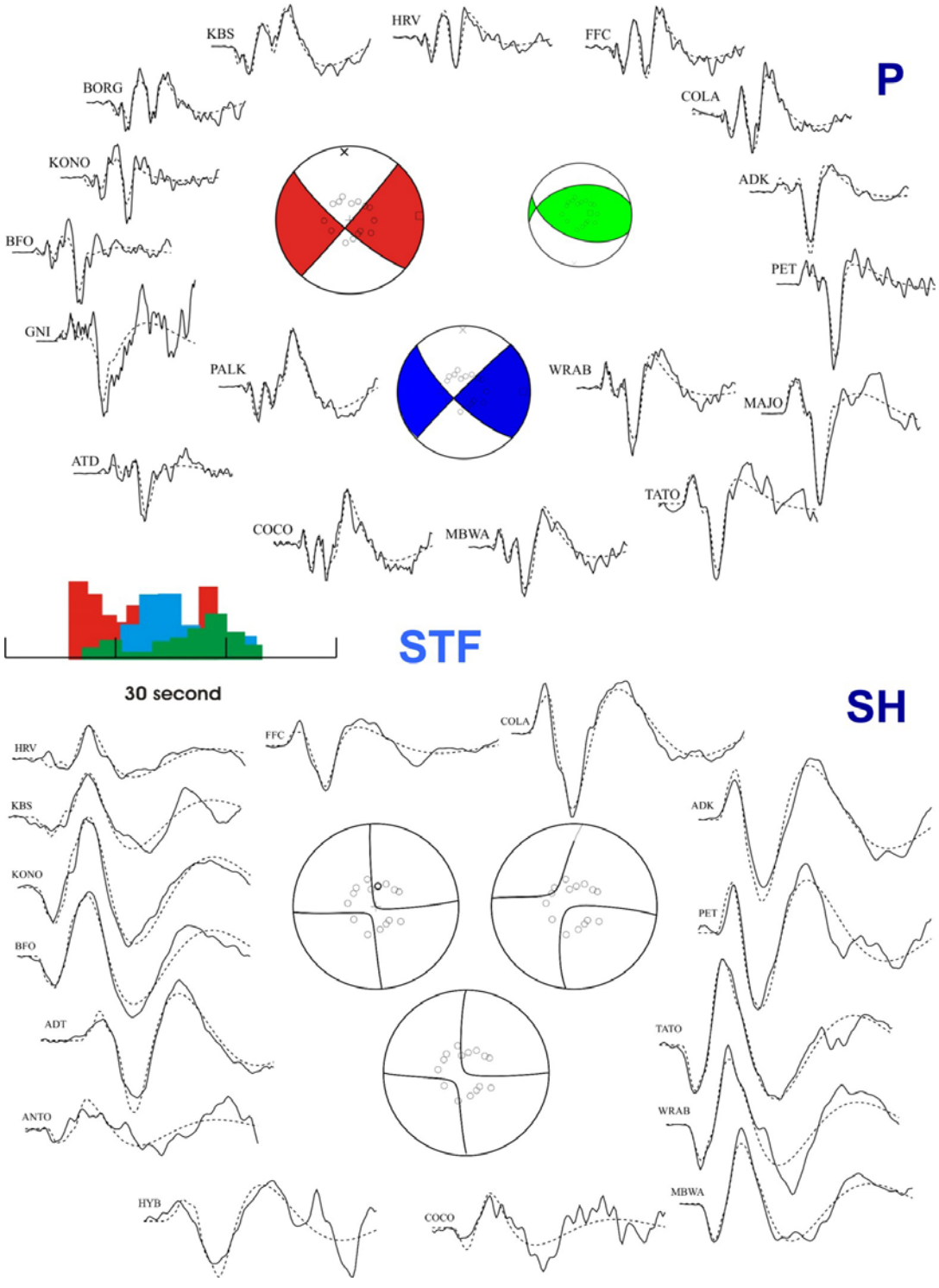

Figure V.14 Comparison between observed (solid line) and synthetic (dashed line) seismograms for the final model composed of 3 subevents (a) P waves, (b) SH waves. In the center is represented the focal solutions obtained for these subevents.

Let us assume that the rupture length in each subevent is roughly the time function duration multiplied by rupture velocity (*~2.5 km/s* for the 1 and 3 subevent, *~1.5 km/s* for the 2 subevent). The first subevent can then account for *~22.5 km* of faulting along southwestern margin of Chagan-Uzun horst and probably propagated northwest. The second subevent can account for *~11 km* of rupture to the eastern slope Chagan-Uzun horst. The third subevent can account *~19 km* of nearly pure strike slip which propagating to the southeast through the Chagan, Elangash low hills and river basins. The total length of rupture covered by these three subevents add up to a total fault length of L = 52.5 km.

To calculate average slip D from the seismic moment we apply the relation:

$$D = \frac{cM_0}{\mu WL} \qquad \text{(V.11)}$$

Where c is a factor depending on the fault's shape (for strike slip faults c is $2/\pi$), μ the crustal rigidify modulus (Stein *et al.*, 2003), **W** and **L** the dimensions of the fault (length and width). In case of large events these parameters are generally constrained by aftershock distribution. In our case was aftershocks concern mainly to large events (27th November and 01st October), for each individual event we will consider that **L** is constrained by the rupture modelling and that **W** has a common value of 20 km given by the depth of the deepest aftershock activity. If we consider the estimated total value of the seismic moment, the length of surface rupture and the vertical wide of aftershock distribution, we can find an average slip for Chuya earthquake of ***D = 270 cm***, which is almost twice larger than what (1.5 m) was reported by Russian scientists (Geodakov *et al.*, 2004) but in good agreement with values obtained for strike-slip events of similar magnitude (Kunlun, 2001; Izmit, 1999; Denali, 2003...). This value is also comparable to the average slip of 2-3 m horizontal slip deduced along the surface rupture on SPOT image autocorrelation (Fig III.16).

The stress drop of strike-slip on rectangular fault with length **L** and width **W** yields:

$$\sigma = \frac{2}{\pi} * \frac{M_0}{W^2 L} \qquad \text{(V.12)}$$

Using this equation we obtain a stress drop of ***6.0 MPa.***

V.4.2 The first large aftershock

Within the first month after the main shock of Chuya earthquake several thousands of aftershocks occurred in the epicentral area. Among these aftershocks two significant strong events of magnitude 6.6 and 7.0 occurred few days after the main shock.

The first strong aftershock is located about 12 km to the NW from the main shock of Chuya earthquake (Chapter III). The focal mechanism estimated from long period seismogram modelling by Harvard shows a right lateral strike slip fault were striking 120°, dipping 79°. The Table V.6 and Fig.V.15 show the focal mechanism solution of first large aftershock of Chuya earthquake obtained different data centres.

SOURCE	TIME (UTC)	EPICENTER		H (KM)	M_W	MOMENT (NM)		NODAL PLANES			
		LAT (DEG)	LON (DEG)			VAL	EX	P1		P2	
								STK	P	STK	P
USGS	18:52:46.9	50.091	87.765	15.0	6.4	5.0	18	120	79	211	83
HRV	18:52:52.9	50.090	87.750	15.0	6.4	4.5	18	117	67	217	68
OBN	18:52:46.9	50.091	87.765	15.0	6.2	2.2	18	226	82	134	82

Table V.6. Location, seismic moment and focal mechanism solution from different data centers: GS - USGS data set, HRV - Harvard Seismology Group, OBN - Obninsk International data center (strike and plunge of the 2 nodal planes are given in degrees).

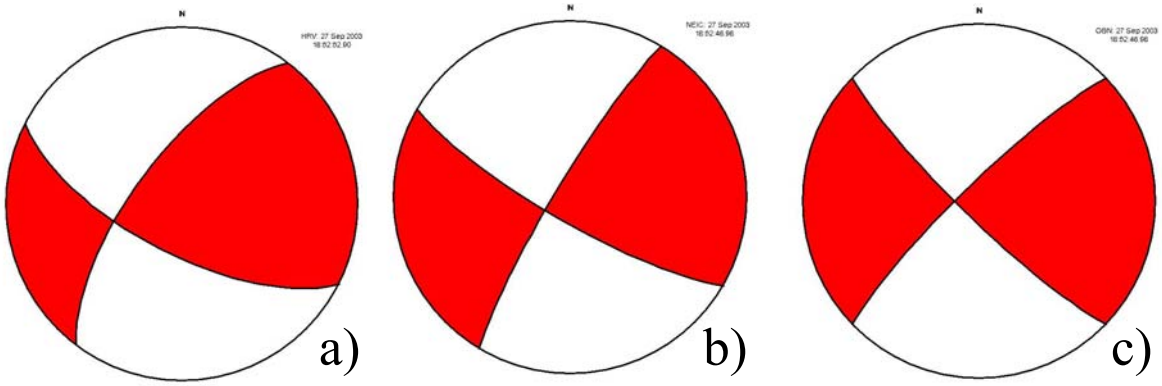

Figure V.15 Focal solutions obtained by different international data centers. (a) Harvard CMT solution. (b) USGS moment tensor solution. (c) Obninsk data source

For the body waves modelling of the first strong aftershock we used 20 broad-band stations data for P wave and 10 long period data for SH wave. Signal quality and azimuth coverage of chosen stations was acceptable. The Fig.V.16 shows location of these seismic stations.

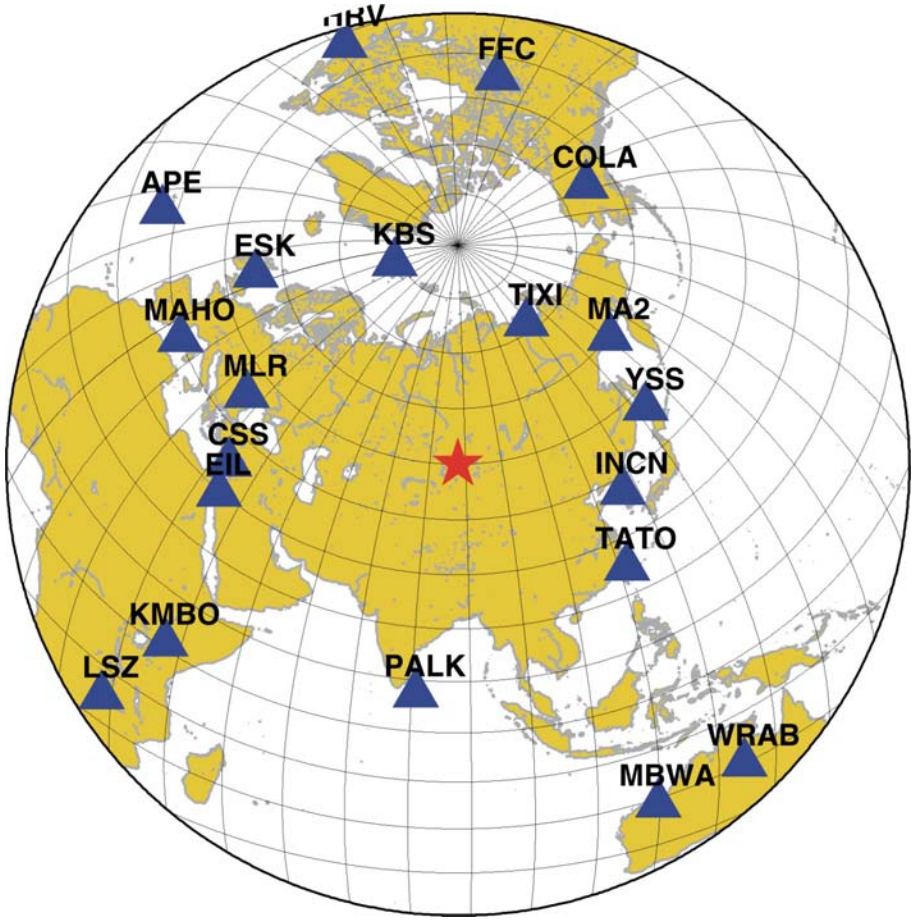

Figure V.16. The distribution of the seismic stations used for P and SH body wave inversion of source function of the first large aftershock. Red star show location of this aftershock which occurred 7 hour after the main shock with Ms=6.6. Azimuth coverage of the stations was sufficient for the modelling

. P and SH waves from broad band and long period stations were inverted together for focal solution, depth and source time function. The first 25s from the onset of the P wave and 30s for SH wave were used for the analysis. The P phase arrivals were picked manually and during inversion sequence realignment was performed by cross correlation of synthetic and observed seismograms.

The source time function was parameterized by a series of 8 overlapping triangles with 0.8 second duration for each element. We choose this short duration of elements mainly to determine centroid depth.

On Fig.V.17 are presented P-waves recorded signals. A first observation of these signals shows that a characteristic of the onset of P wave is clearly depending of the azimuth: SE stations have more impulsive onset which is not easily compatible with the HRV solution. At NW stations we can observe smaller amplitudes of direct P phases. Moreover, as the event duration is short, sP waves can be identified and we can observe clear sP phases on all the records; signal frequency depends strongly from the azimuthal position of the station which shows that a strong directivity effect should be present from SE to NW. These observations are well explained by strong rupture directivity.

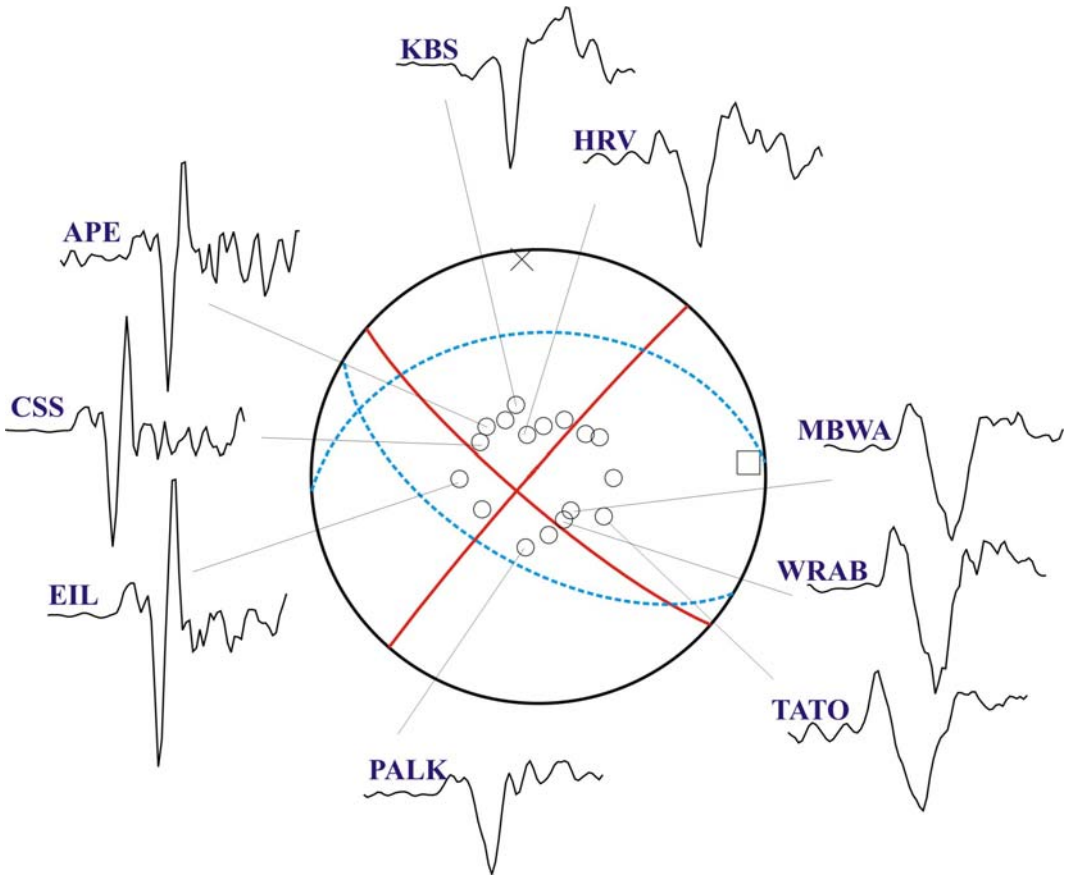

Figure V.17 Selected P waves signals which show clearly that the strike-slip solution (in red) as it is proposed by Harvard is not compatible with P waves polarities observed. In blue our better point source solution.

The modelling is performed only using simple half space crustal model for source and receiver region (Table V.2); general values of weighting of seismograms are used 1.0 for P waves and 0.5 for SH waves. Three set of starting models were used for inversion of this data set which is described here after.

V.4.2.1 Point source modelling

We used first a simple point source model with parameter giving in Table V.6 to obtain the mean characteristics of the source. As starting focal solution we take a 130°N striking strike-slip fault with a dip of 85° given by Harvard solution. We fix centroid depth at 10 km. We inverted focal solution and seismic moment, fixing centroid depth. After we fixed estimated result of focal mechanism and let vary seismic moment and centroid depth. This procedure was repeated until we get a stable solution.

The inversion shows 122°N striking and 56° dipping pure reverse faulting with strike slip component and around 3s of source duration. Centroid depth and seismic moment are estimated at 13 km and 3 x 10^{18} Nm respectively. The result of this modelling is summarized in Table V.7 and fitting synthetic and observed waveforms showed Fig.V.18

Fit of seismograms is relatively poor and we obtained error value of RMS = 6.0 x 10^{-1}. As expected from the observation of seismograms, this simple model cannot explain the azimuth variation of onset shapes and amplitudes of P-waves (lower amplitude of synthetic seismogram compared to observed seismogram at the NW stations: CSS, APE and others) and reverse for the stations SE direction (WRAB, MBWA, TATO). We notice also a large misfit at the two stations located very close to the nodal line (KBS MLR). Therefore we tested model with propagating rupture.

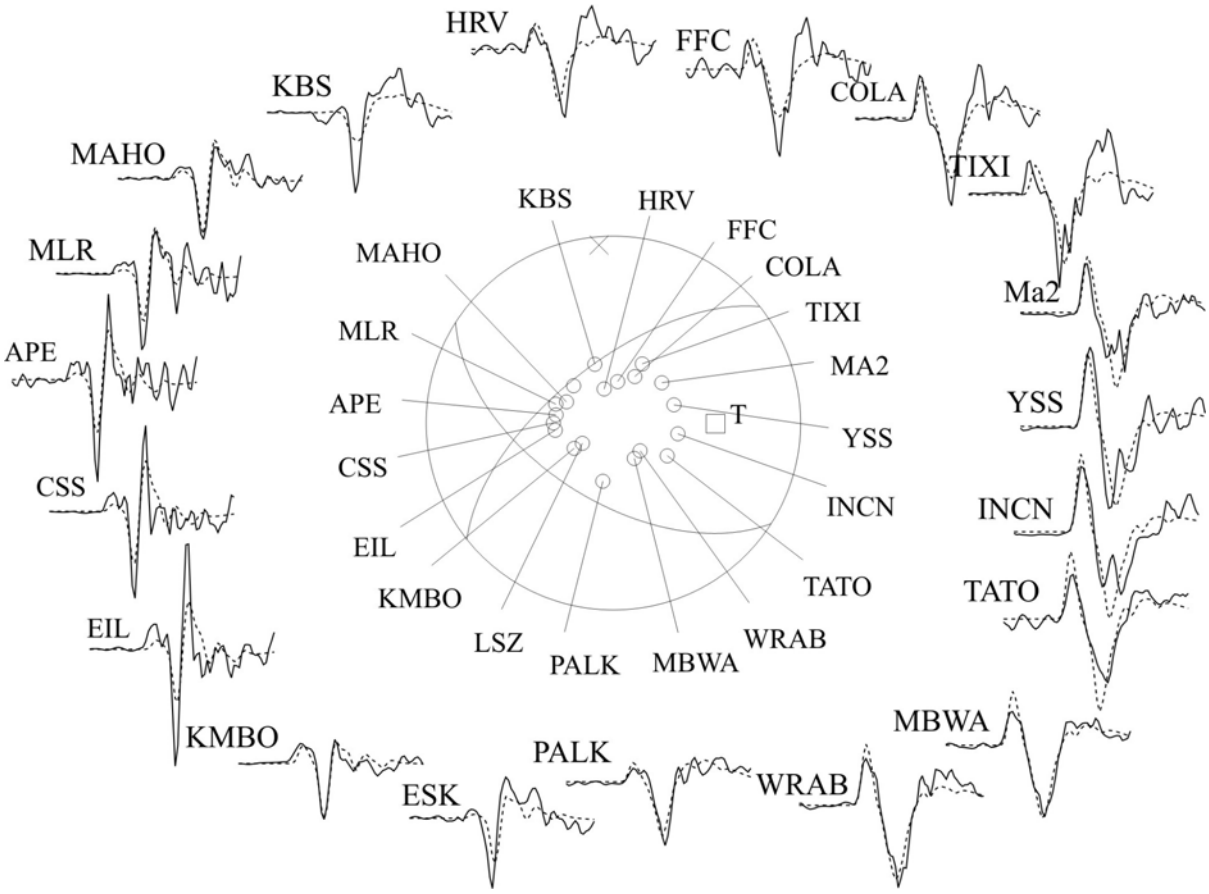

Figure V.18. Comparison between observed (solid line) and synthetic (dashed line) seismograms of the point source model. Some amplitudes are not well modelled (TATO, MBWA, EIL, CSS).

V.4.2.2 Unilateral rupture model

For the unilateral rupture model we start from the same initial parameters than the previous ones but search the solution as a propagating line source along the strike 130°N, with rupture propagating SE to NW with a 2.5 km/s velocity. These parameters allow converge to a solution in which the fit between synthetic and observed seismograms is increased. Nevertheless, still the low amplitudes observed at NW stations are not explained by the modelling.

We explore inversion results increasing the rupture velocity. The best fit is obtained for a high rupture velocity value of Vr = 4.5 km/s. Such high velocity rupture (Vr = 4.7 km/s) has been noted during for Izmit event on 17th August, 1999 (Tibi *et al.*, 2000; Bouchon *et al.*,

2000), Kunlun event on 14th November, 2001 (Bouchon *et al.*, 2002). Corresponding to this model, we obtain a 117°N striking and 55° dipping reverse faulting that ruptured during 3 s. The result of P and SH body-wave inversion by unilateral line source model is represented in Table V.7.

Fit of seismograms is slightly improved (we found a smaller value of RMS = 5.1 x 10^{-1} which remain relatively high) but the same discrepancies are still observed for north-western stations. The Fig.V.19 illustrates the fit improvement between synthetic and observed waveforms for different steps of source models.

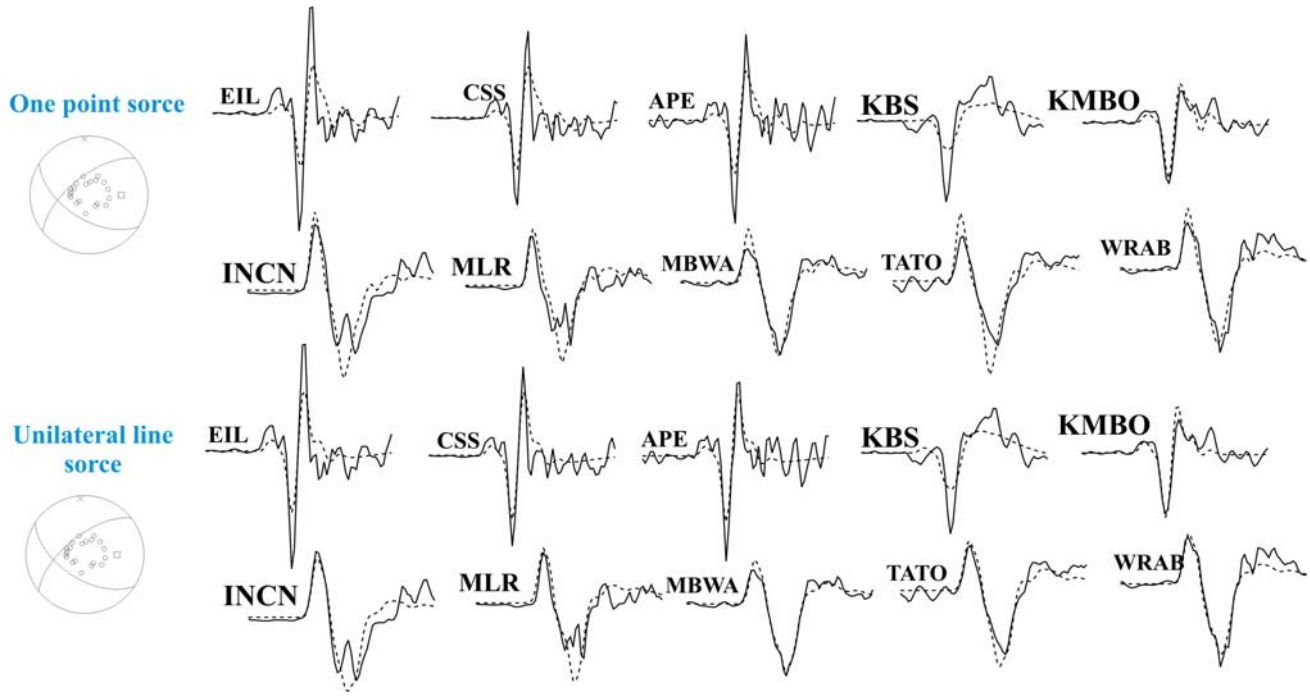

Figure V.19. Comparison of synthetics (dashed lines) and observed seismograms at the most critical stations for point source models. Amplitudes modelling are improved with a propagating source.

Therefore we tried to improve fit of two nodal stations by varying focal mechanism solutions. It was impossible to explain these data by one point or line source model and we need more complex model to explain those two nodal stations data.

V.4.2.3 Two propagating line sources

In the next model, for the starting parameters we used results of previous inversion procedures except of focal solutions. We parameterized SE-NW propagating 2 line sources along the giving fault azimuth with a rupture velocity of 2.5 km/s. In the starting model, the same focal solution (strike 130°N, dip 70°, slip 170°) and the same depth (10 km) was assigned to the 2 segments. Position and origin time of the second subevent is given relatively to the first subevent. It is assumed to be located in a 280°N azimuth to the north, at a distance of few km and nucleated 2s after the first subevent.

First, we inverted the following parameters for each of the sources: seismic moment, focal mechanism and centroid depth, fixing them one by one. The inversion procedure was continued until stabilization of source mechanism solution has given in Table V.7. Different focal solutions are obtained (first subevent as dip-slip, second subevent as strike-slip).

In the next step, we examined rupture velocities in the range 1.0-5.0 km/s, and achieved the best match between observed and synthetic waveforms with a value of 1.5 km/s and 4.5 km/s, respectively for first and second subevents (Fig.V.20). The high rupture velocity (4.5 km/s) found in this inversion is similar to the one obtained for the previous unilateral propagating line source model. The low rupture velocity (1.5 km/s) obtained for the dip-slip subevent is less well defined. It could be related either to none a circular fault, either to the fact that resolution for such small moment it is not good. Nevertheless the similarity to results on the second subevent of the main shock allows us to propose a specific character in this region for the reverse faulting which will be related as the break of asperities of smaller size than the surrounding faults and on which the rupture as a low horizontal velocity.

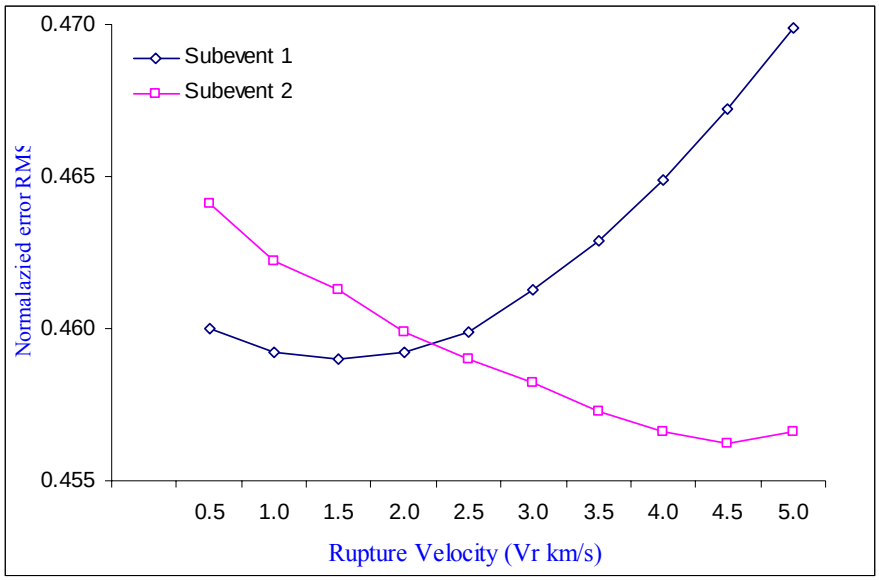

Figure V.20. Ruptures velocities determination of the first and second subevents.

We then examined rise times of 0.5s, 1.2s and 2.0s, assuming the source time function consisting of eight ramp functions. We found that 1.2s gave a better fit than the others. We also examined a distance and azimuth between these subevents. According to the smallest estimated value of RMS, the nucleation point of second subevent is located at a distance of 6 km and a 280°N azimuth relative to the first subevent. Fig.V.21 shows determination of best nucleation distance and azimuth of second subevent.

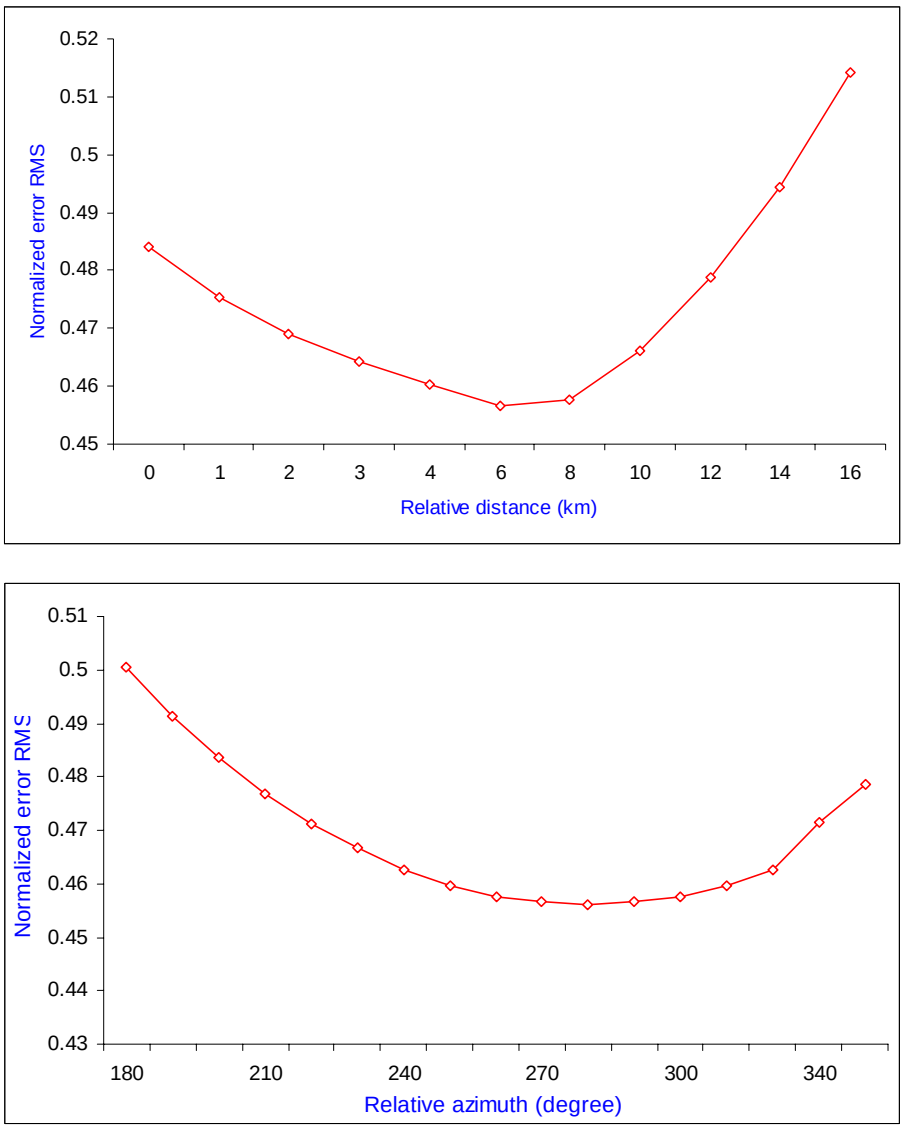

Figure V.21 Relative location determination for the second subevent compare to the first one.

The final selected result for this large aftershock is illustrated in Table V.7. The focal solution and best fitting observed and synthetic seismograms are shown in Fig. V.22. Fitting at northern and north-western stations is improved. SH waveform modelling is again not very sensitive to parameters controlling the rupture description

Event	Strike (°)	Dip (°)	Slip (°)	Vr (km/sec)	STF (sec)	Depth (km)	Mo (Nm)	Rms
Inversion results of the point source model								
	122	56	81	-	3	13	3.0x10**18	
Inversion results for the unilateral propagating line source model								
	177	55	72	4.5	3	13	2.9x10**18	
Inversion results for the bilateral propagating line source model								
Sub1	66	54	89	1.5	2	11	1.3x10**18	
Sub2	125	65	72	4.5	2	14	3.3x10**18	

Table V.7. Summary of the body wave inversion result of the first large aftershock.

Results of inversion suggest that the first large aftershock is produced by the combination of two subevents. The episode of rupturing is described by a first part represented the unilaterally slowly toward 66° NE propagating rupture followed by a second part represented by a propagating to the NW rupture. Centroid mechanism of the first subevent corresponds to the reverse faulting with little strike slip component.

The second biggest subevent is characterized by right lateral strike slip faults with small vertical displacement component. If we consider the estimated rupture velocities and source time function duration, the first subevent is produced by a 3 km length rupture to the NW and the second subevent by a 9 km length rupture to the same direction. The moments released by first and second subevents add up to 4.6 x 10^{18} Nm. The estimated average centroid depth is 13 km which is in good agreement with depth reported bulletin of NEIC, calculated by depth pP phases.

Using the equation V.11, an event with a total seismic moment of 4.6 x 10^{18} Nm might be expected to occur on a total fault of ~9 km long that slipped ~0.6 m. Applying V.12, we obtain the stress drop of *3 MPa*. Finally we obtained Mw = 6.4 moment magnitude by Kanamori relation (V.10) (Kanamori, 1977). These values of moment magnitude and average stress drop are in good agreement with values of surface magnitude Ms = 6.6 estimated by USGS and Harvard Mw estimated by CMT (Mw = 6.4).

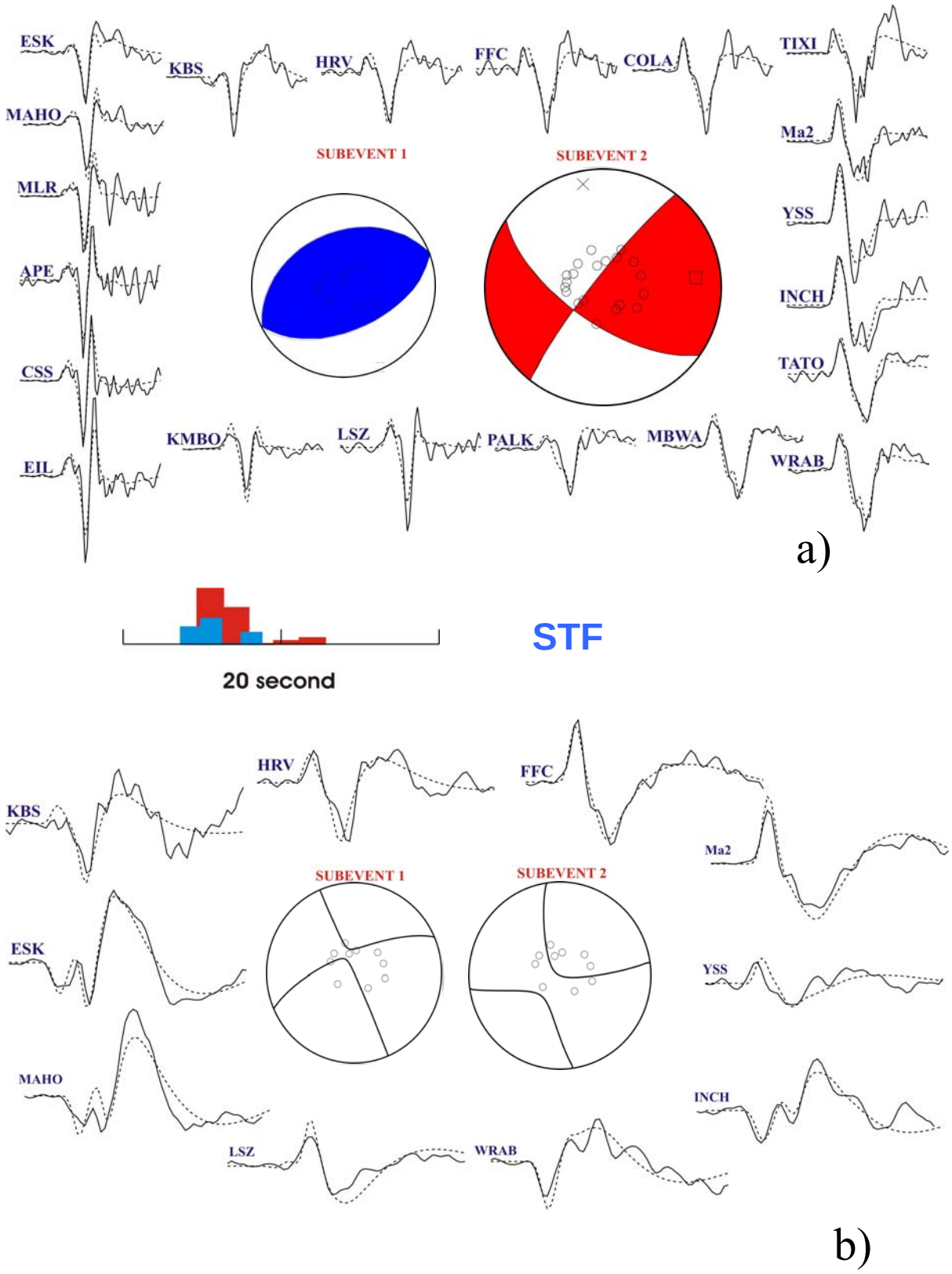

Figure V.22. Teleseismic waveform modelling result of first large aftershock of the Chuya earthquake. The fitting between observed (solid line) and synthetic (dashed lines) P (a) and SH (b) waveforms are improved. Stations are ordered clockwise by azimuth.

V.4.3 Second large aftershock

On 01st October, occurred the largest aftershock (Ms = 7.0) of the Chuya earthquake. This event occurred four days after the main shock and was located 25 km away to the NW from main shock by relative relocation result obtained by our study (see chapter IV). The Harvard fault plane solution based low frequency seismograms modelling, suggests this largest aftershock was caused by a pure right lateral strike slip faulting. If considering the aftershock distribution and the position of the epicenter determined by relative relocation method, the fault direction is 128°N striking and 82° dipping at depth 14 km. The estimation seismic moment is 1.3 x 10^{19} Nm and calculated magnitude Mw is equal 6.7. First motion focal solution results from different databases are shown Fig.V.23.

SOURCE	TIME (UTC)	EPICENTER		H (KM)	M_W	MOMENT (NM)		NODAL PLANES			
		LAT (DEG)	LON (DEG)			VAL	EX	P1		P2	
								STK	P	STK	P
USGS	01:03:25.2	50.21	87.71	14.0	6.7	1.3	19	37	81	128	82
HRV	01:03:30.0	50.24	87.59	15.0	6.7	1.1	19	221	67	129	85
OBN	01:03:25.2	50.21	87.72	14.0	6.3	3.5	19	142	74	51	88

Table V.8. Locations, seismic moments and focal mechanism solutions from different data centers. GS - USGS data set, HRV - Harvard Seismology Group, OBN - Obninsk International Data Center (strike and plunge of the 2 nodal planes are given in degrees).

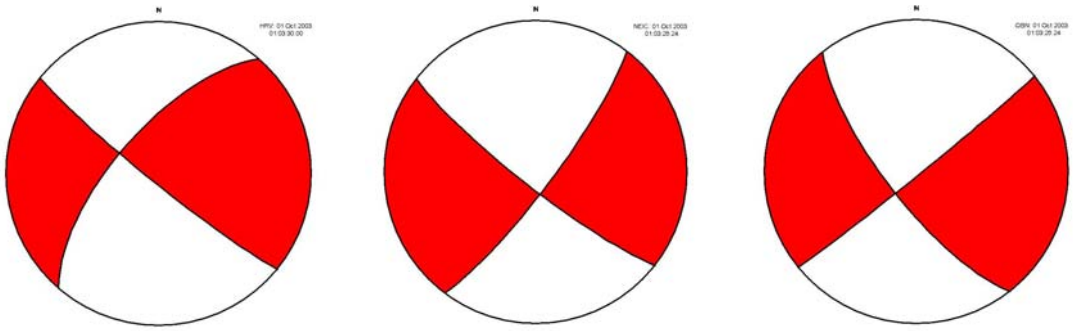

Figure V.23 Focal solutions obtained by different international data centers. (a) Harvard CMT solution. (b) USGS moment tensor solution. (c) Obninsk data source

Data were obtained from IRIS DMC database did not fully cover all azimuths: information is missing from south and south-east direction, because data of some stations were we used previously was not acceptable (high noisy or signal is not well). To complete this distribution we used TAM, ATD, HYP data from GEOSCOPE database. The station positions (used for this inversion) are shown Fig.V.24.

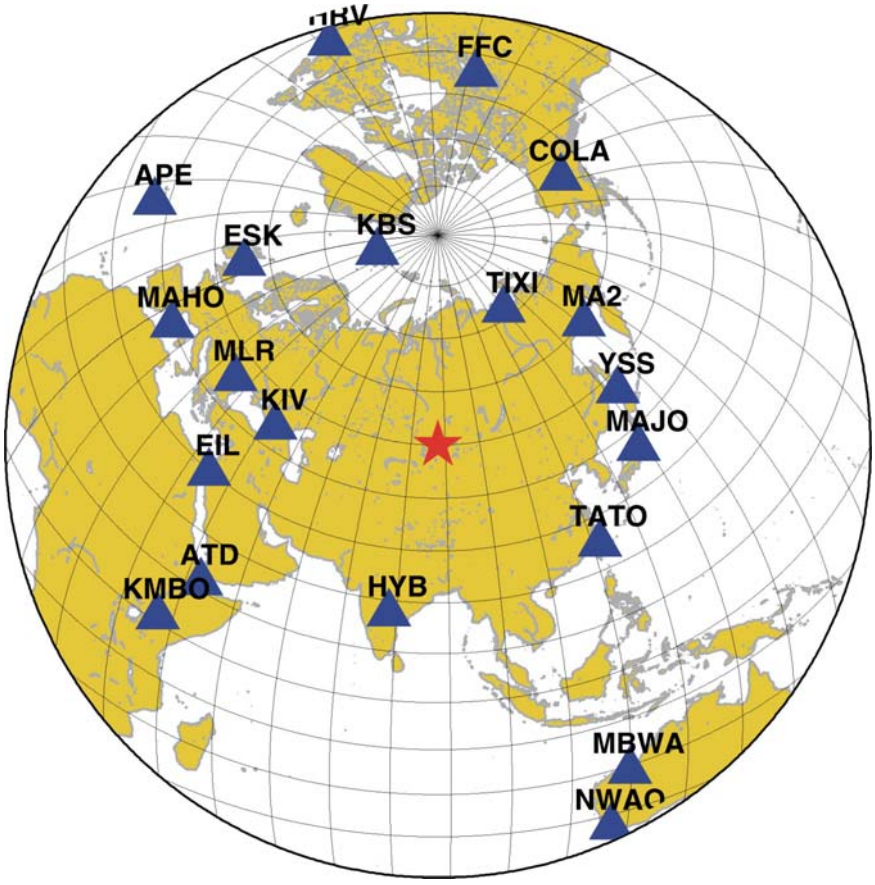

Figure V.24. The distribution of the seismic stations used for P and SH body wave inversion of source function of the second large aftershock. Red star shows location of this event on 01st October.

The observed signals are suggesting that aftershock is more complex than the previous one. After data collection, we examined each signal quality, polarization of horizontal components and selected 20 broad band data for P wave, 13 long period data for SH wave acceptable to be inserted in the inversion process.

For weighting of the stations we used early mentioned criteria but, because of less density of stations in south east direction, we increased weight of HYB station until 3 for the first steps of inversion, to get reasonable solutions. For the final inversion procedure we used almost same weights for the all stations.

In this inversion procedure we used 8 overlapping triangular source time functions of 1.0 second duration each. The inversion window is chosen at 25 second after onset of P phase by duration of first energy phases. Three inversion processes have been performed for this aftershock.

V.4.3.1 Point source model

As first test of inversion, like as before, we had begun with a single point source. By using this model first we inverted focal solution and seismic scalar moment for the P and SH waveforms together. The parameters corresponding to the best data fit are given in Table V.9 and the estimated focal mechanism is shown Fig.V.25.

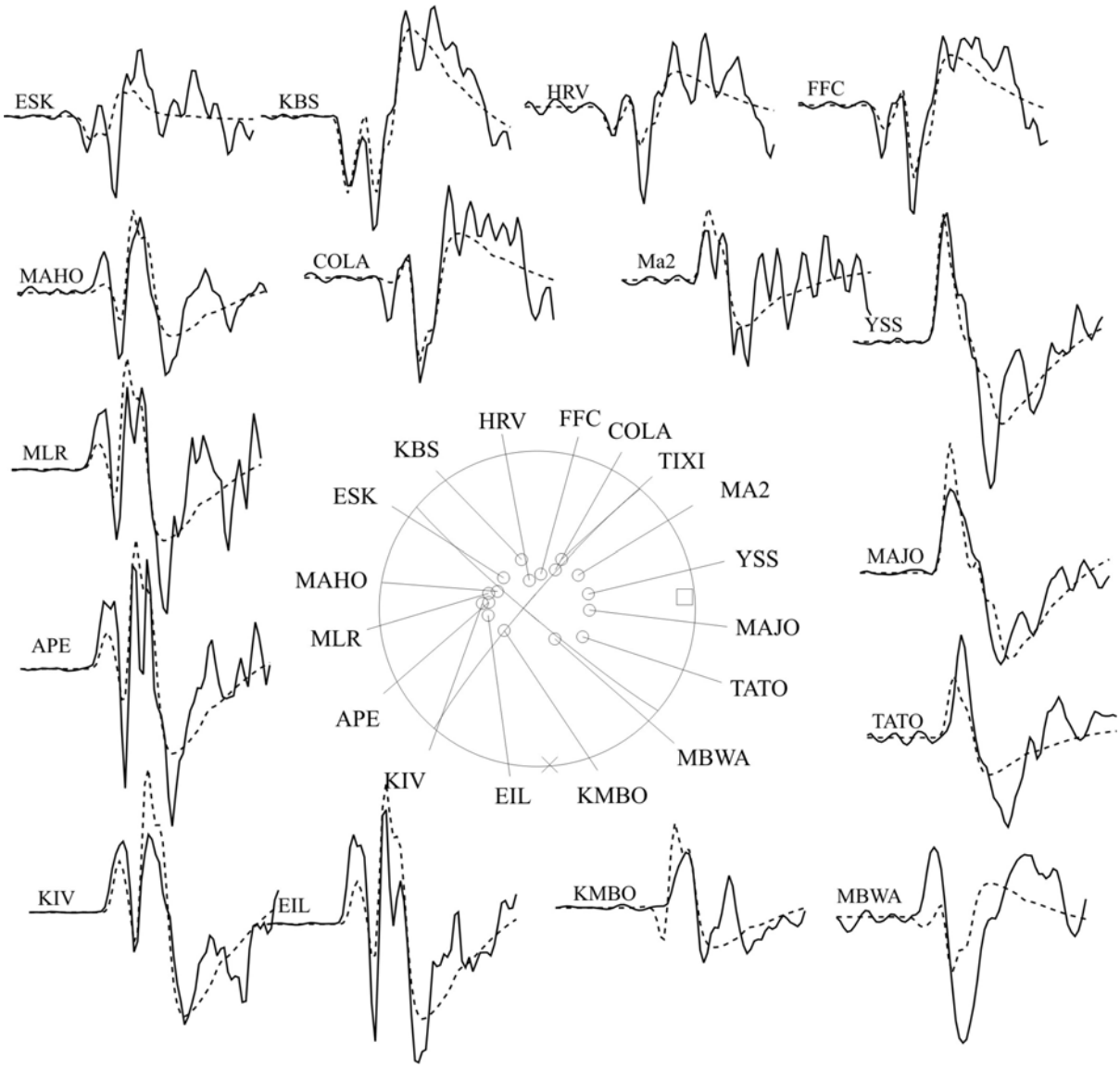

Figure V.25. Teleseismic P waveform modelling result of the 01st October aftershock. The fitting between observed (solid line) and synthetic (dashed lines).

The inversion shows that event was caused by an oblique right lateral strike slip faulting with 130°N strike, almost vertical 85° dip. Epicentral depth is 9 km. Result of inversion shows us again an azimuthal separation in the fitting of the observed seismograms like as the main shock study.

The most noticeable aspect of this model is the large misfit to the southern and south eastern stations (HYB, MBWA, and KMBO) compared to the observed seismogram (Fig.V.25). P waves first motion polarity modelled at these stations are dilations and

incompatible with compressions on the observed seismograms. No reasonable solution can be found by the inversion procedure. So these results show us that this aftershock is a complex earthquake. We did not invert for a unidirectional propagating rupture because by observing raw signal we did not find some a clear indication of directivity.

V.4.3.2 Bilateral propagating line source

In the second model, the point source is replaced by line source that propagates bilaterally from the nucleation point with a rupture velocity of about 2.5 km/s. As starting parameters for this second inversion we used the results obtained at the end of the first inversion (Table V.9).

First we inverted seismic moment, focal mechanism and centroid depth, fixing them one by one. After several inversions the result of focal solution stabilized and this provide the first reasonable solution of this event.

Then in the following steps, we examined rupture velocities in the range 1.0-5.0 km/s, and achieved the best match between observed and synthetic waveforms with a value of 1.5 km/s and 3.0 km/s, respectively for the first and second subevents (Fig. V.26). In this inversion procedure we also observed relatively high and low velocity combination in two fault segments rupture.

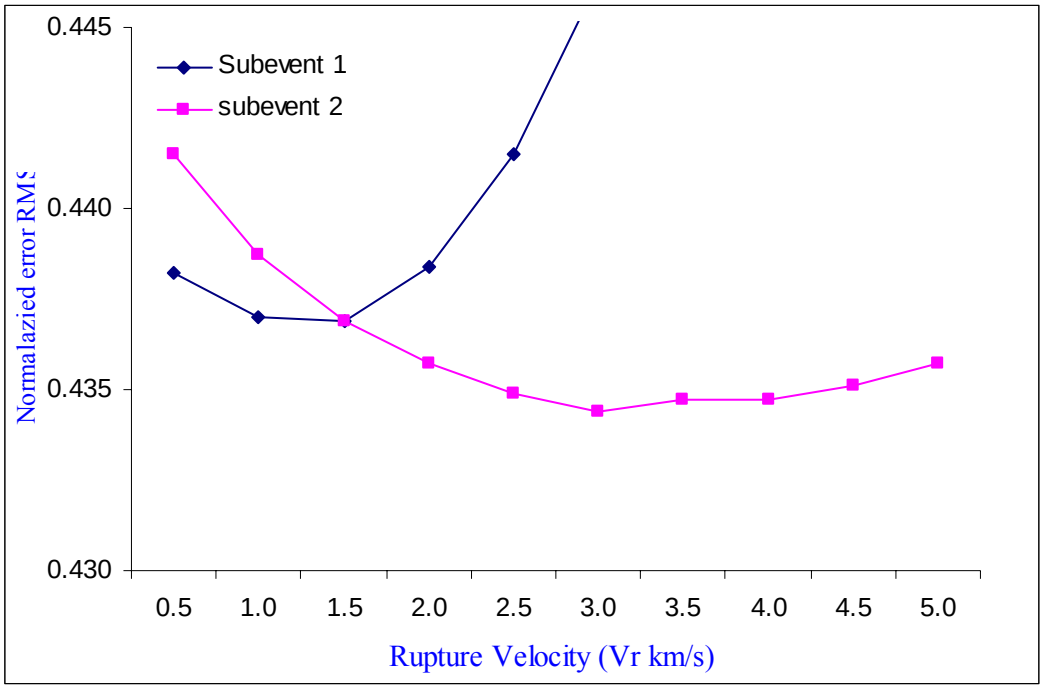

Figure V.26. Estimation of rupture velocity for the first and second subevents of the second large aftershock.

Next we examined rise times of between 0.5 and 2.0 s, assuming the source time function to consist of eight ramp functions, and found that 1.0s gave a better fit than the others. We also examined distance and azimuth between these subevents. According to smallest estimated value of RMS, the nucleation point of second subevent is located at a distance of 3.5 km and 280°N azimuth relative to the first subevent. Fig.V.27 shows determination of best nucleation distance and azimuth of second subevent.

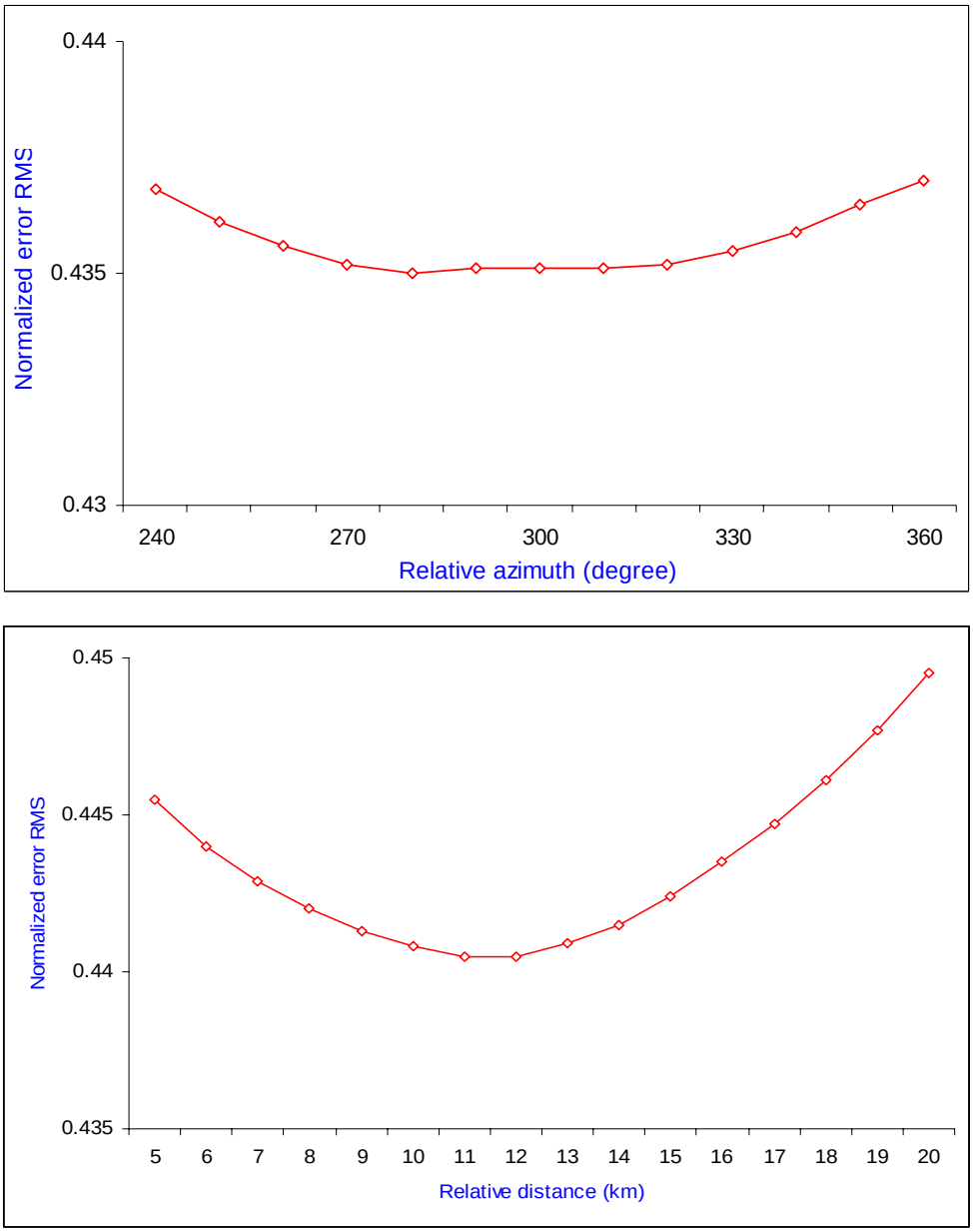

Figure V.27 Determination of the relative location of the second subevent compare to the first one.

This second model is considered to be the best fitting model. The inversion results are shown in Table V.9

Event	Strike (°)	Dip (°)	Slip (°)	Vr (km/sec)	STF (sec)	Depth (km)	Mo (Nm)
Result of the inversion for the single point source model							
Sub1	310	85	174	2.5	9	9	9.4x10**18
Parameter of the inversion for the bilateral propagating sources							
Sub1	310	85	174	2.5	9	9	9.4x10**19
Sub2	130	85	174	2.5	4	9	4.0.x10**18
Result of the inversion for the bilateral propagating source model							
Sub1	122	89	183	1.5	5	8	9.4x10**18
Sub2	147	55	142	3.0	4	8	4.0.x10**18

Table V.9 Body wave inversion result for the second large aftershock of October 1st

Fit of observed waveforms is significantly increased at all stations in different azimuth ranges. It is quantified by a significant decrease of the normalized rms error value of RMS = 4.3 x 10^{-1}. Step by step improved fit between observed and synthetic seismograms are shown in Fig. V.28

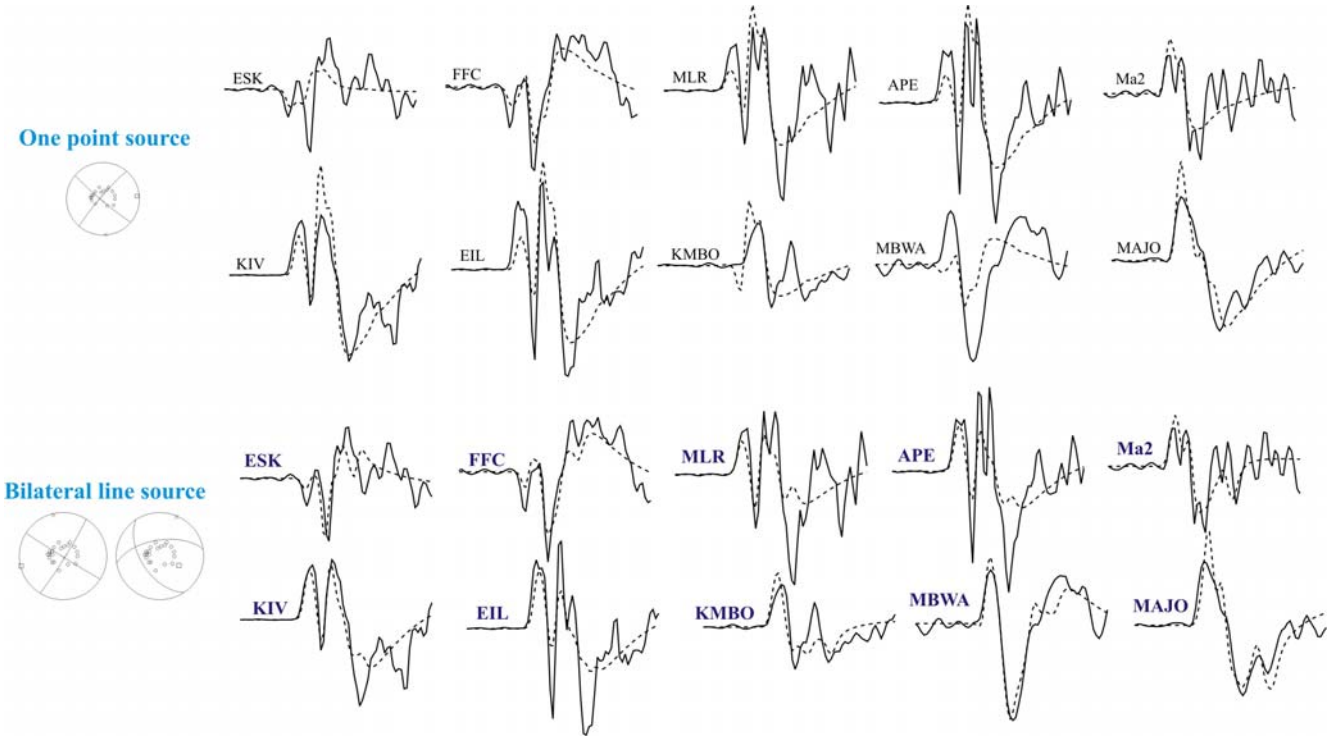

Figure V.28. Examples of improvement of the modelling using a bilateral line source description of the event.

The final modelling of 01st October large aftershock records show that again this event can be explained with a combination of two subevents. The observed and best-fit theoretical seismograms for the second large aftershock are shown in Fig.V.29.

The first subevent is modelled as a right lateral strike slip faulting striking 122°N and dipping 89°. The second subevent is a line source located 3.5 km north-west of the nucleation point of the first subevent in a 280° azimuth. The deduced source mechanism is a 55° dipping inverse fault with a strike of 147°N. Time delays between the two events are estimated of 2 seconds. Associated seismic moment to the first subevent is two times larger than the one of the second subevent and respectively 9.4×10^{18} Nm and 4.0×10^{18} Nm.

The first rupture episode propagated to the north westward direction during 5s and two seconds after the second shock occurred and rupture developed to the SE direction during 4s. As before, we assume that the rupture length in each subevent is roughly the time function duration multiplied by the rupture velocity of 1.5 km/s and 3.0 km/s respectively for the first and the second subevent. The first subevent can then account for a ~8 km long rupture propagated to the NW. The second subevent can account for a ~12 km of faulting along the near southern margin of Kurai basin.

Total scalar seismic moment is Mo = 1.35×10^{19} Nm. Estimated source duration is about 9s and total length of rupture is 20 km.

Average slip and stress drop derived from equation (V.11) and (V.12), using total seismic moment and size of fault area is *D = 280 cm* and *4.3 MPa*. Then we obtained Mw=7 magnitude by Kanamori relation (V.10) (Kanamori, 1977) comparable to the magnitude reported by USGS (Ms=7.0).

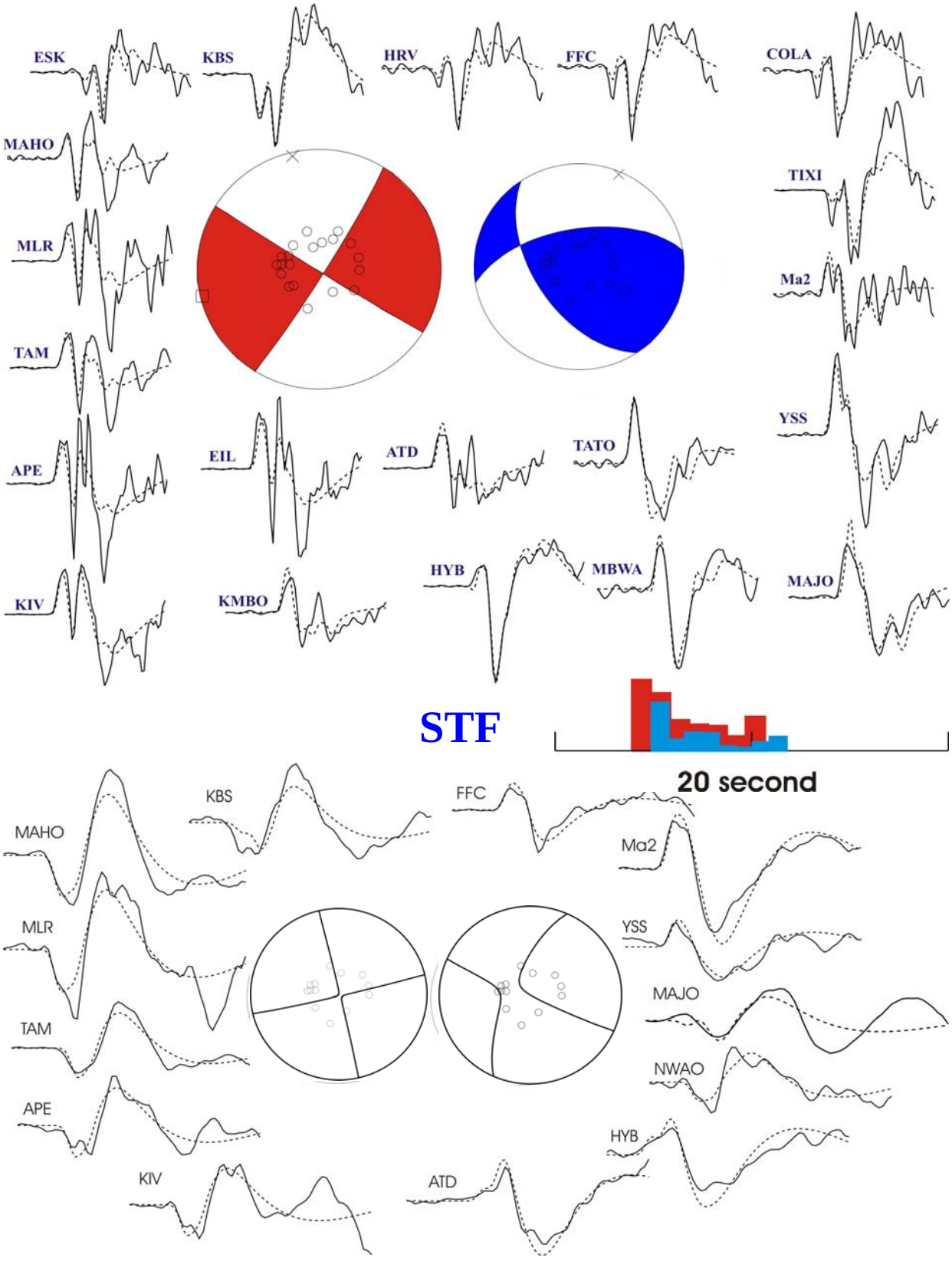

Figure V.29. The observed (solid line) and the best-fitted synthetic (dashed line) P and SH seismograms for the model bilateral propagating line source. This model has been choose to be the best model on the fitting of observed and synthetic P wave forms criteria for the last

V.5 Rupture process model of Chuya earthquake

The previous results show that all three events were complex with several subevents: as some slight changes in fault plane solutions are observed among these subevents, we can suspect that the complexity in the rupture is induced by the changes in the fault direction. Fig.V.30 shows model of the rupture process of Chuya earthquake.

The main shock of the Chuya earthquake started first with right lateral oblique strike slip faulting that propagated to the NW 311°. The rupture propagated during 9 seconds with 2.5 km/s rupture velocity and extended up to ~22 km. One second after the first subevent (sub1), occurred a second shock 0.6 km away in 40° N direction. Soon after (1.5s after the sub1 event) occurred a third subevent 12 km away in 106°N direction, east from first subevent. Second sub event produced reverse faulting with strike slip component and third event was caused by oblique strike slip faulting striking 134° to the SE. Coseismic faulting length estimated to be 11 km and 19 km respectively. Reverse fault occurred with a slow rupture velocity of 1.5 km/s propagated during 7.5 second. Third subevent propagated during 7.5s with a rupture velocity of 2.5 km/s. The first subevent released highest seismic moment of 3.9×10^{19} Nm.

Seven hour after the main shock occurred to the NW a large aftershock of magnitude Ms = 6.6. This aftershock is modelled as a combination of two subevents; the largest second subevent occurred out of general fault traces. The event started with small reverse faulting striking 66° to the NE with a fault length of 3 km. Like during the main shock, this reverse fault exhibits a slow rupture velocity that was propagating during 2s. One second after the first subevent, a second subevent occurred 6 km away to the SW from general fault traces of Chuya earthquake. Rupture of this second subevent extent on a 9 km length and exhibits very high rupture velocity of 4.5 km/s. For this aftershock a clear directivity of P wave propagation is observed in SE to NW direction compatible with the high rupture velocity. This evidence of directivity gives us a chance easily to define the rupture process. The azimuth of the strike slip faults are slightly changing from $\sim 311^0$ N to $\sim 305^0$ N.

The second large aftershock, with magnitude Ms = 7.0, occurred four day after the main shock. This aftershock nucleated northwest of the first aftershock initiation. It is modelled as a combination of two subevents that propagates bilaterally. Estimation of the rupture duration is 5s and 4s respectively for the two subevents. The rupture velocity determined is respectively 1.5 km/s and 3.0 km/s. The first subevent is produced by pure strike-slip motion along 8 km fault striking 300°N. The second subevent caused by reverse faulting with horizontal displacement, extents at the northern part of the main shock rupture. A slight change in the rupture direction was observed also during this large aftershock process.

Finally, we would like to point out once again that Chuya earthquake was caused by right lateral strike slip faulting with combination of small reverse faulting. Total length of the surface ruptures extents around 70 km with the strike SE-NW (310°N). Considering the global sequence as a whole event, the focal mechanisms and rupture characteristics of the different subevents exhibit a complex behaviour: variation of fault plane strikes, variation of mechanism type, but also a great variability of the delay between subevents (from seconds to days) and on rupture velocities. This can be related to the presence of heterogeneity on the fault on which the rupture occurred, which pass from the border of the Kurai basin to the border of the Chuya basin, through the Chuya range.

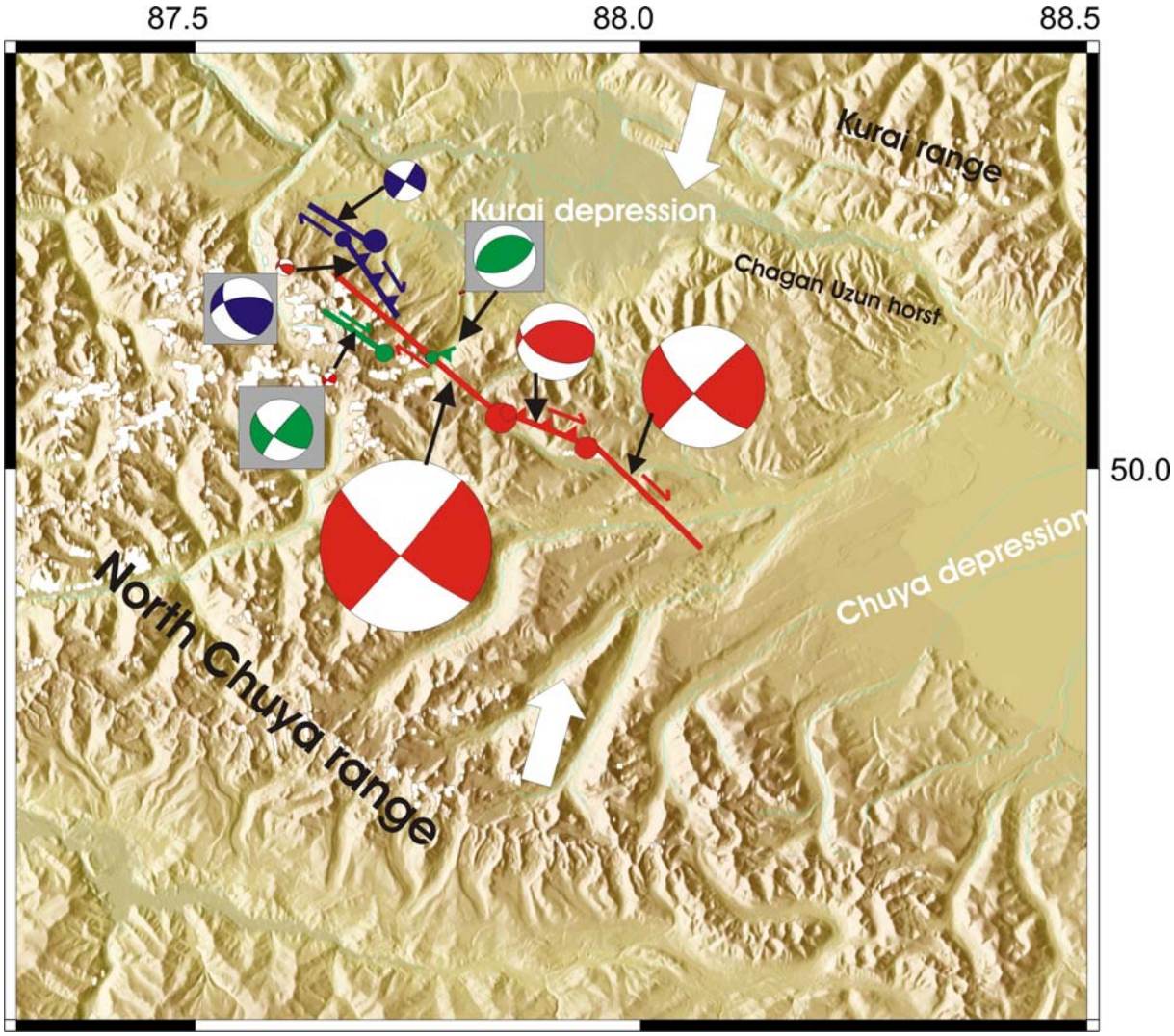

Figure V.30. Proposed model for the fault rupture during the Chuya 2003 sequence. Sizes of the focal solutions are proportional to the seismic moment (focal solutions of 3 small moment sources are enlarged in grey boxes). Each subevent hypocenter is represented by a small points and a line striking in the direction of the determined rupture propagation. Red colors are for main shock, green one for first aftershock on 27th September and blue one for second aftershock on 01st October.

V.6 Discussion and conclusion

The rupture process of Chuya earthquake and its two large aftershocks were investigated using teleseismic P and SH waveform-matching technique. Broad band and long period seismograms were employed to deduce the source time function of these events and their focal mechanisms. The investigated shallow depth events are characterized by a complex pattern of multiple shocks as function of spatial position and distribution of moment release with time.

The main shock of Chuya earthquake is modelled as a combination of three subevents. The best constrained parameters of the models are shown in the Table V.14. The general strike ~ 130°N and total length of rupture of 52.5 km determined is significantly smaller than

the aftershock distribution length (90 km), more similar to observed surface rupture in the field (~60 km). The Chuya earthquake is modelled as oblique right lateral strike slip faulting with vertical dipping fault plane which is also well correlated with observed surface rupture by field investigation.

The estimated seismic moment and calculated Mw magnitude are in good agreement with other information using the empirical relations for large strike-slip events. Our estimated magnitude value of Mw = 7.2 well fit with magnitude (Ms = 7.3) estimated by USGS. The stress drop of *6.0 MPa* of the Chuya earthquake is consistent when compared with the average stress drops commonly found for large events.

We have estimated a much shallower centroid depth (8 km) than reported in the IDC (CTBTO) bulletin. But this shallow depth is confirmed by location result of Novosibirsk Centre. They obtained using local seismic network a similar depth of ~8 km. This shallow depth is also confirmed by Harvard CMT centroid solution. The value of 2.4 m for average slip displacement is little smaller than what could be expected for this kind of large events. Observed displacement at the surface is even smaller than this value which can be explained by the presence of a soft soil layer in the basins. Our estimated average slip displacement is in excellent agreement with obtained by SPOT image correlation method.

It was mentioned earlier that the results obtained by our inversion for the Chuya earthquake leads to a geologically acceptable solution. The strike slip motion took place on the almost vertical fault planes. The strike of this plane can change along the global fault. The reverse faulting on the central part of the ruptured area is compatible with the same regional stresses.

All that evidences are showing that the match between field evidence on coseismic rupture of main shock and the corresponding parameters deduced from teleseismic body waves are remarkable and is well correlates with geodynamic condition of the region.

The two large aftershocks of Chuya earthquake are modelled as complex earthquakes with combination of two subevents. First aftershock nucleated relatively deeper than other two large events but this depth is well correlated with depth estimation have done by depth phase pP. The HRV moment tensor solution shows not significantly deeper value of 15 km. The second large aftershock nucleated at a similar depth value of 8 km than the main shock, again shallower than depth estimation of HRV (14 km) and IDC (10 km).

The extent of aftershock activity is about 90 km. As the rupture of the first large aftershock extents parallel to the main shock rupture we consider that only the second large aftershock can participate to the extension of the global rupture; we propose a total length of ruptured fault of around ~ 73 km. The difference between this length and the aftershock distribution is clearly related to the occurrence of a high aftershock activity at the south eastern edge of the distribution which seems to be neither related to surface breaks, or to part of fault which could have been ruptured during the main shock if source duration and rupture velocity are correct for the southern subevent. This is a still pending question on this study.

The seismic moment released during the second aftershock was larger than the seismic moment released during the first one. The corresponding moment magnitudes are respectively Mw = 7.0 and Mw = 6.4. These magnitude estimations are similar to the results given by Harvard. For the first large aftershock we estimated an average slip displacement of 0.7 m and average stress drop of 4.0 MPa. The second large aftershock produced an average displacement of 1.2 m with an average stress drop of 4.3 MPa. This result is also shows that stress drop is not much depending from earthquake size a relatively low in this sequence.

Event	Strike (°)	Dip (°)	Depth (km)	Vr (km/s)	STF (sec)	Length (km)	Slip (m)	Mo (Nm)
Mainshock (27/09/2003; 11h; Ms = 7.3)								
Sub1	131	80	8	-2.5	9	~22.5		3.9 x 10**19
Sub2	111	49	12	1.5	7.5	~11		1.8 x 10**19
Sub3	134	74	12	2.5	7.0	~19		2.8 x 10**19
Total					**24**	**~52.5**	**2.7**	**8.5 x 10**19**
First large aftershock (27/09/2003; 18h; Ms = 6.6)								
Sub1	66	54	11	1.5	2	~3		1.3 x 10**18
Sub2	125	65	14	4.5	2	~9		3.3 x 10**18
Total					**4**	**~12**	**0.6**	**4.6 x 10**18**
Second large aftershock (01/10/2003; 01h; Ms=7.0)								
Sub1	122	89	8	1.5	5	~8		9.4 x 10**18
Sub2	147	55	8	3.0	4	~12		4.0 x 10**18
Total					**9**	**~20**	**2.8**	**3.4 x 10**19**

Table V.10 Summary of source parameters of Chuya earthquake and the two large aftershocks studied.

The estimation of rupture velocity was one noticeable result of this inversion. In this sequence is observed low and high velocity combination for each large earthquake. In all those event reverse faulting is associated with low velocity rupturing. A high velocity has been observed on the southern most segmental during the main shock rupture.

Finally, these studies give us the opportunity to constrain ongoing tectonic process of the Chuya and Kurai region where is very important to understand transpressional zone expecting counterclockwise rotation.

General conclusion and perspectives

Mongolia is a continental region well known to have suffered largest intraplate crustal events. During last century occurred there four large earthquakes with magnitude larger than 8 and several tens of earthquake with magnitude $M \geq 7$.

The instrumental seismic study of Mongolia started in 1957 only after the Gobi-Altay large earthquake (M = 8.2) which occurred the 4th December 1957. Two seismic stations were installed at that time. Actually we have installed more than 20 seismic stations and, if we include two mini arrays stations, the seismic network of Mongolia contains more than 40 stations. This development of seismic instrumentations in Mongolia was supported by several developed countries like France, USA, Japan and Russia.

We analyzed the seismic catalogue covering the period from 1964 to 2002 with about 50 000 events. Recently we have published a map "One century seismicity of Mongolia" which included this data set and an early instrumental data set. From the seismicity map we can observe that the earthquakes of Mongolia are not evenly distributed over the region but are rather well correlated with the major active structures. Other specific character of seismicity in Mongolia is the anomalous frequent occurrence of very large earthquakes ($M \geq 8$) during the last century. Our seismicity analysis shows that the most seismic active regions on the territory are Khubsugul and Altay region with respectively 20% and 30% of the events of the whole catalog.

Little is known about the aftershock activity duration after very large intra-continental events. So an other interesting questions was to determined if seismic activity of Mongolia is due to aftershock swarms after the large earthquakes or is related to a more tectonic activity of the region. By using a method of clustering events, we identified 629 clusters that include a total of 9040 clustered events. So it concerns approximately 20 % of the events of our database. But this level is quite different for each region: it can be very high in region like Huvsugul where 60% of the seismic activity is clustered in aftershock activity or quite low in region like Ureg-Nur where aftershock activity concerne only about 5% of the general regional activity.

Our test of Gutenberg - Richter relation shows that seismic activity of Mongolia is fairly high. We have estimated $a = 6.2$ and $b = 0.8$. B value is relatively small compare to the worldwide mean value. These results are related to frequent occurrence of large events which can be interpreted as the possibility of large stress accumulation on the main faults on which large events occurred.

Altay is one of the most seismically active regions in Mongolia. Altay range was struck by several large earthquakes during last century. The most recent event was the Chuya 27th September 2003, Ms = 7.3 event. This work on Chuya event was the first

pluridisciplinary detailed study on a large event in this broad region where large intracontinental events have occurred (Bulnai, Fu-yun, Gobi-Altay).

Several informations were already available on the Altay range deformation, some of them quite recently. Detailed kinematic studies of faults systems of the Altay range based on field observations and on earthquakes slip motion indicates that right-lateral strike-slip faults oriented NW-SE are ending to the northwest on thrust faults oriented then E-W to N100° (Schlupp 1996, Bayasgalan *et al*., 1999) which can be explained by a global counterclockwise rotation of Altay. Paleomagnetic study (Thomas *et al.,* 2002) on Tertiary rocks from southeastern Kazakstan (Zaisan basin) and the northwestern Altay (Chuya depression) has shown such a rotation relative to stable Asia of the Chuya depression (a Tertiary counterclockwise rotation of 39° ± 8°) when no significant latitudinal displacement or rotation in Zaisan basin (Thomas *et al*., 2002) have been detected. Finally, recent GPS measurements of crustal velocities in Northern Asia (Baikal rift zone and Mongolia) show a N-S shortening in westernmost Mongolia (Calais *et al*., 2003). Concerning the Altay deformation, interpretation of GPS survey gives NNE velocities relative to a stable Siberian block, with rates decreasing from south to north: from 10 mm/yr at Urumqi, south of the Altay, to ~ 4 mm/yr in Altay. Bayasgalan *et al*. (2005) used source parameters of earthquakes to constrain slip vector azimuths in Altay and found a mostly NNW direction. They proposed that the discrepancy between slip vectors and GPS vectors also suggest a counterclockwise rotation of Altay range.

From a first observation of fault description and seismicity, it is clear that the Altay range cannot be considered as an undeformed block, but is consisting of several micro blocks separated by active continuous fault zones. The tectonic activity of the Altay range is illustrated by the high seismic activity with four large earthquakes of magnitude between 7 and 8 (Fun-Yun, 1931 M = 8.1; Ureg 1970, M = 7.0) and several moderate size earthquakes with magnitude larger than M = 5.

We worked on Landsat ETM+ images and, for some parts of the region, SPOT images to characterize major active fault zones in these intra blocks. The satellite image analysis shows us that it is possible to define four major fault zones cutting the block; each of them consisting of several segments, two of them defined the NE and SW border of the range; the two others are intra-block faults. On these faults, right-lateral motion can be observed, compatible with most of earthquake focal solutions. We observed also sometime finite horizontal displacements quantified using drainage or streams offsets. From NE to SW we found:

The Khovd fault zone is the most active. Three recent surface ruptures are known on this fault (Chihtei, Ar-Hotol, Bidj) and we measure a cumulative right-lateral strike-slip between 3.5 and 4.8 km.

The Tolbo fault zone shows cumulative offsets between 1.3 – 1.5 km.

Sagsai fault system is difficult to map precisely even if a continuity of segments can be proposed. We were not able to detect clear cumulative displacement which could have been very small.

Fu-Yun fault zone, which marks a sharp boundary between the Junggar and Altay blocks and on which we measured a right-lateral cumulative offsets between 1.5 km and 2.5 km.

Because river stream dating is missing in the region, we used our observed cumulative rivers displacement and rate of deformation obtained by previous published work, to only confirms a beginning of the deformation in Altay during Pliocene - Quaternary. Indeed, we deduced a beginning of the deformation one to four millions years ago. We will propose two hypotheses related to these difference of cumulative offset induced by the regional stress along on the different faults: either the rate of motion on each fault is constant but the rivers have different ages, either the Khovd fault is two times more rapid that the others showing then a partitioning of the deformation over the Altay block.

If we follow the partitioning proposition, it seems that horizontal movements along the major faults are more intense at the border, on Khovd and Fu Yun structures, than in the middle part of Altay block, on Tolbo and Sagsai structures. This partitioning also can be explained by the backward rotation of Altay range. If we believe that the Altay range is rotating in a counterclockwise direction with a rotation pole inside the block, it should be more intense movement on the extremity of Altay range relatively to its center.

A last point is that our observations of offsets are not confirmed up to now by the recent GPS measurements. Indeed, GPS shows a similar N-S shortening compared to Siberai plateform with the same velocity for the 2 Altay points (ULGI and HOVD), ~ 4 mm/year, despite they are separated by the Khovd fault zone (Calais *et al*., 2003). So it seems, from the GPS, that there were no motions across this fault during the period of GPS measurements. The contradiction between the morphology and seismic activity and the GPS should be interpreted. We think that the deformation expressed on images, which cover a longer period, is more reliable to explain Altay tectonics.

It is thus difficult to give a definite proposition on the Altay deformation, without more focussed studies: we could propose 2 main directions for this purpose:

- Detailed continue GPS measurements during an at least 5 years period across the main observed faults. RCAG maintain already a permanent GPS stations in Hovd city located on the extreme northeastern block of the system. At least 2 more instruments should be installed on the middle and west site of Altay range to obtain the present deformation rates across the faults and confirm a possible variation from central part to borders.
- An effort on dating is necessary for a better use of river stream offsets observations. This will allow quantifying the cumulative deformation on a broader period but this can only be done in collaboration with foreigner's collaborations. Such dating should be supported by detailed geological mapping and trenching at selected points across fault zones. Paleomagnetic studies can be continued inside RCAG as we have one section who is working on this topic.

The seismological analysis of Chuya aftershocks and main shock sequence gave us the opportunity to focus on the northwestern part of the Altay range where it occurred. Our main study concerns the rupture mechanism description and its relation with the geologically complex area of Kurai and Chuya basins.

The tectonic of Chuya and Kurai is complex. The tectonic and fault geometries indicate that neotectonic activity in the Chuya-Kurai zone is controlled by NS compression expressed in active faulting and block tilting. The northern margin of these two depressions (Chuya and Kurai) is the most active zone in the region where are expressed clear strike-slip and thrusting or high angle reverse faults. Compared to this active zone, the southern margin of the depressions shows less active structures.

Nevertheless the Chuya earthquake occurred at the southern margin of Chuya and Kurai depression and was associated on its main part with right-lateral strike slip ruptures observed along 60 km of surface breaks (Geodakov *et al*., (2003). Observed slip on this surface rupture is about 1.5 m. The southeastern part of the surface rupture is clearly visible on the field and is described in details but the northwestern part of the rupture is poorly described.

We have done also SPOT image correlation study in the southeastern part of Chuya and Kurai region. The SPOT image correlation has been processed at DASE (France), in the frame of collaboration between DASE and RCAG, by Remi Michel and Renaud Binet. Only two third (about 40 km) of the surface ruptures at the south east part was possible to image. The result of subpixel correlation of SPOT image shows us a clear feature with linear segments which correlates well with surface breaks in the southern part of Chuya basin. The observation of a clear change in strike to the South is also consistent with the field observations. We obtained an average horizontal displacement on profiles across this line in the southern part of rupture 2.8 – 3.5 m. This measure is twice as large as the displacement reported from the surface breaks. This can be explained either by the fact that it is always difficult on the field to take into account all possible ruptures in such context where “en echelon” features are present, or by the possibility that the thick layer of quaternary deposits at surface have absorbed a part of the displacement.

Some parts of reverse component associated with the source history of the 2003 earthquakes in the northern part of the ruptured zone could easily be explained by the complexity of the geological structures.

After the mainshock of Chuya earthquake, two large aftershocks occurred respectively 7 hours (Ms=6.6) and 4 days after (Ms=7.0). Locations by different data centers of these two aftershocks are largely dispersed. We define more precise locations of these earthquakes using a double difference relative relocation procedure applied to regional arrival time data. Our result shows that the mainshock of Chuya earthquake is located on the south margin of Chagan-Uzun tilted block with the Chuya range, as it was proposed by NEIC and IDC. But locations of the two large aftershocks are improved. The first aftershock was located 10 km NW from the mainshock along the strike of the fault. The second large aftershock occurred more north at 25 km from the main shock, at a place where direction of surface breaks is reported to change from NW-SE to WNW-ESE. The horizontal statistical errors on these epicenter locations are less than 1 km, but the real uncertainties could be of the order of 2 km.

After the main shocks occurred, eight portable stations were installed along the Mongolian border and in the Chuya basin, thanks to a Mongolian-French-Russian collaboration, to study aftershock sequence. The aftershock study shows a main activity

along the Southern margin of Chuya and Kurai depression in good agreement with the observed surface rupture as well for the general direction and for they positions. But the resolution on epicenter location does not allow us to infer any specific segmentation. In the central part of the activated area, several moderate aftershocks have occurred just after the main shock but during the period of the temporary network, the activity was less important than on the two external segments of the area. The release of stress migrated bilateraly from the main shock epicenter towards the north western and south eastern edges of the zone. The southwestern end of aftershock distribution was significantly active during our observation time with the occurrence of several moderate size earthquakes with magnitude between 4 and 5. This activity occurred mostly on the south margin of the Chuya basin. According to information on surface rupture, the fault did not reach the surface in this zone. Majority of earthquakes occurred in a depth range between 5 and 20 km. The activity in the north western and south eastern zones may be a little shallower than in the central part. It is difficult to propose a vertical fault on cross section perpendicular to the general strike of aftershock sequences even if the main activity lies below the surface breaks. On both sides aftershock activity extend more than the surface breaks. It seems that the southern part of the rupture did not reach to the surface. In this place we are observing several moderate size earthquakes.

Finally we have done teleseismic body wave inversion study to constrain source history and fault mechanism. Our results show that Chuya earthquake has a complex history. Mainshock of Chuya earthquake is modelled as a combination of the three subevents with two oblique and pure right lateral strike-slips and one reverse faulting. A total length of rupture of 52.5 km is determined considering observed velocity and source duration. We estimated Mw = 7.2 and 6.0 *MPa* of stress drop, values which are consistent when compared to the surface wave magnitude (Ms = 7.3) and to average stress drop commonly found for large events. We have estimated a much shallower centroid depth (8 km) than reported in the IDC (CTBTO) bulletin. But this shallow depth is confirmed by the location result of Novosibirsk Center.

The two large aftershocks of Chuya earthquake are modelled with a combination of two subevents including, each of them, a strike-slip and a reverse faulting. A total length of 12 km and 20 km is inferred as fault length for first and second large aftershock, respectively. The hypocentral depths are 13 km and 8 km, respectively.

One of specific point in our source inversion study is the rupture velocity of these large earthquakes. Different rupture velocities are associated to the different mechanisms. Most reverse faults are associated with super low velocity value of about 1.5 km/s and strike slip rupturing exhibits normal values. For the first large aftershock we get super high velocity with 4.5 km/s. Such high velocities have been reported for some recent large strike slip intra-continental events: the most clearly identified is the mean rupture velocity of 3.5-4.0 km/s observed during the Kunlun event (Bouchon *et al.*, 2002). We can suppose that the northern part of the surface breaks can be related to the surface rupture of the second large aftershock. The complexity of the faulting can explain the fact that observations on the field were difficult and the total displacement not able to be well observed.

We summarize our modelling results and compare them to the other results of the other part of the sudy the following figure.

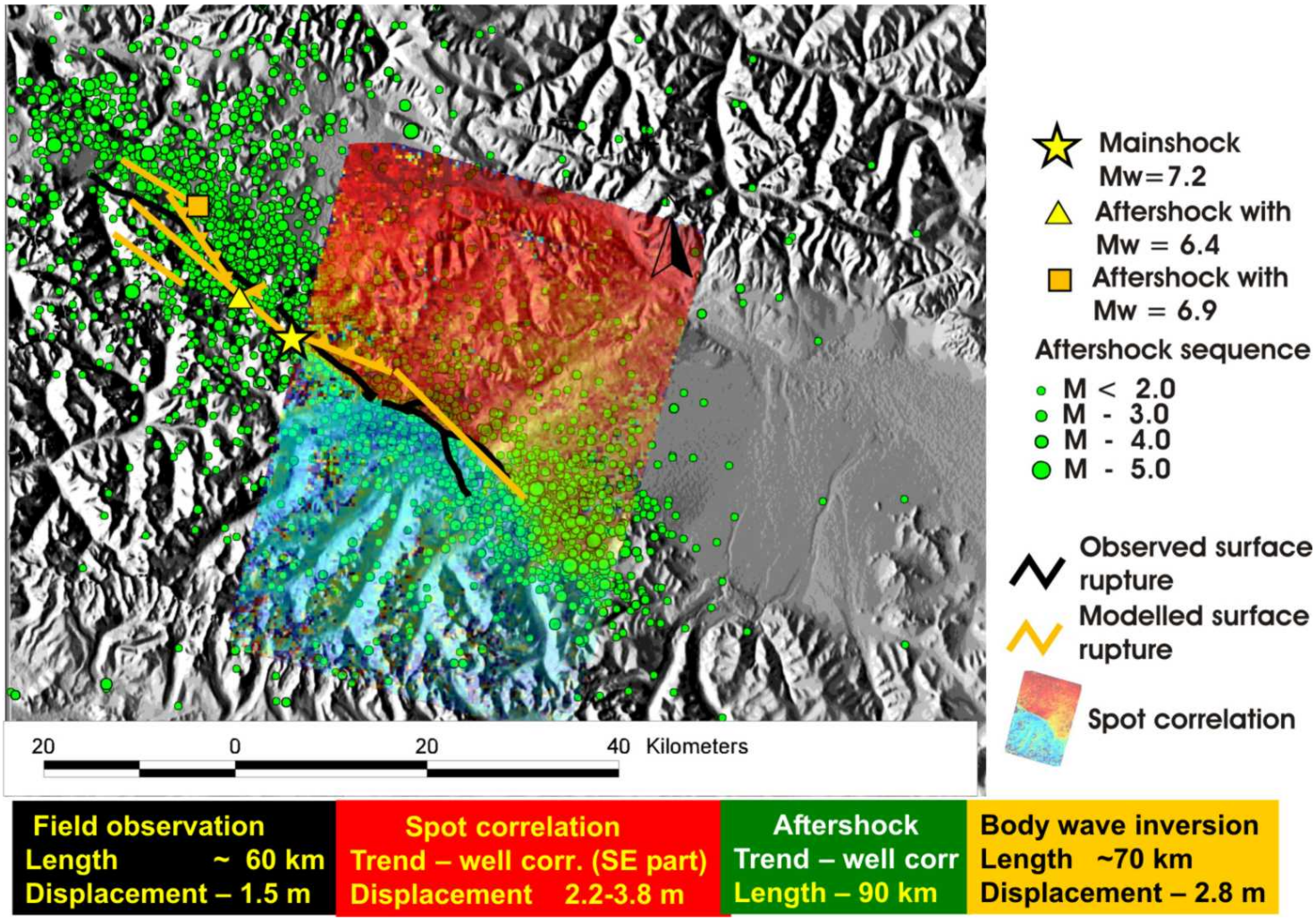

Final results of study Chuya earthquake sequences

On the field relatively small surface offsets were observed (maximum 1.5 m) if we compare with the length of fault and the estimated magnitudes (Ms = 7.3 or Mw = 7.2). If we refer to the usual scaling laws relating coseismic slip, moment magnitude and fault dimensions (Wells and Coppersmith, 1994), more than 3 m of average coseismic slip would be consistent with fault rupture of 70 km length and moment magnitudes of order of Mw 7.2. The aftershocks are spread over 90 km suggesting a possible longer rupture than 60 km. Our estimated displacement deduced from SPOT correlation (horizontal displacement), and consistent with our body wave inversion, show larger displacement with an average value of about 2.8 to 3.8 m.

How can we explain that the horizontal slip deduced from SPOT correlation and source inversion are larger than the field measurements?

The expected surface offset is proportional to the length of the activated fault. For intracontinental earthquakes, the proportionality factor is typically $\alpha = 5x10^{-5}$ (Scholz *et al*., 1986). This ratio is related to the static stress drop on the fault, and it is equivalent to say that stress drops are typically between 1 and 10 MPa (Berberian *et al*., 2001). However, the value of α for the Chuya earthquake is 2.5×10^{-5}, thus 2 times smaller than global average pattern. The difference is nevertheless too small to argue that Chuya surface rupture has particular mechanical properties. Another explanation is that rupture in the Chuya earthquake occurred deeply and that only a part of the displacement reached the surface. But this explanation is not consistent with the centroid depth obtained by source inversion and by calculation of local networks which give a depth value of 8 km. But why the SPOT correlation, which is a surface measurement as field observations, gives also large offsets?

We can consider that each local observation on the field were accurate. But it is possible that the offsets reported were for a specific segment and did not took into account all offsets of parallel segments of ruptures. This problem is very often when the surface ruptures are expressed as pure strike-slip and consist of several en-echelon rupture systems. The other possibility is that there is a part of deformation which was spread at the surface near the fault without any clear break and thus impossible to observe from the field without previous detailed measurements as a local dense GPS network. This would explain the higher value obtained with SPOT correlation, consistent with the body waveform inversion and would not bring into question the field observations. Also we note that, in the report of the field survey, the surface ruptures of the northern part are poorly described probably related to difficulties to access the area.

This study confirms that the SPOT correlation method is a tools that give us a detailed mapping of the fault rupture geometry as well as surface horizontal offsets. These results are important because the area was difficult to access and we could not observe clearly the fault trace on the original SPOT images, despite a ground resolution of 5 m. We did not have the possibility to complete these images with InSar differential observations which should have brought a complementary observation. Despite the field measurements are generally accurate, they are ponctual measurements and do not show always all the deformation due to an earthquake. More global images are also very important.

The different approaches (relocation, aftershocks, main shock modelling, large scale displacement analysis by SPOT image) that we used provide a relatively good and coherent image of the Chuya sequence.

But there are still some questions in our study and we think that we will have the possibility to address some of them in the near future:

1. Aftershock distribution: we have still some possibility to increase our dataset and get a better azimuthal coverage of stations for the Chuya aftershock locations thanks to potential future cooperation with the Novosibirsk seismological centre. That may increase our resolution of aftershock distribution and could allow us to better individualize some segments in the activity.
2. It will be interesting to see what the focal solutions are for some of the main aftershocks. This can be done with classical polarity analysis within the collaboration with the Novosibirsk team, but also for 3 or 4 main aftershocks by a local waveform modelling of the broad band 3 components records. That work would improve the description of the complexity of the sequence.
3. In our study we did not include deep structure of Altay region. But it will be our next intense study of the region. As we explained, the seismic network of Mongolia is still increasing. Actually are working 2 VBB station in Altay region and it is planned to add 3 BB stations in the next years. Despite a thick crust generally is assumed in the region, it seems that the aftershocks did not occurred deeper than in places where the thickness is more standard. The understanding of crustal structure should help to understand how the lower crust breaks.

The already mentionned possible developpements of this work are focused more on the studied region. But each large event should be also the opportunity to understand the tectonics and seismic activity in Mongolia. In countries like Mongolia which is a developing country, it is difficult to have immediately field survey in order to follow aftershock sequence as the necessary instrumentation is not available in the country. At the time of the Chuya earthquake, thanks of PICS project and collaboration with DASE (France), we had the possibility to install several portable stations. But in case of next large earthquake it will be more difficult because of the absence of portable stations in the country. RCAG have long-term technical and scientific cooperation with French scientists (DASE, GEOAZUR and Strasbourg Institute) and now a strong engineer team. This can give us the opportunity to plan cooperation, between French and Mongolian teams willing to work this region in case of large earthquakes. If instrumentation can be send from France, Mongolian scientists can take in charge most of the field study, administration question and instrumentation maintenance.

For a more applicated goals, such studies will increase the knowledge on seismic hazard which is necessary to the development of the cities in Mongolia.

References

[1] Adija, M., Ankhtsetseg, D., Baasanbat, Ts., Bayar, G., Bayarsaikhan, Ch., Erdenezul, D., Mungunsuren, D., Munkhsaikhan, A., Munkhuu, D., Narantsetseg, R., Odonbaatar, Ch., Selenge, L., Tsembel, B., Ulziibat, M., Urtnasan, Kh, One Century of Seismicity in Mongolia (1900 - 2000), RCAG - DASE, Ulaanbaatar, 2003.

[2] Adija, M., On the aftershocks of the Busiingol earthquake. - In: Search investigations of forerunners of earthquakes in Siberia, Nauka, Novosibirsk. (in Russian), 115-118, 1988.

[3] Aki, K., Earthquake mechanism, Tectonophysics, 13, 423-446, 1972.

[4] Aki, K., Characterization of barriers on an earthquake fault, J. Geophys. Res., 84, 6140-6148, 1979.

[5] Aki, K., and P. Richards, Quantitative seismology, 872 pp., Mir, Moscow, 1983.

[6] Allen, C.R., Geologic criteria for evaluating seismicity, Geol. Soc. Am. Bull., 86, 1041-1057, 1975.

[7] Allen, C. R., Luo, Z., Qian, H., Wen, X., Zhou, H., and Huang, W, Field study of a highly active fault zone: The Xianshuite fault of southwestern China, Geol. Soc. Am. Bull., 103, 1178-1199, 1991.

[8] Allen, M. B., and S. J. Vincent, Fault reactivation in the Junggar region, northwest China: the role of basement structures during Mesozoic- Cenozoic compression, J. Geol. Soc. London, 154, 151-155, 1997.

[9] Ankhtsetseg, D., Dugarmaa, T., D., Bayar, J., Baasanbat, Battulga, B., Bayarsaikhan, Ch., Selenge, L., The report of field investigation of the Chuya earthquake, RCAG, MAS Mongolia, Ulaanbaatar, 2003.

[10] Avouac, J. P., P. Tapponnier, M. Bai, H. You, and G. Wang, Active thrusting and folding along the northern Tien Shan and Late Cenozoic rotation of the Tarim relative to Dzungaria and Kazakhstan, J. Geophys. Res., 98, 6755-6804, 1993.

[11] Baljinnyam, I., A. Bayasgalan, B.A. Borisov, A.A. Cisternas, M.G. Dem'yanovich, L. Ganbaatar, V.M. Kochetkov, R.A. Kurushin, P. Molnar, P. Herve, and Y.Y. Vashilov, Ruptures of major earthquakes and active deformation in Mongolia and its surroundings, 181 pp., Geol. Soc. Am., 1993.

[12] Baljinyam, I., D. Munkhuu, and B. Tsembel, Seismicity of the Mongolia, Publication of MAS Mongolia, 105, 1975.

[13] Bayarsaihan, C., Bayasgalan, A., Enkhtuvshin, B., Hudnut, K., Kurushin, R. A., Molnar, P., Ulziibat, M., 1957 Gobi Altay, Mongolian earthquakes as a prototype for southern California's most devastating earthquake, Geology, USA, 1996.

[14] Bayasgalan, A., J. Jackson, J.F. Ritz, and S. Carretier, 'Forebergs', flowers structures, and the development of large intra-continental strike-slip fault: The Gurvan Bogd fault system in Mongolia, J. Struct. Geol., 21, 1285-1302, 1999.

[15] Bayasgalan, A., and J. Jackson, A re-assessment of the faulting in the 1967 Mogod earthquakes in Mongolia, Geophys. J. Int., 138, 784-800, 1999.

[16] Bayasgalan, A., Active tectonics of Mongolia, Univ. of Cambridge, Cambridge, 1999.

[17] Bayasgalan, A., Jackson, J., Ritz J-F., Carretier S, Field examples of strike-slip fault terminations in Mongolia and their tectonic significance, Tectonics, 18 (3), 394-411, 1999.

[18] Bayasgalan, A., Jackson, J and McKenzie, D, Lithosphere rheology and active tectonics in Mongolia: relations between earthquake source parameters, gravity and GPS measurements, Geophys. J. Int., 163, 1151-1179, 2005.

[19] Ben Mehahem, A., Radiation of seismic surface waves from finite moving source, Bull. Seism. Soc. Am., 51, 401-435, 1961.

[20] Berberian, M., Jackson, J. A., Fielding, E., Parsons, B. E., Priestley, K., Qorashi, M., Talebian, M., Walker, R., Wright, T. J., Baker, C., The 1998 March 14 Fandoqa earthquake (Mw 6.6) in Kerman province, southeast Iran: re-rupture of the 1981 Sirch earthquake fault, triggering of slip on adjacent thrusts and the active tectonics of the Gowk fault zone, Geophys. J. Int., 146, 371–398, 2001.

[21] Bijwaard, H., Spakman, W., Engdahl, E.R, Closing the gap between regional and global travel time tomography, J. Geophys. Res., 13, 30055-30078, 1998.

[22] Bogachin, B.M., Tectonic history of Gorny Altai in the Cenozoic, Nauka, Moscow, 1981.

[23] Bouchon, M., Toksoz, N., Karabulut, H., M-R. Bouin, Dietrich, M., Aktor, M., Edie, M., Seismic imaging of the Izmit rupture inferred from near fault recordings, Geophys. Res. Lett., 27, 3013-3016, 2000.

[24] Bouchon, M., Toksoz, N., Karabulut, H., M-R. Bouin, Dietrich, M., Aktor, M., Edie, M., Space and time evolution of rupture and faulting during 1999 the Izmit (Turkey) earthquake, Bull. Seism. Soc. Am., 92, 256-266, 2002.

[25] Bouchon, M., Vallée, M., Observation of long supershear rupture during the magnitude 8.1 Kunlunshan earthquake, Science, 301, 824-826, 2003.

[26] Brace, W.F., and J.D. Byerlee, Stick-slip as a mechanics for earthquakes, Science, 153, 990-992, 1966.

[27] Braitenberg, C., Non-random spectral components in the seismicity of NE Italy, Earth. Plant. Sci. Lett., 179, 379-390, 2000.

[28] Brune, J.N., Tectonic stress and the spectra of seismic shear waves from earthquakes, J. Geophys. Res., 75, 4997-5009, 1970.

[29] Bucknam, R.C., Anderson, R. E., Estimation of fault-scarp ages from a scarp-height-slope-angle relationship, Geology, 7, 11-14, 1979.

[30] Bump, H.A., and A.F. Sheehan, Crustal thickness variations across the northern Tien Shan from teleseismic receiver functions, Geophys. Res. Lett., 25, 1055-1058, 1998.

[31] Burdick, L. J., and G.R. Mellman, Inversion of the body waves from the Borrego Mountain earthquake to the source mechanism, Bull. Seism. Soc. Am., 66, 1485-1499, 1976.

[32] Burdick, L.J., and C.A. Langston, Modeling crustal structure through the use of converted phases in teleseismic body waveforms, Bull. Seism. Soc. Am., 67, 677-692, 1977.

[33] Butler, R., G. S. Stewart, and H. Kanamori, The July 27, 1976 Tangshan, China earthquake: a complex sequence of intraplate events, Bull. Seism. Soc. Am., 69, 207-220, 1979.

[34] Calais, E., Sh.Amarjargal, V.A.San'kov, Global Positioning System measurements of active crustal deformation in Western Mongolia, Ulaanbaatar, 2002.

[35] Calais, E., Lesne, O., Déverchère, J., Sankov, V.A., Lukhnev, A.V., Miroshnichenko, A.I. and Levi, K.G, GPS measurements of crustal deformation in the Baikal rift zone, Siberia, Geoph. Res. Lett., 25 (21), 4003-4007, 1998.

[36] Calais, E., O. Lesne, J. Déverchère, V. Sankov, A. Lukhnev, A. Miroshnitchenko, K. Levi, V. Zalutski, Y. Bashkuev, Amarjargal, B. Bekthur, Active deformation in the Baikal rift zone and Mongolia from GPS measurements, in European Union of Geosciences meeting, Strasbourg, 1999.

[37] Calais, E., and S. Amarjargal, New constraints on current deformation in Asia from continuous GPS measurements at Ulan Baatar, Mongolia, Geophys. Res. Lett., 27, 1527-1531, 2000.

[38] Calais, E., M. Vergnolle, J. Déverchère, V. Sankov, A. Lukhnev, and S. Amarjargal, Are post-seismic effects of the M=8.4 Bolnay earthquake (July 12, 1905) still influencing GPS velocities in the Mongolia-Baikal area, Geophys. J. Int., 148, 1-12, 2002.

[39] Calais, E., Vergnolle, M., San'kov, V., Lukhnev, A., Miroshnitchenko, A., Amarjargal, Sh., Déverchère, J., GPS measurements of crustal deformation in the Baikal-Mongolia area (1994-2002): implications on current kinematics of Asia, J. Geophys. Res., 108 (10), 2003.

[40] Carretier, S., J.-F. Ritz, J. Jackson, and A. Baysagalan, Morphological dating of cumulative reverse fault scarp, examples from the Gurvan bulag fault system, Mongolia, Geophys. J. Int., 148, 256 - 277, 2002.

[41] Carroll, A.R., Yunhai, L., Graham, S.A., Xuchang, X., Hendrix, M.S., Jingi, C. and McKnight, C.L, Junggar basin, northwest China: trapped late Paleozoic ocean, Tectonophysics, 181, 1-14, 1990.

[42] Charles, A.L., John K. Hammer, The Vertical Component P-Wave Receiver Function, Bull. Seism. Soc. Am., 2000.

[43] Chen, W.P., and H. Kao, Seismotectonics of Asia: some recent progress, in The Tectonic Evolution of Asia, Cambridge Univ. Press, 37-62, 1996.

[44] Cunningham, D.W., B. F. Windley, D. Dorjnamjaa, G. Badamgarov, and M. Saandar, A structural transect across the Mongolian Western Altai: Active transpressional mountain building in central Asia, Tectonics, 15, 142 - 156, 1996.

[45] Cunningham, W.D., Windley, B.F., Dorjnamjaa, D., Badamgarov, J., Saandar, M, Late Cenozoic transpression in southwestern Mongolia and the Gobi Altai-Tien Shan connection, Earth. Plant. Sci. Lett., 140, 67-81, 1996.

[46] Cunningham, D.W., B. F. Windley, L. A. Owen, T. Barry, D. Dorjnamjaa and J. Badamgarav, Geometry and style of partitioned deformation within a late Cenozoic transpressional zone in the eastern Gobi Altai Mountains, Mongolia, Tectonophysics, 277, 285 - 306, 1997.

[47] Cunningham, W.D., Lithospheric controls on late Cenozoic construction of the Mongolian Altay, Tectonics, 17, 891-902, 1998.

[48] Cunningham, W.D., Cenozoic normal faulting and regional doming in the southern Hangay region, central Mongolia: implications for the origin of the Baikal rift province, Tectonophysics, 331, 389-411, 2001.

[49] Dahlen, F.A., Tromp, J., Theoretical Global Seismology, Princeton University Press, Princeton, 1998.

[50] Das, S., and B.V. Kostrov, An investigation of the complexity of the earthquake source time function using dynamic fault models, J. Geophys. Res., 93, 8035-8050, 1988.

[51] De Grave J, V.D.H.P., Denudation and cooling of the Lake Teletskoye Region in the Altai Mountains (South Siberia) as revealed by apatite fission-track thermochronology, Tectonophysics, 2001.

[52] Dehandschutter, B., Vysotsky, E., Delvaux, D., Klerkx, J., Buslov, M.M., Seleznov, V.S., De Batist, D, Structural evolution of the Teletsk graben (Russian Altai), Tectonophysics, 351 (1-2), 139-167, 2002.

[53] Delouis, B., Déverchère, J., Melnikova, V., Radziminovitch, N., Lonke, L., Larroque, C., Ritz, J.F. and San'kov, V, A reappraisal of the 1950 (Mw 6.9) Mondy earthquake, Siberia, and its relationship to the strain pattern at the south-western end of the Baikal rift zone, .TenaNova, 14, 491-500, 2002.

[54] Delouis, B., Vallée, M., Meghraoui, M., Calais, E., Maouche, S., Lammali, K., Mahsas, A., Briole, P., Benhamouda, F., Yelles, K., Slip distribution of the 2003 Boumerdes-Zemmouri earthquake, Alger,ia, from teleseismic, GPS, and coastal uplift data, Geophys. Res. Lett., 31, 1-4, 2004.

[55] Delvaux, D., Theunissen, K., Van der Meer, R., Berzin, N., Formation dynamics of the Gorno-Altaian Chuya-Kurai depression in Southern Siberia: paleostress, tectonic and climatic control, Russian Geology and Geophysics, 36(10), 26-45, 1995.

[56] Delvaux, D., Klerkx J., Matton C., Selegei V., Theunissen K., Vysotsky E., Evidences for Active Tectonics in Lake Teletskoye (Gorny Altai, South Siberia), Russian Geology and Geophysics, 36(10), 109-122, 1995.

[57] Delvaux, D., Meoys D., Stapel R., Petit C., Levi K., Miroshnichenko A., Ruzhich V., San'kov V., Paleostress reconstructions and geodynamics of the Baikal region, Central Asia, Part 2: Cenozoic Rifting, Tectonophysics, 282, 1-38, 1997.

[58] Dergunov, A.B., Structure of the zone of conjugation between Gorno-Altai and West-Sayan, 213 pp., Nauka, Moscow, 1967.

[59] Dergunov, A.B., Quaternary compression and extension structures in the eastern Altai, Geotektonika, 3 (in Russian), 99-110, 1972.

[60] Deschamps, A., Mordvinova, V., Dugarmaa, T., Déverchère, J., Perrot, J., Ulziibat, M., Artemyey, A., Urtnasan, H., Bayar, J., Bayarsaikhan, C., The MOBAL'03 experiment a seismological lithospheric transect from South Siberia to Gobi-Altai range, in EGU 1st General Assembly, Nice, 2004

[61] Déverchère, J., Houndry, F., Diament, M., Solonenko, N.V., Solonenko, A.V., Evidence for a seismogenic upper mantle and lower crust in the Baykal rift, Geophys. Res. Lett., 98, 19 895-19 912, 1991.

[62] Déverchère, J., Petit, C., Gileva, N., Radziminovitch, Melnikova, V. and San'kov, V, Depth distribution of earthquakes in the Baikal rift system and its implications for rheology of the lithosphere, Geophys. J. Int., 146, 714-730, 2001.

[63] Devyatkin, E.V., Structures and formational complexes of the Cenozoic activated stage, 182-195 pp., Nauka, Moscow, 1974.

[64] Devyatkin, E.V., Neotectonic strucutres of western Mongolia, 264-282 pp., Nauka, Moscow, 1975.

[65] Devyatkin, E.V., Cenozoic of the Inner Asia (stratigraphy, geochronology, and correlation), 196 pp., Nauka, Moscow, 1981.

[66] Devyatkin, E.V., Nikolaeva, T.V., Shuvalov, V.F., Structural-geomorphological situation and basic steps of development of basaltic magmatism in Mongolia in the Mesozoic and Cenozoic, 124-134 pp., Nauka, Novosibirsk, 1990.

[67] Devyatkin, E.V., Inner Asia, 92-100 pp., Moscow, 2000.

[68] Dobretsov, N.J., G.G. Lepezin, and O.S.Pukinskaya, Petrography of Altai-Sayan fold zone, Dok. Akad Nauk. SSSR, 206(1), 200-203, 1972.

[69] Dobretsov, N.L., Buslov, M. M., Delvaux, D., Berzin, N. A., Ermikov, V.D, Meso-Cenozoic tectonics of the Central Asian orogenic belt: collison of lithospheric plates and mantle plume, Inter. Geol. Rev., 38, 430-466, 1996.

[70] Dominguez, S., J. P. Avonac., Remi, M., Horizontal coseismic deformation of the 1999 Chi-Chi earthquake measured from SPOT satellite images: implication for the seismic cycle along the western foothills of Central Taiwan, J. Geophys. Res., 108, 2083, 2003.

[71] Dorjnamjaa, D., G., Badarch, O. Gerel, B. Windley, Geodynamic map of Mongolia, Ulaanbaatar (in English), 1998.

[72] Dunn, M.M., Relocation of Eastern Tennessee Earthquakes Using hypoDD, MS thesis, Virginia Polytechnic Institute and State University, Blacksburg, Virginia, 2004.

[73] Ekstrom, G., and P. England, Seismic strain rates in regions of distributed continental deformation, J. Geophys. Res., 94, 10 231-10 257, 1989.

[74] Engdahl, E.R., Van der Hilst, R., Buland, R., Global teleseismic earthquake relocation with improved travel times and procedures for depth determination, Bull. Seism. Soc. Am., 3, 722-743, 1998.

[75] England, P., Molnar, P, The field of crustal velocity in Asia calculated from Quarternary rates of slip on faults, J. Geophys. Res., 130, 551-582, 1997.

[76] Faure, M., and B.Natal'in, The geodynamic evolution of the Eastern margin in Mesozoic Times, Tectonophysics, 208, 397-411, 1992.

[77] Filina, A.G., The Altai and Sayan earthquakes. - In: Earthquakes in the USSR in 1991, Trud. Inst. Fiz. Zemli. (in Russian), 38-39, 1997.

[78] Fitch, W.E., D. W. McCowan., M.W. Shields, Estimation of the seismic moment tensor from teleseismic body wave data with application to intraplate and mantle earthquakes, J. Geophys. Res., 85, 3817-3828, 1980.

[79] Florensov, N.A., and V. P. Solonenko, The Gobi-Altai Earthquake, 391 pp., Akademiya Nauk USSR, Moscow, 1963.

[80] Futterman, W. I., Dispersive body waves, J. Geophys. Res., 67, 5279-5291, 1962.

[81] Geodakov, A.P., Obsuchenko, A. H., Platonova, S. G and Rogojin, E. A, Prelimenary result of study large earthquake occured 2003, in the Gorny Altay, Scien. Infor. Elect. J., 1(21) (in Russian), 1-22, 2003.

[82] Goldin, S.B., Seleznev, B.S., Emanov, A.F., The Chuya earthquake, 2003 (M=7.5), Scien. Infor. Elect. J., 1(21), (in Russian), 1-7, 2003.

[83] Golenetsky, S.I., Demjanovich, V.M., Filina, A.G., The comprehensiveness of earthquakes in South Siberia and Mongolia in 1960-1990. - In: Seismicity and seismic zoning in the North Eurasia, Trud. Inst. Fiz. Zemli, 1, (in Russian), 83-85, 1993.

[84] Got, J. L., Okubo, Paul, Machenbaum, Roland and Tahigawa, Wilfred, A real time procedure for progressive multipled relative relocation of the Hawaiian Volcano Observatory, Bull. Seism. Soc. Am., 92, 2019-2026, 2002.

[85] Grachev, A.F., Intraplate geodynamics and seismic activity, J. Earth. Pred. Res., 1, .87-106, 1992.

[86] Gross, S., Magnitude distributions and slip scaling of heterogeneous seismic sources, Bull. Seism. Soc. Am., 86, 498-504, 1996.

[87] Gutenberg, B., and Richter C. F, Frequency of earthquakes in California, Bull. Seism. Soc. Am., 34, 185-188, 1944.

[88] Haskell, N.A., Crustal reflection of plane P and SV waves, J. Geophys. Res., 67, 4751-4767, 1962.

[89] Haskell, N.A., Total energy and energy spectral density of elastic wave radiation from propagating fault, Bull. Seism. Soc. Am., 54, 1811-1841, 1964.

[90] Haskell, N.A., Elastic displacements in the near field of a propagating fault, Bull. Seism. Soc. Am., 59 (3), 865-908, 1969.

[91] Hearn, T.M., James, F.N, Pn velocities beneath continental collision zones: the Turkish-Iranian plateau, Geophys. J. Int., 117, 273-283, 1994.

[92] Helmberger, D.V., Generalized ray theory for shear dislocation, Bull. Seism. Soc. Am., 64, 45-64, 1974.

[93] Hirata, N., Sakai, S., Liaw, Z. S., Tsai, Y. B., Yu, S. B., Aftershock observations of the 1999 Chi-Chi, Taiwan earthquake, Bull. Earthq. Res. Inst. Tokyo Univ., 75, 33-46, 2000.

[94] Holt, W.E., Haines, A.J., Velocity felds in deforming Asia from the inversion of earthquake-released strains, Tectonics, 12, 1-20, 1993.

[95] Huang, J., Chen, W-P, Source mechanisms of the Mogod earthquake sequence of 1967 and the event of 1974 July 4 in Mongolia, Geophys. J. R. Astr. Soc., 84, 361-379, 1986.

[96] Husebye, E.S., and Dainty, A.M., Monitoring a Comprehensive Test Ban Treaty, Kluwer, Dordrecht, 1996.

[97] Jackson, J.A., Molnar, P, Active faulting and block rotations in the Western Transverse Ranges, California, J. Geophys. Res., 95, 22 073- 22 087, 1990.

[98] Kagan, Y.Y., Seismic moment distribution revisited: I. Statistical results, Geophys. J. Int., 148, 521-542, 2002.

[99] Kanamori, H., The energy release in great earthquakes, J. Geophys. Res., 82, 2981-2987, 1977.

[100] Kennet, B.L.N., England, E.R., Buland, R, Constrain on seismic velocities in the Earth from trivel times, Geophys. J. Int., 122, 108-124, 1995.

[101] Khilko, S.D., Kurushin, R.A., Kochetkov, V.M., Baljinnyam, I. Monkhoo, D, Report of field investigation of Seismogeological and seismological expedition in Western Mongolia, RCAG, Mongolia, Ulaanbaatar, 1977.

[102] Khilko, S.D., Florensov, N.A., Kurushin, R.A., Lastochkin, S.V., Baljinnyam, I., Seismotectonic lineaments and paleoseismic dislocations of the Mongolian Altai, 75-88 pp., Nauka, Moscow, 1978.

[103] Khilko, S.D., The Neotectonic and seismotectonics of Mongolia, in XI -th Conference INKBA., 285-286, 1982.

[104] Khilko, S.D., Kurushin, R.A., Kochetkov, V.M., Baljinnyam, I., Monkhoo, D., Strong earthquakes, paleoseismological and macroseismic data, in Earthquakes and the Bases of Seismogenic Zoning of Mongolia, Nauka, Novisibirsk Transactions, 41 (in Russian), 19-83, 1985.

[105] Kikuchi, M., H.Kanamori, Inversion of complex body waves, Bull. Seism. Soc. Am., 72, 491-506, 1982.

[106] Kissling, E., Program VELEST user's guide- Short Introduction, Institute of Geophysics and Swiss Seismological Service, Zurich, 1994.

[107] Kissling, E., U. Kradolfer, H. Maurer, VELEST user's guide short introduction, Inst. of Geophys. and Swiss Seismol. Serv, Zurich, Switzerland, 1995.

[108] Kiureghian, A.D., and A.H.S. Ang, A fault-rupture model for seismic risk analysis, Bull. Seism. Soc. Am., 67, 1173-1194, 1977.

[109] Klyuchevskii, A.V., Dynamic parameters of aftershock sources of the North-Mongolian earthquake, Russian Geology and Geophysics, 6, (in Russian), 136-141, 1993.

[110] Klyuchevskii, A.V., Selenge, L, Comparative analysis of dynamic parameters of the sources of earthquakes in Mongolia, 55-64 pp., Nauka, Novosibirsk, 1995.

[111] Kochetkov, V.M., Khilko, S.D., Zorin, Yu.A., Ruzhich, V.V., Turutanov, E.Kh., Arvisbaatar, N., Bayasgalan, A., Kozhevnikov, V.M., Erdenbeleg, B., Chipizubov, A.V., Monkhoo, D., Anikanova, G.V., Klyuchevskii, A.V., Naidich, V.I., Bayar, G., Borovik, N.S., Gileva, N.A., Ady, Seismotectonics and seismicity of Prikhubsugulye, 182 pp., Nauka, Novosibirsk, 1993.

[112] Kolmogorovo, P.P., Kolmogorov, V.G, Recent vertical crustal movements in the Altai-Sayan province in relation to neotectonic and sesimicity, Russian Geology and Geophysics, 6 (in Russian), 567-578, 2002.

[113] Kopnichev, Y.F., Spilker, G.L, Spatio-temporal characteristics of large earthquake sources of different-type motions, Trud. Ints. Fiz. Zemli, 9 (in Russian), 3-11, 1980.

[114] Kozhevnikov, V.M., Erdenbileg, B., Baljinnyam, I., Ulemzh, I., Structure of the crust and upper mantle beneath the Khangai uplift (Mongolian People's Republic) from the data on the dispersion of phase velocities of Rayleigh waves, Trud. Ints. Fiz. Zemli, 3 (in Russian), 12-20, 1990.

[115] Kurushin, R.A., Bayasgalan, A., Olziybat, M., Enhtuvshin, B., Molnar, P., Bazyarsayhan, Ch., Hudnut, K.W. Jian Lin., The surface rupture of the 1957 Gobi-Altay, Mongolia earthquake, 320 pp., The Geol. Soc. Am., Colorado, 1997.

[116] Langston, C. A., and D.V. Helmberger, A procedure for modeling shallow dislocation sources, Geophys. J. R. Astr. Soc., 42, 117-130, 1975.

[117] Langston, C .A., Source inversion of seismic waveform: The Koyna, India, earthquakes of 13 September 1967, Bull. Seism. Soc. Am., 71, 1-24, 1981.

[118] Lay, T., Wallace, T. C., Modern global seismology, 495 pp., Aczdemic press, San Diego, 1995.

[119] Lienert, B.R., and R. Barry, HYPOCENTER, Hawaii Institute of Geophysics SOEST, Honolulu, 1994.
[120] Lienert, B.R., and J. Havskov, A computer program for locating earthquakes both locally and globally, Seis. Res. Lett., 66, 26-36, 1995.
[121] Lukk, A.A., and Yunga, S.L, Geodynamics and state of stress and strain of the lithosphere in Central Asia, 234 pp., Donich, Dushanbe, Tajikistan, 1988.
[122] Luzgin, B.M., G. G. Ruzanov., Characteristics of formation of Neogenic deposits in the Southeastern Gorny Altai, Russian Geology and Geophysics, 33, (in Russian), 23, 1992.
[123] Marinov, N.A., Zonenshain, L.P., Blagonravov, V.A., Geology of the Mongolian People's Republic, 750 pp., Nedra, Moscow, 1973.
[124] McCaffrey, R., Abers, J, A program for inversion of teleseismic body wave form on microcomputers, Hanscomb Air Force Base, Air Force Geophysical Laboratory, Massachusetts, 1988.
[125] Micheal, H.R., Mikhail P. Barmin, Antonio Villasenor, Pn and Sn tomography across Eurasia to improve regional seismic event locations, Tectonophysics, 358, 39-55, 2002.
[126] Molnar, P., Tucker, B.E., Brune J.N., Corner frequencies of P and S waves and models of earthquake sources, Bull. Seism. Soc. Am., 63, 101-104, 1973.
[127] Molnar, P., and P. Tapponnier, Cenozoic Tectonics of Asia: Effects of a continental collision, Science, 189, 419 - 426, 1975.
[128] Molnar, P., and D. Qidong, Faulting associated with large earthquakes and the average rate of deformation in Central and eastern Asia, J. Geophys. Res., 89, 6203 - 6227, 1984.
[129] Mooney, W. D., and Goleman, R. G., The crustal structure in northwest China, 21st Seismic Research Symposium, 182-189, USGS., CA USA.
[130] Mordvinova, V.V., Zorin, Yu.A., Gao, Sh., Devis, P., Estimations of thickness of the earth's crust along the Irkutsk-Ulan Bator-Undurshil profile from spectral ratios of bodily seismic waves, Trud. Inst. Fiz. Zemli., 9 (in Russian), 3-11, 1995.
[131] Morozova, E.A., Morozov, I. B, Smithson, S. B., and Solodilov, L.N, Lithospheric boundaries and upper mantle heterogeneity beneath Russian Eurasia: evidence from the DSS profile QUARTZ, Tectonophysics, 329, 333-344, 2000.
[132] Nabelek, J., Determination of earthquake source parameters from inversion of body waves, Ph.D thesis, MIT, Massachusetts, 1984.
[133] Natsag-Yum, L., Monkhoo, D., Baljinnyam, I., Lkhanaasuren, G., Adyaa, M., Tsembel, B., Medvedev, S.V., Shteinberg, V.V., Popova, E.V., Tokmakov, V.A., Seismic zoning in Ulan Bator, 206 pp., Nauka, Moscow, 1971.
[134] Nelson, M.R., McCaffrey, R., Molnar, R., Source parameters for 11 earthquakes in the Tien Shan, Central Asia, determined by P and SH waveform inversion, J. Geophys. Res., 92, 12 629-12 648, 1987.
[135] Nelson, M.R., R.McCaffrey and P.Molnar, Source parameters for 11 earthquakes in the Tien Shan, central Asia, determined by P and SH waveform inversion, J. Geophys. Res., 12, 12,629-12,648, 1992.
[136] Novikov, I.S., Tectonic role for the evolution relief of the Gorny Altai, Russian Geomorphology., 1, (in Russian), 82-91, 1998.

[137] Novikov, I.S., Geomorphological effect of intracontinental collision on the example of Gorny Altai, Russian Geology and Geophysics, 37 (in Russian), 52, 1996.

[138] Novikov, I.S., Late paleozoic, middle mesozoic, and late cenozoic stages of the Altai orogeny, Russian Geology and Geophysics, 5 (in Russian), 434-445, 2002.

[139] Novikov, I.S., Morphotectonics of the Altai, 311 pp., Filial "Geo", Novosibirsk, 2004.

[140] Okal, E.A., A surface-wave investigation of the rupture mechanism of the Gobi Altai (December 4, 1957) earthquake, Phys. Eart. Plan. Int., 12, 319-328, 1976.

[141] Okal, E.A., The July 9 and 23, 1905, Mongolian earthquakes: A Surface wave Investigation, Earth. Plant. Sci. Lett., 34, 326-331, 1977.

[142] Owen, L.A., B. F. Windley, D. W. Cunningham, J. Badamgarav, and D. Dorjnamjaa, Quaternary alluvial fans in the Gobi of southern Mongolia: Evidence for neotectonics and climate change, J. Quat. Sci., 12, 239 -252, 1997.

[143] Owen, L.A., B. Richards, E. J. Rhodes, D. W. Cunningham, B. F. Windley, J.Badamgarav, and D. Dorjnamjaa, Relic permafrost structures in the Gobi of Mongolia: Age and significance, J. Quat. Sci., 13, 539 - 547, 1998.

[144] Owen, L.A., D. W. Cunningham, B. W. Richards, E. Rhodes, B. F. Windley, D. Dorjnamjaa, and J. Badamgarav, Timing of formation of forebergs in the northeastern Gobi-Altai, Mongolia: Implications for mountain up-lift rates and earthquake recurrence intervals, J. Geol. Soc. London, 156, 457 - 464, 1999.

[145] Ozacar, A.A., Beck, S. L., The 2002 Denali fault and 2001 Kunlun fault earthquakes: Complex rupture processes of two large strike-slip events, Bull. Seism. Soc. Am., 94, 1159-1165, 2004.

[146] Parfeevets, A.V., San'kov, V.A., Miroshnitchenko, A.I., Lukhnev, A.V., The evolution of the state of stress of the earth's crust of the Mongol-Baikal mobile belt, Pacific Geology, 21 (in Russian), 14-28, 2002.

[147] Petit, C., Déverchère, J., Houdry, F., Sankov, V.A., Melnikova, V.I., Delvaux, D., Present-day stress field changes along the Baikal rift and tectonic implications, Tectonics, 15, 1171-1191, 1996.

[148] Petit, C., Déverchère, J., Calais, E., San'kov, E., Fairhead, D., Deep structure and mechanical behaviour of the lithosphere in the Hangai-Hovsgol region, Mongolia: new constraints from gravity modelling, Earth. Plant. Sci. Lett., 197, 133-149, 2002.

[149] Petit, C., J. Déverchère, and E. Calais, Topography genesis in Mongolia: present-day tectonics and/or mantle dynamics Constraints from gravity modeling, Earth. Plant. Sci. Lett., 197, 133-149, 2002.

[150] Philip, P., and J.-F. Ritz, Gigantic paleolandslide associated with active faulting along the Bogd Fault (Gobi-Altay, Mongolia), Geology, 27, 211- 214, 1999.

[151] Prentice, C.S., Kendrick, K., Berryman, K., Bayasgalan, A., Ritz, J.F., Spencer, J.Q., Prehistoric ruptures of the Gurvan Bulag fault, Gobi Altay, Mongolia, J. Geophys. Res., 107(B12), 2321, 2002.

[152] Rautian, T.G., On determination of energy of earthquakes at distances up to 3000 km, Trud. Inst. Fiz. Zemli., 32 (in Russian), 86-93, 1964.

[153] Reasenberg, P., Cluster 2000 user's guide, http://quake.wr.usgs.gov, 2000.

[154] Richter, C.F., Elementary Seismology, 768 pp., W. H. Freeman, San Francisco, 1958.

[155] Ritz, J.F., E.T.Brown,D. L.Bourle`s, H. Philip, A. Schlupp, G. M. Raisbeck, F. Yiou, and B. Enkhtuvshin, Slip rates along active faults estimated with cosmic-ray-exposures dates: Application to the Bogd Fault, Gobi-Altay, Mongolia, Geology, 23, 1019 - 1022, 1995.

[156] Ritz, J.-F., D. Bourlès., E. T. Brown., S. Carretier., J. Chery., Enhtuvshin B., Galsan, P., Finkel, R. C., Hanks, T. C., Kendrick, T. C., Philip H., Raisbeck, G., Schlupp, A., Schwartz, D. P. , Yiou F, Late Pleistocene to Holocene slip rates for the Gurvan Bulag thrust fault (Gobi-Altay, Mongolia) estimated with 10Be dates, J. Geophys. Res., 108, X-1-16, 2003.

[157] Schlupp, A., Neotectonique de la Mongolie Occidentale analysé à partir de données de terrain, sismologiques et satellitaires, Univ. Louis Pasteur, Strasbourg, 1996.

[158] Scholz, C.H., Aviles, C. A., and Wesnousky, S. G., Scaling differences between large interplate and intraplate earthquakes, Bull. Seism. Soc. Am., 76, 65-70, 1986.

[159] Scholz, C.H., The mechanics of earthquake and faulting, Cambridge Univ. Press, Cambridge, UK., 1990.

[160] Schwartz, D., and K. Coppersmith, Fault behavior and characteristic earthquakes: Examples from the Wasatch and San Andreas faults, J. Geophys. Res., 89, 5681 - 5698, 1984.

[161] Shi, J.-B., Feng Xian-yue, Ge Shu-mo, Yang Zhang and others, The Fuyun earthquake fault zone in Xinjiang, China, in Continental seismicity and earthquake prediction., pp. 325-346, Seismology Press, Beijing, 1984.

[162] Scholtz, C.H., The frequency-magnitude relation of microfracturing in rocks and its relation to earthquakes, Bull. Seism. Soc. Am., 58, 399-415, 1968.

[163] Stein, S., Wysession, M., An Introduction to Seismology, Earthquakes, and Earth Structure, Blackwell, 2003.

[164] Stump, B.W., and L.R Johnson, Determination of source properties by the linear inversion of seismograms, Bull. Seism. Soc. Am., 67, 1489-1502, 1977.

[165] Tapponnier, P., Molnar, P., Active faulting and Cenozoic tectonics of the Tien Shan, Mongolia and Baykal regions, J. Geophys. Res., 84, 3425 - 3459, 1979.

[166] Thomas, J.C., Lanza, R., Kazansky, A., Zykin, C.V.S., Semakov, N., Mitrokhin, D., Delvaux, D., Paleomagnetic study of Cenozoic sediments from the Zaisan basin (SE Kazakhstan) and Chuya depression, RAS, GJI., 163, 1151-1179, 2002.

[167] Tibi, R., Bock, G., Y. Xia., M. Baumbach., H. Groscer., C. Milkereit., S. Karakisa., S.Zuhbul., R. Kind., J. Zschau, Rupture processes of the 1999 August 17 Izmit and November 12 Duzce (Turkey) earthquakes, Gephys. J. Int., 144, F1-F3, 2000.

[168] Tikhonov, V.I., Faults, in Tectonics of the Mongolian People's Republic, pp. 196-209, Nauka, Moscow, 1974.

[169] Timofeev, V.Y., Ardukov, D.G., Zapreeva, E.A., Calais, E., Duchkov A.D., Arnautov G.P., Kalish E.N., Stus Y.F., Smirnov M.G., Visotskyi E., Kazantsev S.A., Timofeev A.V., Altay GPS and gravity network for geodynamic studies, Institute of Geophysics UIGGM SB RAS, Novosibirsk, 2003.

[170] Traynor, J.J., Sladen, C., Tectonic and stratigraphic evolution of the Mongolian People's Republic and its influence on hydrocarbon geology and potential, Mar. Petrol. Geol., 12, 35-52, 1995

[171] Treskov, A.A., and M.B. Vertlib, Objective determination of the epicenters of near earthquakes, 75 pp., Nauka, Moscow, 1973.

[172] Trifonov, V.G., Late Quaternary tectogenesis, 224 pp., Nauka, Moscow, 1983.

[173] Trifonov, V.G., Features of active faulting, Geotektonika, 2 (in Russian), 16-26, 1985.

[174] Ulziibat, M., Mongolia Network for Detection Earthquakes, Bulletin of the IISEE., (Tsukuba, Japan), 1996.

[175] Ulziibat, M., Bayarsaikhan Ch., Ankhtsetseg D., Calibration of local magnitude Ml in the Mongolia, Special report of the RCAG., (Ulaanbaatar, Mongolia), 2000.

[176] Vallée, M., Stabilizing the empirical Green function analysis: Development of the projected Landweber method, Bull. Seism. Soc. Am., 94, 394- 409, 2004.

[177] Van der Woerd, J., F. J. Ryerson, P. Tapponnier, Y. Gaudemer, R. Finkel, A. S. Meriaux, M. Caffee, Z. Guoguang, and H. Qunlu, Holocene left-slip rate determined by cosmogenic surface dating on the Xidatan segment of the Kunlun fault (Qinghai, China), Geology, 26, 695 - 698, 1998.

[178] Van Puymbroeck, N., Micheal, R., Binet, R., Avouac, J.P. and J. Taboury, Measuring earthquakes from optical satellite images, Appl. Opt., 39, 3486-3494, 2000.

[179] Waldhauser, F., William L. Ellsworth, A Double-Difference Earthquake Location Algorithm: Method and Application to the Northern Hayward Fault, California, Bull. Seism. Soc. Am., 6, 1353–1368, 2000.

[180] Waldhauser, F., HYPODD--A program to compute double-difference hypocenter locations, U.S. Geologic Survey, Menlo Park, 2001.

[181] Wells, D.L., and K. J. Coppersmith, New empirical relationships among magnitude, rupture length, rupture width, rupture area, and surface displacement, Bull. Seism. Soc. Am., 84, 974-1002, 1994.

[182] Wiemer, S., Wyss, M, Seismic quiescence before the Landers (M=7.5) and Big Bear (M=6.5) 1992 earthquakes, Bull. Seism. Soc. Am., 84, 900-916, 1994.

[183] Wiemer, S., and Katsumata, K., Spatial variability of seismicity parameters in aftershock zones, J. Geophys. Res., 104, 13,135-13,151, 1999.

[184] Windley, B.F., Allen, M.B., Mongolian plateau: Evidence for late Cenozoic plume under central Asia, Geology, 21, 295-298, 1993.

[185] Wyss, M., Towards a physical understanding of the earthquake frequency distribution, Geophys. J. R. Ast. Soc., 31, 341- 359, 1973.

[186] Yanshin, L.D.e.a., Tectonics of the Mongolian People's Republic, 284 pp., Nauka, Moscow, 1974.

[187] Yunga, S.L., On the mechanism of deformation of seismoactive volume of the Earth's crust, Phys. Solid. Eart., 15 (in Russian), 693-699, 1979.

[188] Zhalkovsky, N.D., and V.I. Muchnaya, On accuracy of plotting the slope of earthquake recurrence curve, Russian Geology and Geophysics, 10, (in Russian), 21-129, 1987.

[189] Zhang, P. Z., Surface rupture associated with the 1931 Fu-yun, northeastern China, earthquake, MS thesis, Chinese University of Science and Technology, Beijing, 1982.

[190] Zhao, X., Coe, R. S., Zhon, Y.,Wu, H., Wang J., New paleomagnetic results from Northern China: Collision and suturing with Siberia and Kazakhstan, Tectonophysics, 181, 43-81, 1990.

[191] Zorin, Y.A., M.R. Novoselova, and V.A. Rogozhina, Deep structure of the territory of MPR., (in Russian), Nauka, Novosibirsk, pp. 93, 1982.

[192] Zorin, Y.A., Geodynamics of the western part of the Mongolia-Okhotsk collisional belt, Trans-Baikal region (Russia) and Mongolia, Tectonophysics, 306, 33-56, 1999.

[193] Zorin, Y.A., Mordvinova, V.V., Turutanov, E.Kh., Belichenko, B.G., Artemyev, A.A., Kosarev, G.L., Gao, S.S., Low seismic velocity layers in the Earth's crust beneath eastern Siberia (Russia) and central Mongolia: receiver function data and their possible geological implication, Tectonophysics, 359, 307-327, 2002.